

**Investigations into Non-Conventional¹⁰
Materials for High-K Dielectrics and the
Unique Production of Permalloy Oxides for
GMR Devices**

THESIS

*Presented to the Graduate Council of
Southwest Texas State University
In Partial Fulfillment of
The Requirements*

For The Degree of

Master of SCIENCE

In the Department of Physics

By

Albert A. Tijerina, B.S.

*San Marcos, Texas
May 2002*

For my mother, Amanda Tijerina. Without your love, help, and support I never would have finished college, much less gone on to graduate school. Thank you for being the amazing person you are.

And for Amy. Sweetheart, you have been more than a man could ever hope for in a wife. You put up with the long nights, the evenings and weekends in the lab, and all the hours I spent at my computer. And all the while, you have been my best friend, my caretaker, my inspiration, my guardian angel, and the best part of my life since the day we met. I could never have done this without you! I Love You, Baby!

Copyright

By

Albert Anthony Tijerina, M.S.

2002

ACKNOWLEDGMENTS

I would like to thank Dr. James Crawford and Dr. Victor Michalk for giving me the opportunity to teach when I was still a student myself. You never learn anything as well as when you teach it to someone else. In addition, I would like to thank Dr. Don Olsen for his infectious delight in seeking to broaden one's boundaries of knowledge. To the faculty of the Physics Department at Southwest Texas State University, my thanks go as well. Your dedication to teaching is an inspiration. Thanks also belong to Pat Parks for all the assistance she has given me during my stay here at SWT and to Steven Rios and Anup Bandyopadhyay for their invaluable help in getting the D-1 operational. I would also like to thank Dr. Larry Larson of International SEMATECH. Without the position as an intern working for you I would never have learned so much, so quickly. You have also become the standard I hope to equal when I enter the management ranks. Most importantly, I would like to thank Dr. Carlos J. Gutierrez for the support he has given me. He has not only been a graduate advisor and mentor, but a friend as well. His guidance and instruction have been an integral part of my education as a physicist and as a person. Thank you for all you have done.

Forward

In the process of writing this thesis, a number of thoughts came to my mind on how I wanted to write it: what level of detail I felt was necessary for the satisfaction of the requirements of a Master's level thesis, who my audience will be, what type of background information I felt was needed to describe the motivation behind why I studied the materials that I did, and others that came and went. Early on in the process of developing an outline, two main themes came to me that had an effect on the style and format that I wanted to use in writing my thesis. The first is that I wanted it to be readable to those who have had little or no scientific background. This was specifically with the hopes that my friends and family could read it and get a better understanding of what I have devoted so much time and energy towards and why I have done so. I also decided to write each chapter, as closely as possible, as a "stand alone" chapter, for use by future graduate students as introductory reading material. My hope is that each chapter can serve as a basic introduction to the analytic methods available at SWT so that when future students read the more advanced texts, their understanding of the material will be easier to comprehend and follow.

Table of Contents

1	INTRODUCTION.....	1
1.1	HIGH DIELECTRIC CONSTANT INSULATING FILMS.....	1
1.2	MAGNETIC RANDOM ACCESS MEMORY.....	4
2	SEMICONDUCTORS AND TRANSISTORS..	10
2.1	BASIC TRANSISTOR PHYSICS.....	11
2.2	MOS TRANSISTOR OPERATION.....	19
2.3	CAPACITANCE IN MOS TRANSISTORS.....	22
2.4	CMOS TRANSISTORS.....	23
2.5	LIMITS TO SiO ₂ DIELECTRICS.....	24
2.6	DRAM TRANSISTORS.....	29
2.7	ALTERNATE DIELECTRICS.....	32
2.8	FERROELECTRIC DIELECTRICS.....	35
2.9	BARIUM-ZIRCONIUM-TITANATE DIELECTRICS.....	38
3	MAGNETIC DEVICES.....	42
3.1	BASIC MAGNETISM.....	42
3.2	EXCHANGE COUPLING.....	47
3.3	TRADITIONAL READ-WRITE PROCESSES.....	52
3.4	ANISOTROPIC MAGNETO-RESISTIVE EFFECT.....	56
3.5	GIANT MAGNETORESISTANCE.....	59
3.6	SPIN-VALVE SENSORS.....	64
3.7	SPIN-VALVE TRANSISTORS.....	66
3.8	MAGNETIC PROPERTIES AND PERMALLOY.....	68
4	VACUUM FUNDAMENTALS.....	75
4.1	PRODUCING A VACUUM.....	75
4.2	ROUGH VACUUM.....	76
4.3	HIGH VACUUM.....	78
5	DUAL ION-BEAM SPUTTERING.....	82
5.1	INTRODUCTION.....	82
5.2	COMPONENTS.....	82
5.2.1	PRESSURE.....	83
5.2.2	CATHODE.....	83
5.2.3	ANODE.....	83

5.2.4	SCREEN GRID AND ACCELERATOR GRID.....	84
5.2.5	NEUTRALIZER.....	85
5.3	BASIC OPERATION.....	85
5.3.1	GENERATION OF THE ION BEAM.....	85
5.3.2	NEUTRALIZING THE ION BEAM.....	87
5.3.3	BEAM BEHAVIOR.....	89
5.3.4	TARGET INTERACTIONS.....	91
5.3.5	FILM GROWTH.....	93
5.3.6	SECOND (DUAL) ION BEAM.....	96
6	VIBRATING SAMPLE MAGNETOMETRY	100
6.1	BASIC OPERATION.....	100
6.2	CALCULATION OF FILM THICKNESS USING VSM.....	102
6.3	MAGNETIC VS. NON-MAGNETIC FILMS.....	106
7	X-RAY ANALYSIS	109
7.1	PROPERTIES OF X-RAYS.....	110
7.1.1	PRODUCTION OF X-RAYS AND CHARACTERISTIC X-RAYS.....	111
7.1.2	CHARACTERISTIC X-RAYS.....	116
7.1.3	X-RAY CHARACTERIZATION.....	120
7.1.4	ABSORPTION.....	123
7.1.5	DETECTION OF X-RAYS.....	127
7.2	X-RAY FLUORESCENCE.....	130
7.2.1	ABSORPTION JUMP RATIOS.....	131
7.2.2	RELATIVE LINE INTENSITIES WITHIN THE K, L, AND M SERIES.....	133
7.2.3	FLUORESCENCE YIELD.....	133
7.2.4	X-RAY ENERGY DISPERSIVE DETECTOR AND THE KEVEX MODEL 771.....	135
7.3	THE GEOMETRY OF CRYSTALS.....	143
7.3.1	LATTICE DIRECTIONS AND THE ZONE AXIS.....	144
7.3.2	MILLER INDICES.....	146
7.3.3	LATTICE PLANE SPACING.....	148
7.3.4	CRYSTAL SYSTEMS.....	150
7.4	X-RAY REFLECTIVITY.....	153
7.5	HIGH ANGLE AND PARALLEL BEAM X-RAY DIFFRACTION.....	160
7.5.1	HIGH ANGLE X-RAY DIFFRACTION.....	161
7.5.2	PARALLEL BEAM X-RAY DIFFRACTION.....	166
8	OPTICAL ANALYSIS	171
8.1	THIN FILMS AND BASIC OPTICS.....	171
8.1.1	OPTICAL CONSTANTS.....	173
8.1.2	REFLECTION.....	174
8.1.3	MODELS FOR <i>n</i> AND <i>k</i>	177
8.2	FILMETRICS F-20.....	178

9 CONCLUSIONS BASED ON DATA.....180

9.1	WHAT I LEARNED ABOUT BZT GROWTHS	180
9.2	WHAT I LEARNED ABOUT PY GROWTHS	187
9.2.1	PERMALLOY METAL FILMS	187
9.2.2	PERMALLOY OXIDE FILMS	198

10 RAW DATA.....208

10.1	FILM PRODUCTION PARAMETERS	208
10.1.1	PERMALLOY METAL FILMS	208
10.1.2	PERMALLOY OXIDE FILMS	209
10.1.3	BARIUM ZIRCONIUM TITANATE FILMS.....	210
10.2	VIBRATING SAMPLE MAGNETOMETRY DATA.....	211
10.2.1	FILM 010315	211
10.2.2	FILM 010319	211
10.2.3	FILM 010505A.....	212
10.2.4	FILM 010505B.....	212
10.2.5	FILM 010506A.....	213
10.2.6	FILM 010506B.....	213
10.2.7	FILM 010312	214
10.2.8	FILM 010314	214
10.3	OPTICAL DATA	215
10.3.1	BARIUM ZIRCONIUM TITANATE FILMS.....	219
10.3.1.1	FILM 010206, 010208, AND 010209	219
10.3.1.2	FILM 010326.....	219
10.3.1.3	FILM 010410.....	224
10.3.1.4	FILM 010413.....	229
10.3.2	PERMALLOY OXIDE FILMS	234
10.3.2.1	FILM 010312.....	234
10.3.2.2	FILM 010314.....	239
10.3.2.3	FILM 010323	244
10.3.2.4	FILM 010415.....	249
10.3.2.5	010501	254
10.4	X-RAY FLUORESCENCE DATA.....	259
10.5	HIGH ANGLE X-RAY DIFFRACTION DATA	265
10.5.1	PERMALLOY METAL FILMS	265
10.5.1.1	FILM 010315.....	265
10.5.1.2	FILM 010319	266
10.5.1.3	FILM 010505A.....	267
10.5.1.4	FILM 010505B.....	268
10.5.1.5	FILM 010506A.....	269
10.5.1.6	FILM 010506B.....	270
10.5.2	PERMALLOY OXIDE FILMS	271
10.5.2.1	FILM 010312.....	271
10.5.2.2	FILM 010314.....	272

10.5.2.3	FILM 010323.....	273
10.5.2.4	010415	274
10.5.2.5	FILM 010501.....	275
10.5.3	BARIUM ZIRCONIUM TITANATE FILMS.....	276
10.5.3.1	FILM 010206.....	276
10.5.3.2	FILM 010208.....	277
10.5.3.3	FILM 010209.....	278
10.5.3.4	FILM 010326.....	279
10.5.3.5	FILM 010410.....	280
10.5.3.6	FILM 010413.....	281
10.5.3.7	FILM 010415B	282
10.5.3.8	FILM 010501B	283
10.5.3.9	FILM 010504AB	284
10.6	PARALLEL BEAM X-RAY DIFFRACTION DATA.....	285
10.6.1	PERMALLOY METAL FILMS	286
10.6.1.1	FILM 010315.....	286
10.6.1.2	FILM 010319.....	287
10.6.1.3	FILM 010505A.....	287
10.6.1.4	FILM 010505B	288
10.6.1.5	FILM 010506A.....	289
10.6.1.6	FILM 010506B	289
10.6.2	PERMALLOY OXIDE FILMS	290
10.6.2.1	FILM 010312.....	290
10.6.2.2	FILM 010314.....	291
10.6.2.3	FILM 010323.....	291
10.6.2.4	FILM 010415.....	292
10.6.2.5	FILM 010501.....	292
10.7	X-RAY REFLECTIVITY.....	293
10.7.1	PERMALLOY METAL FILMS	294
10.7.1.1	FILM 010315.....	294
10.7.1.2	FILM 010319.....	296
10.7.1.3	FILM 010505A.....	297
10.7.1.4	FILM 010505B	298
10.7.1.5	FILM 010506A.....	299
10.7.1.6	FILM 010506B	300
10.7.2	PERMALLOY OXIDE FILMS	301
10.7.2.1	FILM 010312.....	301
10.7.2.2	FILM 010314.....	302
10.7.2.3	FILM 010323.....	303
10.7.2.4	FILM 010415.....	304
10.7.2.5	FILM 010501.....	305

11 APPENDICES.....306

11.1	HOW TO OPERATE THE VSM.....	306
11.1.1	MOUNTING A SAMPLE	306
11.1.2	TURNING ON THE SYSTEM COMPONENTS	306

11.1.3	CALIBRATION SETUP	307
11.1.4	OPTIMIZATION	307
11.1.5	CALIBRATING THE LOCK-IN AMPLIFIER.....	308
11.1.6	TAKING A MEASUREMENT.....	309
11.2	HOW TO OPERATE THE KEVEX MODEL 771 XRF	310
11.2.1	STARTING AND PREPARING THE COMPUTER AND THE MACHINE.....	310
11.2.2	SETTING UP A MATRIX FILE.....	311
11.2.3	SETTING THE SAMPLE CONDITIONS IN PREPARATION FOR MAKING A STANDARD.....	313
11.2.4	TAKING A SCAN	315
11.2.5	CREATING A RESULTS FILE	316
11.2.6	DEFINING THE STANDARD	318
11.2.7	CREATING A FILE THAT WILL HOLD THE CALIBRATION DATA.....	319
11.2.8	COMPARING AN UNKNOWN SAMPLE TO THE CALIBRATION STANDARD.....	321
11.2.9	SETTING UP A JOBS FILE TO AUTOMATE THE PROCESS OF ANALYZING MATERIALS.....	324
11.3	HOW TO OPERATE THE DUAL ION-BEAM SYSTEM.....	328
11.4	HOW TO OPERATE THE F-20.....	331
11.5	HOW TO OPERATE THE D-1	332
11.5.1	ALIGNING THE BEDE D-1 FOR PARALLEL BEAM AND HIGH ANGLE XRD SCANNING.....	333
11.5.2	ALIGNING THE SAMPLE	337
11.5.3	PERFORMING A HIGH ANGLE X-RAY DIFFRACTION SCAN	343
11.5.4	PERFORMING A PARALLEL BEAM X-RAY DIFFRACTION SCAN.....	344
11.5.5	ALIGNING THE D-1 FOR AND PERFORMING A REFLECTIVITY MODE X-RAY SCAN	346
11.5.6	ALIGNMENT AND SCANNING OF SAMPLE FOR REFLECTIVITY MODE.....	349
12	BIBLIOGRAPHY.....	351

Table of Images

Figure 1-1: Cross-Section Diagram of DRAM¹	2
Figure 1-2: Principle of the Magnetic Recording Process used in Magnetic Hard Disk Drives²	4
Figure 1-3: MRAM Spin-Valve.....	7
Figure 2-1: Diamond Structure Bonding of Si in a Perfect Crystal	12
Figure 2-2: EHP Formation in a Perfect Si Crystal ¹	13
Figure 2-3: EHP Formation with Dopant Atoms Present¹.....	14
Figure 2-4: Depletion Region¹	16
Figure 2-5: Effects of Biasing on Depletion Region¹	17
Figure 2-6: Typical Enhancement Mode N-Type MOSFET⁴.....	19
Figure 2-7: CMOS Transistor⁵	23
Figure 2-8: Schematic Diagram of Typical DRAM⁸	30
Figure 2-9: Perovskite Crystal Structure³.....	34
Figure 3-1: Direction of Magnetic Field in a Conductor²⁵	43
Figure 3-2: Electron Spin Orientations of an Iron Atom in Free Space.....	46
Figure 3-3: Exchange Coupling Ratio²⁶.....	48
Figure 3-4: Three Common Types of Magnetic Ordering.....	49
Figure 3-5: Magnetization (M), Magnetic Field (H), and Flux Density (B) Fields of a Bar Magnet	51
Figure 3-6: Idealized Write Head²⁵	53
Figure 3-7: Fringing Field at the Top of the Write Head	54
Figure 3-8: Fringe Field and Written Magnetization Pattern.....	55
Figure 3-9: Flux Near the Read Head.....	55
Figure 3-10: Spin Dependant Scattering in GMR Multilayers.....	60
Figure 3-11: GMR Lattice with Py-Cu Layers	63
Figure 3-12: Example of Hysteresis Curve Demonstrating Exchange Biasing	64
Figure 3-13: Example of the Structure of a Spin-Valve Transistor³⁰	66
Figure 3-14: Energy band diagram of a Spin-Valve Transistor³¹	67
Figure 3-15: Magnetization Curve (Green) and Hysteresis Loop (Blue)	68
Figure 3-16: Cubic (NaCl) Crystal Structure³	70
Figure 3-17: Body Centered Cubic (bcc) Crystal Structure³.....	71
Figure 3-18: Rhombohedral Crystal Structure of Fe₂O₃ ³	72
Figure 4-1: Two-Stage Oil-Immersed Rotary Vane Pump.....	76
Figure 4-2: Detail of Rotary Vane Pump Module	77
Figure 4-3: Cryopump and Compressor	79
Figure 4-4: Insides of a Typical Cryopump	80
Figure 4-5: Gas Molecules Undergoing Cryosorption.....	81
Figure 5-1: Gridded Ion Source	82

Figure 5-2: Discharge Chamber	86
Figure 5-3: Target Atom Distribution	91
Figure 5-4: Island Formation	94
Figure 5-5: Layer Growth	94
Figure 5-6: Stranski-Krastanov Film Growth	96
Figure 5-7: Dual Ion-Beam Sputtering System.....	97
Figure 6-1: Schematic Diagram of a Typical Vibrating Sample Magnetometer	101
Figure 6-2: Bohr Magneton Number and Curie Point of Iron-Nickel Alloys	102
Figure 6-3: Face-Centered Cubic (fcc) Crystal Structure³.....	103
Figure 6-4: Lattice Constants of Fe-Ni Alloys in the bcc and fcc Condition ³⁸	104
Figure 6-5: Hysteresis Curve for Magnetic Py Film.....	107
Figure 6-6: Hysteresis Curve for Non-Magnetic Material.....	108
Figure 7-1: Incoming Electron	111
Figure 7-2: Electron Escaping from Parent Atom	112
Figure 7-3: X-Ray Emitted as Electron Fills a Vacancy	113
Figure 7-4: Example of a Typical X-Ray Source	114
Figure 7-5: Bohr Model of a Silicon Atom	117
Figure 7-6: Characteristic X-Ray Lines.....	119
Figure 7-7: Example of a NaI(Tl) Crystal Scintillation Detector... 	128
Figure 7-8: Distribution of Secondary Targets for Kevex Model 771	135
Figure 7-9: XRF Scans Of Same Material Using (a) Germanium and (b) Iron Targets.....	137
Figure 7-10: Lithium Drift Solid State X-Ray Detector	138
Figure 7-11: XRF Film Thickness vs VSM Thickness	141
Figure 7-12: Graph of XRF Thin Film Measurements.....	142
Figure 7-13: Primitive Unit Cell	145
Figure 7-14: Primitive Unit Cell with Two Planes Defined	147
Figure 7-15: Intercepts of a Lattice Plane	148
Figure 7-16: The Fourteen Bravais Lattices³⁸	152
Figure 7-17: Reflection of a Plane Wave by Crystal Planes.....	155
Figure 7-18: Example of Reflectivity Spectra	156
Figure 7-19: Poorly Fit Analysis of Reflectivity Scan.....	157
Figure 7-20: Well Fit Analysis of Reflectivity Data	158
Figure 7-21: Bragg-Brentano Diffraction Geometry.....	161
Figure 7-22: HAXRD Diffraction Geometry	164
Figure 7-23: Example of High Angle X-Ray Diffraction Spectra....	165
Figure 7-24: Seemann-Bohlin Geometry for Parallel Beam XRD....	166
Figure 7-25: Parallel Beam XRD Benefits	168
Figure 7-26: Example of Parallel Beam XRD Spectra	169
Figure 7-27: Combined PBXRD Spectra from Three Incident Angles	170
Figure 8-1: Single Interface Reflection.....	174

Figure 8-2: Reflection in Multiple Interfaces³⁹	175
Figure 8-3: Filmetrics F-20 Setup and Operation³⁹	178
Figure 8-4: Reflectance Spectra from F-20³⁹	179
Figure 9-1: Typical Scan from BZT Films	180
Figure 9-2: Example of Uneven Film Growth	182
Figure 9-3: Side View of Old SWT Platen	183
Figure 9-4: Diagram Showing Side View of New SWT Platen.....	184
Figure 9-5: SWT Platen Details of Part #1.....	184
Figure 9-6: Details of SWT Platen Part #2.....	185
Figure 9-7: Details of SWT Platen Part #3.....	185
Figure 9-8: Film after New Platen Installed on DIBS	186
Figure 9-9: Example VSM Scan of Py Film.....	188
Figure 9-10: Typical High Angle X-Ray Diffraction Scan for a Permalloy Metal Film.....	189
Figure 9-11: Example of a Typical Parallel Beam X-Ray Diffraction Scan on a Py Metal Film	192
Figure 9-12: REFS Mercury Data Input Page	193
Figure 9-13: Example of REFS Mercury Model vs Experimental Data	194
Figure 9-14: Details of Fit Information for REFS Mercury Calculations.....	195
Figure 9-15: Example of Permalloy Oxide Vibrating Sample Magnetometry Scan	199
Figure 9-16: Example of HAXRD Scan of Permalloy Metal Film	200
Figure 9-17: Example of PBXRD Scan for a Permalloy Oxide Film	203
Figure 9-18: Example of REFS Mercury Data Input for PyO Film .	204
Figure 9-19: REFS Mercury Fit to Experimental Data for a PyO Film	206
Figure 9-20: REFS Mercury Calculated Details of PyO Film	206
Figure 10-1: F-20 Data Collection Locations	215
Figure 10-2: XRF Data From Scan Used to Create Py Standard....	259
Figure 10-3: XRF Scan Data of BZT Target Used to Produce BZT Films	260
Figure 10-4: XRF Scan of Film 010413 Using Gd Secondary Target	261
Figure 10-5: XRF Scan Film 010413 Using an Fe Secondary Target	262
Figure 10-6: XRF Scan of Film 010413 Using a Silver (Ag) Secondary Target.....	263
Figure 11-1:Kevex WinXRF Monitor Pop-Up Window	310
Figure 11-2: Kevex WinXRF Main Program Window Example.....	311
Figure 11-3: Condition Code Pop-up Window.....	312
Figure 11-4: Kevex WinXRF Spectrum Display Panel (SDP) Menu Bar	313
Figure 11-5: Setup Sample Data Pop-up Window	313
Figure 11-6: "Layers" Example for Sample Data Setup	314

Figure 11-7: "Component" Example for Sample Data Setup	315
Figure 11-8: Sample Names Pop-up Window	315
Figure 11-9: Spectrum Save/Recall Pop-up Window	317
Figure 11-10: "Deconvolution" Example for Spectrum Processing Window.....	317
Figure 11-11: Chart to Select Elements from for Deconvolution Processing	318
Figure 11-12: Setting the Layer Thickness of the Standard Film ..	319
Figure 11-13: Creating a Least Squares File	320
Figure 11-14: Calibration Pop-up Window	321
Figure 11-15: Calibrated Data for Use in Future Analysis Window	321
Figure 11-16: Results File for the Unknown Sample.....	322
Figure 11-17: Selecting the Least Squares File to Compare to the Unknown Sample	323
Figure 11-18: Results File for the Unknown Sample Showing Film Thickness	323
Figure 11-19: Jobs Manager Pop-up Window.....	324
Figure 11-20: Sample Naming Pop-up Window.....	325
Figure 11-21: Condition Codes for the Jobs Menu.....	325
Figure 11-22: Spectrum Processing Window for the Jobs Menu	326
Figure 11-23: Job Setup Quantitation Pop-up Window	327
Figure 11-24: Export Pop-up Window	327
Figure 11-25: Bede Control Opening Window	333
Figure 11-26: Align in Powder Mode Opening Script.....	334
Figure 11-27: Powder Mode Alignment PUW.....	335
Figure 11-28: Pop-up Window for Step G.....	335
Figure 11-29: PUW for Step I.....	336
Figure 11-30: PUW for Step K	336
Figure 11-31: PUW for Step M	337
Figure 11-32: PUW for Step A.....	338
Figure 11-33: Control Pane Main Window for Sample Alignment ..	339
Figure 11-34: Main Window for Scan Setup	340
Figure 11-35: Scan Peak Selection for Scan on Omega	341
Figure 11-36: Sample Information Window	343
Figure 11-37: Sample Information Window	345
Figure 11-38: Bede Control Opening Window	346
Figure 11-39: Opening PUW of D-1 XRR Alignment	347
Figure 11-40: Opening Pop_Up-Window for XRR Sample Alignment and Scanning.....	349

1 INTRODUCTION

1.1 High Dielectric Constant Insulating Films

Since its introduction in the late nineteen seventies, Dynamic Random Access Memory (DRAM), made from one transistor and one capacitor as the cell structure, has played a key role as a technology driver for ultra large-scale integration (ULSI) silicon technology. With each successive generation of transistors, the density of DRAM on a chip has increased, following a pattern of quadrupling every three years.¹ As the density increases, the minimum feature size has been scaled down to the point where a chip only 1.5 times larger than the generation before it has four times the number of DRAM devices. In addition to decreasing the size of DRAM devices, the chip speed has improved. While there have been many advances in the production of DRAM, current DRAM technology cannot be extended to the giga-bit era and beyond because of many challenges, the largest of which comes from the extremely small size needed to put on the order of 10^9 devices on a chip that is only a few square centimeters in area. This is due to the requirements placed on the DRAM such as sufficient device charge, small leakage current, and fast charge transferring into and out of the DRAM capacitor.

DRAM capacitance is a key parameter in the determination of a DRAM operation. The Capacitor-over-bit line structure for DRAM (see

Figure 1-1 below) seems to be the best candidate for giga-bit technology because it can provide more area for the device capacitor. However, due to the extremely small size required for next generation chips, there are still many challenging obstacles that must be overcome if it is to become the structure of choice for future DRAM technologies.

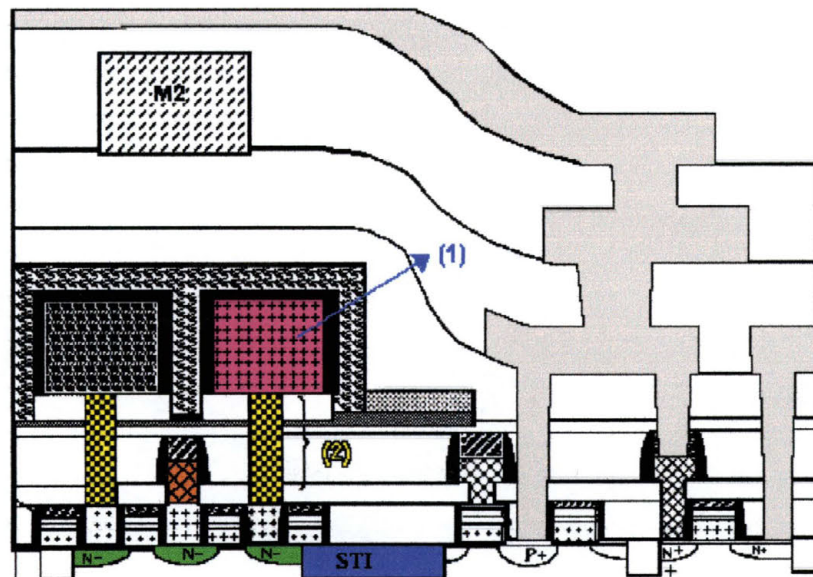


Figure 1-1: Cross-Section Diagram of DRAM¹

One of the most challenging of these obstacles to overcome is the insufficient device capacitance and the large leakage current at the storage junction that would be seen if existing technology were to be applied to next generation devices. The capacitance determines the

signal speed margin, the sensing speed, and data retention time as well as other parameters such as soft breakdown. Capacitance of DRAM can be described by using the simple equation (Equation 1-1) used for parallel plate capacitors, which is determined by the area of the plates (A), the dielectric constant (ϵ), and the thickness of the capacitor dielectric (d) as follows:

$$C_s = A \times \frac{\epsilon}{d}$$

Equation 1-1: Capacitance for Parallel Plate Capacitor

In the past, most methods of trying to solve the minimum capacitance required for DRAM technologies have been focused on trying to increase the memory cell capacitor area, as well as decrease the dielectric thickness. For future generations of devices, unless the capacitor dielectric thickness is reduced to around half of the preceding generation or the dielectric constant is at least doubled, the total surface area of the capacitor will have to be doubled. This will not allow for continued scaling down for future generations of DRAM devices. Because of the dielectric leakage current for extremely thin films, the only possible way to satisfy the required memory cell capacitance seems to be either to increase the thickness of the dielectric or to increase the surface area of the capacitor. An increase in the height of the capacitor causes other undesirable effects, such as a high global topology

difference, which can lead to difficulties in the production process of devices, including contact hole etching and storage node separation.

This thesis intends to investigate the viability of producing superior oxide films for use as High Dielectric Constant (High 'K') thin films for use in DRAM transistors using the non-conventional ferroelectric material Barium-Zirconium-Titanate grown in a Dual Ion-Beam Sputtering system.

1.2 Magnetic Random Access Memory

Another important technology in today's computer industry is memory. The storage capacity of hard disk drives in computers increases by 60% to 100% every year, while the physical size of the devices remains relatively constant. In order to maintain this increase in storage capacity, there is a strong ongoing demand for the reduction of critical feature sizes in magnetic storage components as well as for the development of increasingly complex film structures.

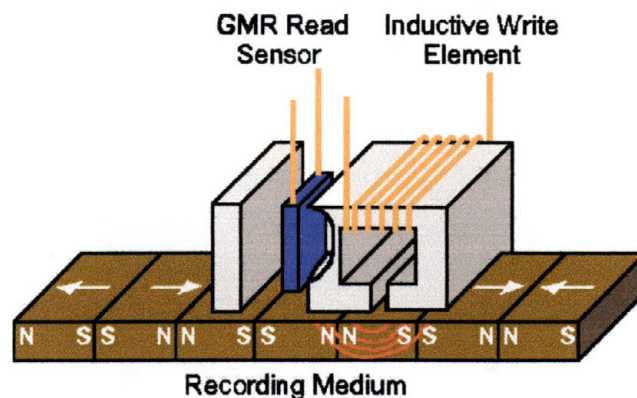


Figure 1-2: Principle of the Magnetic Recording Process used in Magnetic Hard Disk Drives²

In a typical recording device (see Figure 1-2 on previous page) an inductive write element is combined with a separate giant-magnetoresistive read sensor and is passed above a magnetic disk which stores information in terms of isolated bits. The width of the GMR sensor read head is much smaller than the write head, which guarantees that the read head can function properly even when the read/write element is not perfectly aligned with the magnetic disk tracks. Typically, for corrosion and wear-and-tear protection, both the thin film and the read/write element are coated with a thin layer of carbon film.

Current technology produces close to 20,000 read/write heads on a single five-inch wafer substrate, usually made of a ceramic material. The magnetic write operation is done inductively, where a magnetic field in the write element is strong enough to induce the magnetic material of the disk to align in one direction or the other. The heart of the modern magnetic read head, however, is the Giant Magneto-Resistance (GMR) sensor, also known as a Spin-Valve.

The GMR effect is based on the interaction of three functional layers: two magnetic films separated by a non-magnetic conducting spacer. One of the magnetic layers is known as the pinned layer and the other is known as the free layer. Due to the electron scattering behavior in such a system, a property that is dependant on the relative orientation of the magnetic field of both the free and the pinned layer in addition to the direction of the electrons spin, a GMR sensor exhibits a change in its

resistance, ΔR , to the flow of electrical current. By measuring this change in resistance the direction of the magnetic field in the free layer can be determined. One direction would represent a binary “1” while the other a binary “0”.

Random Access Memory (RAM) is another possible application where the use of the GMR effect can be useful. RAM is the type of memory that is read from and written to by the Central Processing Unit (CPU) of a microprocessor and by the supporting hardware that runs a computer. The more RAM a computer system contains, the more information it can manipulate and the more programs it can run at one time. RAM only holds information that a program is currently using, and it can only hold that information while the computer is turned on. For this reason, RAM is called volatile memory: as soon as the computer is turned off, all the information that was stored in RAM is lost.

As a data storage tool, magnetic thin-film devices (Hard Disk Drives) have been the most commonly used. For non-volatile memory applications, Magnetic RAM (MRAM) is not able to compete against traditional RAM due to many properties of the magnetic materials and device characteristics such as material substrates, process compatibility with existing technologies, lack of address decode logic increasing read time, small read-back signal from the cell decreasing sensitivity and large write current requirements increasing power consumption.²

Nonetheless, with the introduction of spin-valve and spin-tunneling materials (i.e. GMR materials), the design and the performance characteristics of non-volatile MRAM transistors has been considerably improved.

Spin-valve structures have been proposed for high-density non-volatile magnetic random access memory applications. The use of GMR materials to replace anisotropic magnetoresistive materials used in current devices shows promise to alleviate one of the most difficult problems which has faced MRAM technology- that of a small signal size.

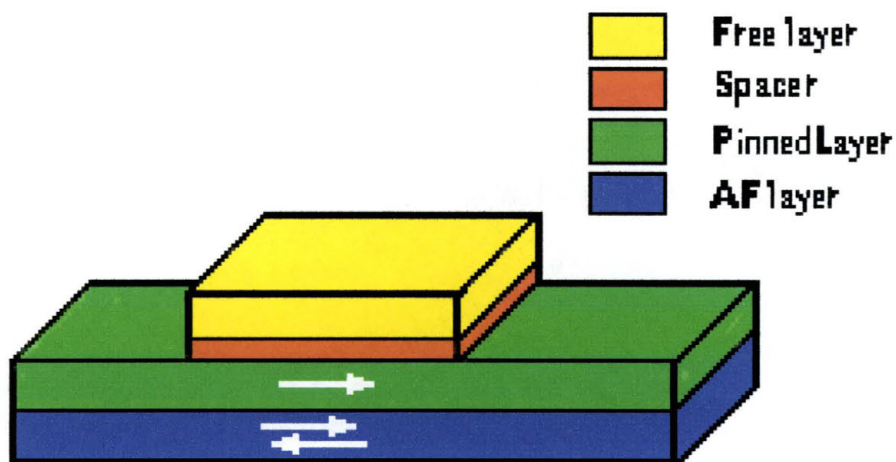


Figure 1-3: MRAM Spin-Valve

This problem leads to relatively long read access times for memory applications. A typical MRAM spin valve (see Figure 1-3 above) device consists of a sandwich structure of two magnetic thin film layers, the Free layer and the Pinned Layer, that are separated by a non-magnetic

conducting spacer layer. The magnetization of one of the layers (green) is pinned along the long dimension of the device by an anti-ferromagnetic exchange-biasing layer (blue), while the magnetization of the second layer (yellow) is free to rotate. A system of current-carrying conductors connect the device to external current sources and generate a magnetic field, H , for operating it. This field is directed along the long dimension of the device. The conductors form part of a larger circuit that implements the read and write functions of a MRAM transistor. For normal operation, magnetic fields of limited magnitude are applied so that only the magnetization of the free layer reverses completely, while that of the pinned layer remains relatively unchanged. The ideal spin valve structure requires a stable uniformly pinned magnetization of the pinned layer, a free magnetic layer that switches in a bi-stable manner, and switching thresholds that are symmetrical about a given magnitude of magnetic field.

Recall that with GMR, the resistance of a device depends on the angle between the directions of the magnetization in the two layers of the magnetic thin films. The resistance is also independent of the direction of the current flow being used to sense the direction of these magnetic fields. As a result, it is possible to sense the state of magnetization by measuring the resistance of the device with very small currents. The direction of current flow does not need to be in any particular direction with respect to the direction of magnetization.

Another benefit that would be seen from the development of MRAM using the GMR effect is that they would not have a leakage current like typical DRAM devices. Once a magnetic field has been aligned, it will not lose its direction with a loss of power to the device. This would be particularly attractive for portable electronic devices, as it would greatly extend the battery lifetimes for such applications as mobile telephones, pagers, and personal digital assistants. For these and other reasons, Giant Magneto-Resistive Spin-Valve devices are actively being investigated for use as memory elements in non-volatile solid-state magnetic random access memory applications.

This thesis also intends to investigate the viability of producing superior GMR spin-valves using Nickel-Iron and Nickel-Iron Oxide materials grown in a Dual Ion-Beam Sputtering system.

2 Semiconductors and Transistors

Semiconductors are a group of materials that have electrical conductivities somewhere between that of metals and insulators. They also possess the ability to have their conductivity modified by a number of factors such as temperature, optical excitation, and impurity content. Because of these properties, semiconductor materials have been used for the fabrication of electronic devices since the bipolar transistor was first invented by Bardeen, Brattain, and Shockley at Bell Telephone Laboratories in 1948. Of the different types of semiconductor materials available the most understood and, consequently the most employed, is Silicon (Si). The vast majority of all commercial applications for semiconductor materials are devoted to building transistors on Si wafers.

Every atom has electrons that are very tightly bound to them. Due to quantum-mechanical principles that will not be discussed in great detail for this thesis, electrons orbit the nucleus of an atom in high probability, very distinct locations. These locations are based on the number of electrons in the atom (one for every proton of the nucleus) and on which shell of the atom the electrons are located. The first shell (the lowest energy state shell) can only hold two electrons, the second can hold only eight, and the third can hold eighteen. There are other shells, but they are not relevant to this discussion. The way that electrons fill

the shells is that the lowest energy shell is always filled first, then the next lowest energy shell (the second), etc. The highest shell of an atom to possess an electron is known as the valence shell. One fundamental property of Si is that it has a total of 14 electrons orbiting the nucleus. Subtracting the 2 from the first shell and 8 from the second shell being filled leaves four electrons in the valence shell that are free to interact with the surroundings of the atom. An additional property of Si is its ability to be manipulated to alter its electrical conductivity. There is another property of Si that has served to make it ubiquitous among semiconductor materials- when exposed to oxygen the Si undergoes a chemical reaction that turns it into an excellent insulator- Silicon Dioxide (SiO_2).

2.1 Basic Transistor Physics

When isolated atoms are brought together to form a solid crystal, there are a number of interactions that occur electronically between neighboring atoms. For Si, in a perfect crystal, the electronic interaction that occurs is that the four electrons of the outer shell of the atom form covalent bonds, where each atom shares its valence electrons with its four neighbors. Due to the electrical properties of charged particles, the bonds of the Si atom in a perfect crystal will be spaced evenly apart (in three-dimensional space) in what is known as the diamond structure (see Figure 2-1 next page). When electrons form a covalent bond between two

atoms, the electrons are said to no longer belong to an individual atom, but belong instead to the bond.

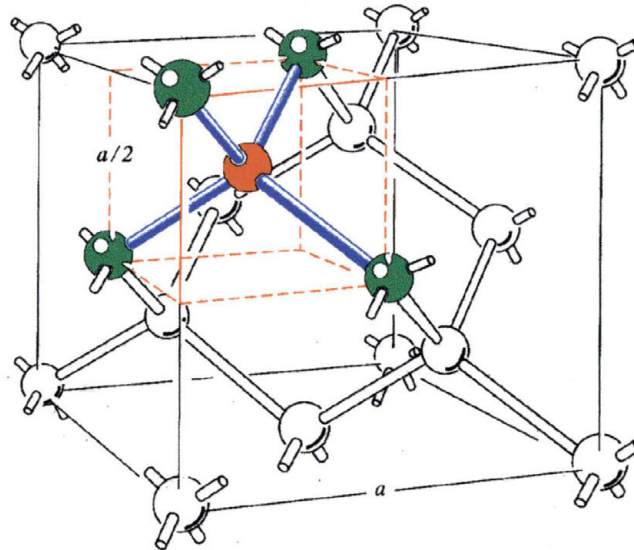


Figure 2-1: Diamond Structure Bonding of Si in a Perfect Crystal ³

Another property of atoms is that every solid has its own characteristic energy band diagram. Energy bands describe the wide range of electrical characteristics observed in various materials. The mathematics involved in calculating energy band diagrams is beyond the scope of this thesis and will not be discussed here as it touches on quantum mechanical principles and the use of a mathematical construct known as the reciprocal lattice. However, based on the calculations used in the creation of an energy band diagram, the amount of energy needed to excite an electron from a state where it will remain with its parent atom to a state where it will escape its parent atom and travel through

the crystal lattice of a material can be calculated. In semiconductor materials, when an electron has an energy level that makes it prefer to remain with its parent atom, it is said to be in the valence band. When an electron has enough energy to escape its parent atom and travel throughout the crystal lattice, it is said to be in the conduction band. One method of giving electrons additional energy is to heat them up. As the temperature of a semiconductor increases, some electrons from the valence band will receive enough thermal energy to be excited to the conduction band. This will leave a vacancy in the number of electrons that the parent atom should have, which is commonly called a hole. A hole can be thought of conceptually as a small positive charge, although this is not completely accurate. Holes are also said to “travel” in the valence band. If the conduction band electron and the hole are created by the excitation of a valence band electron to the conduction band, they are called an electron-hole pair (EHP) (see Figure 2-2).

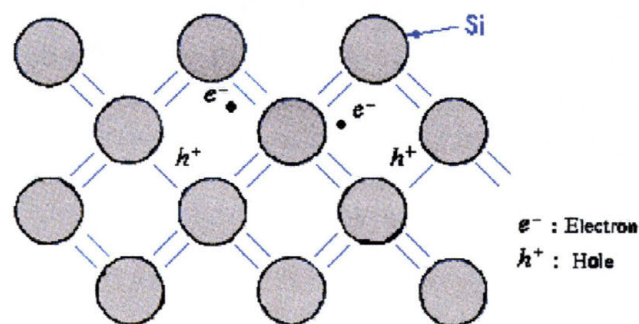


Figure 2-2: EHP Formation in a Perfect Si Crystal ¹

What occurs is that one of the four atomic bonds of a Si atom is broken and the electron becomes free to travel through the crystal lattice until it is absorbed by another atom. When a perfect semiconductor crystal (with no impurities or lattice defects) is at a given temperature (above 0° K) there will be EHPs present, typically on the order of 10^{10} per square centimeter. These are known as intrinsic charge carriers.

In addition to the intrinsic carriers, it is possible to create carriers in semiconductors by purposely adding impurities into the crystal. This process is known as doping and is the most common technique used to manipulate the electrical characteristics, the band diagram, of a semiconductor. By doping a semiconductor with the proper atoms, the crystal can be altered so that it contains an excess of either electrons or holes (see Figure 2-3).

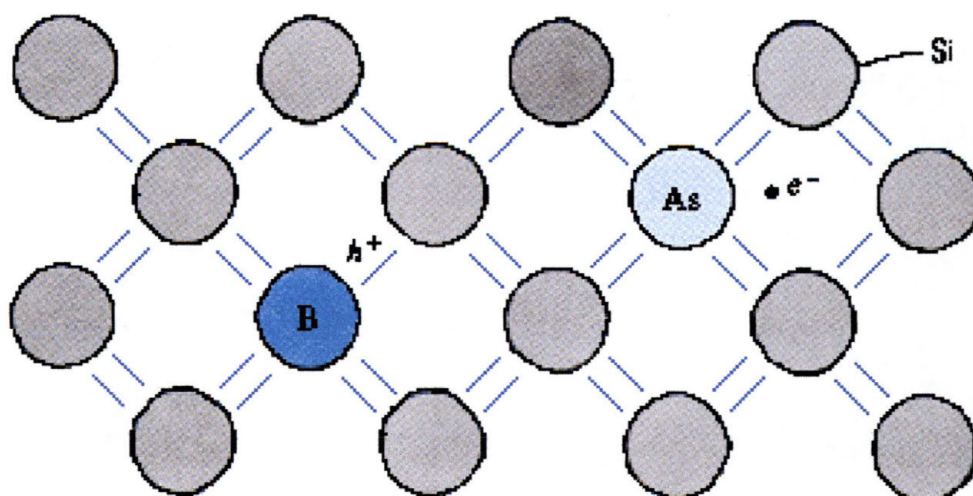


Figure 2-3: EHP Formation with Dopant Atoms Present¹

There are thus two types of doped semiconductors, n-type (which have an excess of electrons or negative charge) and p-type (which have an excess of holes or positive charge). Atoms that have five electrons in their valence shell (Group V on the Periodic Table of the Elements) will provide an excess of electrons when they bond with the four Si atoms of the crystal. The most commonly used element for n-type doping is Arsenic (As). Atoms that only have three valence electrons (Group III on the Periodic Table of the Elements) will be missing an electron compared to Si. This will cause one of the surrounding Si atoms to not have an electron to form a bond with creating an excess of holes in the crystal. This is because the Si atom would like to form a bond and will “grab” any passing electron, causing it to ‘fall into a hole’ and no longer be free to travel in the crystal lattice. The most commonly used element for p-type doping is Boron (B). When there are excess electrons in the crystal (n-type material), there will still be some holes formed from the intrinsic EHPs. These holes are known as minority charge carriers, while the electrons are known as the majority charge carriers. The same is true for excess holes in the crystal (p-type material), where the holes are the majority charge carriers and the electrons are the minority charge carriers.

When a region of the bulk material, or substrate, that is predominantly n-type comes in contact with a region of the substrate that is predominantly p-type, the electrical interactions form what is

known as a depletion region (see Figure 2-4). The excess holes of the p-type region are attracted to the excess electrons of the n-type region and the two combine, forming a region between the two types of doped semiconductors that is essentially electrically neutral. The depletion region also acts as an insulator in that charge does not very easily cross from one side of the depletion region to the other, although there is a small number of minority charge carriers crossing from one region to the other.

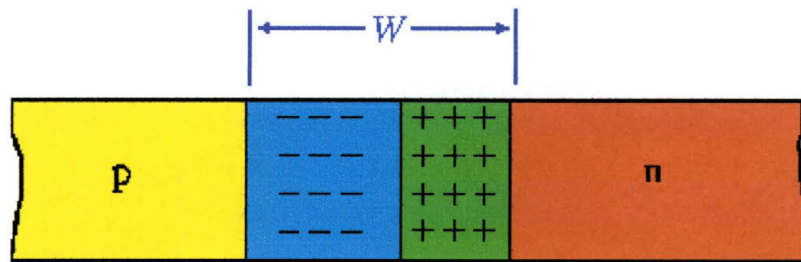


Figure 2-4: Depletion Region¹

The size of the depletion region depends on the number of dopants in the substrate and on any electrical potential that may be applied to the n-type and p-type regions. The depletion region forms as holes from the p-type region attempt to combine with electrons from the n-type region. As this electrically neutral region grows, it sees a net positive electrical potential on one side and a net negative electrical potential on

the other side. This causes the formation of an electric field in the depletion region that tends to counter the effects of the net positive and net negative regions of the substrate. Indeed, it is the electric field that in the end limits the size of the depletion region when the force of the electric field on the charge carriers in one direction balances the force of electrostatic attraction between the positive and the negative charges in the other direction. By changing the amount of doping in either the p-type or the n-type region, the depletion region width will be shifted to one side or the other of the center of the interface. This is due to the electrostatic repulsion/attraction caused by having a net increased amount of charge in one region as compared to the other.

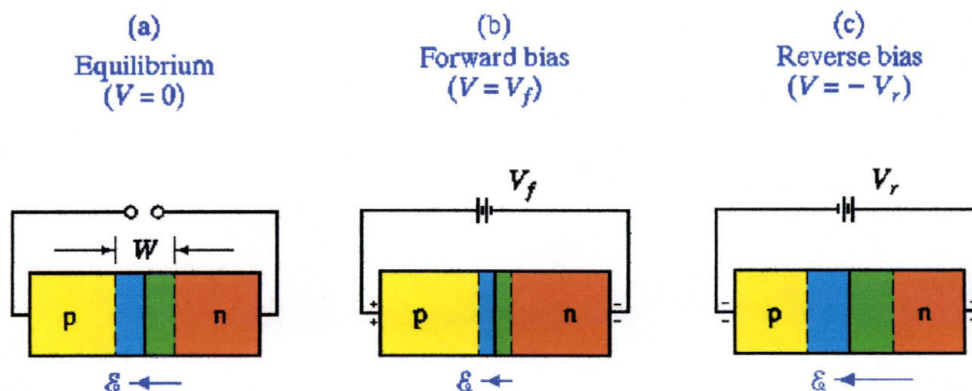


Figure 2-5: Effects of Biasing on Depletion Region¹

The size of the depletion region can also be modified by applying a voltage to one or both of the doped substrate regions. This is known as biasing. In forward biasing, a positive voltage is applied to the p-type

region (or a negative voltage is applied to the n-type region) and the electrostatic force of attraction tends to make the charge carriers move towards the electrodes on the opposite side of the depletion region (i.e. electrons to the p-type electrode, holes to the n-type electrode). This causes the size of the depletion region to shrink (see Figure 2-5(b) on previous page). In reverse biasing, a negative voltage is applied to the n-type region (or a positive voltage is applied to the p-type region) and the electrostatic force of attraction pulls the electrons towards the electrode on the same side of the depletion region (i.e., electrons to the n-type electrode, holes to the p-type electrode). The size of the depletion region would then increase (see Figure 2-5(c) on the previous page).

If the junction is forward biased with a large enough voltage, the depletion region can completely disappear and charge carriers can travel from one electrode to the other with little or no resistance. If the junction is reverse biased with too large a voltage, a condition known as reverse breakdown occurs. When this occurs, the number of minority charge carriers increases sharply, and large currents can flow with little or no increase in the applied bias voltage. An interesting characteristic of reverse breakdown is that once the bias voltage is lowered below the breakdown voltage, the junction is restored to its original condition and the depletion region has only a small minority current.

This discussion describes, in a very basic manner, the operation of one of the simplest of electronic devices, the diode. A diode allows

current to flow in one direction (forward bias) and prevents it from flowing in the other direction (reverse bias).

2.2 MOS Transistor Operation

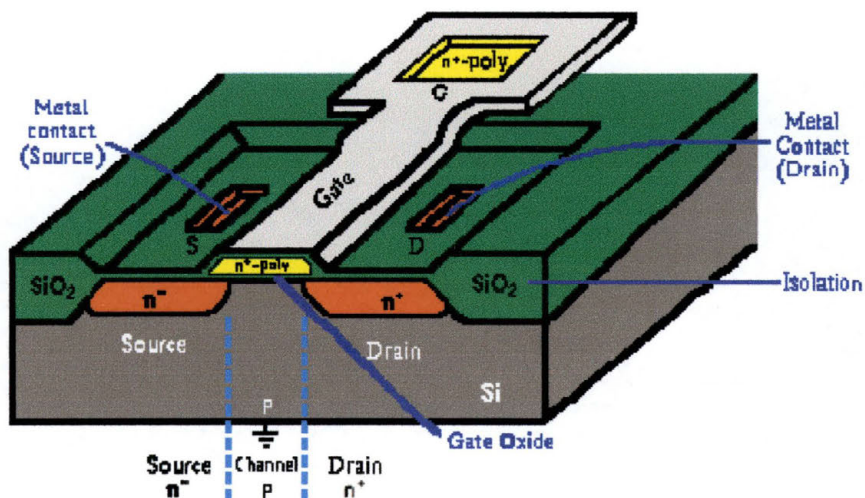


Figure 2-6: Typical Enhancement Mode N-Type MOSFET⁴

Arguably, the most important electronic device is the transistor. Figure 2-6 shows the construction of a typical n-type Metal-Oxide-Semiconductor Field Effect Transistor (MOSFET). Ignoring the details of how and why, the operation of a FET is relatively simple to explain. For an enhancement-mode n-channel transistor formed on a p-type Si substrate, the n^+ source and drain regions are implanted into a relatively lightly doped p-type substrate. A thin oxide layer (a dielectric insulator) separates the conducting gate, which is typically made from polycrystalline Si, from the Si surface (the substrate). No current will flow from the source to the drain unless an n-type channel can be

formed between them. When a positive voltage is applied to the gate relative to the substrate, one way of thinking about what occurs is to think of positive charges being deposited into the gate. Since like charges repel and opposite charges attract, the positive charges in the area just below the gate oxide will be repelled from the gate structure and the negative charges will be attracted there. This serves to convert a region below the gate that is normally a p-type material into a region that is an n-type material. This is caused by the formation of an inversion region where there will be a thin surface region containing mobile electrons. These induced electrons form the channel that is needed to allow charge carriers to travel from the drain to the source. The threshold voltage (V_t) is the minimum amount of voltage needed to form this inversion layer. Similarly, for a p-channel transistor (made on an n-type substrate with p-type source and drain implants), the voltage applied to make the device work will be a negative voltage and the charge carriers will not be electrons but holes.

The MOS transistor is particularly useful in digital circuits, where it is switched from the off-state (with no channel) to the on-state (with a channel present). The drain current (the amount of charge carrier conductivity) is controlled by the application of a voltage to the gate electrode, which is separated electrically from the channel region by the gate insulator, or dielectric. The most commonly used gate dielectric is Silicon Dioxide (SiO_2). While both types of MOS transistors are

commonly used today, the n-type MOS transistor is more preferred than the p-type MOS transistor. This is mainly due to the fact that electrons travel faster in the Si substrate than “holes”, giving the n-MOS transistor faster operational speeds.

One electrical characteristic of a MOS transistor is that it is, in some ways, nothing more than a fancy capacitor. A capacitor, comprised of two metal electrodes separated by a dielectric, is a device used to store energy. In a MOS transistor, one electrode is the gate and the other is the Si substrate. The dielectric is the gate oxide, SiO_2 . When charging a capacitor, if a negative voltage is applied to one electrode, it effectively deposits negative charge onto that electrode. This causes an equal but opposite charge to accumulate on the other electrode. When a positive charge is applied from the metal (the gate electrode) of an n-type MOSFET to the p-type substrate (the channel), the positive voltage deposits positive charge on the metal and induces a corresponding negative charge at the surface of the semiconductor. This is similar to the formation of a depletion region in a diode. In the depleted region, the number of holes is decreased while the number of electrons is increased giving the region near the semiconductor surface conduction properties seen in an n-type material, with an electron concentration formed not by doping, but by a process known as inversion. This inversion layer, separated from the p-type Si in an n-MOS transistor by a depletion region, is a major key to MOS transistor operation. A transistor is said to

be in strong inversion whenever the channel becomes as strongly n-type as the substrate is p-type.

2.3 Capacitance in MOS Transistors

An ideal gate insulator does not allow any charge to travel through it. This is not what happens in the real world, though, due to the quantum mechanical effect of tunneling. Classically, the gate dielectric acts as a barrier to the conduction of charge carriers from the gate to the channel. Quantum mechanically, however, there is always a probability, no matter how small, that an electron can tunnel through the gate dielectric. This probability is raised as the thickness of the dielectric is lowered.

One form of tunneling is called direct tunneling. As the gate dielectrics are made thinner, which occurs whenever transistors are made smaller due to scaling factors, the tunneling barrier becomes so small that the electrons can tunnel directly from the gate to the channel. This serves to increase the current flowing in the transistor causing degradation in the transistors electrical characteristics. If the charge transport through the gate dielectric continues for too long it can ultimately lead to the catastrophic failure of the dielectric, which, in turn, leads to the failure of the transistor.

2.4 CMOS Transistors

For many applications of electronic devices, the type of transistor used is a Complimentary MOS (CMOS) transistor (see Figure 2-7). In a CMOS transistor, the drains (V_{out}) of two opposite types of MOS transistors are connected together to form a shared output connection, while the input terminal (V_{in}) is a common connection to the two transistor gates. To turn them on, the p-channel device requires a negative V_t and the n-channel device requires a positive V_t .

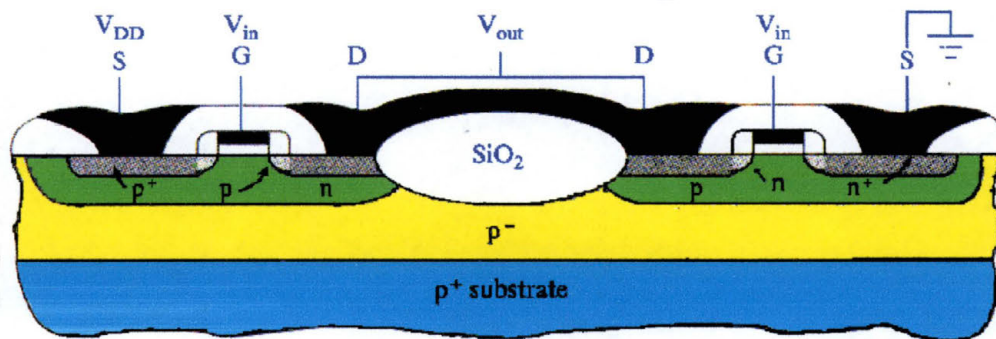


Figure 2-7: CMOS Transistor⁵

When there is no voltage applied to the gate ($V_{in} = 0$) there is no voltage for the n-channel device and the device is off. At the same time, the voltage between the gate and the source of the p-type device has a relative negative value ($V_{in} < V_{DD}$) and the device is on. When a positive voltage is applied to the gate, the n-type device turns on and the p-type device turns off. This behavior allows the CMOS transistor to be used as an inverter. When the device has a binary “1” at the input the output

state will be a “0”. When the device has a binary “0” at the input the output state will be a “1”.

One very advantageous property of a CMOS transistor is that one of the devices will be turned off no matter what the input state of the gate is. Since the two transistors are connected electrically in series, there will be no current flowing except the small amount needed to change the transistor from one state to the other. This results in the CMOS transistor using very little power to operate. As can be imagined, for portable electronic devices extending the lifetime of a battery power supply is an important feature and makes the use of CMOS transistors an ideal choice. In addition to portable devices, CMOS transistors are the transistors of choice for ultra-large scale integrated circuits where there are billions of transistors on a single microprocessor chip.

2.5 Limits to SiO₂ Dielectrics

The success of Si CMOS technologies has been achieved during the recent past due to the remarkable properties of SiO₂ as an insulator for the gate region of a CMOS transistor. Its excellent performance in terms of interface quality, dielectric isolation, stability and reliability has led to the tremendous development of MOS-based integrated circuits. This development relies on the continuous miniaturization of MOS devices in following Moore’s Law, which states that the number of transistors in computer chips doubles every 18 months. For this to occur in a

financially advantageous manner for the semiconductor manufacturing industry, the size of the transistors must shrink while the price of building them must remain relatively constant.

In the process of shrinking a transistor, the characteristic dimensions of the transistors are downsized in a regular manner for every technology generation, yielding increased integration density, circuit complexity and operation speed. The gate oxide insulator is therefore thinned down in order to increase the coupling capacitance between the gate electrode and the device channel, and, in turn, the current drive capability of the transistor.

The thinning of the oxide is also very helpful in controlling the short-channel effects that take place in submicron MOS transistors, such as threshold voltage roll-off or drain-induced barrier lowering. Recall that the threshold voltage is the minimum gate voltage required to induce the channel. Threshold voltage roll-off occurs when the electric field lines from the source and the drain depletion regions of the transistor overlap each other underneath the gate on very short-channel transistors. This causes difficulty in controlling the threshold voltage for a device. Drain-Induced Barrier Lowering (DIBL) is caused when the source and drain junctions are too deep with respect to the transistor size or when the channel doping is too low. DIBL leads to punchthrough leakage of the transistor when the depletion region of the source expands and merges with the depletion region of the drain. When this occurs, the

ability to turn the transistor off and on is removed and you lose complete control of the gate.

The ultimate step of oxide depletion is dielectric breakdown. This breakdown corresponds to the sudden, irreversible loss of the insulating properties of the SiO₂ layer. Classically, two main processes are in competition to explain the oxide breakdown phenomenon.⁴ The first one is based on the anode hole injection and states that the breakdown is triggered as soon as a critical hole fluency is reached or when a critical defect density is attained.⁵ What occurs is that charge traps are generated during the electrical stress across the oxide layer, and as the stress continues, several neighboring traps form defect clusters. Breakdown of the dielectric occurs as soon as a cluster reaches the source to drain regions, forming a path between the electrodes of the transistor. The second process is based on a thermo-chemical approach.⁶ Stress induces dipolar coupling of defects with the local electric field. When this occurs, breakdown is regarded as the result of thermal Si-Si bond breakage with the oxygen vacancy as a possible precursor.

When scaling down the oxide thickness below 10 nanometers (nm), new degradation phenomena arise.⁷ This is manifested in three ways. First, the ability of the bulk oxide to trap charges thus preventing them from quantum mechanically tunneling from the gate to the channel vanishes. The trapping efficiency decreases because with the oxide

thickness scaling down, the distance beyond the tunneling distance that electrons have to cross is smaller allowing for less charge trapping. Second, Stress-Induced Leakage Currents (SILC) appear for oxides below 10 nm in thickness. This event was first seen in 1982.⁸ A change in the low electric field range is superimposed onto the initial MOS gate current characteristics. The associated current is attributed to a trap-assisted tunneling conduction through the uniformly distributed stress-induced interface with bulk oxide traps acting as “stepping stones” for electrons to tunnel from the cathode to the anode. Third, for ultra-thin oxides below five nm, a different failure mode, occurring at the same time as the classical dielectric (Hard) breakdown, appears.⁹ This is called a soft-breakdown. This mode corresponds to a sudden, irreversible, noisy and localized gate leakage current. Unlike the relatively large currents seen in hard breakdown, soft breakdown leakage current is rather small.

While the application of ultrathin gate oxides has resulted in enhanced MOSFET performance, direct gate tunneling currents and oxide reliability remain the biggest challenges to their continued use as devices are scaled to even smaller sizes. The defects in the oxide will significantly enhance the gate leakage current which, in turn, increases the standby power requirements, degrades device performance, and eventually will cause the device to fail. Of the failure modes present in the gate oxides, direct tunneling current is the most sensitive quantity to the oxide thickness. It has been shown that direct tunneling currents

between the source/drain extension region and the gate dominate the off-state drain currents and strongly contribute to off-state power consumption.¹⁰

Another mode of failure in using ultra-thin oxides is poly-gate depletion effects (PDE). PDE, caused by insufficient active dopant concentration near the poly-gate/SiO₂ interface, becomes too large a problem to ignore as devices continue to get smaller. A lower effective surface electric field, due to an additional voltage drop across the depletion layer, causes a significant reduction in the drive current, difficulties in determining accurate oxide thickness, and overestimation of the dielectric lifetime. Since the depletion width from the poly-gate/SiO₂ interface increases if the oxide electric field increases, the PDE gets worse for ultra-thin oxide layers because the applied gate voltage does not usually get scaled with the device physical features. With a gate oxide thickness of 3.5 nm, and a typical gate doping of $1 \times 10^{20} \text{ cm}^{-3}$, there is a 20% degradation of the gate capacitance. When the oxide thickness is reduced to 1.5 nm, there is a 35% degradation in the oxide capacitance.¹¹

2.6 DRAM Transistors

Dynamic Random Access Memory (DRAM) transistors are fabricated using MOS technology and are noted for their high capacity, low power requirements as well as their moderate operating speed. Unlike Static RAM (SRAM) that stores information in a digital circuit called a Flip-Flop, DRAM stores 1's and 0's as charges on a small MOS capacitor. The charge of this capacitor tends to leak off with the characteristic of its time constant, τ , where $\tau = R_s \cdot C_s$, where R_s is the leakage resistance and C_s is the DRAM capacitance (typically $C_s \approx 10$ pico-Farads and $R_s \approx 10^9 \Omega$). Using these typical values, the information stored in the DRAM would be lost in approximately 10 microseconds.

Because of the tendency for charge to leak off after such a short period of time, DRAMs require constant recharging of their memory cells. This process is called refreshing the DRAM. The need for refreshing is a drawback for DRAM as compared to SRAM because it often requires external support circuitry that makes the chip architecture more complex.

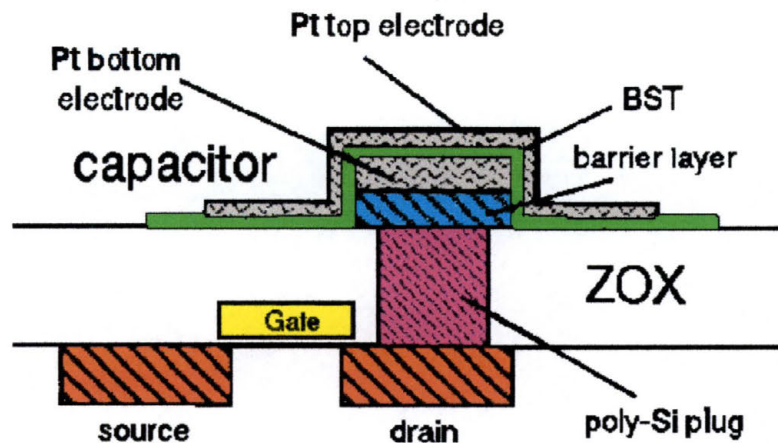


Figure 2-8: Schematic Diagram of Typical DRAM^s

A typical DRAM transistor is built as shown in Figure 2-8. The information is stored as charge on a MOS capacitor. When a voltage is applied to turn on the MOS transistor of the circuit (the pass transistor), charge is allowed to flow to the drain, through the polycrystalline Si plug, and onto the bottom plate of the capacitor sitting above the transistor. The gate of the capacitor (the capacitor top plate) is permanently connected to the power supply voltage for the MOS transistor (V_{DD}) creating a potential well beneath it that tends to be full of inversion electrons for a p-type substrate. When there is no voltage applied to the gate of the pass transistor, the transistor is off and the inversion charge under the storage capacitor stays the same; this is the stable state of the capacitor. When a positive voltage is applied to the gate of the pass transistor, the bottom capacitor plate “sees” the positive voltage of V_{DD} .

This causes the electrons stored on the bottom plate of the capacitor to leave the bottom plate and travel through the pass transistor. When the pass transistor is cut off, there is an empty potential well on the bottom plate of the capacitor. There is still a positive potential applied to the top electrode of the capacitor, and over time, the potential well will be filled with minority charge carriers created thermally. This is the process by which DRAM loses its information, and it occurs in a matter of picoseconds (1×10^{-12} sec.).

As DRAM devices are scaled-down, in order for them to operate properly, the capacitance of the cell must remain at a value of approximately fifty pico-Farads. The challenge thus becomes to store more charge per unit area of the surface of the Si substrate. Treating the MOS capacitance (C) as a fixed, voltage independent capacitor, the amount of charge (Q) stored on the capacitor can be calculated using the following equation:

$$Q = C \cdot V = \left(\frac{\epsilon \cdot A_c}{d} \right) \cdot V$$

Equation 2-1: Charge Stored in a Capacitor

where ϵ is the permittivity of the dielectric, d is the thickness of the dielectric, V is the voltage, and A_c is the area of the capacitor. Traditionally, the method of achieving the desired capacitance has been to scale down the dielectric thickness, d . This leads to the same problems concerning ultra-thin oxide layers discussed earlier. One

alternative solution to the problem of shrinking oxide thickness is to use a different material for the dielectric. Ferroelectric materials, crystalline substances having spontaneous electric polarization reversible by an electric field, have much higher dielectric constants and offer larger capacitance without increasing the area of the capacitor or reducing the dielectric thickness.

2.7 Alternate Dielectrics

One way to extend CMOS technology is by replacement of the current gate dielectric (SiO_2) with alternative insulators having a dielectric constant, K , higher than SiO_2 thus enabling reliance on increased physical thickness to reduce tunneling effects while at the same time reducing the equivalent oxide thickness. These high- K materials, as they are known, can provide the same equivalent electrical thickness using a physically thicker layer than would be used with SiO_2 which will then be, hopefully, more controllable and easier to manufacture. These films fall into three main categories. The first group is nitride-related materials including oxynitride grown on nitrogen-implanted substrates. The second group employs stack gate structures such as nitride/oxide, metal oxide/oxide, and metal oxide/nitride. The third group belongs to the metal oxides, such as Tantalum Oxide (Ta_2O_5), Titanium Oxide (TiO_2), Barium Strontium Titanate (BaSrTiO_3 , also known as BST), and Barium Zirconium Titanate ($\text{Ba}(\text{Ti}_{1-x}, \text{Zr}_x)\text{O}_3$, also known as

BZT). The third group of oxides are materials that have a perovskite crystal structure and are also known as ferroelectrics.

Oxynitrides and oxide/nitride stacks are a promising alternative for SiO_2 because of their compatibility with CMOS process flow and equipment already available in microelectronics process lines. The advantages also include an excellent thermal stability, a barrier for impurity/dopant diffusion and a good interface with the underlying Si. Recent results show that oxide/nitride stacks with 1.6 nm Effective Oxide Thickness (EOT) exhibit more than 100 times lower tunneling current than 1.6 nm of pure SiO_2 .³ However, at a thickness of around 1.5 nm a large amount of gate leakage is present limiting the lifetime of oxide/nitride dielectrics to two or three generations of devices. Ferroelectric materials offer a good alternative solution.

The principle perovskite structure found in ferroelectric materials is a simple cubic structure containing three different ions of the form ABO_3 (see Figure 2-9 on next page). The A and B atoms represent +2 and +4 ions (in this case $A = \text{Ba}$, $B = \text{Ti/Zr}$), respectively, while the O atom is the -2 Oxygen ion. This ABO_3 structure in a general sense can be thought of as a face-centered cubic (FCC) lattice with the A atoms at the corners and the O atoms on the faces. The B atom completes the picture and is located at the center of the lattice. The A atom is the largest of the atoms and consequently increases the overall size of the AO_3 (fcc) structure. As a result, there are minimum energy positions off-centered

from the original octahedron that can be occupied by the B atom. Shifting of this atom due to applied electric fields causes the structure to be altered, creating electric dipoles.

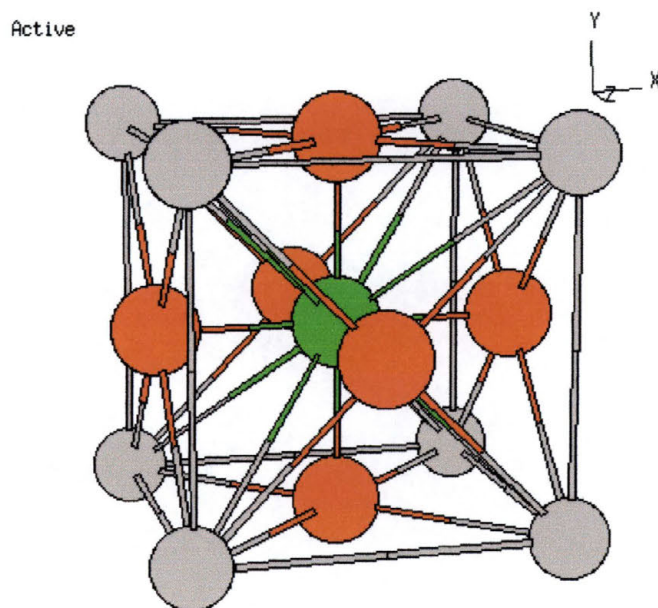


Figure 2-9: Perovskite Crystal Structure³

Ferroelectric perovskite films have been receiving much attention since the late eighties. Initially, they were looked at for ferroelectric non-volatile memories. This led to their development as ferroelectric films, in the paraelectric phase, for use as high permittivity dielectrics for DRAMS. There has also been a great deal of interest lately in the use of high permittivity oxides as a replacement for SiO_2 as the gate dielectric in CMOS transistors.

2.8 Ferroelectric Dielectrics

Typical materials that have been studied in the effort to create a material with a higher dielectric constant are Strontium Titanate (SrTiO_3) and Barium/Strontium Titanate $[(\text{Ba}/\text{Sr})\text{TiO}_3]$. With these materials, an equivalent SiO_2 thickness of less than 10\AA has been reported.¹² These films may extend the integration of DRAM transistors a few more generations but will not be able to overcome many of the restrictions of further scaling. Ferroelectric memories are expected to meet many of the needs of ULSI technology including low power non-volatile operation for portable and general use, and low voltage non-volatile memory for embedded memory of microcontrollers.

The first experimental verification of a ferroelectric memory was reported by J.L. Moll and Y. Tarui in 1963 based on work they did at Stanford University.¹³ Their experimental device demonstrated nonvolatile memory action, but it was also determined that a better interface between the semiconductor and the ferroelectric material was needed. Since then, there have been many experiments with different combinations of materials using a thin-film structure: Tellurium on Barium-Titanate (BaTiO_3), Tellurium on Trigricine Sulfate (TSG), Cadmium Selenium (CdSe) on BaTiO_3 , and Tin Oxide (SnO_2) on Lead Zirconate-Titanate (PbZrO_3) ceramic.¹¹

To make a good ferroelectric gate type transistor it is important that the interface between the Si and the ferroelectric material do three

things: prevent carrier injection at the interface, prevent intermixing of materials at the interface, and have few or no interface states and traps at the interface. This will probably mean that good hetero-epitaxy must exist between the Si and the ferroelectric.

Barium Strontium Titanate ($(\text{Ba,Sr})\text{TiO}_3$ (BST) thin film has been widely investigated as a possible alternative dielectric for use in ULSI DRAM storage capacitors due to its high dielectric constant ($\epsilon > 200$), low leakage current, low temperature coefficient of electrical properties, small dielectric loss, lack of fatigue or aging problems, high compatibility with current device processing, linear relationship between electric field and polarization, and low Curie temperature.¹⁴ The success of BST as a replacement dielectric for SiO_2 depends greatly on understanding its material properties in more detail. Literature on the subject details experiments that indicate the electrical and dielectric properties of BST rely heavily on the deposition process, post-annealing process, composition, base electrodes, microstructure, film thickness, surface roughness, oxygen content and film homogeneity. The key issues regarding BST as a dielectric are barrier height between metal electrodes and the dielectric, the strong thickness dependence on the dielectric constant, the temperature at which BST shifts from an amorphous film to a crystal, and the barrier layers between the storage electrode and poly-Si plug and its resistance to oxidation during crystallization temperature and electrode formation.

For use in storage capacitors, a dielectric film must have a very small leakage current in order to maintain adequate charge retention. Although as-deposited sputtered films of BST have low leakage currents due to their amorphous structure, the high temperature treatments necessary for standard DRAM processes lead to the crystallization of the film. This leads to drastic increases in the leakage current of the transistor.

The dielectric constant of BST is also known to be dependant on the thickness of the film.¹⁵ As the film thickness decreases, the dielectric constant decreases. This can be explained by the lower dielectric constant resulting in a depletion region being formed between the metal gate and the dielectric film. It has also been reported that the dielectric constant of BST films is influenced by oxygen vacancies. Oxygen vacancies seem to be the origin for trap defects that are of an elementary nature affecting the conducting properties of BST films.¹⁶

Although BST films have a very low leakage current when low electric fields are applied across them, the leakage current increases by orders of magnitude as the voltage applied to the dielectric exceeds a critical field of several hundreds of kV/cm. The films also exhibit complete breakdown if the field is in the neighborhood of 2 MV/cm.¹⁷ This will put a limit on the minimum thickness of BST films still maintaining the required electrical characteristics for DRAM

applications, making the search for an alternative dielectric a worthwhile endeavor.

2.9 Barium-Zirconium-Titanate Dielectrics

It is known that there are several isovalent substituents in BaTiO_3 besides Sr that are also able to shift the Curie temperature below room temperature.¹⁸ Zirconium (Zr) is one of the more interesting because a different character of dielectric response with respect to the paraelectric-to-ferroelectric phase transition can be achieved by the substitution of Zr from that of Sr in BaTiO_3 , due to the disparate distortions of oxygen octahedral in the perovskite lattice.¹⁹ In addition, the Zr^{+4} ion is more chemically stable than the Ti^{+4} ion and has a larger ionic size to expand the perovskite lattice. This serves to limit the amount of electron hopping from the Ti^{+4} atoms to the Ti^{+3} atoms of the crystal.

In a study of the Zr content in $\text{Ba}(\text{Ti}_{1-x}\text{Zr}_x)\text{TiO}_3$ (BZT) films it was discovered that the orthorhombic-tetragonal phase transition increases and the tetragonal-cubic phase transition decreases with increased Zr content.²⁰ It was discovered that this leads to a broadening of the Curie temperature curve. When a material is ferroelectric it means that, when placed within a magnetic field, the electron spins of the materials atoms tend to align with the applied magnetic field, allowing the material to develop a magnetic field of its own. When these materials are heated, their electrons are excited such that, above a certain temperature, their

electron spins can no longer align; they are no longer ferromagnetic. This temperature is called the Curie temperature. A broadening of the Curie Temperature range would thus inhibit the development of a stable magnetic field in the dielectric.

Aging properties, a decrease in permittivity in the absence of electrical or mechanical stress of BZT, was also reported on. Generally, aging is assumed to be caused by the decreasing mobility of the domain walls of a material, which leads to a decrease in the permittivity and loss factor of the material with time. It was shown that for ceramics with a Zr content of around 2% (by weight) there was exhibited a decrease in aging when compared to BaTiO₃.²¹

For DRAM applications, spontaneous polarization, a property of ferroelectric materials, is not necessary. The important factor is whether or not a film has a high dielectric constant and good insulating properties. Methods of producing thin films include: Direct Current or Radio-frequency Sputtering, Chemical Vapor Deposition, Metal-Organic Deposition, and Sol-Gel Processing. Of these methods, DC or RF-sputtering deposition has the advantage of depositing films at low temperatures, relative to the other methods. Ion beam sputtering of BaTiO₃ films has been shown to be an effective method of depositing the Barium-Titanate films onto substrates as well. It has been reported that ion beam sputtered films showed smaller leakage current and a more

narrow distribution of breakdown voltage when compared to RF-sputtering.²²

Ion bombardment during thin film growth has been widely used to change the properties of a film being grown. Properties such as morphology, orientation, stress, and magnetic anisotropy can be affected, as well as the optical properties of the films being produced. It has been shown that when thin films of BaTiO₃ were deposited on unheated Pt-coated Si wafers, the as-grown films were essentially amorphous.²³ An amorphous film is one in which there is no large ordered arrangement of atoms in the crystal lattice. Instead, the film is made up of many small crystals with lattice dimensions in many random directions. An experiment was performed in which Barium-Titanate films were grown with and without direct ion bombardment by a low-energy oxygen ion beam from a Kaufman ion source.

The films with and without bombardment showed random orientation, but the bombarded films showed a more densely packed microstructure rather than grain growth. This resulted in the ion-bombarded films showing a dielectric constant roughly 10% higher than the non-bombarded films. The bombarded BaTiO₃ films showed improved physical properties: more dense structure, higher dielectric constant, lower dissipation factor, lower dc resistivity degradation rate, and lower leakage current.

For this thesis, it is the investigation of BaTiO₃ with Zr incorporation in addition to the ion bombardment of the films as they are deposited on the substrate that is one of the central goals of my investigations.

3 Magnetic Devices

In the late 1980's, two European scientists working independently: Peter Gruenberg of the KFA research institute in Julich, Germany, and Albert Fert of the University of Paris-Sud, discovered a property known as Giant Magneto-Resistance (GMR).²⁴ The GMR effect is the phenomenon that the resistance of a material depends on the angle between the directions of magnetization at different locations in a material. It is the application of this effect that is important for this thesis.

3.1 Basic Magnetism

When electric current flows in a conducting material, a magnetic field, H , will be produced in the space surrounding the conductor. A magnetic field, while invisible to the human eye, none-the-less has many properties which are easier to imagine if one thinks about water flowing in a river, or air flowing over the wings of an airplane. If the magnetic field is created by a very long, straight conductor (i.e. a wire), then some very definite properties of the magnetic field are known. Using what is known as the right-hand rule, if the thumb is placed along the wire in the direction of current flow then the direction of the magnetic field will be in the same direction as the way that the fingers are curled. In

Figure 3-1, current is traveling up the wire in the direction of the thumb. It can be seen that the magnetic field is orthogonal to both the direction of current in the conductor and to a straight line from the conductor to a position in space where the magnetic field is being measured (known as the radius vector). Note also that the direction of the magnetic field changes such that it is always perpendicular to the direction of the current and the radius vector.

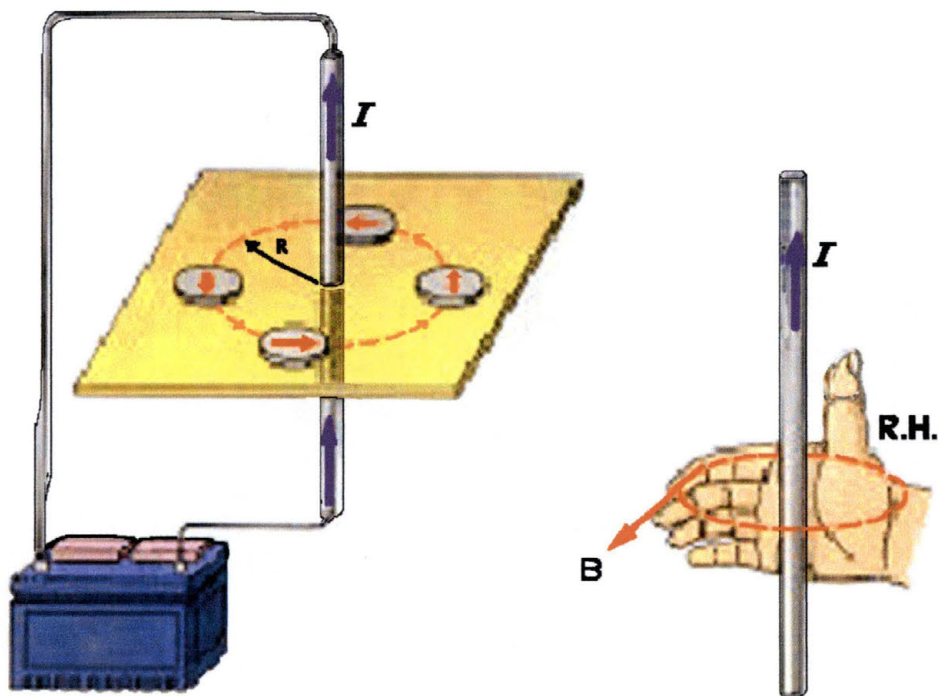


Figure 3-1: Direction of Magnetic Field in a Conductor²⁵

Magnetization is a property of materials that is caused by the motions of electrons within atoms. In all atoms, electrons orbit the nucleus in certain specific locations based on the principals of quantum mechanics. These electrons have two separate motions. While not an accurate picture of how electrons travel, and ignoring most of the real quantum mechanical descriptions of how electrons really travel, the two motions of electrons can be thought of semi-classically as follows (this is essentially the Bohr model of the atom). The first is that electrons orbit the nucleus much like the Earth orbits the Sun. The second is that the electron spins on its own axis, again like the Earth rotates every day (Again, let me stress that this is not really how electrons travel, but in order to accurately describe the probability functions that do describe electron travel I would have to spend much effort describing quantum mechanics and the Schrödinger and Dirac functions. This is well beyond the scope of this thesis and the reader is encourage to read any number of excellent resources available in any college bookstore.). An electric current is defined as the movement of charge carriers through a given point in space per unit time. Since electrons are small negative charge carriers, all motions of an electron produce an electric current. The orbital motion of electrons create what is known as an orbital magnetic moment, while the spinning of the electrons causes what is known as a spin magnetic moment. As a tributary adding water to a river makes the current of the river get stronger, when magnetic fields are added in the

same direction they too become stronger. If two equal magnetic fields are in opposite directions, they will cancel each other out. In most bulk materials the usually random spin magnetic moments of the atoms that make up the material tend to cancel each other so that the overall magnetic moment of the material tends to be relatively small. At the same time, while the magnetic moment of an individual atom may be relatively weak, when most of the atoms in a material are aligned in the same direction, the overall magnetic moment of the material can be quite large.

The magnetic moment of an individual spinning electron is called the Bohr magneton, μ_B and can be calculated by:

$$\mu_B = \frac{e \cdot h}{4 \cdot \pi \cdot m} = 0.93 \times 10^{-20} \text{ emu}$$

Equation 3-1: Bohr Magnetron

where e is the charge of an electron (1.602×10^{-19} Coulombs), h is Planck's constant (6.63×10^{-27} Joule-seconds), and m is the mass of an electron (9.11×10^{-31} kg). For most atoms in free space the total electron spin moment is not more than one Bohr magneton. In some elements such as the transition metals, however, due to quantum mechanical properties, the outer electron shells begin to become filled before some of the inner shells are completely filled. This results in partially filled inner shells that have a large net electron spin moment (see Figure 3-2)

because you have more magnetic moments aligned in one direction than you have in the other direction.

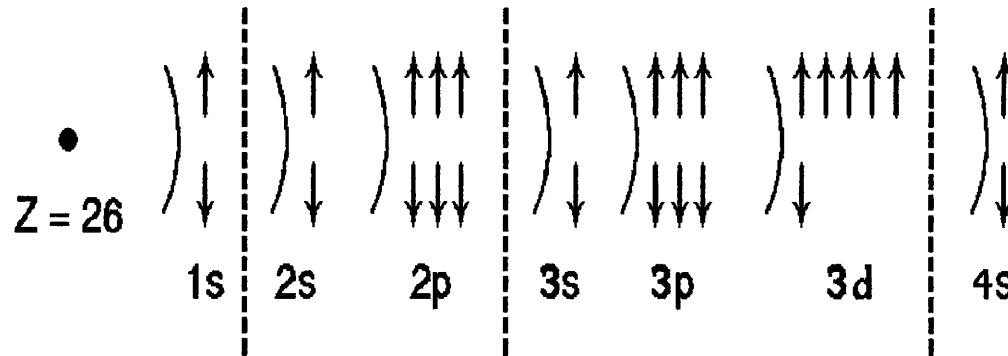


Figure 3-2: Electron Spin Orientations of an Iron Atom in Free Space

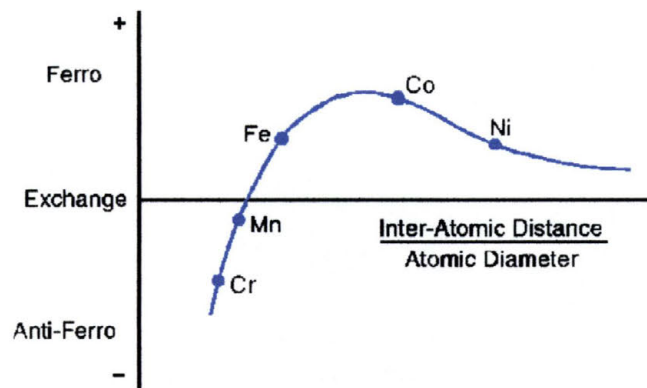
This effect is not the same in a bulk material. As an example of what can happen, when iron atoms condense to form a solid-state metallic crystal, the electronic distribution, called the density of states, changes. This is due to the bonding between atoms and the effects of electrons on neighboring atoms. For example, while some neighboring atoms may have magnetic moments that screen or compensate for the magnetic moment of the atom in question, for all practical purposes, an iron atom in a bulk metallic Fe sample has a magnetic moment equal to $2.2 \mu_B$. For Ni, the magnetic moment is 0.75 , while for Permalloy it is approximately 1.02 .

3.2 Exchange Coupling

It is now relevant to look at the magnetic behavior of atoms in a crystal. This discussion will use iron as an example since it is one of the most well known magnetic materials. The most important question to ask is, "How does one atom relate to its neighboring atoms in the crystal?" A quantum effect called exchange coupling forces all the iron's atomic magnetic moments to point in approximately the same direction. Nature prefers systems to have as little energy as possible. When all the magnetic moments are aligned in a crystal of iron, there is a lowering of the overall energy of the crystal, thus, this is a preferred state in nature. Think of it as taking less energy for one magnetic moment to align with another magnetic moment instead of opposing it, in much the same way that two bar magnets will repel each other in one orientation while they attract each other in the other.

In considering the energy of a system, other ways of adding or removing energy must be considered. Adding heat to a system is one way to add energy to it. When you have a magnetic material, there is a certain temperature, called the Curie temperature, at which the amount of thermal energy (or energy from heat) equals the exchange energy of the electrons in the material and the long-range ordering of the spin moments breaks down. Thermal energy is usually measured in terms of a value obtained from kT where T is the temperature (in degrees Kelvin) and k is Boltzman's constant (where $k = 1.38 \times 10^{-23}$ Joules/Degree

Kelvin). At room temperature (~ 300 K) the thermal energy of a material is 4.14×10^{-21} Joules, or 0.025875 electron-Volts (eV). This is not much energy at all but when this value is reached, it allows the spin moments of the atoms to point randomly in all directions. When a material is in this state, it is said to be paramagnetic. When the material is below the Curie temperature, the magnetic moments align and the material is said to be ferromagnetic.



Element	Cr	Mn	Fe	Co	Ni
Neel Temp. (°C)	311	100	1043	1388	627

Figure 3-3: Exchange Coupling Ratio²⁶

Exchange coupling is very sensitive to the ratio of the inter-atomic spacing to the size of the atoms (see Figure 3-3). When the atoms are closely spaced, the exchange coupling is negative and the adjacent spins are aligned in an anti-parallel orientation. These types of materials are called anti-ferromagnetic (see Figure 3-4a on the next page) because they have no net magnetic moment. When the atoms are more largely spaced,

the exchange coupling is positive and the material is said to be ferromagnetic (see Figure 3-4b). There is a third state, called the ferrimagnetic state, that is a unique sort of anti-ferromagnetic state (see Figure 3-4c). As an example of ferrimagnetism, consider a bulk sample of iron oxide. Some of the oxide will form Fe_2O_3 in which the iron is in an Fe^{2+} state having a magnetic moment of $4\mu_B$, while some of the oxide will form Fe_3O_4 in which the iron is in an Fe^{3+} state having a magnetic moment of $5\mu_B$. The mix of the 2^+ and the 3^+ states causes the Fe oxide, which normally wants to be anti-ferromagnetic, to have two different magnetic moments aligned in opposite directions. The stronger of the two will be partially shielded by the smaller of the two, but will not be entirely quenched.

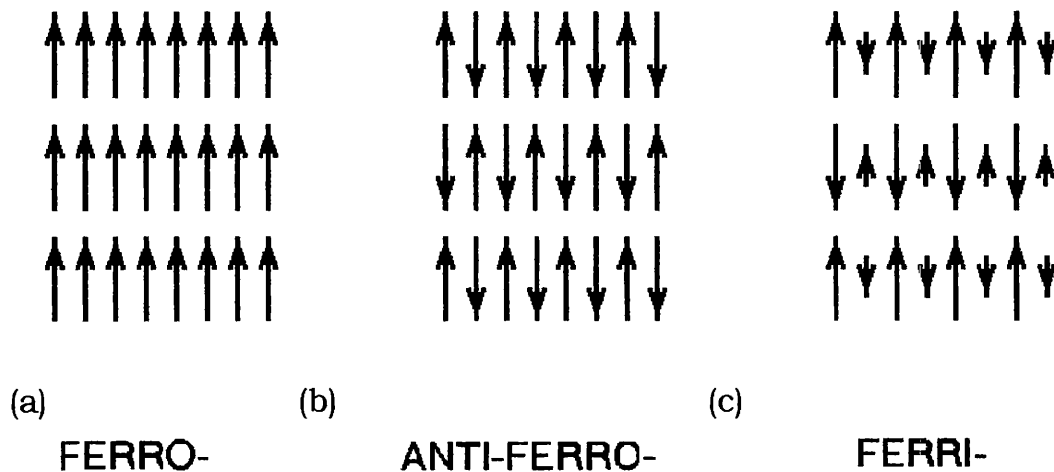


Figure 3-4: Three Common Types of Magnetic Ordering

Another important behavior to consider is what occurs when, instead of a free atom or a small collection of atoms, you have a sample comprised of several million atoms. The term used to describe the spin magnetic moments of the entire sample is called the magnetization (M), and is, by definition, just the sum of all the spin magnetic moments divided by the total volume of the sample:

$$M = \frac{1}{V} \cdot \sum_1^N m$$

Equation 3-2: Magnetization of a Material

where N is the number of atomic moments, V is the volume of the material, and m is the atomic moment in emu. In a large enough magnetic field, the magnetization of the entire material will be parallel, or ferromagnetic. If the external magnetic field is smaller than the internal magnetic field, it may divide into domains, where the direction of the magnetic field will be the same throughout a single domain but the individual domains may not be aligned.

Generally, when a magnetic material becomes magnetized by an external magnetic field, it will create within itself a magnetic field that will oppose the externally applied magnetic field. This can be thought of as a sort of negative feedback. This also leads to the production of magnetic poles. The convention for magnetic poles is that when the magnetization decreases, the poles produced are north or positive. Magnetic poles, just like a moving charge, can produce magnetic fields.

Magnetic fields generated by a magnetic body are extremely complicated and in most circumstances are not uniform. A measure of the strength of a magnetic field and the magnetization of a material can be found by calculating a quantity known as the flux density:

$$B = H + 4 \cdot \pi \cdot M$$

Equation 3-3: Calculation of Flux Density

where B is the flux density in gauss, H is the total magnetic field in Oersteds, and M is the magnetization in electromagnetic units (emu).

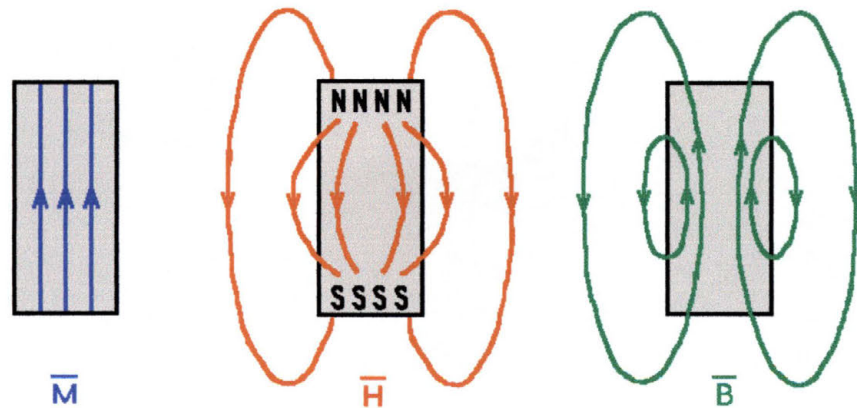


Figure 3-5: Magnetization (M), Magnetic Field (H), and Flux Density (B) Fields of a Bar Magnet

These three quantities, B , H , and M , are typically plotted or demonstrated on paper by lines being drawn through an image of the magnetic material. The lines represent where an effect may exist, while arrows represent the direction of the effect (see Figure 3-5). The spacing between the lines is inversely proportional to the magnitude of the field.

The closer the lines are together, the higher the field strength being represented. These properties of magnetism have been exploited to make a number of devices used every day by millions of people all over the world. One example, relevant to this thesis, is magnetic recording.

3.3 Traditional Read-Write Processes

Magnetic devices are the most common devices used to record information in computers. The hard disk drive of a computer memory is a magnetic device that stores information as binary digits, or bits. These are the ones and zeros of computer code. The hard disk is made of two main components, the magnetic film that stores the information and the read/write head that communicates between the disk drive and the computer. When writing in digital or binary recording, the writing head is toggled from one polarity to another in order to write digital transitions of the remnant magnetization in the recording medium or film. Figure 3-6 on the next page is an example of an idealized write head. Current is passed through a wire to create a magnetic field, with the strength of that field directly related to the number of times the wire is wrapped around the core. The magnetic field is then amplified and directed by the core.

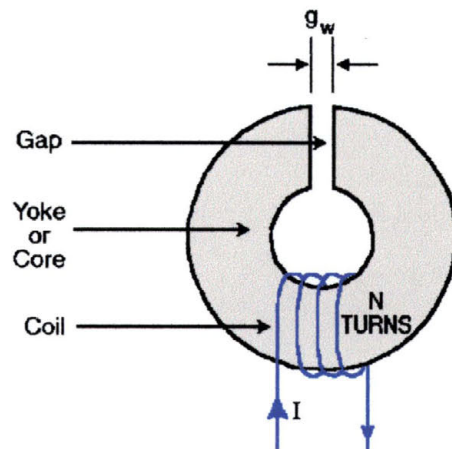


Figure 3-6: Idealized Write Head²⁵

The gap in the core is what allows the magnetic flux circulating inside the core to fringe out and pass through the recording media or thin film (see Figure 3-7 on the next page). The deep gap field, H_o , given in units of Oersteds (Oe) is calculated by the following equation:

$$H_o = \frac{0.4 \cdot \pi \cdot N \cdot I}{g_w}$$

Equation 3-4: Deep Gap Magnetic Field

where N is the number of turns in the wire, I is the current in the wire in Amperes, and g_w is the width of the gap. For high-density recording such as on a computer hard-drive, H_o needs to be at least three times the value of the opposing magnetic intensity that must be applied to a magnetized material in order to remove the residual magnetism (H_c) that exists in that material.²⁵

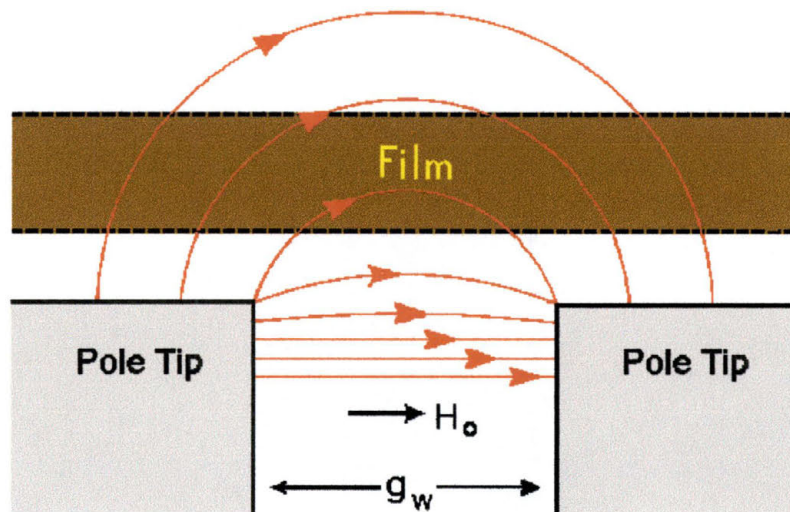


Figure 3-7: Fringing Field at the Top of the Write Head

If the current in the wire of the write head is held constant while the head is near the surface of the recording medium or thin film, then the magnetization of the thin film remains unchanged from whatever previous value it possessed. When the current is suddenly reversed, the written magnetization reverses as well. A north pole in one direction represents a digital '1', while a south pole in the same direction represents a '0'.

Once the data has been written to the recording media, it is then important to be able to read it. The magnetic field and flux fringes are equally distributed above and below the medium (see Figure 3-8 on the next page). Where the magnetization (represented by the blue line) decreases, north magnetic poles exist; where it increases, south magnetic poles exist.

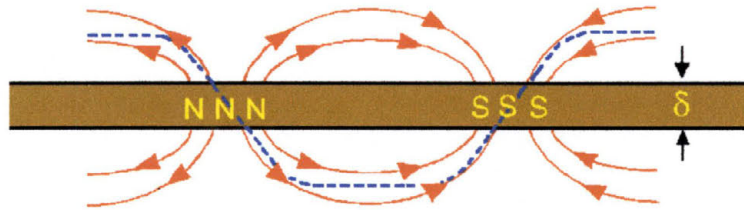


Figure 3-8: Fringe Field and Written Magnetization Pattern

When a reading head made with relatively large pole pieces of a highly permeable material is placed close to the recording medium or film, the field and flux flow patterns of the film are dramatically changed (see Figure 3-9). In this instance, the read head is large in relation to the wavelength of the recorded film. The reading head has the same structure as the writing head discussed above, except that different materials are used in its construction. By using a highly permeable material, when the read head is placed close to the film, most of the fringing flux of the thin film will pass through the coil while not much passes through the air gap.

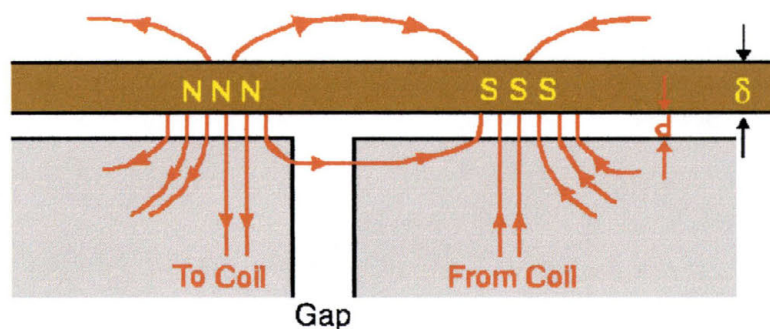


Figure 3-9: Flux Near the Read Head

The direction of the magnetization in the recording film will determine the direction of the flux through the coil. When a magnetic field moves through a conductor, an electrical current is induced based on the direction of the field and the direction of the movement. As this current is created, it will produce a voltage differential across the wire wrapped around the core. The polarity of this induced voltage is what “tells” the electronics whether the read head is reading a ‘1’ or a ‘0’.

3.4 Anisotropic Magneto-Resistive Effect

In 1857, Lord Kelvin discovered that the electrical resistance of an iron bar changed as its magnetization was changed. This phenomenon has come to be called the Anisotropic Magneto-Resistive (AMR) effect. This effect has some interesting applications when applied to thin films of magnetic materials. Two qualities of thin magnetic films are that the magnetization can be a single domain instead being broken up into multiple domains, and that the demagnetizing fields force the magnetization direction to remain parallel to the plane of the thin film. These properties were exploited in the early 1970’s by Bob Hunt²³ who invented a device known as the magneto-resistive head (MRH).

AMR can be described rather simply in the following equation:

$$R = R_o + \Delta R \cos^2 \Theta$$

Equation 3-5: Resistance with Respect to Magnetization Direction

where R is the total resistance of the magnetic material, R_0 is the fixed resistance of the material, ΔR is the maximum value of resistance obtainable in the material, and θ is the angle between the direction of the magnetization of the material and the direction of the current flow through the material. The resistance will be greatest when the direction of the magnetization and the direction of current flow are parallel to each other and smallest when they are perpendicular.

The fundamental idea of a MRH is that the magnetic field produced by the written or recorded magnetization pattern in the tape or disk rotates the MRE magnetization angle. In all MRHs, the output signal voltage is, by Ohm's Law, equal to the current in the material times the resistance to current flow in the material. Since the resistance in a MRH changes when the magnetization direction changes (assuming a constant direction for current flow), the voltage will change as the direction of the magnetization changes.

Resistivity is an intrinsic property of all materials that describes resistance to electrical current without taking the volume of a material into account. The electrical resistance, R , of the MRH, in terms of the resistivity, ρ , of the material is given by:

$$R = \frac{\rho \cdot W}{T \cdot D}$$

Equation 3-6: Electrical Resistance in Terms of Resistivity

Where W is the width of the thin film, T is the thickness of the film, and D is the depth of the film.

For magneto-resistive materials, resistivity is found by:

$$\rho = \rho_o + \Delta\rho \cdot \cos^2 \Theta$$

Equation 3-7: Resistivity of MR Materials

where ρ is the total resistivity of the material, ρ_o is the fixed part of the resistivity and $\Delta\rho$ is the maximum possible value of the part of the resistivity that depends on the MRE. The maximum fractional change in the resistivity of a material is defined as the magneto-resistive coefficient, $\Delta\rho/\rho_o$. This coefficient is often used to describe the qualities of MR materials. For example, Permalloy, a binary alloy of around 81% nickel and 19% iron, has a thin film MR resistivity of around 2%.

The historical growth rate of hard disk drives has been around twenty-five percent per generation, but in the late 1980's the spacing between individual storage locations on a disk began growing considerably closer. This data compression requires more sensitive read/write heads. With AMR based technology, the sensitivity is inadequate to the task. For this reason, a new property of magnetic materials has been a popular area of research- Giant Magnetoresistance.

3.5 Giant Magnetoresistance

Today, read-write devices are made using a similar yet different effect, Giant Magnetoresistance (GMR). The use of GMR materials to replace AMR materials has shown great promise in overcoming one of the most difficult problems in the development of such devices as magnetic random access memory technology- that of small size, which leads to relatively long read access times for memory applications. GMR (the percent change in resistivity with respect to its lowest value under application of a range of magnetic fields) and the magnetic field required to achieve the full range of the material's resistance (saturation field) are two of the most important material properties for GMR material applications. The rate of change of resistance with magnetic field (sensitivity) determines the signal generated by a magnetic field when the field is less than the saturation field.²⁶

GMR devices are built from alternating, ultrathin layers of magnetic and nonmagnetic materials. In a typical device, two magnetic layers are separated by a conductive, nonmagnetic interlayer. As discussed previously, electrons can exist in two quantum states: spin up if their spin is parallel to the magnetic field of their surroundings and spin down if the spin is antiparallel to the magnetic field. While in non-magnetic conductors there are equal numbers of spin up and spin down electrons in all energy bands, due to the ferromagnetic exchange interaction there is little difference between the number of spin up and

spin down electrons in the conduction sub-bands of ferromagnetic materials. This means that the probability of an electron being scattered when it passes into a ferromagnetic conductor depends upon the direction of its spin and the direction of the magnetic moment of the layer. The resistance of two thin ferromagnetic layers separated by a thin non-magnetic conducting layer can be altered by changing whether the moments of the ferromagnetic layers are parallel or antiparallel. Layers with parallel magnetic moments will have less scattering at the interfaces, and thus, a lower resistance to conduction (Figure 3-10A). Layers with antiparallel magnetic moments will have more scattering at the interfaces and consequently, higher resistance (see Figure 3-10B).

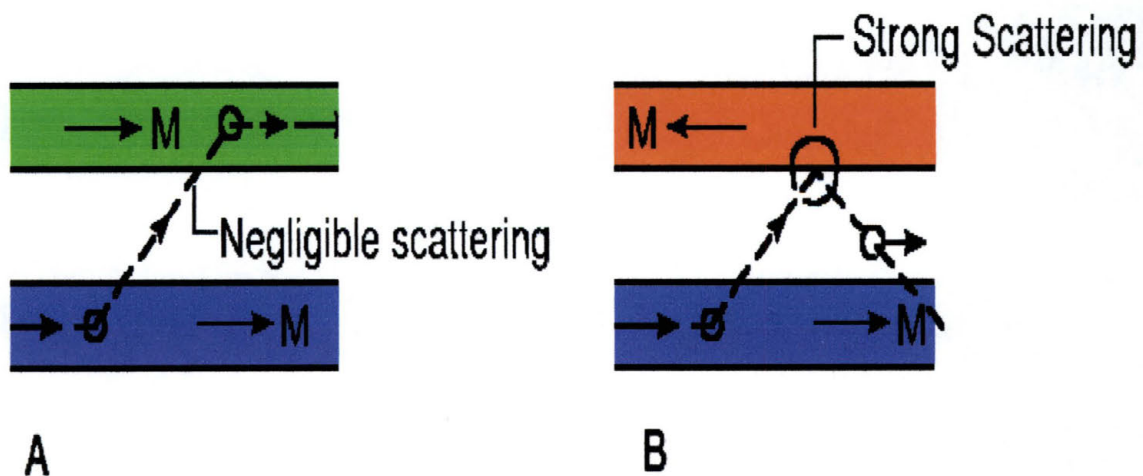


Figure 3-10: Spin Dependant Scattering in GMR Multilayers

Spin-dependant scattering is a quantum mechanical phenomena in which the mean free path of electrons (how far an electron will travel before it interacts with something) in magnetic conductors, and in turn their resistivity, is affected by the relative orientation of the conduction electron spins and the magnetic moment of the magnetic material. The resistivity of metals is directly dependant upon the mean free path of conduction electrons. The shorter the mean free path, the higher the resistance of the metal.

GMR can be quantified by the following equation:

$$GMR = \frac{B * t_B}{n * \left(\frac{F * t_F A}{NM * t_{NM} A} \right) C * t_C}$$

Equation 3-8: Giant Magnetoresistance

where B and C designate a buffer and a capping layer, respectively, F is a transition-metal magnetic layer (Fe, Co, Ni or their alloys), and NM is a non-ferromagnetic transition metal or a noble metal (V, Cr, Nb, Mo, Ru, Re, Os, Ir, Cu, Ag or Au). t_F , t_{NM} , and t_C refer to the thickness of the corresponding layers. The amplitude of the GMR effect depends considerably on the pair of F/NM materials used and on the thickness of the various layers.²⁷ It ranges from 0.1% in V or Mo-based multilayers, to more than 100% in Fe/Cr or Co/Cu multilayers. In all of these structures, GMR is associated with changes in the relative orientation of the magnetizations in successive ferromagnetic layers.

GMR is also seen in antiferromagnetically coupled multilayers. In these multilayers, when there is little or no applied magnetic field, the coupling between the interlayers generates a macroscopic antiferromagnetic alignment of the magnetizations in successive ferromagnetic layers. As the applied magnetic field is increased, the magnetizations in the ferromagnetic layers rotate more and more toward the field (see Equation 3-7 on page 55). The term “spin-valve magnetoresistance” was introduced for the change in resistivity associated with this change in resistance.

Two main factors are necessary to observe spin-valve magnetoresistance: (1) the probability of scattering of the conduction electrons must be spin-dependant either in the bulk of the ferromagnetic layers or at the ferromagnetic/non-ferromagnetic interfaces; and (2) the conduction electrons must have the ability to travel back and forth through the successive ferromagnetic layers.

In general, there are three main categories of spin-valve multilayered systems. These can be distinguished by how the change in the magnetic alignment of the magnetizations in the successive ferromagnetic layers occurs or is produced. The first is antiferromagnetically coupled multilayers, in which GMR was originally discovered. The second is multilayers of ferromagnetic materials with different coercivities. The third, and most important for the purposes of this thesis, is the spin-valve sandwich (see Figure 3-11 on the next page).

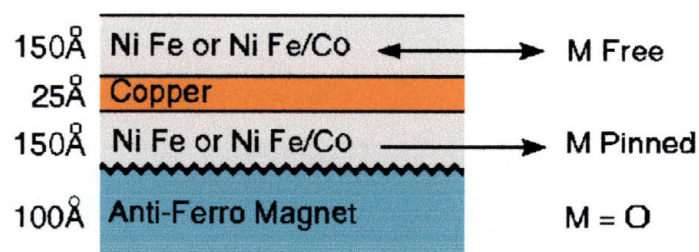


Figure 3-11: GMR Lattice with Py-Cu Layers

Spin-valve sandwiches are constructed by sandwiching two ferromagnetic layers (F1 and F2) around a nonferromagnetic metal (NM). The magnetization of F2 is constrained by coupling to an adjacent antiferromagnetic layer. An interesting feature of these spin-valve sandwiches is that the change in the relative orientation of the magnetizations in the two ferromagnetic layers does not rely on the existence of antiferromagnetic coupling between the ferromagnetic layers. Due to the asymmetric pinning forces acting on the magnetizations of the ferromagnetic layers, it is always possible to switch the alignment of the magnetizations from fully parallel to fully antiparallel. The only requirement is that the thickness of the spacer layer must be large enough to provide sufficient decoupling of the ferromagnetic layers. It is this property that is of most interest to this thesis, in the form of a spin-valve sensor.

3.6 Spin-Valve Sensors

Exchange-biased spin-valve multilayers are among a variety of multilayers displaying the GMR effect. Spin-valves have received, in the recent past, much attention for their use as magnetoresistive sensors, most notably in computer memory storage devices. Another area of interest is magnetic random access memory (MRAM) devices.

A spin valve is generally a sample consisting of a GMR trilayer. All (exchange-biased) spin-valve configurations exhibit the antiparallel configuration that is needed to obtain the GMR effect. Exchange biasing is seen when a layer of ferromagnetic material is put into contact with a layer of antiferromagnetic material and the two are placed in a magnetic field. When this occurs, the magnetic domains of the ferromagnetic layer will obtain a uniform anisotropy along the direction of the field resulting in a shift (biasing) of the magnetization loop of the ferromagnetic material over some field (known as the exchange bias field, H_{eb}), when the field is applied along the anisotropy axis.²⁸

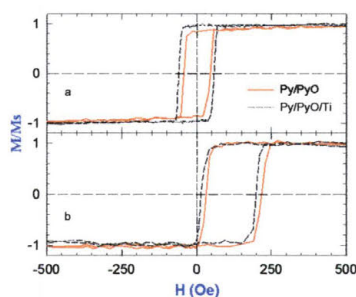


Figure 3-12: Example of Hysteresis Curve Demonstrating Exchange Biasing²⁹

When an external field is applied to the device along the exchange-biased anisotropy axis, which is smaller than the bias-field, only the uncoupled layer (known as the free layer) will change its magnetization direction. This reversal of the magnetization is determined by the anisotropy field of this free layer, in addition to some residual coupling through the nonmagnetic interlayer, which is a small field interval close to zero field.

When the field is increased further until it exceeds the bias field, the second layer will also reverse its magnetization. The second layer, known as the pinned or biased layer, displays a magnetization reversal centered around the bias field. The relative orientation of the magnetization directions of the two ferromagnetic layers is thus parallel for fields below the exchange-biasing field and above zero, while it is antiparallel for fields between these two values. The transition from parallel to antiparallel magnetic configurations is, as the GMR effect describes, accompanied by a transition in the device from a state of low resistance to electrical current to a state of high resistance to electrical current.

3.7 Spin-Valve Transistors

The spin-valve transistor is made up of a silicon emitter, a magnetic multi-layer as the base, and a silicon collector (see Figure 3-13).

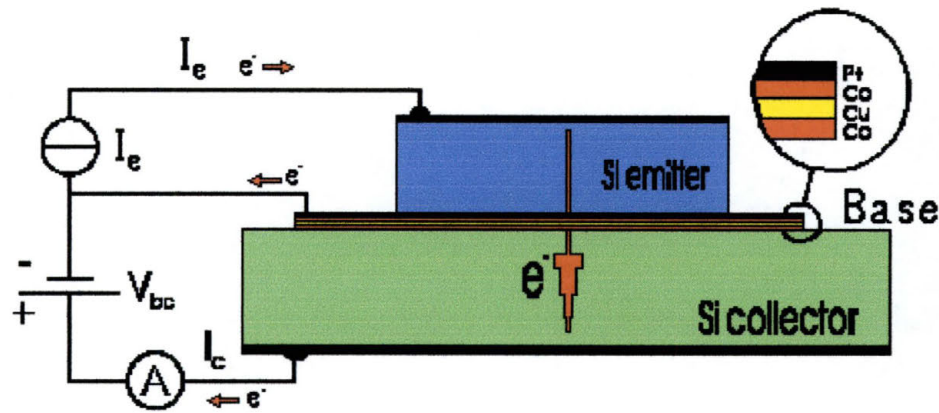


Figure 3-13: Example of the Structure of a Spin-Valve Transistor³⁰

The details of how a normal transistor works can be found in many books, journals and magazines. For the purposes of this thesis, it is enough to say that by controlling the current from the emitter to the collector by the application of a voltage to the base, a transistor is either on (current flow through the device) or off (no current flow through the device). The operation of a basic CMOS transistor can be found in Chapter 2 of this thesis. In a spin-valve transistor, electrons are injected from the emitter, passing the first semiconductor-metal interface into the base. Because of the thin base multi-layer, most of the electrons are not directed to the base contact, but travel instead perpendicular through the multi-layer across the second semiconductor-metal interface. These electrons form what is known as the collector current.

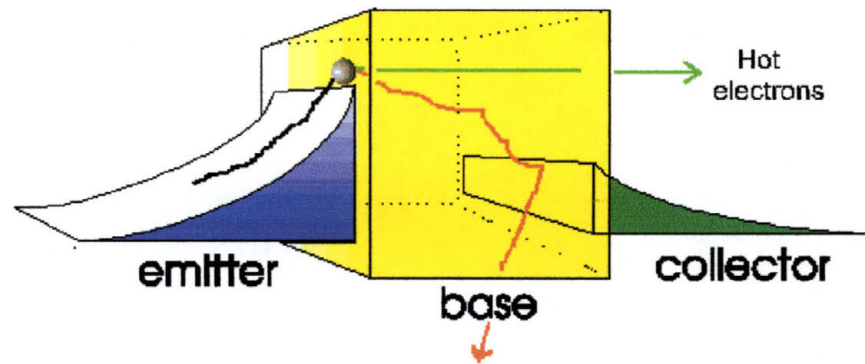


Figure 3-14: Energy band diagram of a Spin-Valve Transistor³¹

The energy band diagram of an example of a spin-valve transistor can be seen in Figure 3-14 above. What it shows is energy on the y-axis as an electron attempts to travel from the emitter to the collector. The blue slope on the left indicates the amount of energy the electron will need to approach and then enter the base. The emitter bias then accelerates the electrons over the emitter barrier (the peak of the blue band diagram). Once electrons enter the base, they interact with the atoms of the base and are called ballistic electrons. The probability of an electron passing the energy barrier of the collector (represented by the green energy band diagram) is limited by the collisions that the ballistic electrons have in the base, which affect their energy and trajectory. The collisions are either by optical phonon scattering in the semiconductors or by quantum mechanical interactions at the base-collector interface. Because the thickness of the individual layers of the base is smaller than the spin-dependent diffusion length of the ballistic electrons, it can be said that there is no spin relaxation within the base. It can also be said

that the ability for electrons to pass through the base (the current in the base) can be described as a series resistance caused by the successive layers and interfaces.³⁰ Since this is a GMR structure, the resistance of the base can be changed by changing the directions of the magnetic moments of the various layers within the base.

3.8 Magnetic Properties and Permalloy

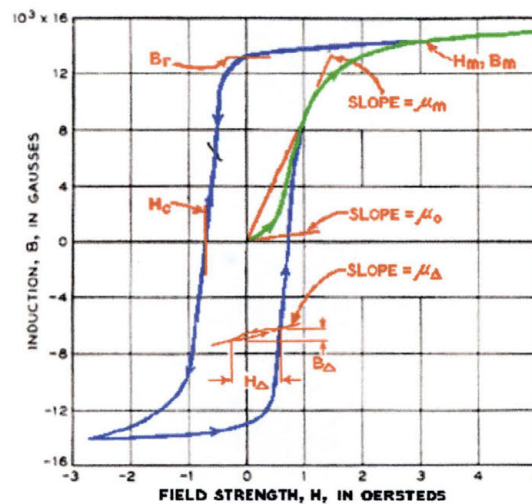


Figure 3-15: Magnetization Curve (Green) and Hysteresis Loop (Blue)

When a piece of unmagnetized iron is brought near a magnet or subjected to the magnetic field of an electric current, the magnetization induced in the iron by the field is described by a magnetization curve plotting the intensity of the magnetic induction, B in *emu*, against the field strength, H in *Oersteds*. Such curves are a fundamental way to describe the magnetic properties of materials (see the Green line of Figure 3-15). The behavior of a material is also described by its

permeability curve and hysteresis. The ratio of B/H is called the permeability, μ , which represents the relative increase in the magnetic flux caused by the presence of a magnetic material.

When testing a material, if the field strength is first increased from zero to a very large value and then decreased again, it can be seen that the original curve will not be retraced. This is because the induction lags behind the field and follows a characteristic curve (see the blue line of Figure 3-15 on previous page). On a loop that is symmetrical about the origin, the value of H for which $B = 0$ is called the coercive force H_c . This value is often used to describe the magnetic quality of a material. The value of induction at which $H = 0$ is called the residual induction, B_r . As H is increased indefinitely, the intensity of the magnetization and the intrinsic induction $B-H$ of a ferromagnetic material approach a finite limit, commonly called saturation. There are many factors affecting a material's magnetic properties. These will not be dealt with in this thesis unless they are directly related to my research, however, there exist many resources that describe in detail what many of these factors are and how they affect the magnetic properties of a material. The reader is encouraged to seek these out if details of magnetic properties are of interest.

Nickel-iron alloys, also known as Permalloy, have been studied since the late 1880's. As a result, there is a great deal of information known about the magnetic properties of Permalloy. It has been shown

that thin films made of NiFe with about twenty percent (by weight) Fe have superior soft magnetic properties, high anisotropic magnetoresistance, and low magnetostriction. It has also been found that the oxidation of NiFe films changes the magnetic properties of the films. For bulk Permalloy, the formation of $\text{Fe}_3\text{O}_4\text{-Fe}_2\text{O}_3$ is found to be formed during air annealing. NiO is also found to form in electrochemical oxidation.³¹ Bulk NiO is an antiferromagnetic material with a NaCl cubic crystal structure (see Figure 3-16) and a Curie point of 250°C .³² In addition, it has been discovered that sputtered NiFe_2O_3 was the preferred atomic formation when Permalloy films are exposed to dry air.³³ The most preferred oxidation of Fe in NiFe films is the Fe_2O_3 structure.³⁴

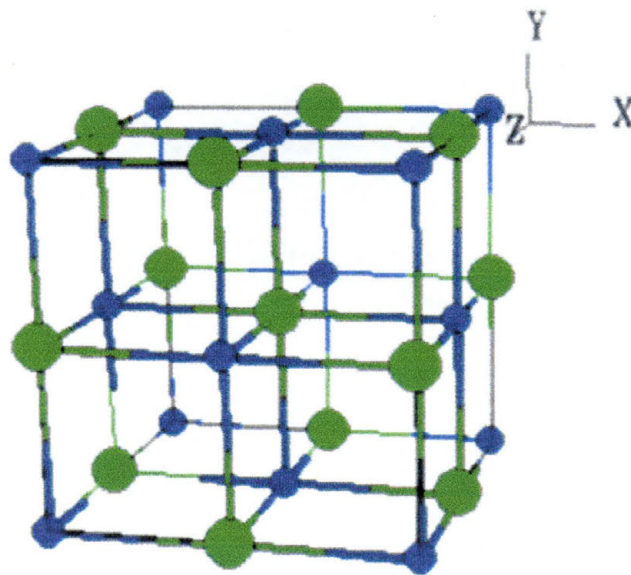


Figure 3-16: Cubic (NaCl) Crystal Structure³

There is also a great deal known about iron itself. Under equilibrium conditions, α iron is the well known structure for metallic iron, having a body-centered cubic structure (see Figure 3-17). When alloyed with fcc Ni, it can form an fcc alloy at the same concentration used for Permalloy.

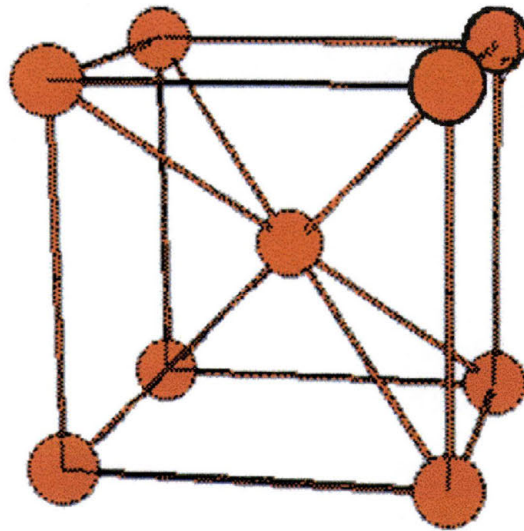


Figure 3-17: Body Centered Cubic (bcc) Crystal Structure³

In addition, there are various iron oxide phases. There is an unstable cubic oxide, γ Fe_2O_3 , that is magnetic and can be produced by sputtering techniques for magnetic media applications; and there is FeO which has cubic (NaCl) structure (see Figure 3-16 on page 70) and is paramagnetic. The thermodynamically preferred state, however, for an iron oxide is Fe_3O_4 and α Fe_2O_3 . Fe_3O_4 , better known as black magnetite, has a simple cubic structure. Fe_2O_3 , however has a rhombohedral crystal structure (see Figure 3-18 on next page).

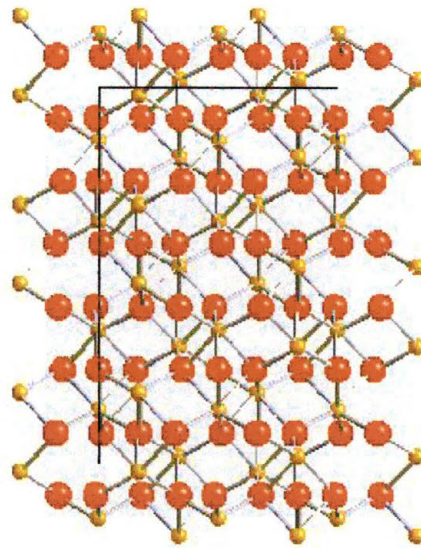


Figure 3-18: Rhombohedral Crystal Structure of Fe_2O_3 ³

Recall that a paramagnetic material has a permeability only slightly greater than one, usually between 1.000 and 1.001. They have permeability's that are independent of field strength and are either independent of temperature or decrease with rising temperature, and they do not generally show hysteresis. This is because the spin moments of the atoms point randomly in all directions.

The addition of nickel to iron increases greatly the strength and corrosion resistance of iron, especially if carbon is present. This is evidenced by the fact that these three elements are the main ingredients in steel. The magnetic properties of such alloys has been studied since the late nineteenth century. It was discovered in the early part of the twentieth century that alloys of NiFe having 30% to 90% Ni had permeability's greater than iron, especially when the alloys were heat-

treated. In modern times, Permalloy (Py) films have already been extensively used in the production of AMR devices (see section 3.4) as well as some GMR devices (section 3.5).

One property of Py that has served to make it such a widely used material in read/write head technology is that its cubic magneto-crystalline anisotropy, K , passes through zero. When magnetizing a material some directions will be easier to magnetize than others. If a material has a K value that is positive, it means that the easy axes of magnetization are the edges of the cubic unit cell. When a material has a negative K value, the easy axes of magnetization are diagonals cut across the cubic body of the unit cell. These are both examples of anisotropic materials. When a material has a K value of zero, the material is isotropic and has no preferred easy (or hard) axis of magnetization. The benefit of having a zero K value material is that it will be easy to magnetize regardless of what direction an external magnetic field is applied.

Another useful property of Py is the fact that when the ratio of Ni to Fe is around 81%:19% the magnetostrictive coefficient, λ , also passes through zero. Magnetostriction describes the phenomenon in which a magnetic material changes its size depending on its state of magnetization. A positive magnetostriction is assigned when a fully saturated magnetic material is larger than when it was demagnetized. A negative magnetostriction is assigned when the size of a material shrinks

when it becomes fully saturated compared to its demagnetized state. Obviously, a zero magnetostriction material will not change its size due to magnetic effects, no matter what level of saturation it has. This property is advantageous when making extremely small devices, such as read/write heads for magnetic storage devices.

The fact that in Py films of approximately the same percentages of Ni and Fe, both $K = 0$ and $\lambda = 0$ has led to the material being called the “magic metal”. It is also the reason that Py is the most dominant material used in the production of thin film and magnetoresistive read/write heads.

The one disadvantage of Py films is that it is a mechanically soft film. This makes it unsuitable for applications where any sort of friction would be required (i.e. contact applications similar to how a needle worked on vinyl records).

For this thesis, it is the investigation of NiFe with the incorporation of oxygen from Dual Ion-Beam Sputtering (DIBS) produced films that is one of the central goals of my investigations. This is because it is believed that the naturally highly unstable FeO cubic structure can be made in the DIBS. If this is possible, it will be feasible to produce a GMR spin-valve using a NiFe/NiFeO/NiFe structure. The ability to produce such a spin valve would have the advantage of ease of production (simply admitting O_2 to the growth chamber when producing a film of NiFe), and would theoretically exhibit all the characteristics of GMR spin-valves.

4 VACUUM FUNDAMENTALS

During the process of producing the films in this research, it was important to perform the work in a good vacuum environment. This is important because as the atoms are deposited on the Si wafer, any contamination can cause the atoms to form non-uniformly across the surface. A non-uniform film can cause irregularities in the electronic and magnetic properties of the films. In addition, since the introduction of any contaminants on the wafer would be a completely random occurrence, any films produced would never be able to be reproduced with exactly the same characteristics.

4.1 Producing a Vacuum

A vacuum is produced by removing the air, and any dust particles that may be suspended in air, from the work chamber. Water vapor, which varies with temperature and humidity, is another common gas that must be removed, as it is one of the largest sources of contamination on a substrate. In the DIBS system used here at SWT, a vacuum is drawn using a roughing pump and a high-vacuum pump. A roughing pump takes the work chamber from atmospheric pressure

(approximately 760 torr) to an ultimate vacuum of about one millitorr, 1×10^{-3} torr. The high-vacuum pump then takes the work chamber to a pressure of around 1×10^{-7} torr. This ultimate vacuum is so clean that it almost equals the emptiness of outer space.

4.2 Rough Vacuum

How the Pump Works

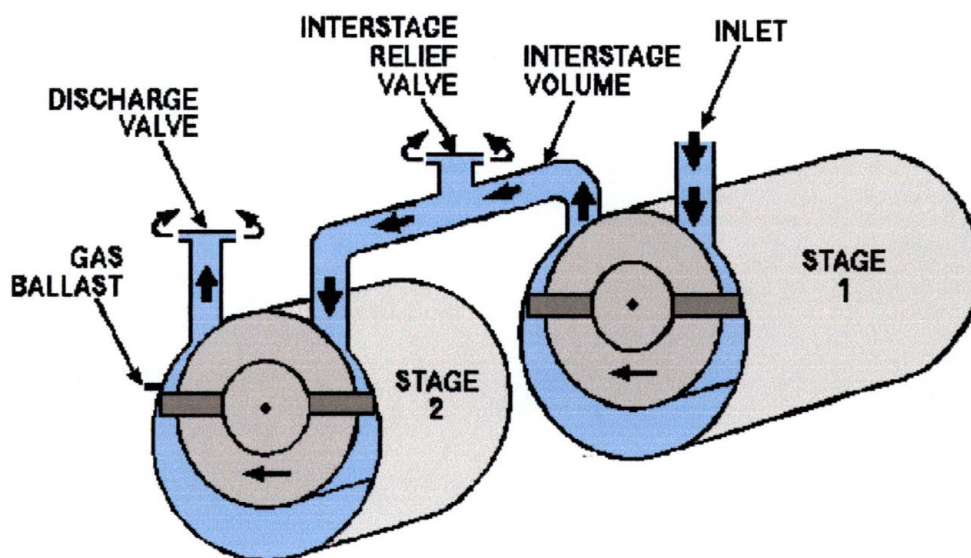


Figure 4-1: Two-Stage Oil-Immersed Rotary Vane Pump

There are many types of roughing pumps in use by industry and in research. The type of pump employed on the DIBS system is called a two-stage rotary-vane, oil-sealed mechanical pump. The pump works by compressing the gases drawn into the inlet to a pressure that is slightly higher than atmospheric pressure. Most rotary-vane pumps can move about one hundred and fifty cubic feet per minute. The pump module is

completely immersed in oil for a number of reasons. The oil serves to cool the pump, lubricate the moving parts of the pump, seal the pump against atmospheric pressure, and it opens the second-stage exhaust valve at low inlet pressures. Gases from the chamber enter the inlet port of the first stage (see Figure 4-1 on previous page), are swept around by the vanes, and compressed.

Compression builds up until it is high enough to overcome atmospheric pressure, at which point the discharge valve opens expelling the trapped gases. These types of pumps can remove up to 99.9% of the air found in the work chamber. The vane does this as it sweeps in a circle around the stator chamber. A small amount of oil is kept in the stator to help the rotary vane maintain its seal on the air being compressed (See Figure 4-2).

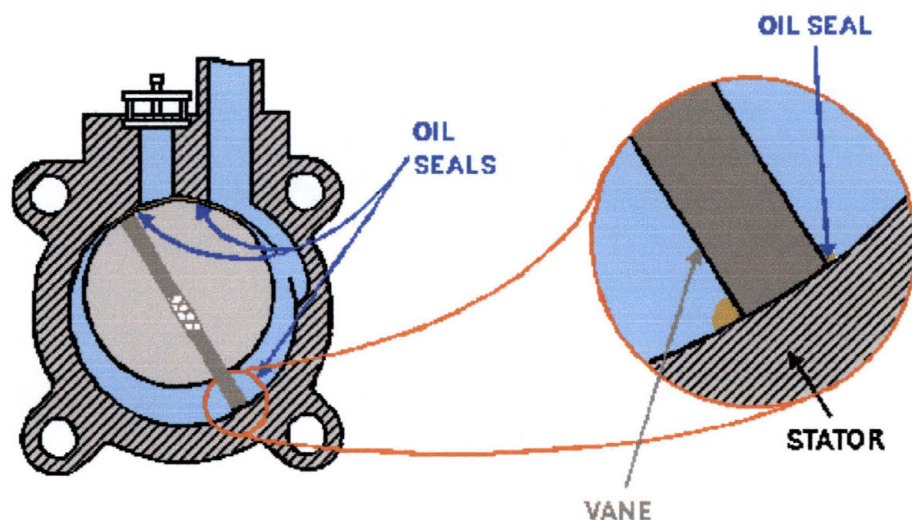


Figure 4-2: Detail of Rotary Vane Pump Module

The base, or ultimate, pressure of the pump is partially determined by the vapor pressure of the oil being used. If the oil becomes dirty with particulate matter or water, the vapor pressure of the oil increases. If the vapor pressure of the oil increases, the pressure at which the oil will change from a liquid to a gas increases. If the oil becomes a gas, or vapor, then it will backstream into the work chamber. Backstreaming not only prevents the pump from removing any of the gases from the work chamber, but also adds a thin coating of oil to the entire chamber. To prevent this from occurring, it is important to regularly change the oil of the pump.

4.3 High Vacuum

Once the working chamber has been taken to a rough vacuum, the high-vacuum pump is employed and the roughing pump is taken off line. The high-vacuum pump on the DIBS system is a cryopump. A cryopump is made up of two main components: a gaseous helium compressor and a pump consisting of a cold head, baffle, and the pump body (See Figure 4-3 on next page). The compressor and the cold head operate a lot like a typical household refrigerator, except that the temperature reached is considerably colder.

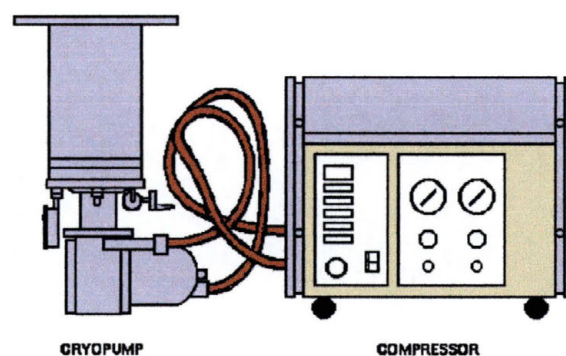


Figure 4-3: Cryopump and Compressor

As the helium is compressed, it gives up its heat to the surrounding walls of the compressor. The heat is removed by air-cooling, which also cools the helium. The cooled, compressed helium is then sent to the pump cold head. In the expander at the cold head, the helium is allowed to expand, lowering its pressure at the same time. As the pressure decreases, it takes in heat from the cold head and the baffle array. This chills the cold head to around 10° Kelvin (-441° F) and the baffle array to around 70° Kelvin (-333° F). These chilled surfaces actually pump the gases from the chamber. Chilled surfaces, in a vacuum, pump gases in one of two ways: The gases are either condensed (called cryocondensation) or adsorbed (called cryosorption) on the cryoarrays (See Figure 4-4 on next page).

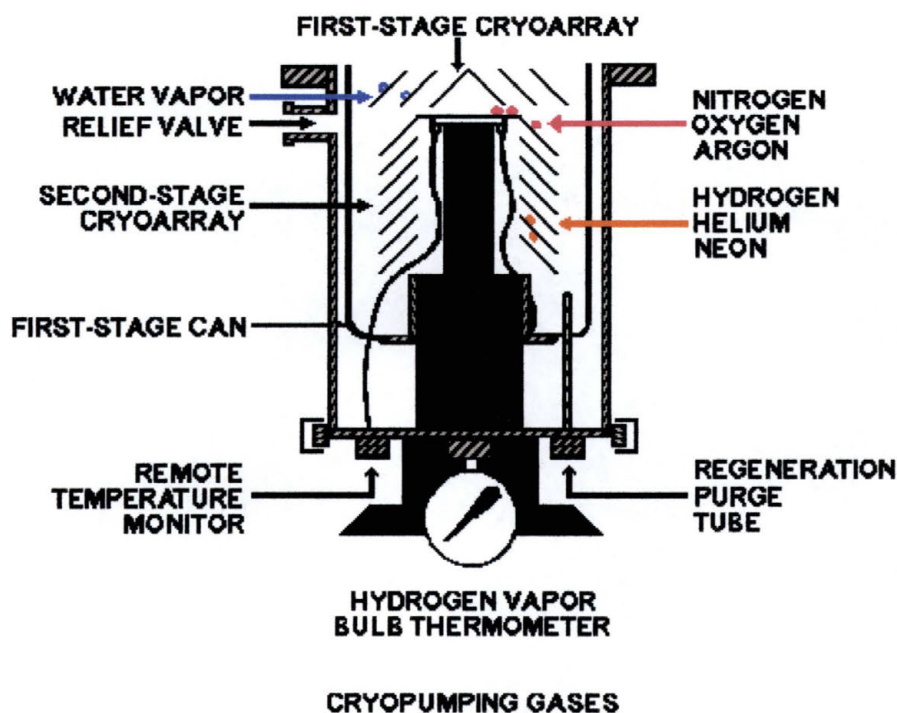


Figure 4-4: Insides of a Typical Cryopump

Cryocondensation is seen on the insides of most freezers in homes. Gases come in contact with the cold surfaces and stick. The first-stage array is cold enough to pump water vapor, while the second is cold enough to pump nitrogen, oxygen, argon, and most other gases. Despite this considerable achievement, however, the arrays are not cold enough to pump hydrogen, helium, or neon. Instead, these gases are pumped by cryosorption. Cryosorption is a surface related technique. A very porous material is attached to the second-stage array. This material is usually just activated charcoal. The gases enter the material and see a maze-like structure in the spaces of the charcoal. This process is similar to the soaking up of water by a sponge. Porous materials are used for three

reasons: First, the surface area available for gases to condense on is increased. Second, as the gases enter the colder regions of the material, they lose thermal energy. When they lose enough energy, they tend to stick to the surface much easier. And Third, it is likely that once inside the “maze” of the material, the trapped gases will not have enough energy to escape (See Figure 4-5).

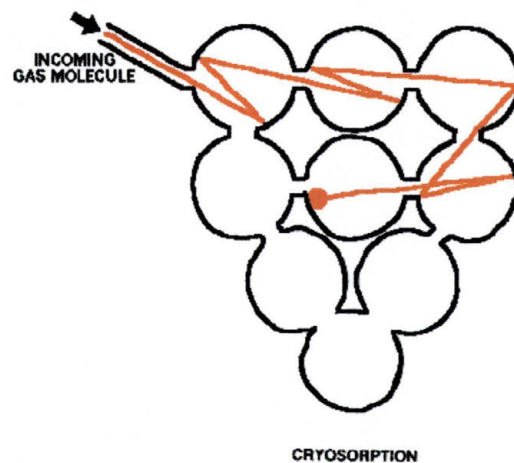


Figure 4-5: Gas Molecules Undergoing Cryosorption

The cryopump takes the ultimate pressure of the work chamber to a vacuum of around 1×10^{-7} torr.

5 Dual Ion-Beam Sputtering

5.1 Introduction

The Dual Ion-Beam Sputtering (DIBS) system in use at SWT is one of many types of broad beam sources for the generation of a beam of ions. The system here is called a gridded ion source, which is the type used most frequently in industrial applications. It provides the advantage of a narrow distribution of energy that is very well defined by the energy of the beam.

5.2 Components

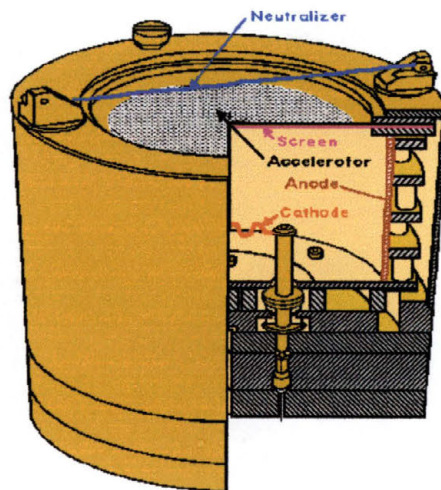


Figure 5-1: Gridded Ion Source

In order to understand the operation of the ion-beam system, it is first important to understand the design of the system that is used to develop the ion beam (see Figure 5-1).

5.2.1 Pressure

The pressure of the discharge-chamber is controlled by the flowing of gas to the ion source. Argon, which is so inert that it rarely reacts with any other atom, is typically used as the gas to be ionized. Gas flow must be above a certain minimum value because if the discharge-chamber pressure is too low, there will not be enough atoms to produce a sustainable plasma.

5.2.2 Cathode

The cathode is usually supplied with an A/C voltage potential. A/C is used to heat the wire of the cathode to the point where it will eject electrons. These electrons will then cause the formation of ions in the discharge chamber.

5.2.3 Anode

The beam voltage is applied to the anode, which is a cylinder that completely surrounds the discharge-chamber. The beam voltage is kept at a positive D/C voltage (ranging from 50 Volts to over 1000 Volts). Electrons from the cathode are attracted to the anode. The voltage of the anode will determine how fast the electrons ejected from the cathode will travel on their way to the anode. When these electrons interact with the gas atoms being injected into the chamber, they strip electrons from those atoms, creating ions. They also transfer energy to the ion through

the collision that strips the electron from the atom. A higher beam voltage will cause the transfer of more energy to the gas atoms.

5.2.4 Screen Grid and Accelerator Grid

The screen grid is an electrically neutral wire mesh that defines the boundary of the discharge-chamber. The accelerator grid is a wire mesh similar to the screen grid. The accelerator grid is kept at a negative potential. When an ion forms in the discharge chamber, it will have a net positive charge (since a negatively charge electron has been stripped from it). The ions will then feel an electrostatic attraction to the negative potential of the accelerator grid. Recall that it is the beam voltage of the anode that gives the ions most of their energy. The accelerator grid voltage, typically kept at 10% to 20% of the magnitude of the beam voltage, merely serves to direct the ions once they have been formed. One reason the grid voltage is kept so low is that if too high an accelerator voltage is used, the ions will tend to sputter the grid itself causing contamination of the target. The two grids are known as the ion optics.

5.2.5 Neutralizer

The neutralizer is a wire (typically made from tungsten) with an A/C voltage potential applied to it, in many ways similar to the cathode but at a lower voltage potential. The electrons generated from the neutralizer are introduced to the ion beam to balance the positive charge of the ions.

5.3 Basic Operation

Regardless of the basic operation of any specific broad beam ion source, a broad beam implies a large beam current relative to the acceleration voltage used. This provides for a large number of possible applications of the generated ion beam. This discussion will deal specifically with the system in use here at SWT.

5.3.1 Generation of the Ion Beam

The neutral atoms or molecules (Figure 5-2 #1 on next page) of the working gas are introduced into the discharge chamber through a port in the back of the discharge-chamber wall. Electrons having a lot of energy are ejected from the cathode (Figure 5-2 #2) (also called the main or discharge-chamber cathode) and will be pulled towards the anode. As they travel towards it, they will become entangled in the gas atoms in the discharge chamber (Figure 5-2 #3) with the result that many of them will undergo collisions with each other.

It is important that the discharge voltage not be too high. If the discharge voltage is too high then when an electron ionizes a neutral gas

atom, the odds increase that the atom will lose two or more electrons when it becomes an ion. These multiply charged ions would then obtain twice as much energy as the singly charged ions when they pass through the ion optics. This is important if small target penetration depths are desired. In addition, these multiply charged ions could obtain so much energy that when they impact the target they can physically damage the surface of the target, or they could contaminate the target with ion-source material.

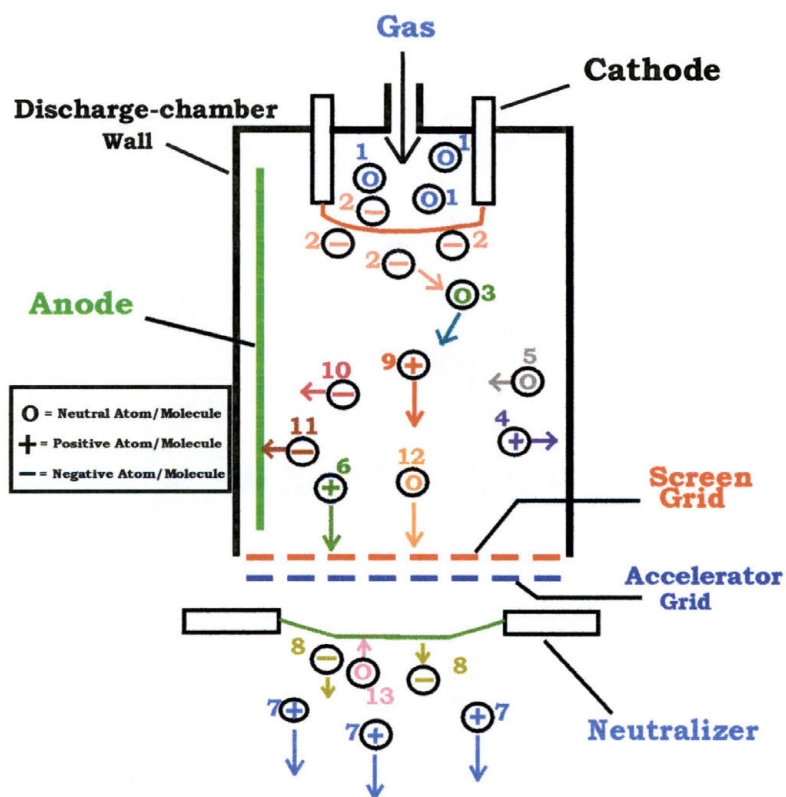


Figure 5-2: Discharge Chamber

Some of the ions (Figure 5-2 #4) produced by these collisions will travel to the surface of the chamber where they will be able to pick up an electron and become electrically neutral again. Most of these neutral atoms (Figure 5-2 #5) will then return to the center of the chamber. Other ions (Figure 5-2 #6) will be attracted by the negative potential of the accelerator grid and form into small beamlets. These beamlets will first travel through the screen grid, then the accelerator grid. They will then be accelerated towards the target. The screens of the two grids are arranged so that any ions passing through them will do so without striking either one. The ion beam (Figure 5-2 #7) is then formed from the individual beamlets after they leave the accelerator grid.

5.3.2 Neutralizing the Ion Beam

The ion beam is then neutralized by electrons from the neutralizer cathode (Figure 5-2 #8). The neutralized beam has equal densities of electrons and ions within the beam volume. The bulk of the energy in an ion beam is carried by the ions. The function of the electrons in the ion beam is to assist the ion beam as it travels from the discharge-chamber to the target through both charge and current neutralization. In charge neutralization, the positive charge of the beam ions is balanced by the presence of the electrons. Without this charge balance, the mutual repulsion of the ions would disrupt the ion beam by causing it to spread out. This neutralization simply means that, on the average, there are the same numbers of ions as there are electrons. It does not mean that

these electrons and ions have recombined, although on rare occasions this does occur. The normal result for an under-neutralized ion beam is that electrons are gradually lost until the beam reaches a high enough voltage to draw an arc, which gives off a visible flash. The arc draws in enough electrons to decrease the beam voltage to near normal.

When charge-neutralizing electrons are not only present, but also have the same average velocity as the ions traveling to the target, then current neutralization of the ion beam can occur. An excess of electrons can be drawn to an ion beam, but this is normally prevented by the fact that they will be drawn to any nearby electrically grounded hardware inside the work chamber. Current neutralization problems are thus caused by an insufficient number of electrons reaching the target. When the target is an insulating material or an electrically isolated conductor, an insufficient arrival rate for electrons will result in an increasing positive charge being built up on the target surface. The electrons are much lighter than the ions and will travel much faster to the target, even though the ions have much more energy. In order for the electron arrival rate at the target to be reduced to the ion arrival rate (which will produce a much more uniform sputtering of the target), a negative sheath forms at the target. This occurs naturally by the ion beam becoming a few volts more positive than the target.

The energetic electrons (Figure 5-2 #2), ions (Figure 5-2 #9), and low-energy background electrons in the discharge-chamber (Figure 9-2

#10) volume make up what is known as an electrically conductive gas, or plasma. This plasma is nearly uniform in potential, typically varying across its volume by only 1-5 Volts. The electric potential of the plasma is typically only a few Volts higher than the anode potential. The anode is thus the electrode that most closely approximates the origin of potential for the ions.

If it is assumed that the target potential is close to the vacuum-chamber ground potential, the ion energy at the target will then be about the same as the beam-supply potential. The neutralizer is also at approximately ground potential, requiring the accelerator grid to maintain a negative potential in order to prevent any of the neutralizing electrons from flowing back into the discharge chamber.

5.3.3 Beam Behavior

Once the plasma passes through the ion optics and is neutralized, it then travels to the target. The pressure in the discharge chamber is normally low enough that the average distance an ion or molecule will travel before it collides with another gas molecule or atom is much larger than the physical size of the discharge chamber. To raise the probability of a working gas atom being neutralized by an energetic electron (Figure 5-2 #2) before it escapes to the anode, a magnetic field is placed between the cathode and the anode. While this magnetic field is designed to contain these energetic electrons, the low-energy background electrons (Figure 5-2 #10) can sometimes diffuse across the magnetic field with

little or no hindrance. These low energy electrons thus complete the current between the cathode and the anode when they reach the anode.

By operating the system at a low pressure, gas backflow from the vacuum chamber into the discharge chamber can occur. The gas normally flows from the gas inlet port to the ion source, through the two grids and into the vacuum chamber. Since the distance between collisions is so large, the outgoing atoms or molecules (Figure 5-2 #12) rarely collide with the incoming atoms or molecules (Figure 5-2 #13). This means that if a different gas is added to the vacuum chamber than is being used in the discharge chamber, this gas will be mixed in the discharge chamber as well.

Interactions with the background gas in the work chamber can modify the ion beam during its passage to the target. Charge can be transferred, through collisions, to neutral atoms in the work chamber, producing electrically neutral but still energetic atoms. These atoms tend not to react with the target surface. In addition, the momentum of the ions in the plasma can be affected by collisions within the beam itself. While these collisions can cause the beam to spread, simply keeping the beam voltage above 100 Volts prevents this event from occurring.

5.3.4 Target Interactions

Once the ion beam reaches the target, a number of processes can occur. The most important process where this system is concerned is sputtering. Sputtering due to ion bombardment can be divided into physical sputtering and reactive sputtering. In physical sputtering, material is removed from the surface of the target as a result from a simple momentum transfer. Ions hit the target with so much energy that they literally knock individual atoms off the surface of the target. In reactive sputtering, the formation of a chemical compound also plays an important role in the removal of atoms from the target.

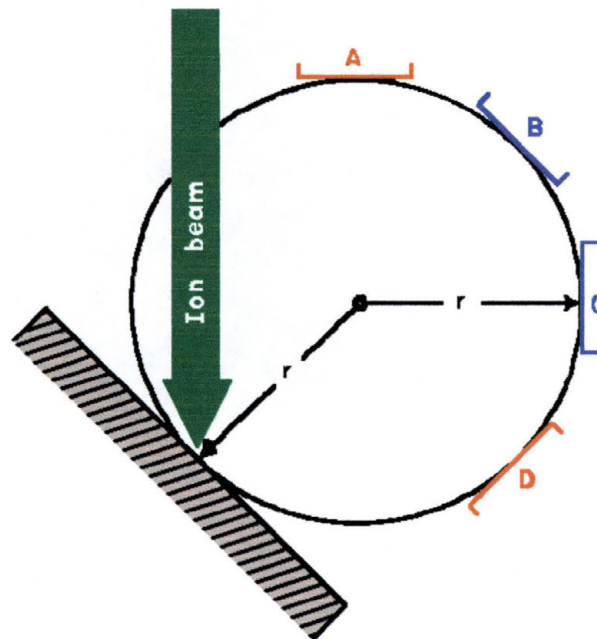


Figure 5-3: Target Atom Distribution

The sputtered atoms leave the target with a relatively even distribution of energies. The peak of this distribution is energies of several electron-Volts. The physical path that these sputtered atoms travel is also known as the spatial distribution, and follows a rough cosine of the angle relative to a line drawn perpendicular to the target surface (see Figure 5-3). Locations A, B, C, and D are regions where the sputtered target atoms would be most likely to travel. Since the ultimate goal is to have these sputtered atoms travel to the surface of a wafer and stick to it (film growth), these would appear to be good locations for the placement of a wafer. There is, however, good reason not to choose locations A or D. Location A is too close to the incident ion beam, and is likely to block part of that beam and become a source of contamination due to collisions with the substrate (the wafer) and the hardware needed to hold the substrate at any given location. Location D is too close to the forward sputtering position and would probably show a highly non-uniform deposition and film properties. Since the goal is to be able to accurately reproduce any films grown with a high degree of accuracy, this is not a good location. Thus, locations B and C are therefore good locations for uniform film deposition.

5.3.5 Film Growth

As the atoms from the target approach the surface of the substrate, they will start to condense and form a film. These atoms are now referred to as adatoms, and the process is known as nucleation. Nucleation follows one of three types of film growth: island growth, layer growth, and Stranski-Krastanov growth.

In island growth, when enough adatoms reach the surface, they will form small but highly mobile clusters or islands (see Figure 5-4 on next page). The formation of these islands occurs when the adatoms are more strongly attracted to each other than to the substrate. The islands continue to grow three-dimensionally until they saturate the surface of the substrate. Once this occurs, the islands will start to merge with each other similar to the way droplets of water will merge, in a kind of coalescence. If the temperature of the substrate is high enough the rate of coalescence will be increased. As the islands join, areas at the edges of the islands will become exposed as the bulk of the islands move toward each other during the coalescence process. Nucleation can then occur on the re-exposed substrate. The coalescence effect continues until the surface of the substrate becomes like a series of connected (but unfilled) channels. New adatoms will then start to fill in the channels causing them to shrink in size until; finally, they are completely filled in.

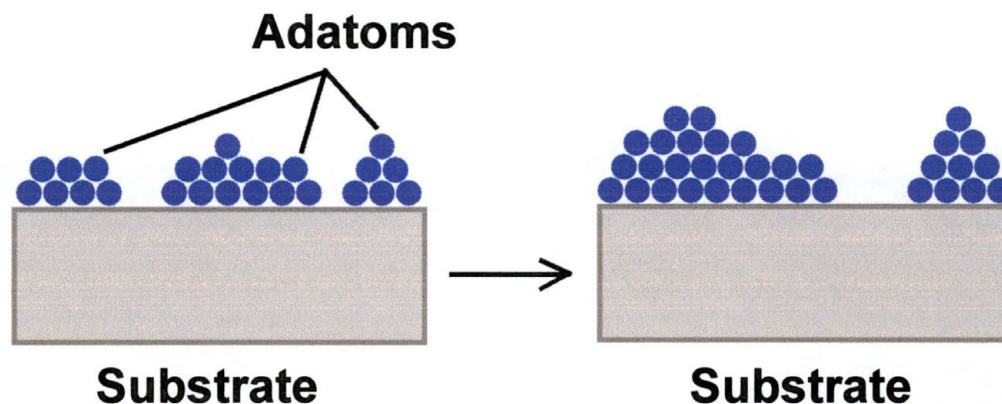


Figure 5-4: Island Formation

In layer growth (see Figure 5-5), the adatoms will feel a stronger attraction to the substrate than to each other. Most adatoms will grow as a sheet of atoms onto the surface of the substrate. When a completely filled plane of atoms (known as a monolayer) is formed, the new adatoms will then start to form a new monolayer. The second monolayer, and each subsequent monolayer as well, will not be bound as tightly as the first monolayer because the adatoms will not be as tightly bound to each other as they were to the substrate.

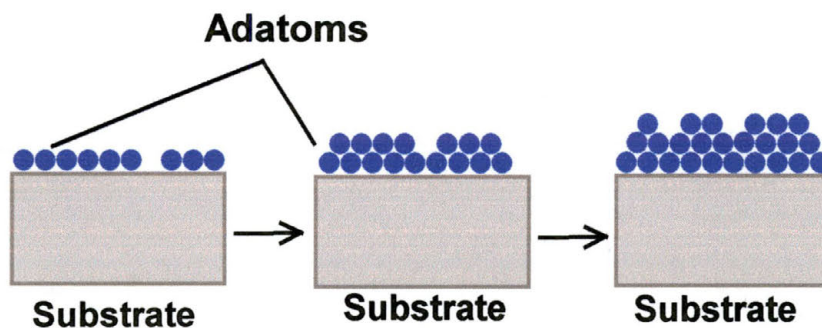


Figure 5-5: Layer Growth

In Stranski-Krastanov (S-K) film growth (see Figure 5-6 on next page), what occurs is a combination of island formation and layer growth. This is the most common form of film growth seen. Normally, a full monolayer of adatoms will form on the surface of the substrate as a layer growth. The new adatoms will then tend to undergo island growth. The exact reasons for this type of growth are not completely understood, but it is believed that this type of growth occurs as a result of the bonding between the atoms of the substrate and the adatoms. As the adatoms bond to the substrate, unnatural angles will be formed in the adatom-adatom bonds that will cause the crystal lattice of the first monolayer to be under a lot of strain. Think of a sealed glass jar filled to the top with water. When the jar is placed in a freezer, the atoms of the water will form a crystal structure commonly known as ice. The bonds between the atoms of water are so strong that the crystal structure of ice is stronger than the crystal structure of the glass the jar is made from. The result is that the jar will break. When subsequent adatoms impact the first layer, the bond energies of the adatom-adatom bonds is strong enough to overcome the strain in the crystal structure of the first monolayer allowing the adatom-adatom bonds to form at angles that have much less strain on them. This results in island growth after the first monolayer has been formed.

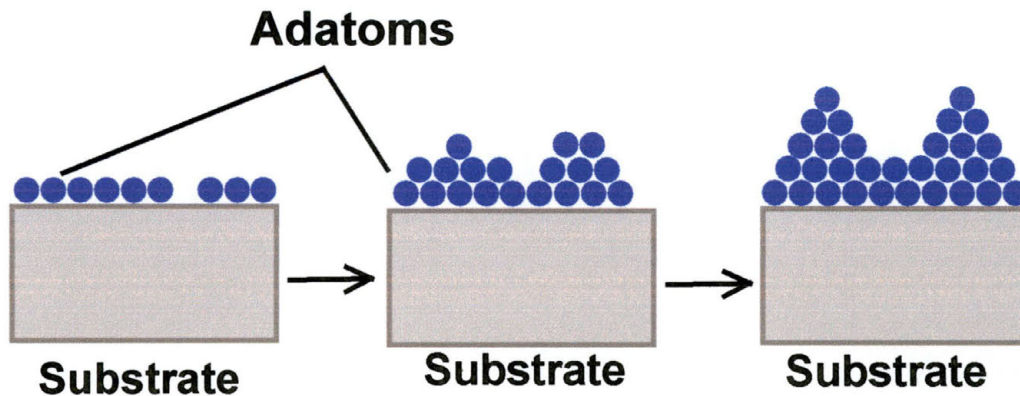


Figure 5-6: Stranski-Krastanov Film Growth

5.3.6 Second (Dual) Ion Beam

It is because of the S-K growth characteristics that the second ion beam is used in a DIBS system. The second ion beam is known as the assist beam. By having a second, much lower energy, plasma focused at the surface of the substrate (see Figure 5-7 on next page), ions of low energy (typically 50 electron-volts) will be impacting the islands of adatoms. These ions can then transfer their energy, in a simple momentum transfer process, to the adatoms. The ions then allow the adatoms on the tops of the islands to “hop” off the island and fill in the spaces or channels between them. This will occur until all the spaces are filled and a complete layer of atoms is present. The result is a more even distribution of adatom deposition and a more uniform film growth.

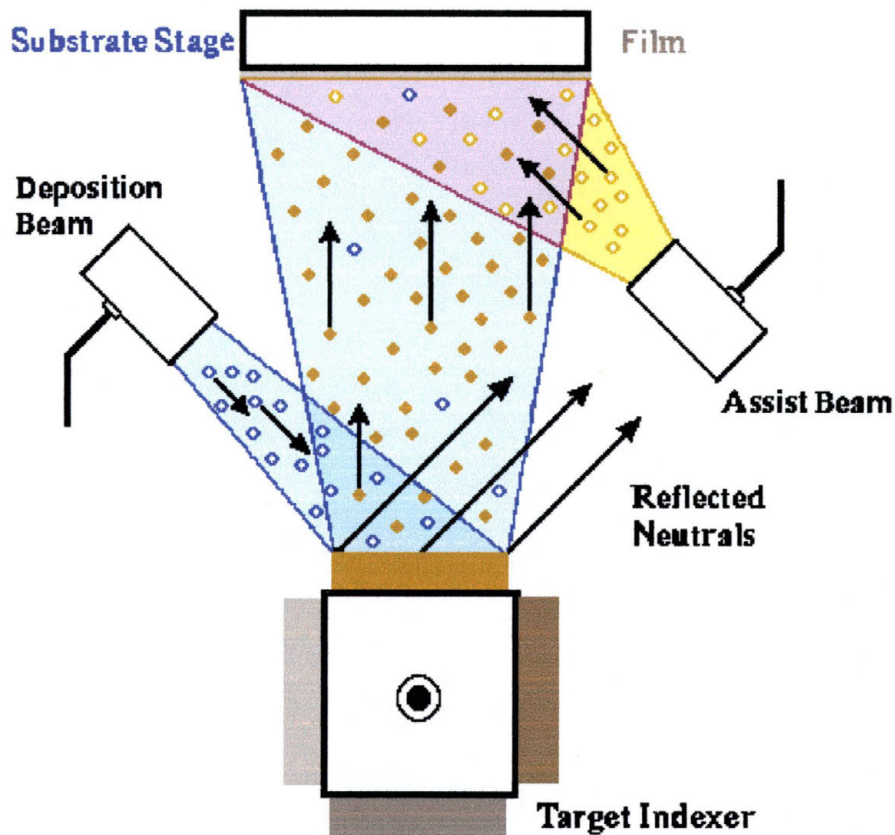


Figure 5-7: Dual Ion-Beam Sputtering System

This can be thought of as occurring like this: Take a handful of sand and drop it slowly onto a plate with high edges. Drop the sand so slowly that only a few grains fall every second. As the first grains of sand land on the plate, they will bounce around the plate and spread out until the edges of the plate stop them from spreading any more. As more sand falls, it will then be stopped by the sand that is already on the plate. Once the grains of sand have covered the plate, they will start to land on top of this layer. Since the grains form a layer that is much more rough

than the plate, the result is that the sand will start to pile up until you have a cone-shaped “island” of sand in the center of the plate. Now, shake the plate. What happens is that by shaking the plate, you are transferring kinetic energy to the grains of sand. As they obtain more energy, they are able to “hop” around. The “hopping” results in a smoother layer of sand left on the plate than when you first deposited the sand. Now think of the adatoms as the grains of sand and the plate as the substrate. When you apply the second ion beam to the surface of the substrate, it transfers energy to the atoms in a manner similar to the way energy was transferred when you shook the plate. This extra energy is what allows the adatoms to “hop” off an island and fill in the spaces between the islands.

Another benefit of using a second Kaufman source is the ability to add elements to the composition of the film as it is being grown. I mentioned earlier that the most commonly used gas for creating the ion beam plasma is Argon, which is a noble gas. Noble gasses are known for being chemically inert- i.e. they do not want to react with anything. What would happen if you used something that is chemically very reactive incorporated into the Argon plasma, like Oxygen? The oxygen atoms would be ionized just like the Argon gas and would travel to the substrate surface. Then, since oxygen is so reactive chemically, instead of just transferring kinetic energy to aid in the smoothing of the monolayers, the oxygen atoms would bond with the adatoms and become

an incorporated ingredient in the film that is being produced. This method of adding elements to the film being grown would be desirable because it would tend to keep the target from becoming contaminated. In an ion-beam sputtering system with only one ion beam, in order to incorporate another element into the film, that element would be ionized along with the sputtering gas and would then travel towards the target. Some of the ions would cause sputtering, but some would become incorporated into the target itself. If the next time you produced a film you did not want to have the second element incorporated into the film, this would be a problem as the contamination atoms would be sputtered along with the target atoms, even if only Argon was used to create the plasma.

The thickness of the film that is grown is controlled by a number of factors. The two most important of which are the substrate temperature and the length of time that the ion beam is allowed to strike the target. The temperature of the substrate directly affects the coalescence, as describe earlier. The correlation between the length of time that adatoms are allowed to bombard the substrate and the thickness of the resulting film is straightforward. The longer the ion beam is allowed to knock atoms off of the target, the more atoms there will be to grow a film and the thicker the resulting film will be. Once the film has been grown, the next step is film characterization which will be dealt with in the next few chapters of this thesis.

6 Vibrating Sample Magnetometry

6.1 Basic Operation

Vibrating Sample Magnetometry is a computer controlled measuring system capable of characterizing a wide variety of magnetic samples. If any material is placed in a uniform magnetic field, a dipole moment will be induced in the sample proportional to the product of the sample susceptibility and the applied magnetic field. This applied field may be produced by an electromagnet. If the sample is made to undergo sinusoidal motion (i.e. vibrations), the resulting magnetic flux changes near the sample will induce an electrical signal in stationary coils if those coils are placed such that the sample is always between them. This signal will be proportional to the magnetic moment, amplitude, and frequency of vibration.

A schematic diagram of a typical VSM set-up is shown in Figure 6-1 on the next page. The material under study in the VSM is inserted in the sample holder so that it rests centered in a pair of pickup coils between the poles of an electromagnet. The sample holder is mounted using a sample rod in a transducer assembly that passes through the center of a driving coil. The transducer is driven by a power amplifier which itself is driven by an oscillator. The magnetic sample under study is constrained such that it vibrates only along the vertical axis. As it does

so, it induces a signal in the sample pickup coils. The magnitude of this signal will be dependent on the magnetic properties of the sample itself.

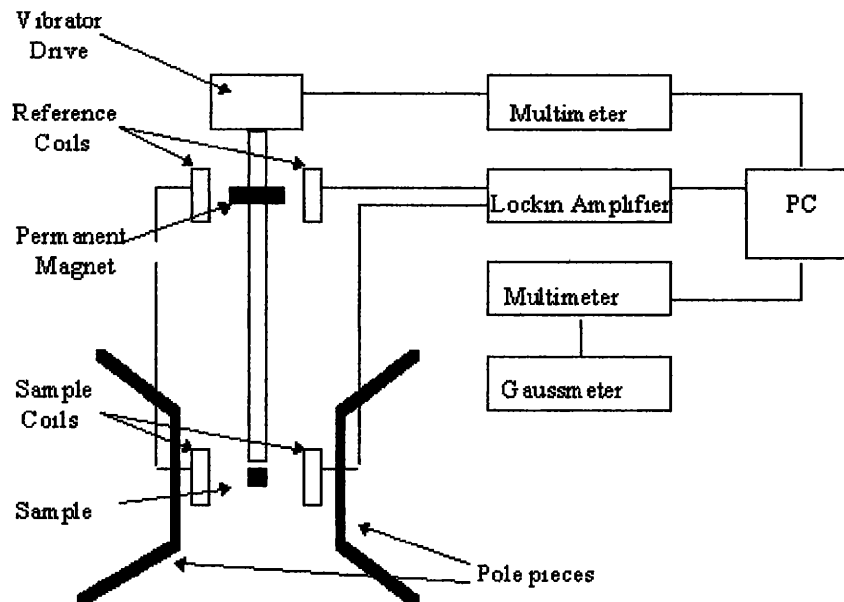


Figure 6-1: Schematic Diagram of a Typical Vibrating Sample Magnetometer³⁵

Attached to the sample holder rod is a permanent magnet. A pair of stationary coils picks up the induced ac signal, which is proportional to the amplitude and frequency of the vibration and is used as a control signal for modulation of the transducer. The output of the sample coil is then fed to the differential input of a lock-in amplifier. The reference input of the lock-in amplifier comes from the sine wave oscillator used to drive the sample holder. The output of the lock-in amplifier goes to the data acquisition computer in addition to the magnitude of the applied magnetic field coming from a gaussmeter. The signal from the lock-in amplifier will be directly proportional to the magnetic moment of the

sample. The computer is then able to graph the magnetic moment of the sample against the applied magnetic field. The system is usually calibrated using a single crystal nickel sample whose saturation magnetization is well documented.

6.2 Calculation of Film Thickness Using VSM

To find the magnetization M_s of the magnetic samples produced for this thesis, the following equation was used from Magneto-Resistive Heads: Fundamentals and Applications by John C. Mallinson:

$$M_s = \frac{x \times \mu_B \times y}{z^3}$$

Equation 6-1: Magnetization Equation

where: x = number of Bohr magnetons per atom, $\mu_B = 9.27 \times 10^{-21}$ emu, y = the number of atoms per unit cell, and z = the lattice constant for the unit cell in Angstroms. The data for x , y and z was obtained from Ferromagnetism by Richard Bozorth and is as follows:

A) x : (from Figure 6-2) with 82% Ni in the mix, you get a value of ~1.02 Bohr magnetons per atom.

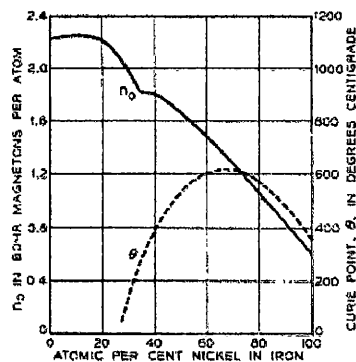


Figure 6-2: Bohr Magnetron Number and Curie Point of Iron-Nickel Alloys

B) y: From the fact that we have a predominantly fcc crystal structure, you get an equivalent value of 4 atoms per unit cell. From Figure 6-3 it can be seen that the unit cell of an fcc structure has one atom at each corner of the cell and one atom in the center of the face of each “wall” of the cell. The four atoms of the corners are shared by the adjacent cells such that only one-fourth of each of them “belongs to the unit cell, for a total of one equivalent atom. In addition, there are six faces of the unit cell, each having an atom positioned in its center. These atoms are shared equally by the adjacent unit cells for a total of six halves, or three equivalent atoms. Add these three to the one equivalent atom from the corners and you get four equivalent atoms.

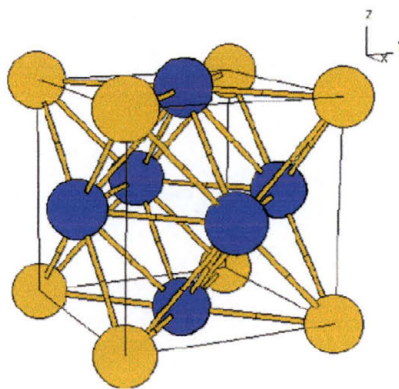


Figure 6-3: Face-Centered Cubic (fcc) Crystal Structure³

C) z: (From Figure 6-4 on the next page) With 82% Ni at $\sim 15^{\circ}\text{C}$ you get a lattice constant of approximately 3.5375 \AA .

When all of this data is plugged into Equation 6-1, you get an $M_s = 854.38 \text{ emu/cm}^3$. The density of Si is $\rho = 2.3283 \text{ g/cm}^3$ and can be found in any number of physics and chemistry references.

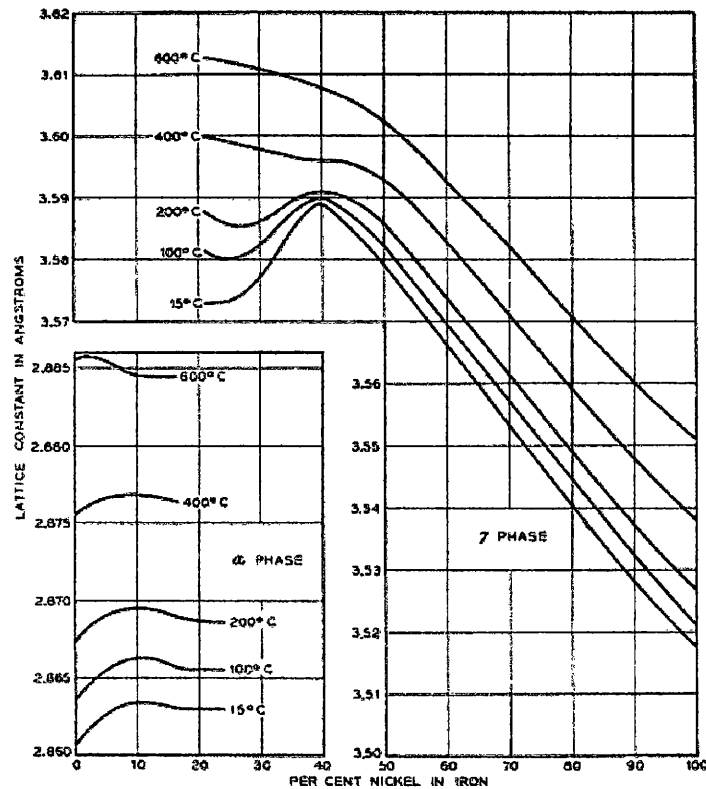


Figure 6-4: Lattice Constants of Fe-Ni Alloys in the bcc and fcc Condition ³⁸

The thickness of the substrate plus the thickness of the film was measured 20 times randomly using an electronic caliper from different locations on various samples and “crunched” using a TI-85 to arrive at 0.0501 cm with an error of 0.012751.

The volume was calculated by dividing the mass of the samples by the density and is given in the Table 1 on page 106 . The area was then determined by dividing the volume by the thickness and is also given in

Table 1. The thickness of the film was then found using the following equation:

$$t = \frac{(\text{Strength} - \text{of} - \text{Magnetic} - \text{Field})}{M_s \times (\text{Area} - \text{of} - \text{Film})}$$

Equation 6-2: Thickness Determination from Magnetic Data

All of the data for the magnetic films I produced for this thesis is listed in Table 1 on the next page. Robert Dail's (a former graduate student of SWT) film was used to calibrate the procedures. The Dail film chosen has a known thickness (from previous VSM and from XRF analysis) of 500 Å.

The analysis for calculating the thickness of the films was performed on May 15, 2001 and again on April 4 and 6, 2002. The reason for this is that once the Bede D-1 x-ray analysis tool was operational and data was being collected on it, the thickness of the films as determined through x-ray analysis did not match that of the VSM data. It was then learned that the sample holders for the VSM were contaminated through many years of use, and all the old data was thus considered suspect. The new data was measured to compare the differences in the thickness of the films using new sample holders. The differences in the results are shown in Table 1 in the columns labeled Mag. Strength (emu) and Thickness (Å). The new data is listed first,

followed by the old data. Note that there are significant differences in the calculated thickness of many of the films.

Film	Gas Used	Growth Time	Mass (g)	Volume (cc)	Area (cm ²)	Mag. Strength (emu)	Thickness (cm)	Thickness (Å)
Dail	???	???	0.2798	0.12017	2.40	8.934E-3	5.25E-6	525
010312	Ar	1200						
010314	Ar	600						
010315	Kr	1200 sec (@ 150C)	0.2563	0.11008	2.20	0.0301 \ 0.02964	1.57E-5	1538 \ 1570
010319	Kr	600 sec (@ 150C)	0.2661	0.11429	2.29	0.0139 \ 0.0141	7.68E-6	710 \ 768
010505A	Ar	600 (@ 21-24 C)	0.1966	0.08444	1.69	0.0054 \ 0.0099	7.90E-6	373.9 \ 790
010505B	Ar	1200 (@ 24-28 C)	0.2339	0.10046	2.01	0.0123 \ 0.0215	1.26E-5	716.2 \ 1260
010506A	Kr	600 (@ 26-28 C)	0.2598	0.11158	2.23	0.0067 \ 0.01189	6.40E-6	351.6 \ 640
010506B	Kr	1200 (@ 21-27 C)	0.25630	0.11008	2.20	0.0121 \ 0.0228	1.25E-5	643.7 \ 1250

Table 1: VSM Data

6.3 Magnetic vs. Non-Magnetic Films

There are many marked differences between a magnetic material and a non-magnetic material. The most common, of course, is that magnetic materials behave in ways that almost everyone is familiar with... magnets attract and repel each other. For the purposes of this thesis, however, another characteristic of magnetic materials is of much

more importance, the hysteresis curve. In Figure 3-15 on page 68, an example was shown of a typical hysteresis curve for a magnetic material. As was just described, in the characterization of films for my thesis research, VSM was used to determine the film thickness of some of the films.

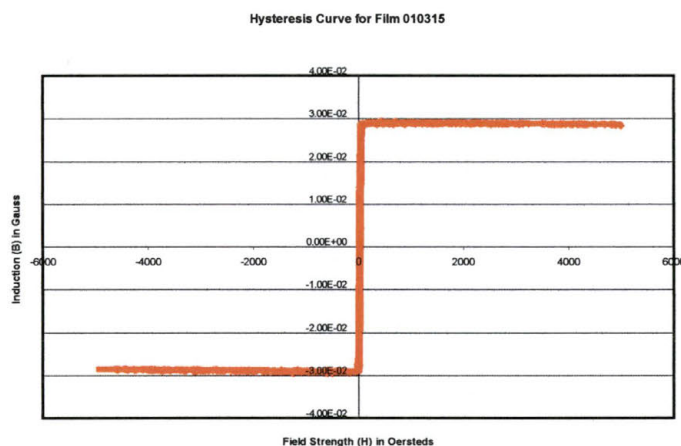


Figure 6-5: Hysteresis Curve for Magnetic Py Film

Figure 6-5 shows the hysteresis curve for a representative magnetic Py film grown in my research. Note that the curve passes directly through zero (one of the properties of Py films discussed in section 3.8 on page 68). Also note that the saturation of the film is achieved rather quickly, an indication of how easy it is to magnetically saturate the material.

Now look at Figure 6-6 on the next page. This film's hysteresis curve looks nothing like the curve above. This is an example of a non-magnetic film. Note how there is no saturation point ever reached. Also,

notice how the induction does not change as the field strength is increased and decreased. These behaviors are both indicative of non-magnetic materials.

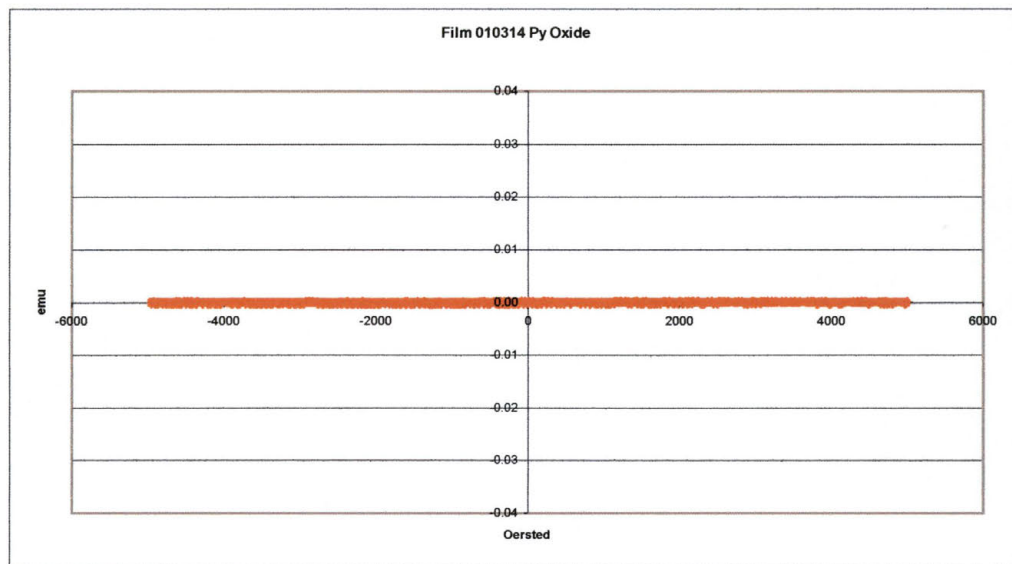


Figure 6-6: Hysteresis Curve for Non-Magnetic Material

The difference between magnetic and non-magnetic materials will be of great importance for the research involved in this thesis. With the production of the anti-ferromagnetic material FeO as one of the principle objectives, the characterization of the films by VSM will be of paramount importance.

7 X-Ray Analysis

X-rays are electromagnetic waves, similar in many ways to light, but having a much shorter wavelength than visible light. The unit of measurement used for describing x-rays is the Angstrom (\AA), which is equal to 1×10^{-10} meters or one-tenth of one billionth of a meter. The reason that x-rays are known to be similar to light is that they behave in many of the same ways that light does: they can be diffracted, they can be reflected, and they can be absorbed. The typical length of visible light has a wavelength around 6000\AA whereas an x-ray wavelength measures from 0.5 to 2.5\AA . Because of their small wavelength, x-rays can be used to obtain information about objects that have sizes ranging from 0.5\AA to 2.5\AA , which just happens to be the typical size of the spacing between atoms in a crystal lattice.

7.1 Properties of X-Rays

When an electric charge, such as an electron, is accelerated or decelerated, it radiates electromagnetic energy. When the electrons strike a sample, often called a target, they are slowed down and eventually come to rest. This is because they are interacting with the atoms of the target, colliding with them and bouncing off in all directions until they run out of energy. When such collisions take place, the momentum that the traveling electrons originally possess is transferred to the target atoms. Since the atom is so large compared to the size of the electron the recoil energy of the atom can be ignored, much like if you rolled a golf ball at a bowling ball. The bowling ball will not move very much, if at all.

There is, however, an interesting phenomenon that occurs, due to the principles of quantum mechanics. The electrons that orbit the atom do so in very distinct energy levels. If a traveling electron has a given amount of kinetic energy before it collides with an atom and has a distinctly lower kinetic energy after it collides, then it has transferred some of its

energy to an electron orbiting the atom. Most of this kinetic energy of the traveling electron (more than 99%) will be absorbed into the target as heat. A small percentage of that energy however, will go into the production of x-rays.

7.1.1 Production of X-Rays and Characteristic X-Rays.

X-rays are produced whenever an electrically charged particle having enough kinetic energy to produce an x-ray decelerates rapidly. As mentioned before, Electrons are the most common source of charged particle used for this purpose.

When an electron passes near an atom, a number of possible interactions can occur. The one we are most interested in here, is one that ultimately leads to the production of x-rays. As the electron passes close to the atom (red dot in Figure 7-1), it transfers some of its momentum to the electrons of that atom.

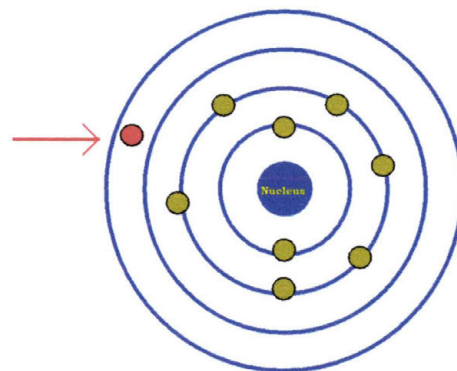


Figure 7-1: Incoming Electron

If the incoming electron has a minimum amount of energy (an amount which varies depending on the incident atom), then the energy transferred to the atom will allow one of the electrons orbiting that atom to obtain enough energy to break free of the atomic bond and become a free electron (orange dot in Figure 7-2).

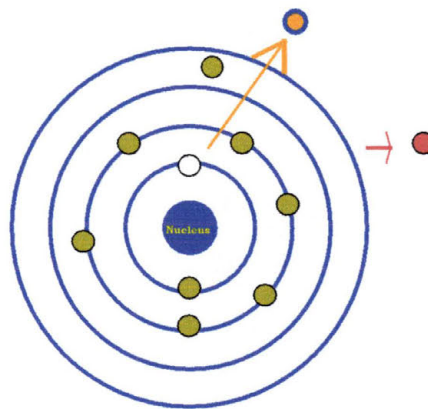


Figure 7-2: Electron Escaping from Parent Atom

This process creates a vacancy in the shell from the electron that just left it causing a condition that is a very unstable energy state for the atom. In order to stabilize the atomic energy state, an electron from a higher energy shell (having more energy than the ejected electron originally possessed) will then fill the vacancy left by the freed electron. In order to do this, the falling electron must get rid of some of its energy. According to the laws of physics, energy can neither be created nor destroyed, only transferred from one energy state

to another. In the case of an electron filling a vacancy, what occurs is that the falling electron will emit a little packet of energy known as a photon (see Figure 7-3). If the photon emitted has enough energy (defined by its wavelength), it is known as an x-ray.

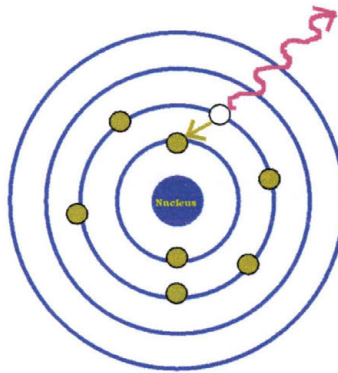


Figure 7-3: X-Ray Emitted as Electron Fills a Vacancy

Electromagnetic radiation, such as a beam of x-rays, carries energy. The rate of flow of this energy through a unit area perpendicular to the direction of the motion of the wave is called the intensity, I . The average value of the intensity is proportional to the square of the amplitude of the wave. According to classical physics³⁶, the spectral profile of a single x-ray emission line can be described by the following equation:

$$\frac{I(\omega)}{I(\omega_o)} = \frac{1}{1 + [(\omega - \omega_o)b]^2}$$

Equation 7-1: Spectral Profile of Electromagnetic Radiation

where ω is the frequency and b^{-1} is a constant equal to $e^2\omega_0^2/2mc^3$. This derived spectral distribution is a Cauchy distribution with a universal profile width of $1.18 \times 10^{-4}\text{\AA}$.³⁴ According to wave mechanics the spectral profile is symmetric, however, in actuality the profile width is dependent upon the sum of the total probabilities of spontaneous transitions from the upper and lower energy states.³⁷ In fact, the profile widths of x-ray emission lines are more broad than $1.18 \times 10^{-4}\text{\AA}$ and are not completely symmetrical at all.

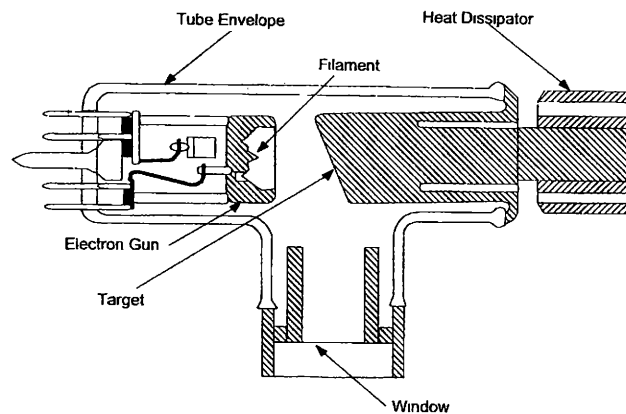


Figure 7-4: Example of a Typical X-Ray Source

To produce x-rays, the most common method today is to employ the use of an X-Ray gun. A typical example is given in Figure 7-4. Any x-ray source must contain a source of electrons, a high-accelerating voltage, and a metal target. In addition, since most of the kinetic energy of the electrons is

converted into heat in the target, the target must have some sort of cooling mechanism, usually just circulating water.

Typically, an x-ray source contains two electrodes, an anode (usually made of copper, Cu) which is usually kept at ground potential, and a cathode which will have an electric potential of approximately 50,000 volts applied to it. The high electric potential is necessary to accelerate the electrons that will be emitted from the cathode to a very high speed, thus ensuring that they will have enough energy when they enter the target to produce x-rays.

The electrons are produced in a filament, which is usually a glass tube that has a vacuum drawn inside of it. The glass helps to insulate the cathode from the anode. A current of around 40 milli-Amps is passed through the metal of the filament (usually made of tungsten) heating the wire. As it glows white hot, it will emit a constant stream of electrons. A section of metal surrounding the filament is kept at the same voltage potential as the filament. This section, having the same potential as the filament, will cause the emitted electrons to be repelled away from it and accelerated towards the metal target. The surrounding metal not only accelerates the electrons, but it also serves to focus the beam of electrons into a very small area of the target metal, known as the focal point. The x-rays,

produced when the beam of electrons impacts the target, are emitted from the focal spot in all directions. Most of these will strike other parts of the x-ray gun and be absorbed. A small percentage of them will, however, travel towards the window seen in Figure 7-4 which is essentially transparent to x-rays. They will pass right through it in a collimated beam directed towards whatever the window is pointed at.

7.1.2 Characteristic X-Rays

As mentioned before, the energy of the x-rays when an electron collides with the target is very characteristic of the elements the target is made from. This is due to principals of quantum mechanics that will not be dealt with in too great a detail in this thesis. A little bit of an explanation, however, is needed to fully describe the monochromatic beam of x-rays that is typically desired for x-ray analysis.

The origin of the characteristic x-ray spectrum is the atoms of the target material. Using the simplified Bohr model of the atom (see Figure 7-5 on the next page), one can think of electrons orbiting the atom at distinct locations.

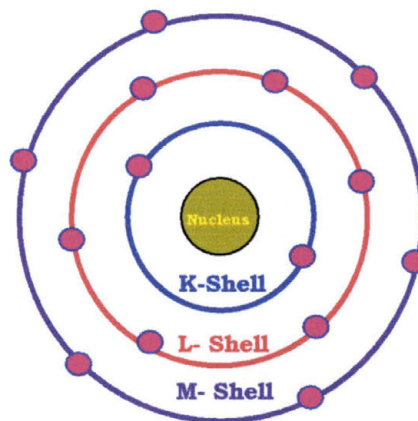


Figure 7-5: Bohr Model of a Silicon Atom

These locations depend on the energy that the electrons possess as they orbit the nucleus. Those electrons with a higher energy level will be orbiting the atom at a greater distance from the nucleus, while those with a lower energy level will be closer to the nucleus. This is because the higher energy electrons have more of the energy they would need to escape from the atom's nucleus, but not quite enough to do it. It's also why it takes less energy to excite a higher shell electron enough to make it a free electron than it takes for a lower shell electron. When an incoming electron collides with the atom, provided it has enough energy, it will knock an electron out of the K-shell, leaving the atom in an excited energy state (see Figure 7-2 on page 112). One of the outer shell electrons immediately falls into the vacancy created when the K-shell electron escaped (see Figure 7-3 on page 113). As the outer shell electron falls into

the vacancy, it will emit energy in the process allowing the atom to return to its least energetic state. The energy emitted when this happens has a distinct wavelength, and hence a distinct energy, that is characteristic of the target atom.

This energy value is so well quantified that the x-rays can be characterized not only by the element from which they originated, but by the shell containing the original vacancy and the shell from which the vacancy was filled. If the vacancy was from a K-shell electron, then the energy of the emitted x-ray is called a K-line (in reference to where on an energy spectrum the energy would lay). This can be further classified by the fact that if the electron that filled the K-shell vacancy originated in the L-shell then the x-ray is called a $K\alpha$ line. If the electron that filled the K-shell vacancy originated in the M-shell, the x-ray line is the $K\beta$ line (see Figure 7-6 on the next page). Each of these “line” energies has a different value and will thus show up at a different location on an energy spectra.

It is possible to fill a K-shell vacancy from the L-shell or the M-shell, or even from the N, O, or P-shell, however, it is considerably more probable that the vacancy will be filled from the L- or the M-shell making the production of a $K\alpha$ or a $K\beta$ line x-ray much more likely.

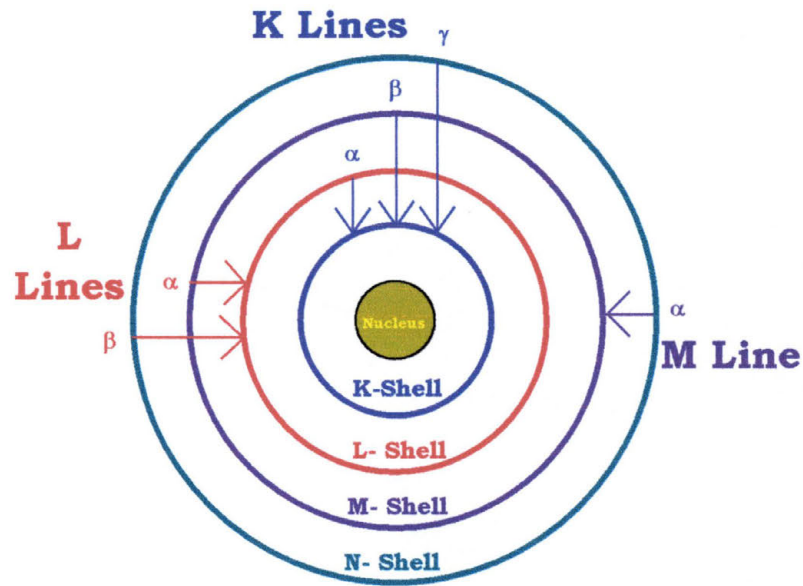


Figure 7-6: Characteristic X-Ray Lines

The intensity of any characteristic line, when it is measured above the continuous spectrum of background radiation, depends on both the filament current and the amount by which the applied voltage exceeds the critical excitation energy for the electrons orbiting the atom. For a K line, the intensity is given by:

$$I_{K-Line} = B \cdot i \cdot (V - V_K)^n$$

Equation 7-2: Intensity of K Line X-rays

Where B is a proportionality constant, V_K is the excitation voltage, V is the voltage of the x-ray source, i is the current in the filament, and n is a constant with a value of about 1.5.³⁸

The intensity of a characteristic line can be very large. As an example of how large, in the radiation from a copper target at 30 kilo-Volts, the $K\alpha$ line radiation has an intensity about 90 times that of the wavelengths immediately to the right and left of it on the continuous spectrum. Besides being very intense, characteristic lines are also extremely narrow, measuring less than 0.001\AA when measured across the peak at half of its maximum intensity (known as Full Width-Half Max, or FWHM). The existence of this very strong and extremely narrow line, the K line, is what makes much of x-ray analysis possible, especially if that analysis requires a monochromatic radiation.

7.1.3 X-Ray Characterization

Now that I have mentioned these characteristic lines, and mentioned that they can be seen on an x-ray spectrum, just what exactly are these lines and how can they be quantified? The energy of an x-ray photon can be quantified in one of two ways: 1) by its particle nature, and 2) by its wave nature.

When discussing the particle nature of an x-ray, the equation used to describe the behavior of an x-ray is:

$$E = h \cdot \nu = \hbar \cdot \omega = h \cdot \frac{c}{\lambda}$$

Equation 7-3: Particle Nature of X-ray Photons

where : h is Planck's Constant = 6.63×10^{-34} *Joule-sec*, \hbar Planck's constant divided by 2π , ν is frequency velocity, ω angular frequency, c is the speed of light in a vacuum, and $E \cdot \lambda = 12400$ eVÅ. The typical range of energy for an x-ray is from 12.4 eV to approximately 1.24 keV.

When discussing the wave nature of an x-ray photon, the way to describe it is by using a set of equations known as Maxwell's equations, after James Clerk Maxwell, the Scottish physicist who discovered the special relationships that describe electromagnetism. Maxwell's equations are really three equations discovered by Charles Coulomb, Jean-Baptist Biot along with Félix Savart, and Michael Faraday, to describe the fundamental properties of electromagnetism plus one equation that Maxwell discovered was the generalized form of a specific law discovered André Ampère. Maxwell's equations relate electric and magnetic fields to each other and to their ultimate source: electric charges.

The theory developed by Maxwell in the late 1870's was even shown by Albert Einstein in 1905 to be in agreement with the special theory of relativity. It predicts the existence of

electromagnetic waves, which travel with the speed of light and are radiated by accelerating charges. The four equations that make up Maxwell's equations are:

1. Coulomb's Law: $\nabla \cdot \vec{E} = \frac{\rho}{\epsilon_0}$ which shows that an

assembly of charge generates a steady electric field.

2. Biot-Savart Law: $\nabla \cdot \vec{B} = 0$ which refers to a steady

state magnetic field.

3. Faraday's Law: $\nabla \times \vec{E} = -\frac{\partial \vec{B}}{\partial t}$ which says that a time-

varying magnetic field causes an electric field.

4. Ampère-Maxwell Law: $\nabla \times \vec{B} = \mu_0 \left(\vec{j} + \epsilon_0 \frac{\partial \vec{E}}{\partial t} \right)$ which

shows that a time-varying electric field causes a magnetic field.

When these equations are applied toward describing an x-ray photon, you arrive at what is known as the wave equation:

$$\nabla^2 \vec{E} = \frac{1}{c^2} \frac{\partial^2 \vec{E}}{\partial t^2}$$

Equation 7-4: The Wave Equation

When the wave equation is solved to find the wave vector, it differentiates to the form:

$$\vec{E}(\vec{r}, t) = \vec{E}_o e^{i(\vec{k} \cdot \vec{r} - \omega t)}$$

Equation 7-5: Solution to the Wave Equation

where E_o is the energy of the wave, k is the wave vector, r is the direction vector of the wave, ω is the frequency of the wave, and t is time. This equation can be solved to find the wave vector, k , which can then be used to find the wavelength by the equation:

$$|\vec{k}| = \frac{2\pi}{\lambda}$$

7.1.4 Absorption

These equations serve to describe how an x-ray photon will travel in space with and without the influence of electromagnetic fields. But for the purposes of this thesis, what is of more concern is what occurs to an x-ray when it interacts with matter. When x-rays interact with matter, they are partially transmitted and partially absorbed. The absorption process was described in section 7.1.1 to some degree and will be discussed further here. Incident x-rays will transfer some of their energy to electrons orbiting the nucleus of the target atoms. This causes electrons to be ejected in the same way that a fast moving electron does, causing K-shell electrons to leave a

vacancy in their shell. This free electron is called a photoelectron. When an L or M shell electron falls down to the K-shell and emits its own x-ray, the process is called fluorescence. The fluorescence yield, ω , for a material is given as:

$$\omega = \frac{\text{the number of atoms that emit K radiation}}{\text{the number of atoms with a K-shell vacancy}}$$

Equation 7-6: Fluorescence Yield

This process will be discussed in much greater detail in section 7.2.

It is also known that the intensity of an x-ray beam as it passes through any material is proportional to the distance it travels in that material. The equation used to describe the intensity of the beam contains a proportionality constant, μ called the linear absorption coefficient that is dependent on the material the beam is passing through, its density, and the wavelength of the x-rays that make up the beam. The intensity can then be described by the equation:

$$I_x = I_o e^{-\mu x}$$

Equation 7-7: Mass Absorption Equation

Where I_o = the intensity of the incident x-ray beam and I_x = the intensity of the transmitted beam after passing through a thickness x .

Because the linear absorption coefficient is proportional to the density of the material being bombarded by the x-ray beam, the ratio of one to the other, $\frac{\mu}{\rho}$, will be a constant independent of the physical state of the material. This ratio is known as the mass absorption coefficient and can be used in equation 7-7 as:

$$I_x = I_o e^{-\left(\frac{\mu}{\rho}\right)\rho x}$$

Equation 7-8: Mass Absorption Equation with Mass Absorption Coefficient

There are two methods by which matter absorbs an x-ray. The first is by scattering of the x-ray by atoms, in a manner very similar to the way that visible light is scattered by dust floating in air. This makes up a very small portion of the total absorption. The second method is known as true absorption and is caused by the electronic transitions within an atom. The second method is what was touched on at the beginning of this section. Just as a fast moving free electron can knock a K

electron from its shell, an incident quantum of x-ray energy can cause the emission of a characteristic x-ray, provided it has the same minimum amount of energy needed to excite a K-shell electron that a fast moving electron would need. When it is emitted by an incident x-ray, the ejected electron is called a photoelectron. Its associated emitted characteristic radiation is called fluorescent radiation.

The amount of energy needed by an x-ray can also be thought of in terms of its wavelength through the use of the quantum mechanical relationship:

$$h\nu_K = \frac{hc}{\lambda_K}$$

Equation 7-9: Frequency-Wavelength Relationship

where ν_K and λ_K are the frequency and the wavelength of the minimum K-shell absorption value. The term $h\nu_K$ is the energy of the x-ray. From this equation, it can be seen that there is an inverse relationship between energy and wavelength. If you have a higher energy, the x-ray will have a shorter wavelength. If you have a lower energy, the x-ray will have a longer wavelength.

In terms of absorption, if the wavelength of the x-ray beam is steadily lowered, raising the energy of the beam at the

same time, the absorption coefficient will go down. This is because the greater the energy of the incident x-ray beam, the more easily it will pass through a potential absorber without interacting with it. When this occurs, less and less of the incident x-rays will create an ejected photoelectron. If the wavelength of the x-ray beam is steadily increased, consequently lowering the energy of the incident x-rays, it will reach a point where it will no longer be able to excite K-shell electrons. It will still be able to excite L, M, etc. shells however. Continued lowering of the energy of the x-ray beam will eventually lead to a point where it will no longer be able to excite L-shell electrons, then M-shell, and so on and so on.

The net effect of knowing what energy is too much for an x-ray to become absorbed and what energy is too little for it to emit a photoelectron from each successive shell allows for the construction of an energy level diagram for the atoms of the target material. This energy level diagram can then be used to calculate the energy values of the characteristic x-ray wavelengths for the target material.

7.1.5 Detection of X-Rays

With all of this discussion on x-ray spectra, the energies of the characteristic x-rays, and energy levels, just how are these x-rays detected? There are a number of methods used for

the detection of x-rays: photographic film, Gieger-Meüller detectors, Everhardt-Thornly detectors, and scintillation detectors. The x-ray system used for this thesis was a Bede Scientific D-1 High Resolution X-Ray Diffractometer with an Enhanced Dynamic Range (EDR) scintillation crystal detector, so that is the type of detector that I will be describing here (see Figure 7-7).

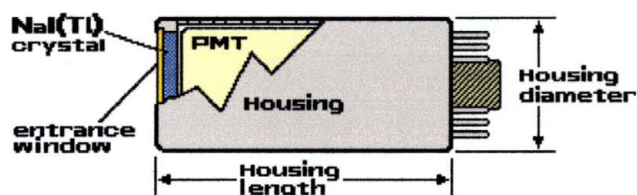


Figure 7-7: Example of a NaI(Tl) Crystal Scintillation Detector³⁹

A scintillation crystal detector is a detector that uses a crystal capable of absorbing x-rays and emitting a photoelectron which will then cause the emission of a photon of visible light when the atom de-excites. I have already discussed what happens when an x-ray is incident upon an atom, so I will explain a little bit more of how this is used in a detector.

The Bede EDR has a 0.5 mm thick beryllium window covering a Yttrium Aluminum Phosphide (YAP) crystal with an 18.0 mm diameter aperture. When an x-ray enters the window, it will interact with the YAP crystal with the end result that a photon of visible light will be emitted. This light will cause a

flash that will be registered by the Photo-Multiplier Tube (PMT). The PMT will then convert the flash of light into an electronic signal (a voltage potential) that some extremely sensitive electronics can then amplify and send to other electronics. The end result is that the x-ray will be counted.

The Bede EDR is specifically tuned to absorb and count x-rays with the $K\alpha$ energy emitted from Cu (8.1 keV). It is capable of recording 1,300,000 individual incident x-rays per second and has an intrinsic background count of 0.15 counts per second (cps).⁴⁰

This type of detector is not capable of dividing the spectra of the incident x-rays to tell you what element it came from. Characterization of the x-ray spectra is not really a concern when the goal is the characterization of the crystal structure of the material under analysis. What is of concern is the intensity of the diffracted x-ray beam so that interference (both constructive and destructive) can be monitored as the sample is analyzed. For this reason, a crystal scintillation type detector is ideal for use in diffraction and reflectivity x-ray analysis (both of which will be explained in greater detail in the following sections).

7.2 X-Ray Fluorescence

X-Ray fluorescence spectrometry has been used since the 1970s as a versatile method for many analytical problems. It allows for the analysis of major, minor, and even trace elements in a sample and it allows for qualitative as well as quantitative characterization. In addition to being a fairly rapid and accurate method for analysis, it also has the benefit of being a non-destructive analytical method. The fundamental physical principle upon which x-ray fluorescence is based is the interaction of a photon with matter at the atomic scale.

X-ray fluorescence can be applied in one of two methods: wavelength dispersive spectroscopy (WDS), and energy dispersive spectroscopy (EDS). In WDS, the important parameter to monitor and detect is the wavelength of the emitted radiation. This method requires the use of multiple detectors, each tuned for an optimal wavelength range. The largest advantage of this method is the excellent wavelength-to-energy resolution. EDS measures all the photons emitted from a sample at the same time using one detector. For the detector to operate optimally, it is usually cooled with liquid nitrogen. It has the advantage of being able to detect many elements in a very short time. This thesis discussion will focus on EDS since that is the type of tool available at SWT.

In both methods, knowledge of characteristic x-ray emission is central to the detection method and will be addressed here. The description given in section 7.1.2 of how a characteristic x-ray is created was a simplified description. It only described the interaction of one incident x-ray or electron causing the emission of a single electron from an atom, which then led to the emission of a single characteristic x-ray. A more realistic approach describes an incident beam of x-rays striking multiple atoms in a given sample. When this occurs, the emission of different characteristic x-rays and their intensities depend upon a number of factors. Three of the more important are: the absorption jump ratio, r ; the relative intensity, f , of a characteristic line within its series; and the fluorescence yield, ω . In the description that is about to be given, Equation 7-10 to Equation 7-15 come from "Quantitative X-Ray Fluorescence Analysis: Theory and Application" by Gerald R. Lachance and Fernand Claisse (1994- John Wiley & Sons).

7.2.1 Absorption Jump Ratios

In order for an element to emit a characteristic x-ray, the first thing that must occur is that its atoms must absorb a photon with sufficient energy to eject a K, L, M, etc. shell electron. As a result, it will be important to quantify each of these absorptions individually. The mass attenuation

coefficient for a given sample will be the sum of the attenuations from each energy level and is given by the following equation:

$$\mu = \mu_K + \mu_{L_1} + \mu_{L_2} + \mu_{L_3} + \mu_{M_1} + \dots$$

Equation 7-10: Mass Attenuation Coefficient for X-Ray Absorption

where μ_K , μ_{L_1} , μ_{L_2} ,... are the partial attenuation coefficients for the K, L₁, L₂, etc. energy levels. If the energy of the incident photon is below the excitation energy for a K-shell electron, the absorption process will be due only to electrons being ejected from the L and M shells (and higher). If the energy of the incident photon is below the excitation energy for an L-shell electron, the absorption process will be due only to electrons being ejected from the M shells (and higher), etc. This leads to the following equation:

$$\tau = \tau_M + \tau_N + \dots$$

Equation 7-11: Photoelectric Absorption Coefficient

where τ is the symbol used to designate the photoelectric absorption coefficient. The magnitude of the change in absorption at any absorption edge is generally referred to by measuring the probability that a specific absorption can even take place. The convention for calculating such a probability is:

$$r_K = \frac{\tau_K + \tau_{L_1} + \tau_{L_2} + \tau_{L_3} + \tau_{M_1} + \dots}{\tau_{L_1} + \tau_{L_2} + \tau_{L_3} + \tau_{M_1} + \dots}$$

Equation 7-12: Absorption Jump for K-Shell Excitation

7.2.2 Relative Line Intensities Within the K, L, and M

Series

It is now important to look at the likelihood that K-L₃, K-L₂, K-M₃, etc. lines will be emitted. The symbol used to represent the intensity of a given energy value is f and is given as a fraction of the total intensity within the characteristic x-ray energy series. As an example, for the emission of a K-shell electron and the subsequent filling of that vacancy by an L_{2,3} electron, $f_{K-L_{2,3}}$ is given as:

$$f_{K-L_{2,3}} = \frac{I_{K-L_{23}}}{I_{K-L_{2,3}} + I_{K-M_3}}$$

Equation 7-13: Probability Equation for Electron Ejection

7.2.3 Fluorescence Yield

In x-ray fluorescence spectroscopy, the most important factor to consider is, of course, the fluorescence yield. When an electron from the inner shell of an atom is ejected, it leaves the atom in an excited energy state. The vacancy created when the

electron was ejected is quickly filled by an electron from a higher energy level than that of the ejected electron, and when this occurs energy is released in one of two ways: 1) as an x-ray photon, and 2) as an Auger electron. An Auger electron is created when the x-ray photon created by a higher energy electron filling the inner shell vacancy gets absorbed by another electron in the same atom, giving it enough energy to become a free electron. Auger electrons are characteristic of the element from which they are ejected and can be used for materials analysis.

The fluorescence yield ω is defined as the probability for a photon to leave the atom without being absorbed within the atom itself. It is given in the following equation:

$$\omega = \frac{n_S}{n_P}$$

Equation 7-14: Fluorescence Yield

where n_p is the number of primary x-ray photons created by the ejection of an electron from any given energy level of an atom, and n_s is the number of secondary x-ray photons that effectively leave the atom without being absorbed. For K-shell fluorescence, the K fluorescence yield ω_K is found by dividing the number of x-ray photons emitted by all the K-shell electrons

during a given time interval, n_K , by the number of K-shell vacancies created during that same time interval, N_K . This is represented as:

$$\omega_K = \frac{n_{K-L_3} + n_{K-L_2} + n_{K-M_3} + \dots}{N_K} = \frac{\sum(n_K)}{N_K}$$

Equation 7-15: Fluorescence Yield

7.2.4 X-Ray Energy Dispersive Detector and the KeveX Model 771

The XRF instrument used in this thesis was a KeveX Model 771 X-Ray Fluorescence machine. The machine uses the x-ray source seen in Figure 7-4 on page 114. For the primary target, the KeveX use Americium. This primary x-ray beam is then collimated and sent to a secondary x-ray target. There are seven secondary targets chosen to give a wide range of excitation energies (see Figure 7-8).

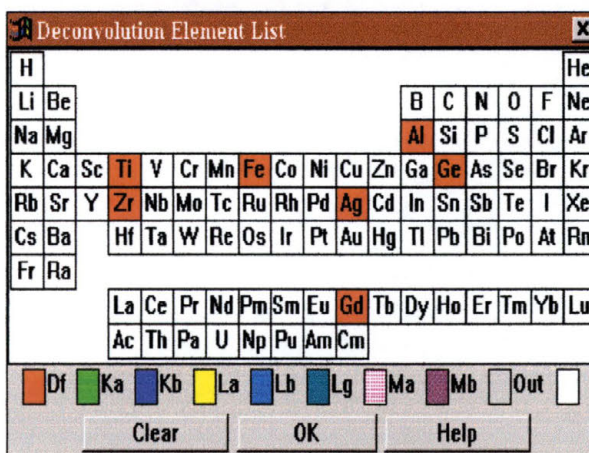


Figure 7-8: Distribution of Secondary Targets for KeveX Model 771

When presenting an x-ray beam to a sample, the closer to the elements of the sample the incident x-ray beam is, the better the resolution of the spectra and the better the signal to noise ratio will be for the energy spectrum generated by the sample. If, for example, the iron secondary target were to be used for analysis of a sample containing nickel (Ni), the x-ray beam would not have enough energy to excite K-shell electrons in the Ni and the spectrum would not have the characteristic Ni K- α peak. If, on the other hand, the same Fe secondary target was used to analyze a sample containing chromium (Cr), the incident x-ray beam would have enough energy to excite the K-shell electrons of the Cr while not having so much energy that they caused a large amount of backscattering of the x-ray beam or high background noise production.

Observe the two scans of Figure 7-9 on the next page. Both spectra are of the same sample, a rock specimen collected in the mountains of Real Viejo, in northern Mexico by Dr. Don Olsen. Figure 7-9 (a) was made with an Fe secondary target, while Figure 7-9 (b) was made with a Ge secondary target. The large calcium (Ca) peaks are from the sample holder. What is interesting to note is that Fe is seen in both samples, but Ni, Zn, and Ge are seen only in (b). This is because the characteristic x-rays emitted by the Fe target are not energetic

enough to eject K-shell electrons from the Ni or the Zn in the sample. The Fe peak is seen because some of the incident Fe x-rays were backscattered off the sample into the detector. In (a) the Ge peak comes from backscattering of the incident x-rays from the Ge secondary target. This is a clear example of why it is advantageous to have multiple secondary targets available for use in causing the phenomenon of fluorescence.

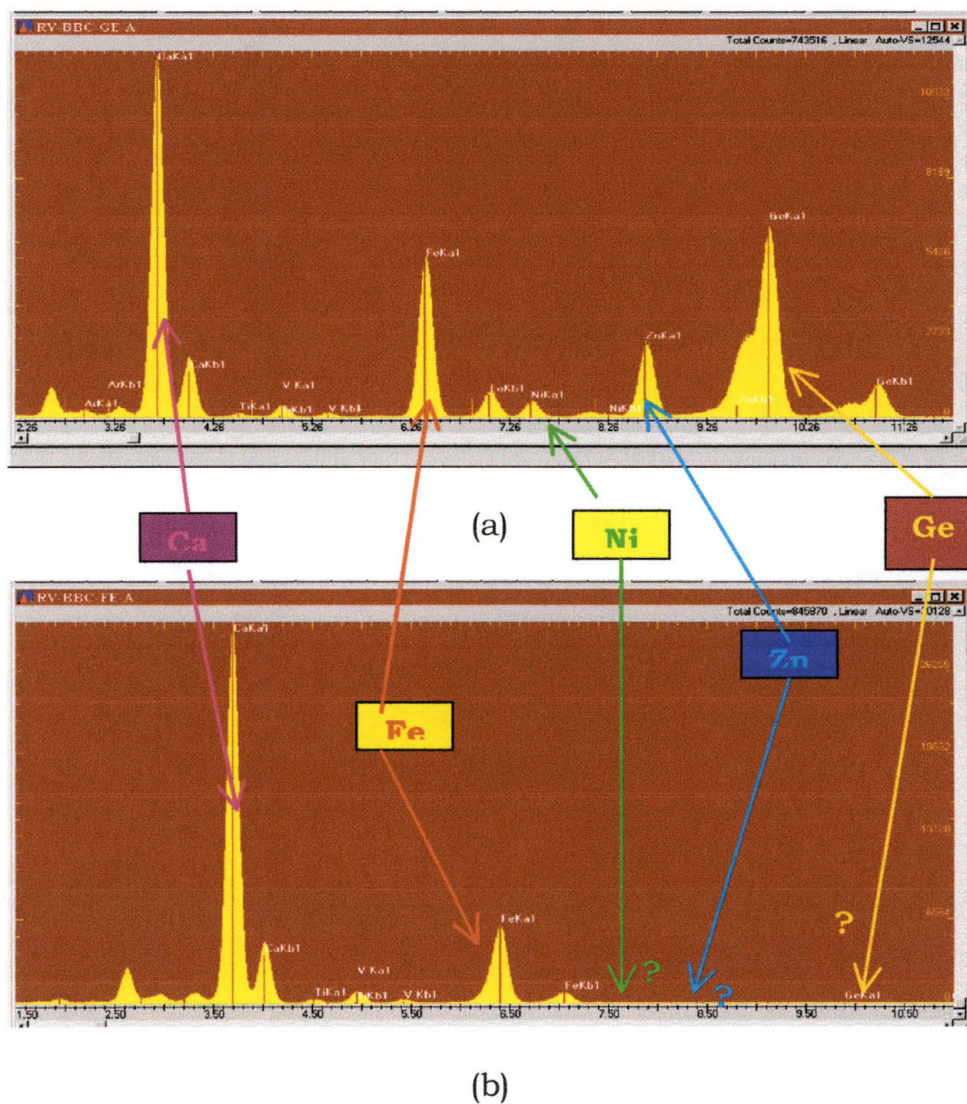


Figure 7-9: XRF Scans Of Same Material Using (a) Germanium and (b) Iron Targets

The detector used in the KeveX is a type known as a Lithium Drift Solid State Detector (see Figure 7-10). A Lithium drift detector works in many ways like a p-n junction diode. Intrinsic silicon (intrinsic meaning that there only thermal electron-hole pairs present) is doped with Li at one end of the detector only. The Li atoms diffuse into the Si substrate creating a neutral zone where electrons can flow freely, or drift. The edge of the detector that has the Li implanted into it will become n-type due to the fact that Li has one valence electron creating an excess of electrons in the crystal.

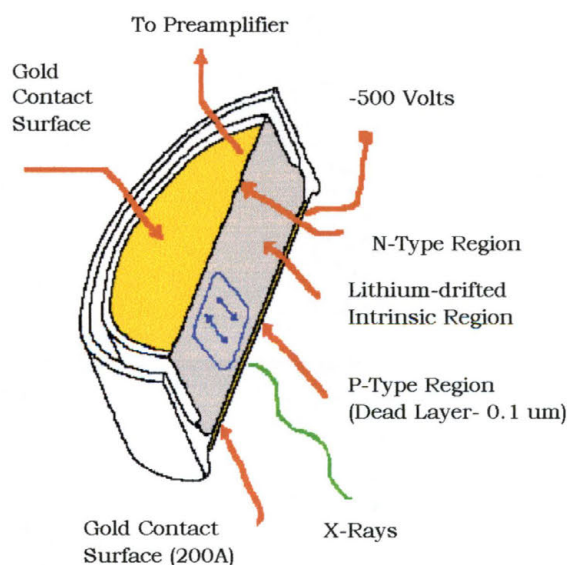


Figure 7-10: Lithium Drift Solid State X-Ray Detector

The end farthest away from the implanted Li region will become p-type, due to the electrons being attracted to the -500 Volt potential placed on one side of the detector and leaving holes behind. As occurs every time there is a material with a difference in electron-hole concentration, a depletion region will form, only this one will be a little bit different. Instead of a p-n junction being formed, what forms is called p-type : intrinsic : n-type junction, or a p-i-n junction.

When an x-ray is incident upon the detector, that x-ray will cause the formation of electron-hole pairs (EHPs) in the intrinsic region by exciting electrons in the intrinsic region of the detector. Due to the high potential applied at one end of the detector, these electrons will quickly travel one way through the detector while the holes will travel in the opposite direction. As these electrons and holes travel throughout the detector, they will interact with the atoms surrounding them with the net result being that they will cause more EHPs to form in what is generally referred to as a cascade. The number of EHPs formed is directly proportional to the amount of energy that the incident x-ray had as it entered the detector. As the EHPs reach the gold contact regions on either side of the detector, a voltage spike will be registered on the preamplifier. This signal is then amplified and recorded electronically for output to the

spectrograph. The more occurrences there are of an x-ray with a specific energy interacting with the detector, the higher the intensity of the peak seen on the spectrum.

One drawback of EDS is that there is a dead-time associated with the Li drift type of detector. The dead-time is defined as that time where, after an x-ray has started a cascade, another incident x-ray will not register on the detectors electronics. The dead-time of the detector is partially related to the number of x-rays being generated in the sample under analysis and can thus be controlled by adjusting the power to the primary x-ray source.

The ability to measure characteristic x-rays allows the realization of many benefits. If a sample is comprised of an unknown material, XRF can provide a qualitative analysis, providing data on the specific elements in that sample. In addition, if a scan is performed on a sample that has a known amount of a particular element (often determined through the use of complimentary analysis methods), then this scan can be used to calibrate the XRF detector for the quantification of elements in a second sample known to have the same elemental composition as the sample used for calibration. In Figure 7-11 on the next page is shown a comparison of the thickness of numerous thin films made by Robert Dail for his master's

thesis. The “old” data was determined using VSM (see Chapter 6 of this thesis). For the “new” data set, the thickest film was chosen as the reference sample and used to calibrate the XRF machine. The other films were then scanned and their film thickness was determined solely by the intensity of their spectral peaks when compared to the reference scan. Note the agreement on all but one of the samples. It was later determined that this one film had deteriorated somewhat.

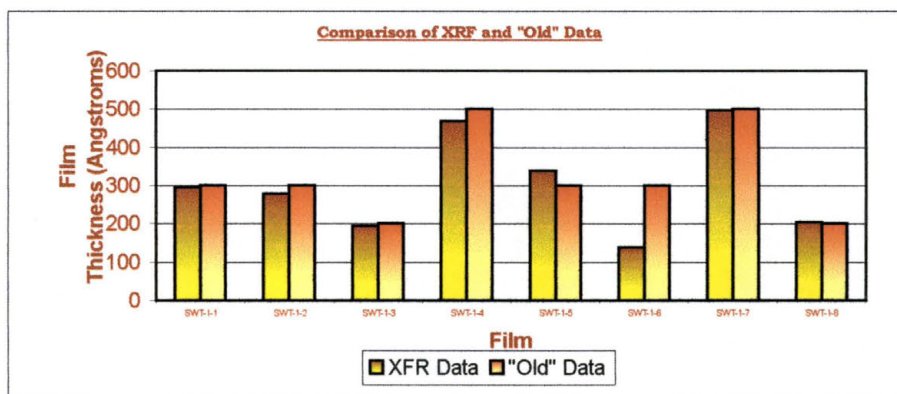


Figure 7-11: XRF Film Thickness vs VSM Thickness

This method is also extremely effective when reproducibility is the question. Again, one of Robert Dail’s films was analyzed twenty times to determine the reproducibility of a film thickness measurement. The range of thickness measurements varied from 501.1Å to 505.15Å, with a mean value of 503.0 Å.



Figure 7-12: Graph of XRF Thin Film Measurements

In conclusion, X-ray fluorescence is a powerful tool for the analysis of thin films. It provides elemental qualitative analysis, as well as thin film quantitative analysis, and it does it non-destructively, rapidly, and accurately.

7.3 The Geometry of Crystals

While the use of x-rays for the analysis of a thin film has seen widespread use for many years, it is becoming more and more an important characterization tool as device features and film thickness becomes smaller and smaller. In order to understand some of the analytical methods that use x-rays to gain information about a thin film, it is first important to understand the details of what a crystal is and how they are defined.

One of the most important of these details involves the geometry and structure of crystals. It is also relevant to describe how these crystals are classified. A crystal is a solid composed of atoms arranged in a periodic pattern in three dimensions. It is noteworthy that not all solids are crystals, i.e. if a solid has no regular arrangement of atoms in its interior it is said to be amorphous.

When discussing and describing crystals, it is often more useful to describe a set of imaginary points with a fixed relationship in space to the atoms of the crystal instead of dealing with the actual atoms that make up the crystal and their arrangement in space. These points then become the framework upon which the crystal is built.

7.3.1 Lattice Directions and the Zone Axis

Over the years, a sort of shorthand notation has been devised to describe the directions and planes in crystals. This has many advantages when describing crystals: the notations are short, they are extremely precise, and they are easy to understand. These notations are direction symbols and plane indices that are based upon the axes of the crystal and that define what is known as the unit cell. Some of these unit cells have been shown in previous sections of this thesis (see Figure 2-9 on p. 34 or Figure 3-16 on p. 70). This discussion will explain how these crystal structures are described.

Because there are different unit cells, each having their own axes, ambiguities can arise from the fact that each axis will have different direction symbols and plane indices. It is therefore important to know which set of crystal axes (which unit cell) is being used and how to change or transform direction symbols and plane indices when the set of crystal axes is changed.

A zone can be defined as a set of faces or planes in a crystal whose intersections are all parallel to each other. The direction of the intersections common to all the planes can be called the zone axis. To make understanding a zone a little easier, think of an octagonal object such as a stop sign placed

on level ground. The face of each side of the sign intersects with the two faces of the adjacent sides. The intersections of these planes are lines that are parallel to each other, and to the lines formed by each intersection of two planes. The direction of these parallel lines is the direction of what is called the zone axis.

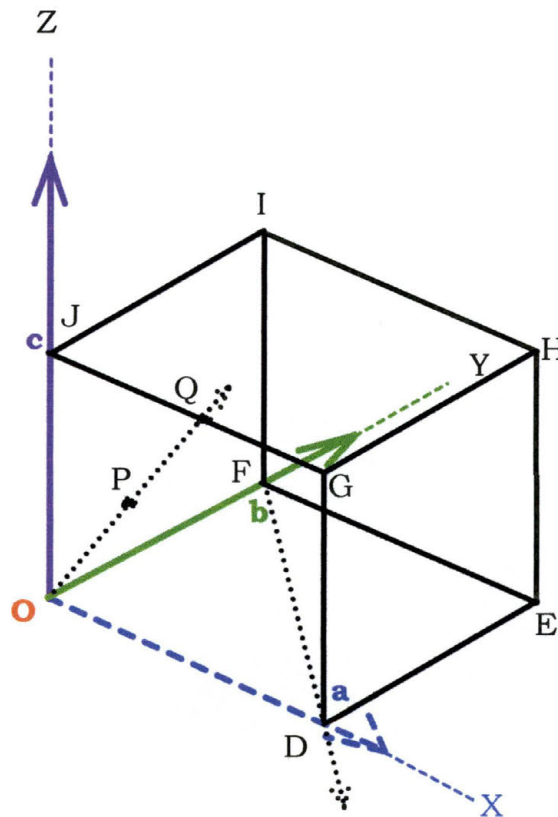


Figure 7-13: Primitive Unit Cell

Now consider the primitive unit cell of Figure 7-13. The cell has edge vectors **a** (blue), **b** (green), and **c** (purple). One corner of the cell is chosen as the origin of the cell (point **O** in red). When describing a point on the unit cell, such as point **Q**

on the J-G line, the coordinates are written in terms of fractions of the lengths a , b , and c respectively. In this example, the coordinates for the point Q would be $\frac{1}{2}$, 0, 1. The convention, however, is to write these coordinates in terms of whole numbers and, since this is a single point, putting those whole numbers in brackets without any commas. Thus the coordinates for Q would be [102].

Directions in crystals are, as can be seen by the description above, vectors that may be expressed in terms of the components of the three unit cell edge or base vectors a , b , and c . The general symbol for any direction would then be $[uvw]$, or when written as a vector:

$$r_{uvw} = ua + vb + wc.$$

Equation 7-16: Unit Cell Direction Vector

7.3.2 Miller Indices

When determining the index of a lattice plane in a unit cell, it is important that the plane not pass through the origin. Using the example shown in Figure 7-14 on the next page, start by observing the lattice plane defined by the points JFK (F is in the same location as it was in Figure 7-13). This plane actually extends beyond the confines of the unit cell, however, the area of concern here is the shaded area inside the unit cell.

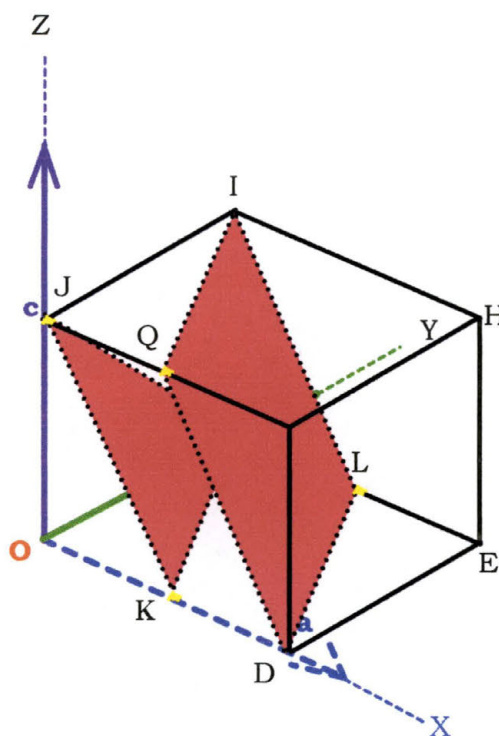


Figure 7-14: Primitive Unit Cell with Two Planes Defined

It is also important to point out that this description is not for just the plane defined by JFK, but by all the planes passing through the crystal parallel to this plane, such as the plane defined by QILD.

To define the plane JFK, first write down the intercepts of the plane with the unit cell axes in terms of the unit cell vectors a , b , and c . In this case, $K = \frac{1}{2}a$, $F = 1b$, and $J = 1c$, or in the appropriate nomenclature, $\frac{1}{2}, 1, 1$. Now, in order to define the planes, take the reciprocal of these numbers and put the whole

numbers into round brackets without commas, resulting in (211). This is the Miller Index of the plane. The general index for a lattice plane is (hkl) .

When a crystal plane lies parallel to an axis its intercept on that axis is infinity, the reciprocal of which will be zero. As an example, when the plane lies on the front face of a crystal parallel to the x-axis, it will have a Miller index of (100). If the plane were along the top of the unit cell, its Miller index would be (001), etc.

7.3.3 Lattice Plane Spacing

One of the results of being able to discuss the Miller indices is to be able, ultimately, to calculate the lattice plane spacing (known as the d-spacing), d_{hkl} . Figure 7-15 shows

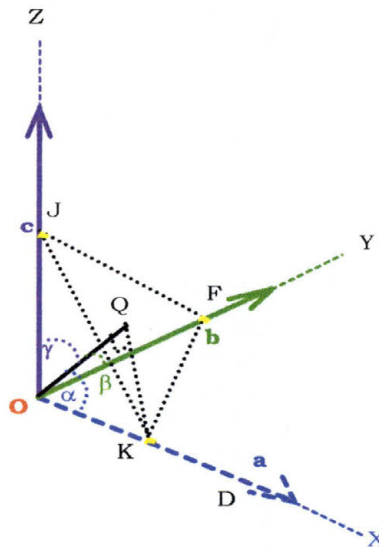


Figure 7-15: Intercepts of a Lattice Plane

a plane drawn some distance away from the origin. A line has been drawn normal to the plane defined by the points JFK and it can be seen that the distance from the plane to the origin is the length of the line OQ. There are also angles α , β , and γ that define angles between the normal to the plane and the x, y, and z axes respectively. Angle α is defined by KOQ and is equal to 90° . Angle β is defined by JOQ while angle γ is defined by FOQ, each angle also being 90° . Using trigonometry to define the angles then leads to:

$$\cos \alpha = \left(\frac{h}{a}\right)d_{hkl}, \quad \cos \beta = \left(\frac{k}{b}\right)d_{hkl}, \quad \text{and} \quad \cos \gamma = \left(\frac{l}{c}\right)d_{hkl}$$

Equation 7-17: Direction Cosines

What this shows is that the ratios of the direction cosines $\cos \alpha : \cos \beta : \cos \gamma$ for a cubic crystal equals the ratios of the Miller indices $h:k:l$. The concept of lattice planes and interplanar spacings is the basis of the concept of the reciprocal lattice and Bragg's law:

$$n\lambda = 2d_{hkl} \sin \theta$$

Equation 7-18: Bragg's Law

where n is the order of reflection, λ is the wavelength, d_{hkl} is the lattice spacing, and θ is the angle of incidence and/or reflection to the lattice planes.⁴¹

7.3.4 Crystal Systems

Now that the lattice parameters and Miller indices have been explained, it can be seen that it is possible to describe the crystal structure of many different solids in a method that is universally understood. This method, however, can be simplified even further. Except for a few rare occurrences, the structures of almost all crystals can be described by one of seven generic lattice systems. These generic lattice systems can be seen on Table 2 below.

System	Axials, Lengths, and Angles	Bravais Lattice	Lattice Symbol
Cubic	Three equal axes at right angles. $a = b = c. \alpha = \beta = \gamma = 90^\circ.$	Simple Body-Centered Face-Centered	P I F
Tetragonal	Three axes at right angles two equal $a = b \neq c. \alpha = \beta = \gamma = 90^\circ$	Simple Body-Centered	P I
Orthorhombic	Three unequal axes at right angles $a \neq b \neq c. \alpha = \beta = \gamma = 90^\circ$	Simple Body-Centered Base-Centered Face-Centered	P I C F
Rhombohedral (also called Trigonal)	Three equal axes, equally inclined $a = b = c. \alpha = \beta = \gamma \neq 90^\circ$	Simple	R
Hexagonal	Two equal coplanar axes at 120 degrees, third axis at right angles $a = b \neq c. \alpha = \beta = 90, \gamma = 120^\circ$	Simple	P
Monoclinic	Three unequal axes, one pair not at right angles $a \neq b \neq c. \alpha = \gamma = 90^\circ \neq \beta$	Simple Base-Centered	P C
Triclinic	Three unequal axes, unequally inclined and none at right angles $a \neq b \neq c. \alpha \neq \beta \neq \gamma \neq 90^\circ$	Simple	P

Table 2: Crystal Systems and Bravais Lattices

By giving special values to the axial lengths and angles, it is possible to produce unit cells of various shapes and thus various kinds of point lattices, since the points of the lattice are located at the corners of the unit cell. The seven different point lattices that describe the possible unit cells can be found by putting the points at the corners of the unit cells of the seven crystal systems. In 1848, French crystallographer Auguste Bravais worked on the problem of defining the unit cell structures and proved that there is a total of only fourteen possible point lattices.⁴² As an example, if a point is placed at the center of each cell of a cubic point lattice, the new array of points also forms a point lattice. The fourteen Bravais lattices are shown in Figure 7-16 on the next page.

The figures are not all that is required to understand the unit cells. Note the letters P, F, I, etc. after the descriptions of the Bravais lattices. These letters help distinguish between what is known as a primitive cell and a non-primitive cell. Primitive cells, denoted only by the letters P and R, have only one lattice point per cell. Non-primitive cells, denoted by all letters except P and R, have more than one lattice point per cell. A lattice point in the interior of a cell is said to belong to that unit cell. This is compared to a lattice point on the face of a unit cell which is considered to be shared between two adjacent unit

cells, and a lattice point at the corner of a unit cell which is considered to be shared between all of the unit cells that share that corner point. The symbol F is used to describe a face-centered unit cell, while the symbol I is used to describe a body-centered unit cell. The symbols A, B, and C are used to describe base-centered unit cells centered on one pair of opposite faces, while the symbol R is used exclusively for the rhombohedral system. Note also the lengths given by a , b , and c .

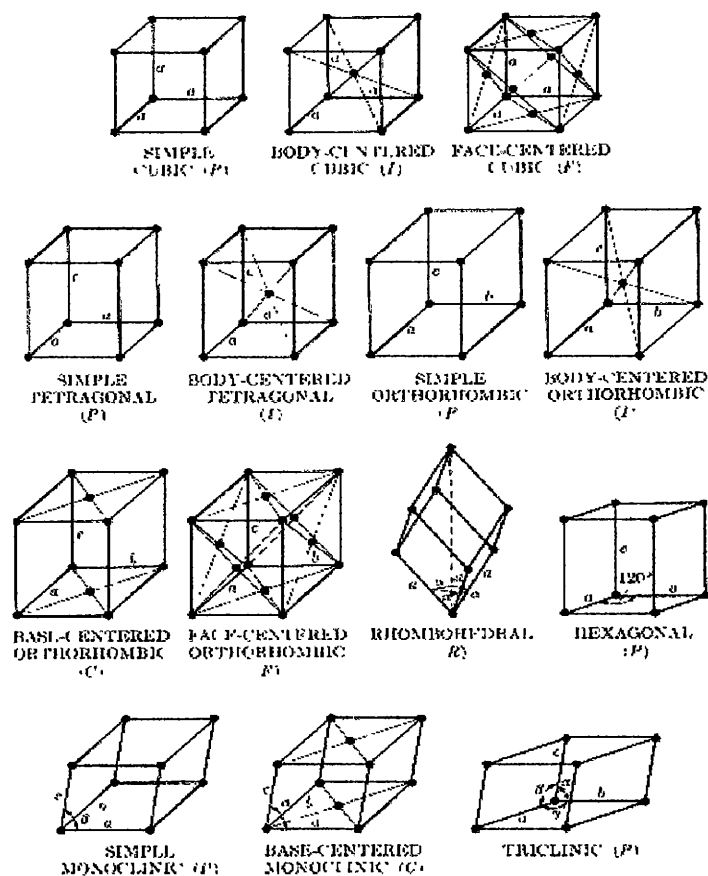


Figure 7-16: The Fourteen Bravais Lattices³⁸

7.4 X-Ray Reflectivity

As mentioned before, x-rays have a wavelength on the order of the atomic spacing of most crystals. When atoms scatter x-rays, interference occurs to the beam of x-rays. When the given angles of incidence for a beam with a given wavelength satisfies Bragg's Law (Equation 7-18 restated below), this interference will be constructive. This constructive interference occurs when the path length for the photons scattered from the adjacent planes of the atoms in a crystal is an integral number of wavelengths, causing the diffracted intensity of the x-rays to be strong. Since crystals are three-dimensional structures, other non-equal values of incident and scattered angles exist, but these are quickly damped when relatively thick crystals are analyzed. The integer n from the Bragg's Law equation represents the order number of the diffraction from the planes of the atoms that make up the crystal that have a separation of d .

$$n\lambda = 2d_{hkl} \sin \theta$$

Equation 7-19: Bragg's Law

At small angles of incidence, θ , below what is known as the critical angle, θ_c , x-rays are totally reflected from the surface of a solid. The critical angle is a function of the density,

scattering factor, and atomic number of the material under analysis as well as the wavelength of the incident x-ray beam. If the angle θ is greater than θ_c , the x-ray beam will penetrate the surface of the material. When this occurs, the interaction of the incident x-rays with the electrons in the crystal cause the intensity of the scattered beam to vary as the angle of incidence is altered. The method of data collection using this geometry (almost a straight line from x-ray source to detector) is called Reflectivity.

When the critical angle is exceeded, the intensity of the reflected beam drops off very quickly. For this reason, when measuring a spectra using reflectivity mode, the scale of the graph is often set to a logarithmic scale. When the incident beam interacts with the planes of a highly uniform crystal, the conditions for satisfying the Bragg law are met and the diffracted beam will produce a diffraction peak. However, in this method, the incident angle is kept at an extremely low, fixed angle. The detector is rotated around such a small angle that the units of the rotation are arcseconds. There are 3600 arcseconds in one degree of rotation. A typical scan will rotate the detector over a range from zero to around 5 or 6 thousand arcseconds.

Because the angle of incidence is so low, typically only 0.1° , the x-ray beam will penetrate the surface and will reflect off of the planes of the crystal that make up the sample under investigation (see Figure 7-17) in a manner similar to the way visible light is reflected off the surface of water or glass.

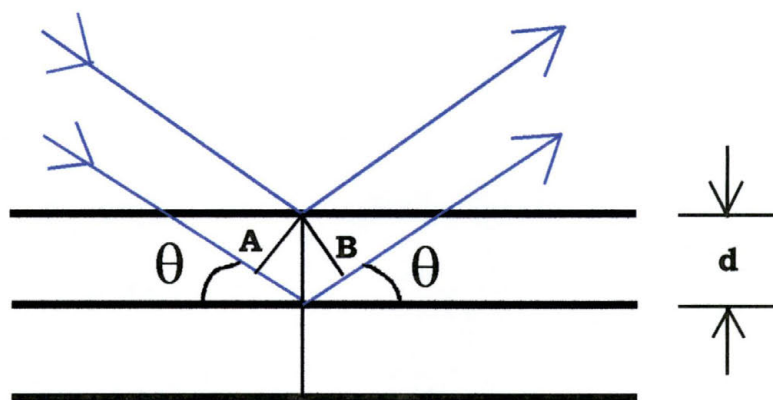


Figure 7-17: Reflection of a Plane Wave by Crystal Planes

The reflected beam will interact, just as any set of plane waves will, by producing interference fringes known as Kiessing fringes (see Figure 7-18 on next page). These fringes will appear in a pattern that is affected by the electronic density of the different layers of the crystal. Because of this interaction information about the unit cell, the lattice constants, the phase of the material, the elemental composition of the layers present, and the thickness of these layers can all be determined by the use of reflectivity. The one drawback is that the sample must have an relatively smooth surface for this method to work. If

the surface is too rough, there will be too much interference for any of the reflected beams to add constructively with the result that the spectra will not be very useful.

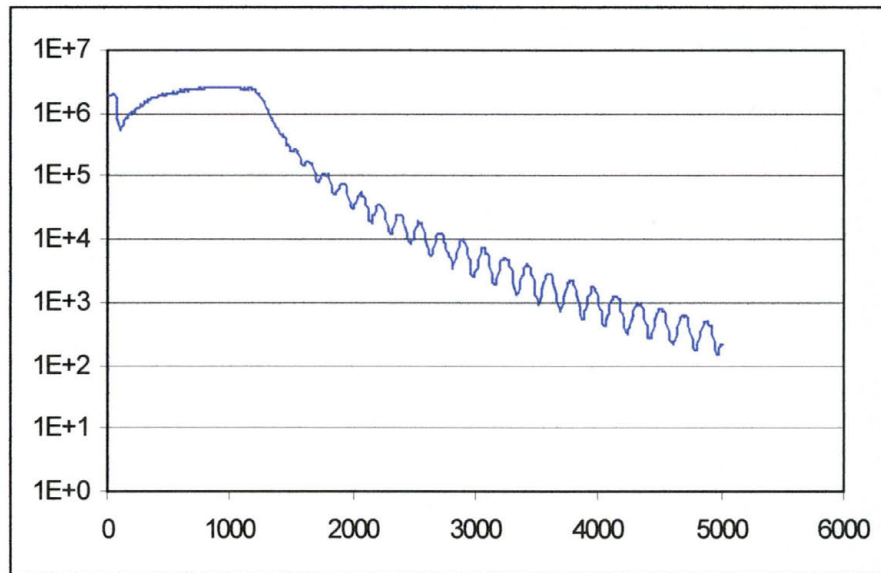


Figure 7-18: Example of Reflectivity Spectra

The amplitude and the spacing of the Kiessing fringes are what help determine the information about the sample under analysis. The periodicity is used to determine the thickness of the film, while the amplitude is used to determine the lattice parameters and crystal structure.

The ability to determine this sort of information is extremely difficult to determine by hand calculations. Instead, an easier method is to use commercially available software, usually provided when an x-ray analysis tool is purchased. After a scan has been performed, the data is collected and input

into the software. The software package used for the purposes of this thesis is REFS Mercury, created by Bede Scientific.

First, the scan under analysis is input into the program. Then, the layer data must be input to define the initial parameters by which the software will attempt to fit the experimental data. This information is crucial to the development of a realistic fit for the data. As an example, observe Figure 7-19. This data was fitted with only three layers: the Si substrate, a SiO₂ layer of approximately 3000 Å, and a Permalloy layer of approximately 800 Å. The software went through over 40,000 iterations yet still did not perfectly match the calculated data to the experimental data.

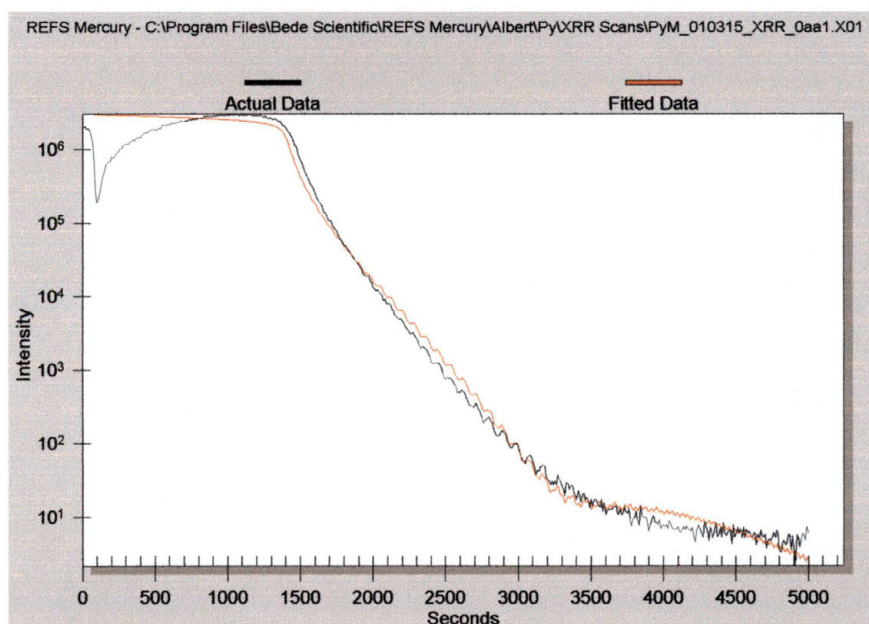


Figure 7-19: Poorly Fit Analysis of Reflectivity Scan

When this same experimental data was fitted with some slightly different parameters, the fit was found to be very close with relatively few iterations of the analysis software (see Figure 7-20). The difference was that in the second attempt, allowances were made for two extra layers of material. The first was an oxide interfacial layer between the SiO_2 and the Py film. The second was an oxide layer on top of the Py film, due to the contamination of oxygen in the ambient air. Recall that Fe reacts vigorously with O_2 , most often forming Fe_2O_3 and Fe_3O_4 .

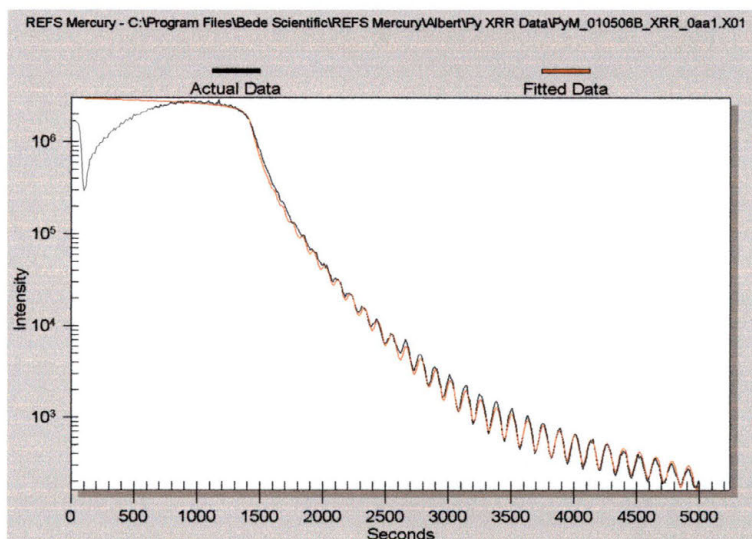


Figure 7-20: Well Fit Analysis of Reflectivity Data

In addition to accounting for the number of layers of different material present in the sample, initial guess must also be given for the density of the materials, and the ratio of one element or molecule to the others present in each individual layer. It is for these reasons that the Reflectivity mode of x-ray

analysis a powerful analysis tool for the examination of a material such as a thin film. By the time the fit is adjusted to a high degree of agreement with the experimental data, intimate knowledge of the films present, including interfacial states, will be determined.

7.5 High Angle and Parallel Beam X-Ray Diffraction

X-ray diffraction is a powerful technique used to identify the crystalline phases present in materials and to measure the structural properties (strain state, grain size, epitaxy, phase composition, preferred orientation, and defect structure) of these phases.⁴³ There are two main methods of using x-ray diffraction for crystal analysis. In both, the diffraction angle, known as 2θ , is the angle between the incident and the diffracted x-rays.

When there is constructive interference from the x-rays being scattered by the lattice planes in a crystal, a diffraction peak is observed. As with reflectivity, the condition for constructive interference is Bragg's law. For this diffraction to be observed, the detector must be placed so that the angle of diffraction is 2θ where θ is the angle of incidence of the x-ray beam when measured from the plane of atoms diffracting it. The crystal must be positioned so that the diffracting plane is coplanar with the incident and the diffracted x-rays.

There are two experimental designs that take advantage of Bragg's law to measure the diffraction of an x-ray beam. The

first is known as Parallel Beam X-Ray Diffraction (PBXRD) and the second is known as High-Angle X-Ray Diffraction (HAXRD).

7.5.1 High Angle X-Ray Diffraction

HAXRD is a method in which the angle of incidence of the x-ray beam is rotated in a designated arc while the angle of diffraction to an x-ray detector is rotated around in an arc across a designated range of angles with the relationship that the detector angle is always twice the angle of the incident beam when measured from the surface of the sample. HAXRD is ideally suited for the analysis of highly ordered thin films due to the geometry of the experimental setup (see Figure 7-22), known as the Bragg-Brentano Geometry.

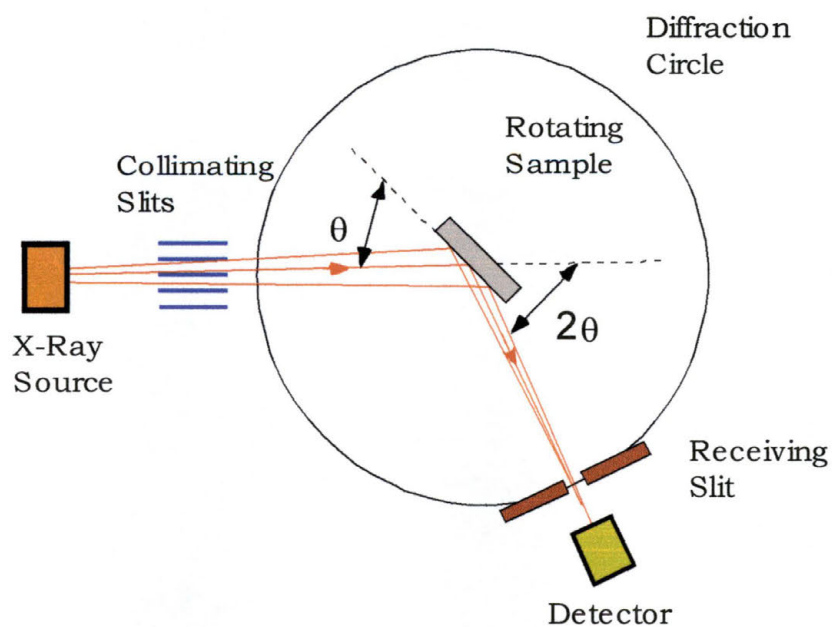


Figure 7-21: Bragg-Brentano Diffraction Geometry

With this geometry, the sample is rotated through a range of angles defined by what type of material you have. The International Center for Diffraction Data (ICDD) has been collecting information on x-ray analysis for many years and has a tremendously useful database upon which to draw some opening parameters when scanning a new film. The database provides locations of angles at which an intense peak should appear, given the elemental composition of your sample. This database also includes information such as crystal structure (which unit cell the element or molecule prefers), atomic lattice constants (the actual lengths of the lattice parameters for the unit cell), and the relative intensities of the expected diffraction peaks when the sample is scanned over a given range of angles. A typical range of angles to scan the detector over would be from around 25° to around 100° . This would rotate the sample over a corresponding range of 12.5° to 50° .

Once the parameters have been selected as to the range of angles that the sample will be rotated, the size of each step along that rotation must be selected. The step size is an important parameter to consider, especially when the width of the diffracted x-ray beam is considered. If the step size is too large, some diffraction peaks may not appear due to the fact that Bragg's law has not been ideally met. If the step size is too

small, the scan time can take an inordinately long time to accomplish. Again, it is a function of how clean you want your data to be and how much time you want to spend collecting your data. Typically, a step size of 0.1° is used.

Another important parameter to consider when analyzing a sample is the speed of the rotation with which the detector will be rotated. Actually, this is only important if you are scanning in a continuous motor movement mode. The motors can be rotated in what is called fixed mode, where the sample and detector are rotated the appropriate step size, stop for the desired length of time while the detector collects data, and then moved to the next location, etc. This is an excellent method when good a signal to noise ratio is desired, but can increase the length of time needed to analyze a sample. The other mode is known as continuous mode. The sample and detector are rotated in a continuous sweep across the angles selected for the scan, with the time between each step determining how fast the motors are rotated. When the sample has an extremely rough surface, a longer time may be needed to reduce the amount of backscattered x-rays that can lead to what is known as background noise. It is preferable to achieve a ratio of at least 10 to 1 for the height of the maximum intensity peak of a scan when compared to the background radiation. The sample scan

time is also selected based on the power level (i.e. the intensity) of the incident x-ray beam. Generally, a time of 2 to 5 seconds is more than sufficient to collect good data.

With the Bragg-Brentano diffraction geometry, the incident and diffracted x-rays make the same angle with respect to the surface of the sample, regardless of the angle of incidence of the x-ray beam (see Figure 7-22). The angle γ is known as the scattering vector and always bisects the angle between the incident and the diffracted beams.

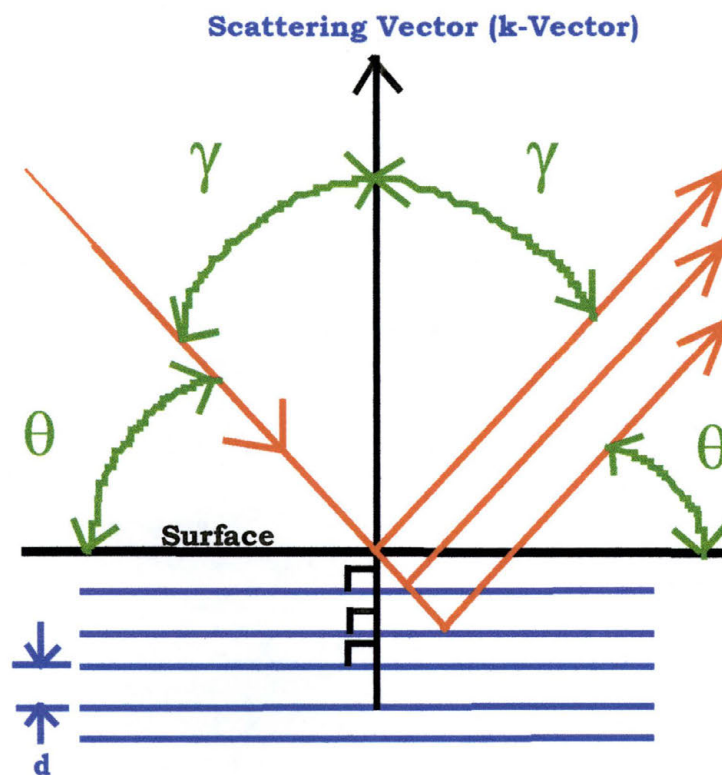


Figure 7-22: HAXRD Diffraction Geometry

This geometry provides structural information only about the (hkl) planes that would be parallel to the surface of the sample. As the sample and detector are rotated, there will only be a few select angles at which Bragg's law will be satisfied. This method provides relatively fast sample analysis. If the surface of the sample is smooth and the material is a highly ordered crystal, the signal to noise ratio will also be quite good (see Figure 7-23).

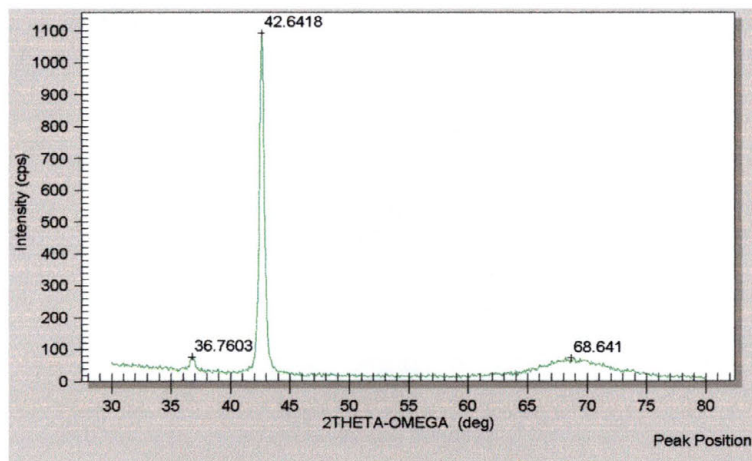


Figure 7-23: Example of High Angle X-Ray Diffraction Spectra

7.5.2 Parallel Beam X-Ray Diffraction

PBXR is a method similar to that of HAXRD in that it uses the principle of Bragg's law to find diffraction peaks. The difference between the two methods of analysis is that in PBXR, the sample is kept at a fixed angle with respect to the incident x-ray beam (see Figure 7-24) using what is known as the Seemann-Bohlin Geometry. The beam is usually kept at a very low angle of incidence, typically from 1° to 5° , while the detector is rotated around roughly the same range of angles that would be used in HAXRD. PBXR is ideally suited for the analysis of highly disordered thin films due to the geometry of the experimental setup (see Figure 7-24).

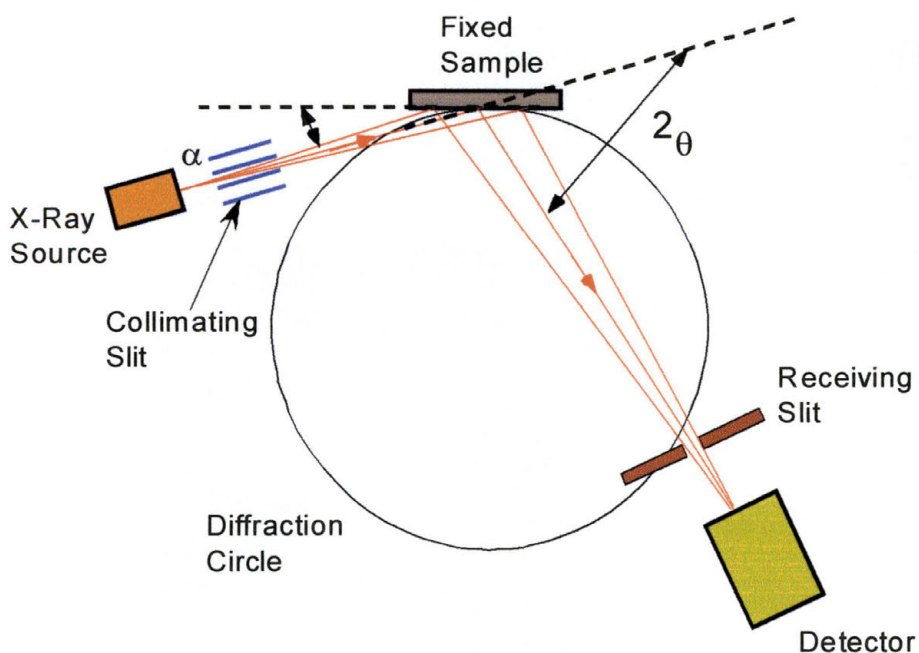


Figure 7-24: Seemann-Bohlin Geometry for Parallel Beam XRD

For the choice of angles, angular velocity for the detector, and scan time, the same selection criteria used for HAXRD applies. The range of angles is still determined by the elemental or molecular composition of the sample being scanned, while the step size and scan time are still determined by surface roughness, beam intensity, and desired signal to noise ratio. A good question to ask is if all of these parameters are the same except for the fact that the x-ray beam is kept at a constant angle of incidence, what exactly is the point of using the Seemann-Bohlin geometry instead of the Bragg-Brentano geometry?

In many thin films, as they are deposited on the surface of a material, there are factors such as the temperature at which the films were produced, the strain between atomic bonds at the film-substrate interface caused when you have materials with different lattice constants attempting to bond to each other, system contamination, and other factors which can cause the deposited film to have an extremely non-uniform structure. Instead of the film being a true crystal with all of the lattice planes lined up perfectly parallel to each other, there will be large areas of individual crystals, each with its lattice planes aligned in a different direction. This would put a severe limitation on the effectiveness of using the Bragg-Brentano

This effect illustrated in Figure 7-25 on the previous page by the maroon and blue lines. The maroon lines are parallel to the surface of the material, but because of the angle of incidence of the incident beam (angle α), they do not satisfy the Bragg equation when the detector is located at angle 2θ so that region of the film does not produce a diffraction peak. The blue lines, representing a different area of the thin film with planes perpendicular to the k-vector, are aligned such that when the detector is at 2θ , the requirements for satisfying Bragg's law are met and a diffraction peak is observed. If the surface of the sample is not entirely smooth and even if the material is far from being a highly ordered crystal, the signal to noise ratio will be quite good (see Figure 7-26) and you will still get a useful spectra.

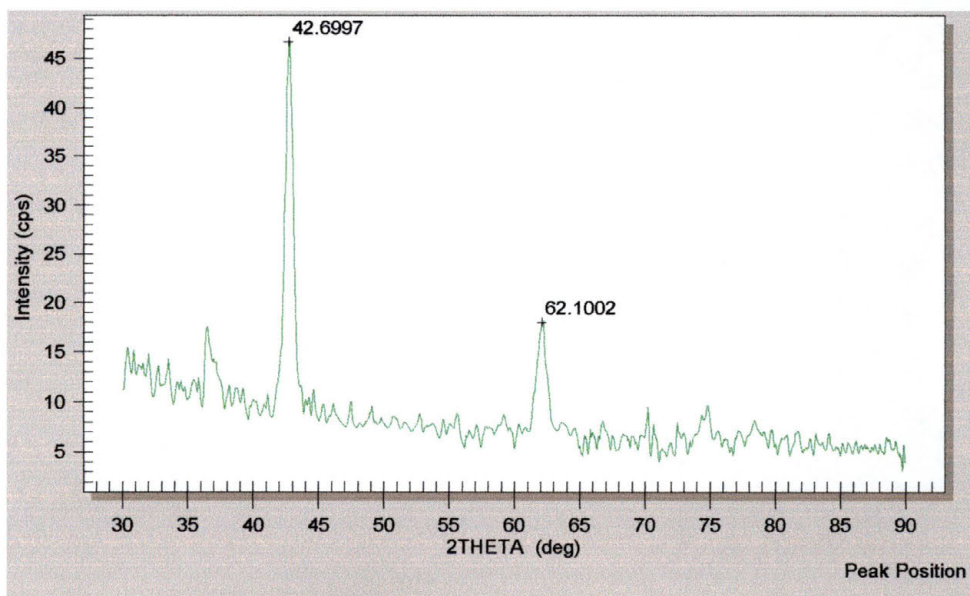


Figure 7-26: Example of Parallel Beam XRD Spectra

Another benefit of using PBXRD instead of HAXRD is that the angle of incidence can be varied for the same sample and the resulting multiple spectra can be combined (see Figure 7-27). The benefit of doing this is that sometimes you can get a peak on the spectra that is the result of layers beneath the film that you are attempting to characterize. Notice the small peaks at around 51° and around 74° . If just one scan had been performed, say the blue one on top, it would be easily possible to mistake the peak at 51° as a characteristic peak of the sample. By observing that it did not appear in the lower two scans, that peak can be ruled out as being a characteristic peak of the sample under investigation.

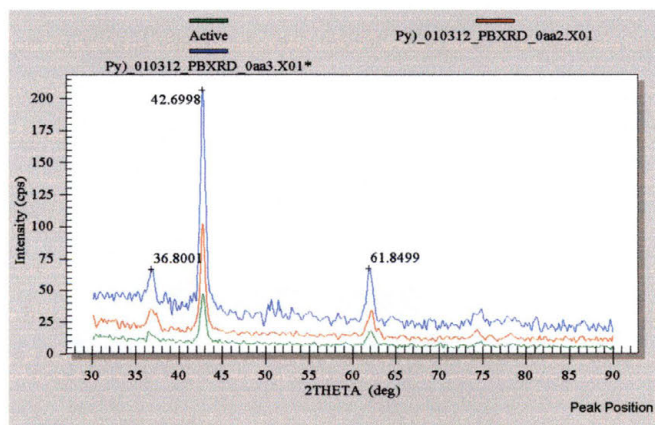


Figure 7-27: Combined PBXRD Spectra from Three Incident Angles

It can thus be seen that the combination of HAXRD with PBXRD is a powerful method for the characterization of thin films.

8 Optical Analysis

8.1 Thin Films and Basic Optics

Thin films are extremely thin layers of material that are deposited onto the surface of another material. They are used extensively in the semiconductor industry as insulating layers, metal interconnects, coatings to harden a surface and for many other uses. For a film to be considered “thin” it must have a thickness on the order of a few hundred microns (the width of a human hair) or much less (dielectrics in transistors are thinner than 3 nanometers!).

In order for thin films to be effective, they must be carefully monitored for thickness, elemental composition, surface roughness, and whatever parameters would be relevant to the application for which they are being employed. These parameters must be measured both during and after the manufacturing process to ensure good quality control. There are two main methods in use to measure the thickness of thin films: optical methods and stylus methods.

A stylus method uses a cantilever-type device that is dragged across the surface of the film. As the stylus travels over the surface of the film its vertical position is carefully monitored, providing information on the film thickness and roughness. One of the limitations of using the stylus method is the limited speed that is available- moving the tip too fast can break it or not give it time to get an accurate measurement. They also often require a step in the film to measure the thickness. While these can be severely limiting factors, they are the preferred method of measurement when the film being studied is a metal (i.e. light absorber).

Optical techniques can measure the thickness, roughness, and optical constants of a thin film by measuring how light interacts with the film. Optical constants describe how light travels through and reflects from a material. They can also be used to determine the elemental composition and the electronic band gap of a material. Optical methods of measurement are often used because they are accurate, non-destructive, and they require little or no sample preparation.

8.1.1 Optical Constants

When discussing optical constants, there are two parameters that are used to describe how light travels, or propagates, in a material. Without getting into too much detail of optical theory, it can be said that the electromagnetic field that describes how light travels through a given material at a fixed time is described by the following equation:

$$E = A \cdot \cos\left(n \cdot \frac{2\pi}{\lambda} \cdot x\right) \cdot e^{\left(-k \cdot \frac{2\pi}{\lambda} \cdot x\right)}$$

Equation 8-1: Light Propagation Through a Material

where x is a distance, λ is the wavelength of the light being used, and the symbols n and k are the refractive index and the extinction coefficient, respectively, of the material. The refractive index is determined by the equation:

$$n = \frac{c}{v}$$

Equation 8-2: Refractive Index

where c is the speed of light in a vacuum and v is the speed of light in the given material. The extinction coefficient is a

measure of how much light is absorbed per unit length in a given material.

8.1.2 Reflection

When light is traveling in one medium, and passes into another medium (such as a light passing from air into glass), the phenomenon of reflection occurs (see Figure 8-1). The fraction of light that is reflected by an interface is determined

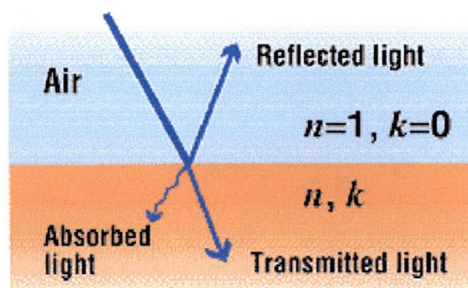


Figure 8-1: Single Interface Reflection⁴⁴

by the discontinuity in the values of n and k at the interface of the two materials. The equation used to describe light being reflected off of a material in air is:

$$R = \frac{(n-1)^2 + k^2}{(n+1)^2 + k^2}$$

Equation 8-3: Reflectance in Air

In order to understand a little better how the spectral reflectance can be used to measure optical constants, think

about an instance where there is light being reflected by a non-absorbing material (i.e. $k = 0$). Then the equation for reflectance changes to:

$$R = \left| \frac{n - 1}{n + 1} \right|^2$$

Equation 8-4: Reflectance in a Perfectly Non-Absorbing Material

It is easy to see that if the value of R can be determined, then the value of n can be calculated.

Now consider a case more likely to be seen in the semiconductor industry, that of light reflecting off of multiple interfaces, as when a thin film is deposited upon the surface of a material (see).

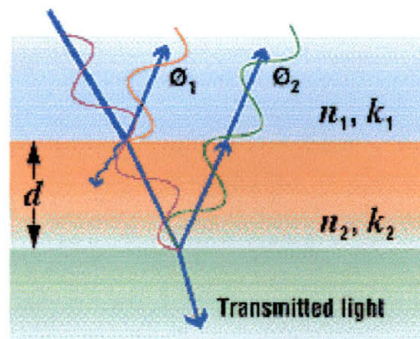


Figure 8-2: Reflection in Multiple Interfaces³⁹

The total amount of light being reflected is now the sum of the reflections from each interface. Due to the wave nature of light,

the multiple reflections will add to each other in one of two ways depending on the phase relationship of the reflected light: either constructive interference will occur, in which the intensity of the light reflections is added positively; or destructive interference will occur, in which the intensity of the light reflections is subtracted. The phase relationship of the reflected light is determined by the differences in the distance that each reflected beam will have to travel. This distance is dependant upon the thickness of the film, the optical constants of the film, and the wavelength of the light being used. The reflections are said to be in phase when the path length of one reflection is equal to an integral multiple of the wavelength of the light being used. For light that is incident at a perpendicular angle on a transparent film, constructive interference occurs when the following equation is satisfied:

$$2 \cdot n \cdot d = i \cdot \lambda$$

Equation 8-5: Constructive Interference of Reflected Light

Where d is the thickness of the film, i is an integer, and λ is the wavelength of the light. The factor of 2 is included because the light passes through the film twice. Reflections are called out-

of-phase and add destructively when the path of the reflected light is on-half of a wavelength different from the in-phase condition, or when the following equation is satisfied:

$$2 \cdot n \cdot d = \left(i + \frac{1}{2}\right) \cdot \lambda$$

Equation 8-6: Destructive Interference of Reflected Light

These equations (8-5 and 8-6) can be combined into a single equation to qualitatively describe the interference of reflected light (note: there is no need to correct for π phase shifting):

$$R = A + B \cdot \cos\left(\frac{2\pi}{\lambda} \cdot n \cdot d\right)$$

Equation 8-7: Combined Reflectance Equation³⁹

8.1.3 Models for n and k

There are many models for describing n and k as a function of wavelength. It is important, when selecting one to use as the model for finding n and k , that the model accurately describe the optical constants over the range of interest in wavelengths using as few parameters as possible. Three of these models are the Cauchy Model, the Amorphous Semiconductor Model, and the Crystalline semiconductor

model. Models for dielectrics (insulators, $k = 0$) generally have three parameters, while non-dielectrics will have five or more parameters.

8.2 Filmetrics F-20

The Filmetrics F-20 is what was used for this thesis to optically characterize some of the films that I grew. The layout of the F-20 can be seen in Figure 8-3.

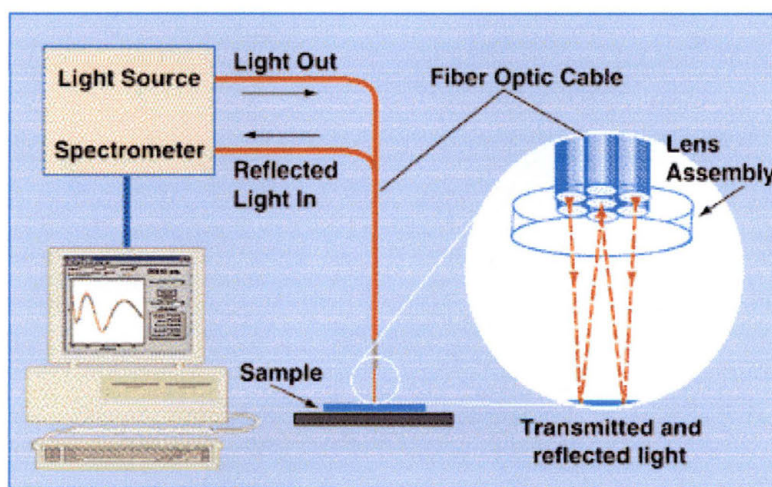


Figure 8-3: Filmetrics F-20 Setup and Operation³⁹

The sample is placed beneath an array of optical fibers. The outer ring of optical fibers that make up the lens assembly has a regulated tungsten halogen light source with an optional He light source for a range of wavelengths from ~220 nm to over 830 nm. An example of a scan can be seen in Figure 8-4.

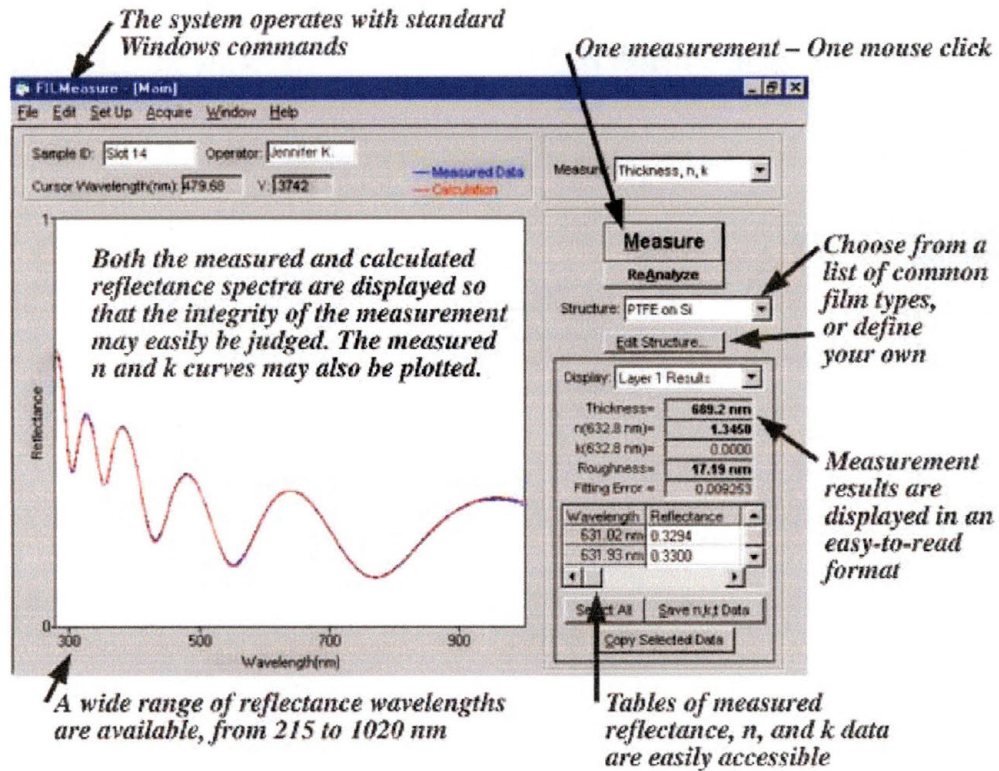


Figure 8-4: Reflectance Spectra from F-20³⁹

As can be seen in Figure 8-4, the results of the scan are presented in easy to read format and include data on film thickness, n and k values, surface roughness, and the fitting error.

9 Conclusions Based on Data

9.1 What I learned about BZT growths

The main goal of the research on the BZT films was to see if we could grow smooth epitaxial films of BZT with the correct stoichiometric phase. BZT Films were grown with the parameters that can be seen in Section 10.1.3 on 210. All the BZT films were measured using the HAXRD mode of the D-1. This was done to determine if the films had enough of a uniform crystal structure to perform PBXRD scans for further data collection. An example of one of the typical HARXD scans can be seen in Figure 9-1.

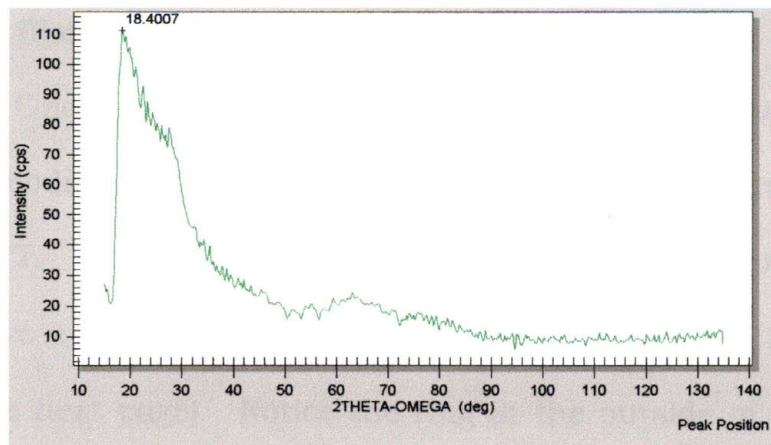


Figure 9-1: Typical Scan from BZT Films

Note the lack of any sharp, distinct peaks in the scan. This is most likely due to the fact that the film produced is a uniformly amorphous film. For the film to be amorphous is actually a success in producing a film for use as a High K dielectric. A pure crystalline film would allow electric current to pass through it much easier than would an amorphous film. With an amorphous film, crystals still exist in the material, they are just rather small and are in all directions. The grain boundaries between individual crystals acts as a barrier to the conduction of electrons, allowing the film to perform as a better insulating material than if it were a single crystal throughout the film. Unfortunately, the analysis equipment at SWT is not sufficient at this time to fully evaluate the dielectric properties of the films. This work will be left for a future thesis.

One by-product of the BZT film growths did however, lead to a modification of the DIBS that will improve future research at SWT. When I first began producing films, the films seemed to have a distinct ring system on their surfaces (see Figure 9-2 on the next page). Notice the ring at the outside of the wafer. This film is an oxide, which means that it is relatively

transparent to light. The different colors of the film are due to the fact that the film has a different thickness at different locations. The thickness of the film determines what wavelengths of light will be reflected, thus determining the apparent color of the film on the wafer.

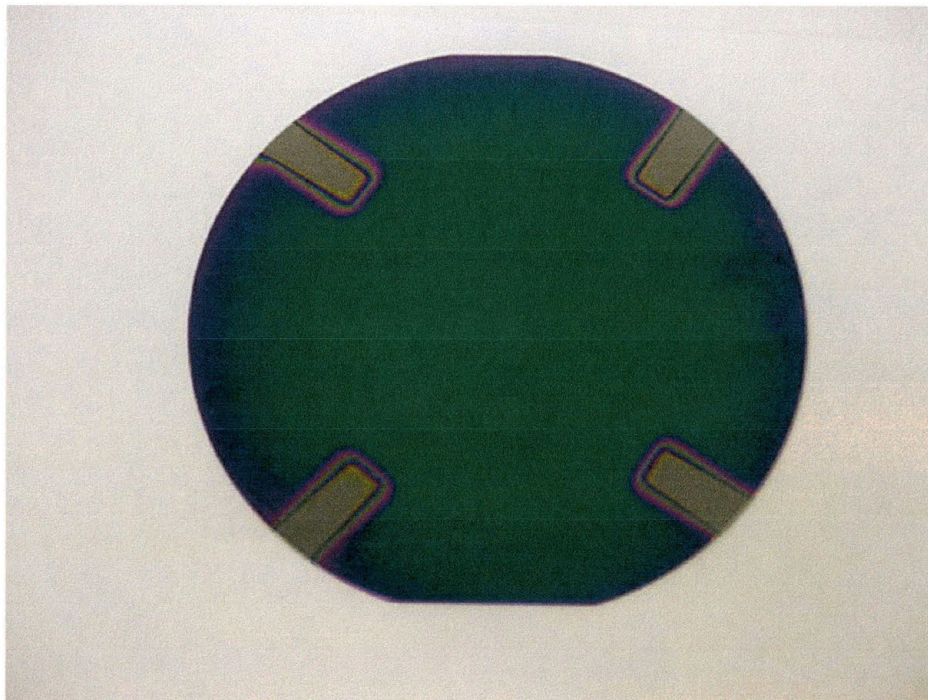


Figure 9-2: Example of Uneven Film Growth

Because the goal was to produce a uniform film over the entire wafer it was decided that the platen, the part of the DIBS that holds the wafers in place and also heats the wafers to the

desired growth temperature (see Figure 9-3), needed to be redesigned. It was also noted that the maximum temperature that the wafers could reach was only around 500°C. Since a literature search indicated that a temperature closer to 600 or even 700 °C would be desirable for the production of BZT films, it was decided to make the new platen much thinner than the old platen.

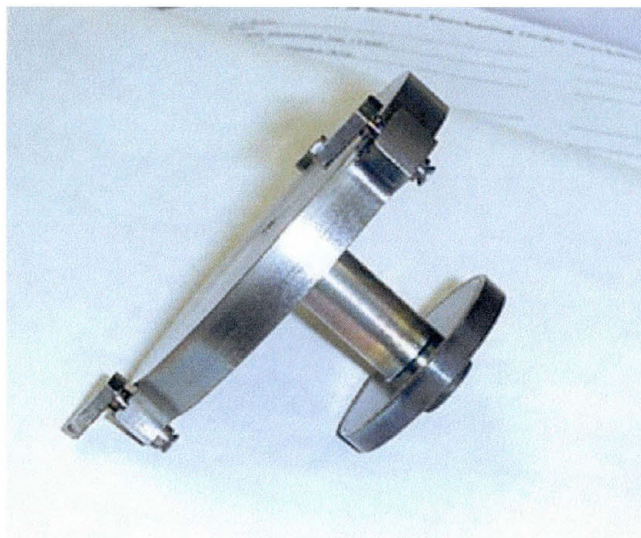


Figure 9-3: Side View of Old SWT Platen

I fully characterized the platen that was in the DIBS at the time to use as a template for a new platen. The diagrams used for the creation of the new, thinner platen can be seen in Figure 9-4 through Figure 9-7.

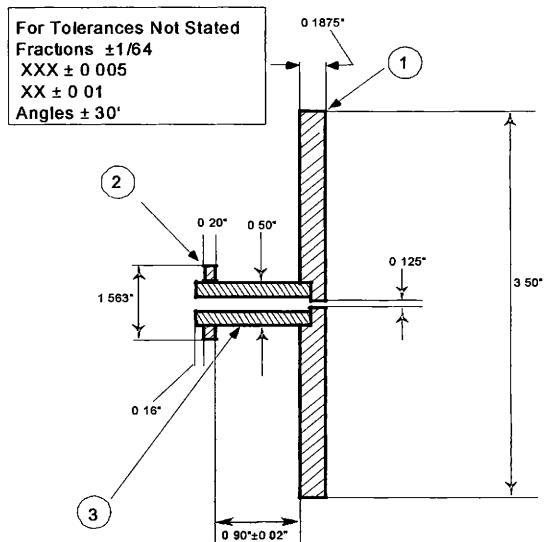


Figure 9-4: Diagram Showing Side View of New SWT Platen

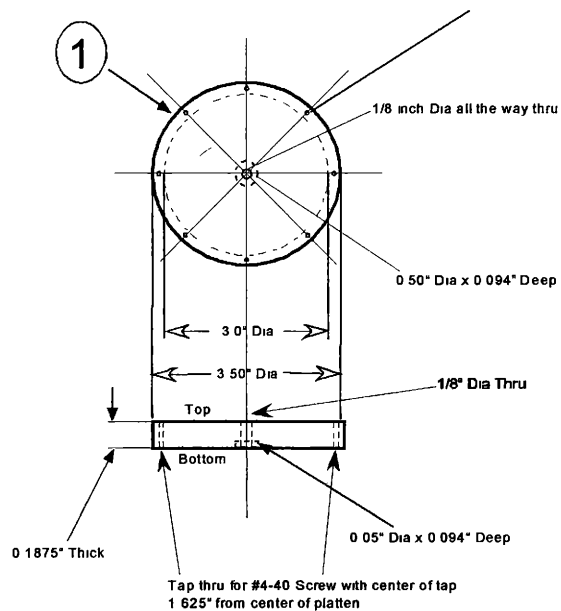


Figure 9-5: SWT Platen Details of Part #1

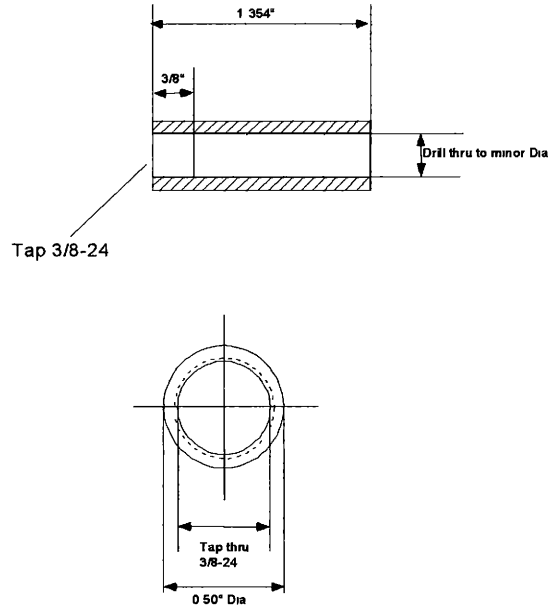


Figure 9-6: Details of SWT Platen Part #2

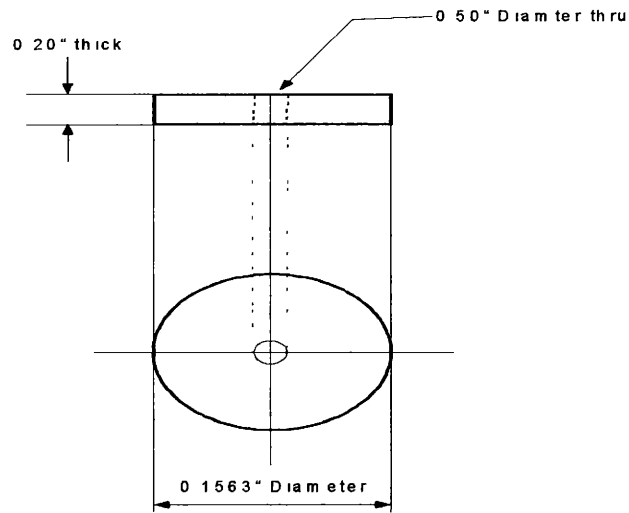


Figure 9-7: Details of SWT Platen Part #3

When the platen was built and installed into the DIBS, the first effect was that the temperature of the wafers was able to reach over 650°C. Still not the ultimately desired 700°C, but much better than the 500°C limit that existed when I first began my research.

The second effect noticed when the new platen was installed was that the uniformity of the films was markedly improved. A close inspection of Figure 9-8 shows a clear improvement of the color uniformity of the film grown on the wafer. Since this color is directly related to the thickness of the film, it is safe to say that the film uniformity has been improved.

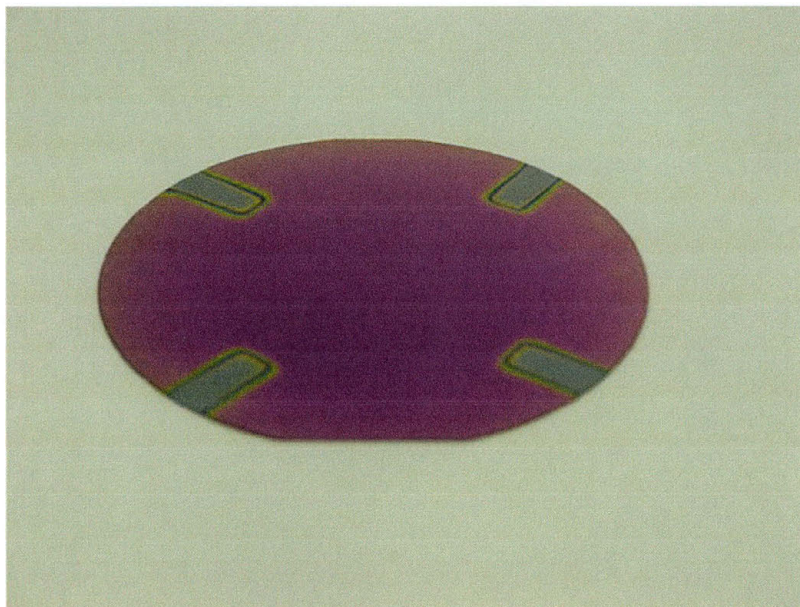


Figure 9-8: Film after New Platen Installed on DIBS

Unfortunately, this was all that was learned in the attempt to produce good films made of BZT. The fact that the films were amorphous is a good sign that the research was at least on the right track but until the films can be fully electrically characterized the question of whether or not these are good candidates for use as High K dielectrics remains open and unanswered.

9.2 What I learned about Py Growths

9.2.1 Permalloy Metal Films

For the Py films that I produced, it is possible to say much more about what I was able to accomplish. The first step in attempting to produce good, high quality films with what I call Permalloy Monoxide (PyMO) is to show that good, high quality films of pure Permalloy can be produced. To this end, I produced a series of films using both Argon and Krypton as the inert gas in the DIBS. The growth parameters for each film can be seen in Section 10.1.1 on page 208.

After the films were produced, they were all analyzed using different techniques. First, they were measured using the

Vibrating Sample Magnetometer. This was to show that the films were indeed magnetic films. A typical scan produced Hysteresis curves showing almost instantaneous shifting from magnetic saturation in one direction to magnetic saturation in the other direction (see Figure 9-9). This behavior is indicative of the magnetic properties of a good Py film: a cubic magnetocrystallization anisotropy (K) that passes through zero and a magnetostriction (λ) that also passes through zero. Details of all the VSM scans performed can be found in 10.2 starting on page 211.

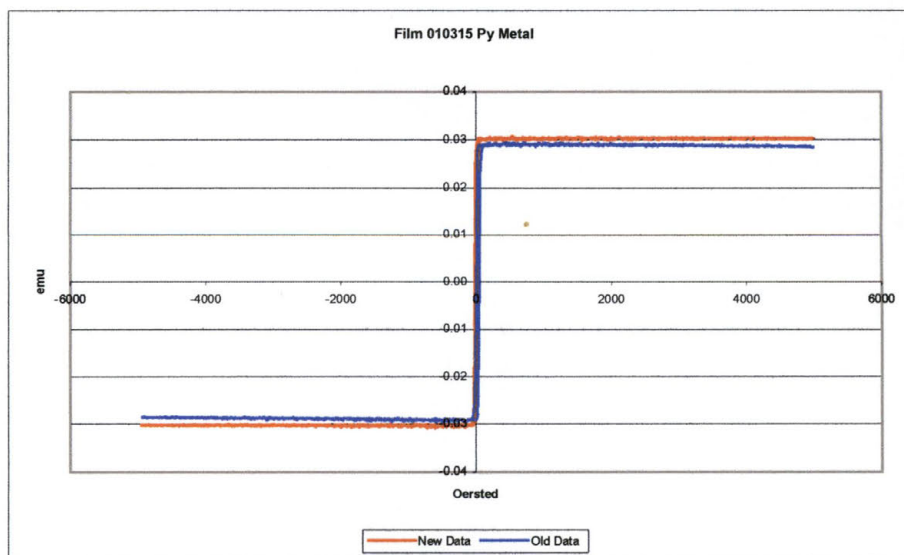


Figure 9-9: Example VSM Scan of Py Film

The films were then analyzed using the Bede D-1 in diffraction and reflectivity modes to obtain detailed information about the uniformity of the films crystallinity, thickness, and phase.

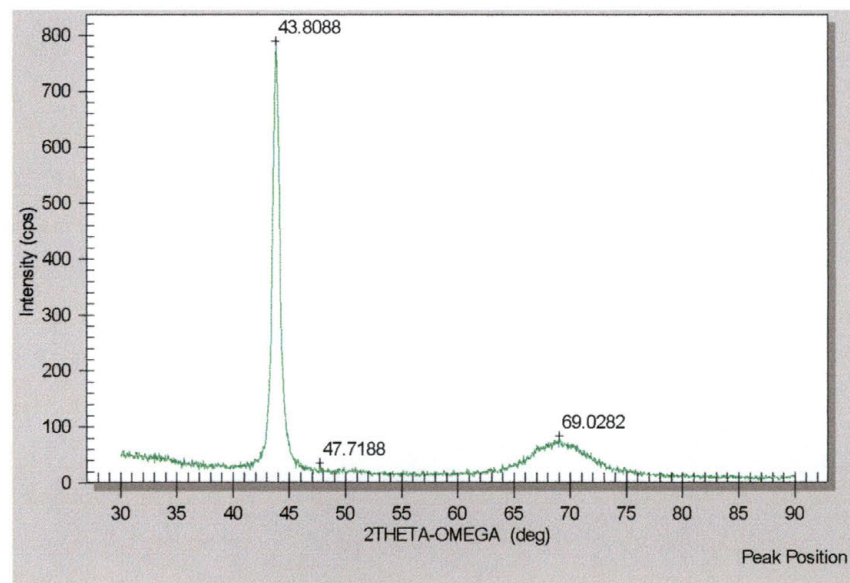


Figure 9-10: Typical High Angle X-Ray Diffraction Scan for a Permalloy Metal Film

The first method of analysis used on the D-1 was High Angle X-Ray Diffraction (HAXRD). This was performed first because it is a relatively short scan to perform (around 45 minutes per scan), and it can quickly give information about the crystal structure of the material being analyzed. Figure 9-10 shows the results of a typical HAXRD scan performed on the

films I produced for this research. Note the peak at 43.9° . This peak is the (111) crystal plane diffraction peak for a NiFe film with a crystal structure of Fm3m (225), also known as Permalloy according to the JCPDS database.

Ni	Fm3m (225)	111	200	220	222
Ni	Fm3m (225)	44.369	51.594	76.082	
Ni	Fm3m (225)	44.599	51.909	77.547	99.397
Ni	Fm3m (225)	46.534			
Ni	???	44.599	51.283	76.082	
Ni	Fm3m (225)	44.832	52.228	76.807	
Ni	Fm3m (225)	44.507	51.846		
NiFe	Fm3m (225)	111	200	220	
NiFe	Fm3m (225)	43.915	51.191	75.442	
NiFe	Fm3m (225)	43.472	50.673	74.677	

Table 3: JCPDS Data for Ni and Py Metal Films

The diffraction peak data for the films I produced were compared to the information found in the International Centre for Diffraction Data (JCPDS) database. Table 3 lists all peaks from the JCPDS database that have an intensity of greater than 30% of the 100% peak for pure Ni and for NiFe films. It also shows the lattice parameters for the peak (i.e. the diffraction plane causing the peak to be seen). Note that the (111) peak is close to 45° for all Ni samples and is close to 44° for the NiFe samples. There is also a peak expected at close to 51° for all of

the samples indicating the (200) diffraction plane, and another peak at close to 76° for pure Ni with peaks at close to 75° for the NiFe samples.

The data collected for all of the Py metal films that I produced is shown in Table 4 on the next page. The information provided shows the angle of a peak, the absolute intensity of the peak, and the relative intensity of the peak to the 100% peak. The actual HAXRD scan data can be seen in section 10.5.1 starting on page 265 . In each film I produced, the 100% peak is within 0.5° of the angle 44.0° , with another peak close to 51.0° and another peak at close to 75.0° . These angle correspond to the (111), (200), and (220) diffraction planes expected from a pure Py sample. Based on this data alone, I feel confident in stating that the films I produced are good quality Py films.

While this is good evidence that the films I produced are indeed good Py films, HAXRD is not the end of the story. PBXRD scans were also performed on all the samples produced. An example of a PBXRD scan can be seen in Figure 9-11 on the next page. Again, note the peaks shown at close to 44° , 51° ,

and 75°. As with the HAXRD scans, these peaks are indicative of Py metal samples, adding further evidence that the films I produced were indeed Py metals.

Film	10315	10319	010505A	010505B	010506A	010506B
Angle		66.3001				
Intensity		28.491				
% Intensity		26.65%				
Angle	75.8505	75.4002	75.4977	75.8308	76.6323	75.4293
Intensity	61.5514	32.3134	51.9489	60.5041	56.6109	74.4724
% Intensity	24.02%	30.22%	36.09%	32.30%	35.59%	33.22%
Angle	51.2951	50.9503	51.1106	50.9927	50.583	50.9869
Intensity	94.8962	47.9533	69.7564	88.8558	69.841	100.923
% Intensity	37.04%	44.85%	48.45%	47.43%	43.91%	45.01%
Angle				38.2176		
Intensity				90.129		
% Intensity				48.11%		
Angle	44.0887	44.15	44.0624	44.052	43.8966	43.9244
Intensity	256.231	106.926	143.962	187.347	159.051	224.205
% Intensity	100.00%	100.00%	100.00%	100.00%	100.00%	100.00%

Table 4: High Angle X-Ray Diffraction Peak Information for All Py Metal Films

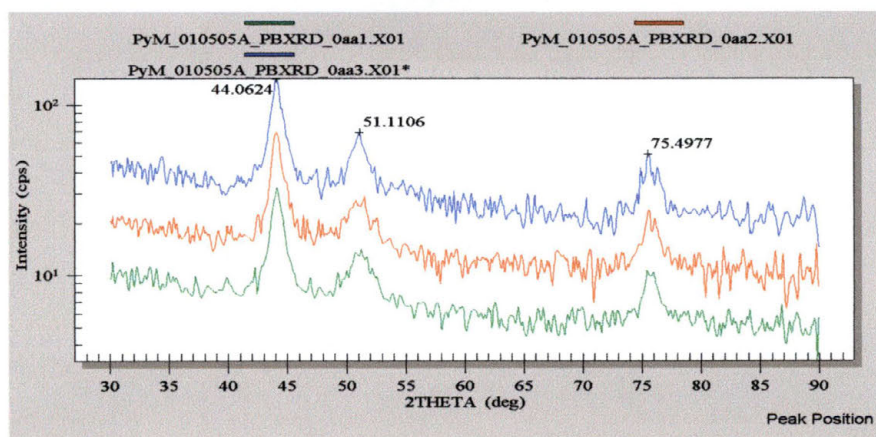


Figure 9-11: Example of a Typical Parallel Beam X-Ray Diffraction Scan on a Py Metal Film

In addition to the diffraction data, reflectivity data was also collected on the Py films that I produced. Once the reflectivity data was collected, the data was input into the Bede REFS Mercury software program to determine details about the films being analyzed. First, details about the suspected film are input into the software (see Figure 9-12). This includes information about the type of substrate used, any interfacial layers that may be produced as a result of different film layers mixing with each other, and information about the suspected films itself.

Layers:	<input type="text" value="5"/>	Points:	<input type="text" value="501"/>	Lambda:	<input type="text" value="1.541"/>	Incident Intensity:	<input type="text" value="3E+6"/>	Range % +/-:	<input type="text" value="0"/>
		Omega Start:	<input type="text" value="0"/>	Omega Finish:	<input type="text" value="5000"/>	Background Intensity:	<input type="text" value="0.1"/>		

	Material		Thickness			Roughness			Density			SL	
	X	Y	Start	Low	High	Start	Low	High	Start	Low	High		
Sub	0.0	0.0	Si	NA	NA	NA	2	5	7	1	.95	1	
1	0.0	0.0	SiO2	1877	1700	1900	100	1	200	1	.9	1	
2	.8	0.0	NiO(x)FeO(y)Fe2O3(1-y)F	30	1	40	20	1	50	1	.7	1.2	
3	.8	0.0	Ni(x)Fe(1-x)	1200	1000	1400	50	1	100	1	.8	1.1	
4	.8	0.0	NiFe2O3(x)NiFe3O4(1-x)	20	1	40	10	1	20	1	.6	1.1	

Divergence (sec):

Figure 9-12: REFS Mercury Data Input Page

Part of the process of inputting this data includes the development of suitable modeling information for the computer program to use. Material properties such as the ratio of one element to another, the density of the material, and the elemental composition of a material are all added into the programs database so that it can use this information in attempting to statistically model the experimental data.

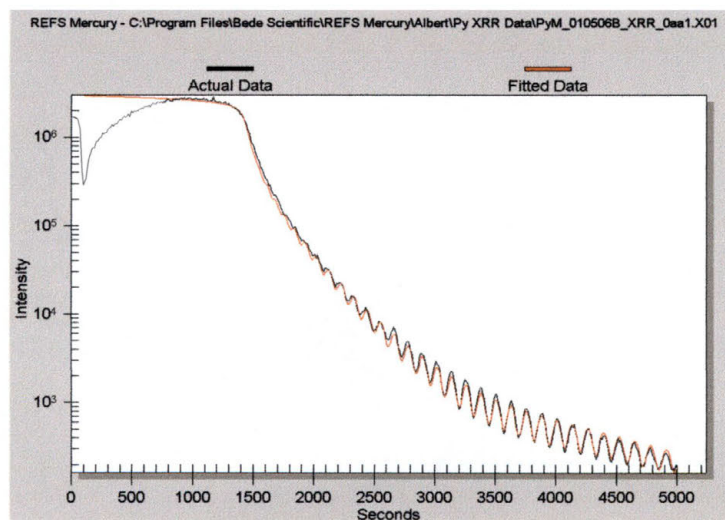


Figure 9-13: Example of REFS Mercury Model vs Experimental Data

Once this information is added to the program, the number of iterations to be calculated is input and the type of mathematical correlation is selected. The simulation is then allowed to run and the calculated data is displayed on the computer screen (see Figure 9-13). In each of these

simulations, the experimentally collected data is shown in black, while the calculated data is shown in red. The closer the red matches to the black, the better the fit, and the more accurate the model is considered to be.

As the computer is modeling the film, based on the information input into the program, it gives a running count of the number of iterations calculated, the best cost, the standardized cost, and the details used in its calculation of the model (see Figure 9-13). The Best Cost and Standardized Cost are an indication of how closely the simulated data fits with the experimental data. The lower both numbers are, the better the fit.

Evaluations: 282360			
Best Cost: 5.695			
Standardized Cost: 0.075			
Incident Intensity: 3000000.000			
TC Mean:		TC SD:	
Thickness	Roughness	Density	SL
Sub	7.00	0.96	
1	1819.16	200.00	1.00
2	1.00	5.36	1.12
3	1139.09	6.64	1.01
4	23.97	6.08	1.10

Figure 9-14: Details of Fit Information for REFS Mercury Calculations

Figure 9-14 shows a table with 4 rows of data. These rows correspond to the 4 rows of data input into the data input

page (see Figure 9-12 on page 193). The numbers indicate the layer number, estimated layer thickness, estimated layer surface roughness, and the density of each layer. These are the numbers used in the actual calculation of the model, and can be considered to be the actual information concerning the layers in the sample being analyzed.

The most important bits of information to take away from this analysis is the thickness of the material under analysis, and the closeness of the fit. The closeness of the fit is the single most important bit of information when attempting to determine the crystal structure and elemental composition of a material. If the starting data input into the program does not closely match the actual conditions of the material under analysis, the standardized cost of the fit will never reach a value under 1.0. For a very poor starting point in modeling the material, the standardized cost will likely not even fall below 20 or 30. In addition, the red curve will not come close to matching the black curve that represents the experimentally collected data.

For these reasons, it can be said that a good fit for the model, with a very low standardized cost, is indicative of a very

good starting point in the modeling of the film, at least as far as the elemental composition and the crystal structure of the material are concerned. In the example shown in Figure 9-12 through Figure 9-14, the model shows an interfacial layer between the SiO_2 of the wafer and the Py metal deposited above it with a mixture of Fe_2O_3 and Fe_3O_4 in it. On top of this is a layer of NiFe with approximately 20% Fe, and on top of this is a layer of Fe_2O_3 and Fe_3O_4 (most likely due to the interaction of the film with ambient air which contains plenty of oxygen for oxidation of the Fe in the film). XRR data along with the REFS Mercury analysis of that data can be seen for all of the Py metal films in section 10.7.1 starting on page 294.

Each of these analytic techniques shows, in some way or another, that the films produced in the course of my research are pure, high quality films of NiFe, also known as Permalloy, with a ratio of approximately 4:1 Ni to Fe. When this information is by itself, it could be considered circumstantial at the best. When it is all combined in an attempt to prove beyond a shadow of a doubt that the Py metal films that I produced are indeed Py metal the evidence is simply too strong to deny. It

can be said with a great deal of confidence that the films I produced are Py metal films.

9.2.2 Permalloy Oxide Films

All Permalloy Oxide (PyO) films were analyzed using the same techniques as were used for the analysis of the Permalloy metal films. The growth parameters for each individual film can be seen in section 10.1.2 on page 209. The goal in producing Py Oxide films was to produce non-magnetic films that could be used as a possible film for GMR Read/Write heads for magnetic hard disk drives and for possible use in spin valve transistors. A major milestone in the production of these films was also to produce films that contained iron oxide in the form of FeO instead of Fe₂O₃ or Fe₃O₄.

Two of the PyO films were chosen for analysis by VSM. It was decided that since the growth parameters from one film to another were not drastically different that if two films were similar magnetically, it would be safe to make the assumption that all the films were similar. Figure 9-15 on the next page shows one of the two PyO film scans using VSM.

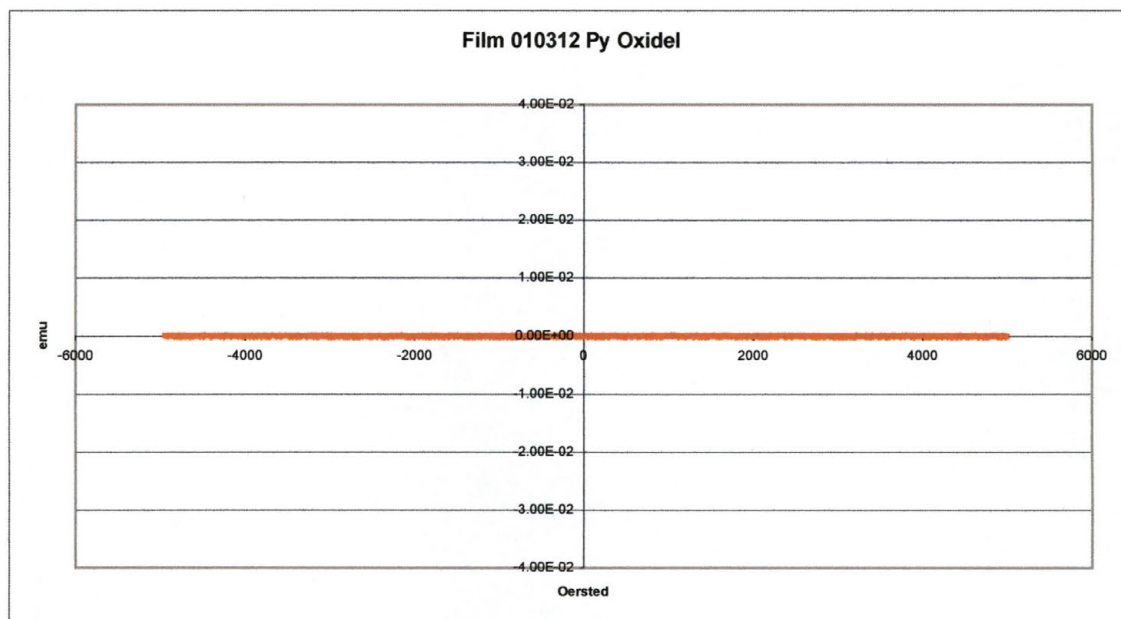


**Figure 9-15: Example of Permalloy Oxide Vibrating Sample
Magnetometry Scan**

Note how the scan data is a straight line, no matter how strong the externally applied magnetic field gets. This is a very strong indication that the material being analyzed has no magnetic moment worth mentioning. The other scan can be seen on page 214.

The films were then analyzed using the Bede D-1 in diffraction and reflectivity modes to obtain detailed information about the uniformity of the films crystallinity, thickness, and phase.

The first method of analysis used on the D-1 was High Angle X-Ray Diffraction (HAXRD). Again, as with the Py metal films, this was performed first because it is a relatively quick scan to perform and it can rapidly provide information about the crystal structure of the material being analyzed.

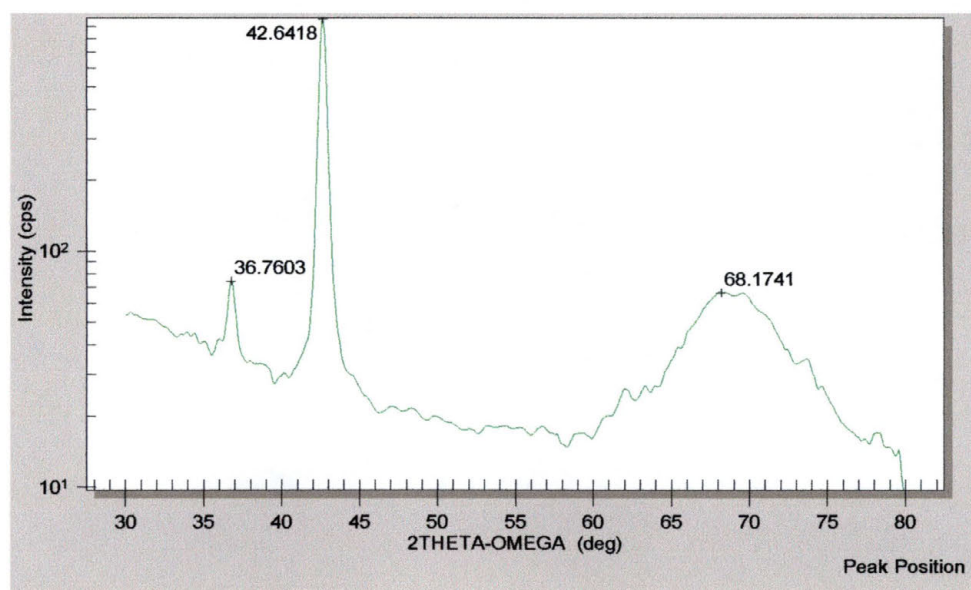


Figure 9-16: Example of HAXRD Scan of Permalloy Metal Film

Figure 9-16 shows the results of a typical HAXRD scan performed on the films I produced for this research. Note the peak at close to 37°. This peak is very close to the (111) peak for Ni Monoxide at around 37.4° but is also extremely close to the (111) peak for Fe Monoxide at around 36.3°. The D-1 has difficulty resolving two such close peaks due to the emission of

$K_{\alpha 1}$ and $K_{\alpha 2}$ x-rays. It is also interesting that the peak seen is almost directly between the expected peaks from NiO and FeO. Table 5 (below) shows all of the expected peaks as obtained from the JCPDS database along with the lattice parameters for the expected peaks.

FeO	Fm3m (225)	111	200	220	311	222
FeO	Fm3m (225)	36.19	41.988	60.897	73.327	76.807
FeO	Fm3m (225)	36.04	41.927	60.764		
FeO	Fm3m (225)	36.342	42.194	61.164	73.13	76.99
NiO	Fm3m (225)	111	200	220	311	222
NiO	Fm3m (225)	37.441	43.472	63.202		
NiO	Fm3m (225)	37.28	43.253	62.726	75.372	79.867
NiO	Fm3m (225)	37.28	43.297	62.916		

Table 5: JCPDS Data for Ni, Fe, and Py Oxide Films

Note that for FeO there are expected peaks at close to 42.0° for the (200) plane, close to 61.0° for the (220) plane, and close to 73.3° for the (311) plane. At the same time, for NiO there are expected peaks at close to 43.3° for the (200) plane, 63.5° for the (220) plane, and close to 75.3° for the (311) plane.

The data collected for all of the PyO films that I produced in the course of my research can be seen in Table 6 on the next page. As with the data for the Py metal films, the information provided gives the angle of all major peaks seen in the scans, the absolute intensity of the peak at each angle, and the relative

intensity as a percentage of the 100% peak. The actual HAXRD scans can be seen in section 10.5.2 beginning on page 271. In each film I produced, the 100% peak was within 0.5° of 42.5° . This is very close to the expected peak from the (200) plane if the film was pure FeO. It is possible that the peak shifted closer to the expected peak for the (200) plane of NiO which should be seen at close to 43.3° , however, it is not definitive in any way.

Film	10312	10314	10323	10415	10501
Thickness (Å)	1665	893.4	967.2		
Assist Gas	O2 1.0	O2 1.0	O2 1.0	O2 1.0	O2 1.0
	(N)	(N)	(R)	(N)	(R)
Angle			86.5554		
Intensity			12.2055		
% Intensity			12.13%		
Angle	74.7999	76.332	77.4954	76.3348	
Intensity	35.10823	28.2281	20.4269	18.6664	
% Intensity	16.73%	21.25%	20.30%	23.48%	
Angle	50.55				
Intensity	41.5309				
% Intensity	19.79%				
Angle	61.9499	61.8186	61.861	61.5261	61.7762
Intensity	66.4871	47.7784	20.7022	22.5987	55.8388
% Intensity	31.68%	35.97%	20.57%	28.43%	45.18%
Angle	36.8001	36.7288	36.5387	36.1754	36.0791
Intensity	68.3939	68.1823	29.5946	28.5454	113.998
% Intensity	32.58%	51.33%	29.41%	35.90%	92.23%
Angle	42.6998	42.6173	42.4663	42.3136	42.0789
Intensity	209.897	132.833	100.641	79.5027	123.6
% Intensity	100.00%	100.00%	100.00%	100.00%	100.00%

Table 6: High Angle X-Ray Diffraction Peak Information for All Py Oxide Films

The peaks on the PyO scans seen at 36° are very close to the expected peaks from the (111) plane in a sample of FeO which is around 36.1° , while the peaks at close to 62° are once again approximately halfway between 61° and 63° which are the peaks of FeO and NiO respectively for the (220) plane. Again, this evidence is close to what would be preferred if the samples I produced were exactly what I was hoping to produce, FeO, but they are not in any way conclusive.

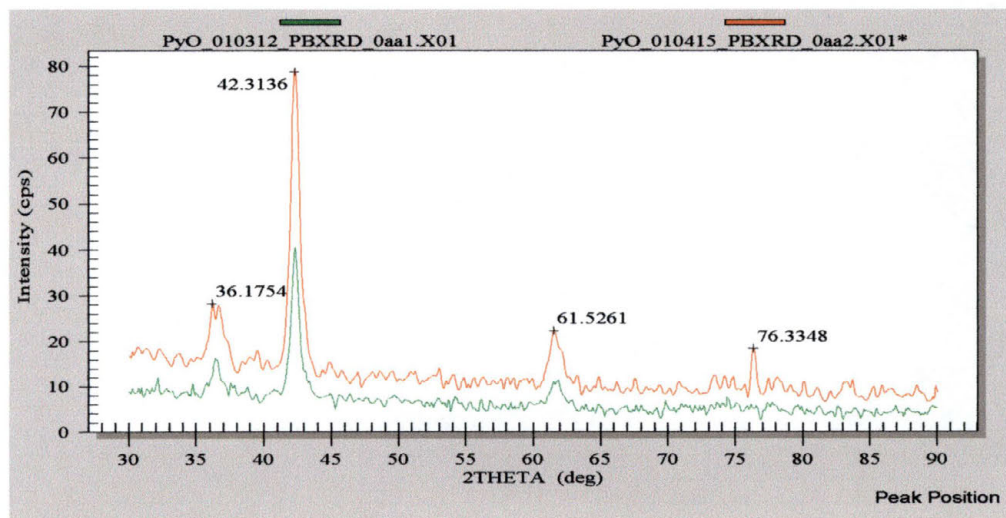


Figure 9-17: Example of PBXRD Scan for a Permalloy Oxide Film

The Parallel Beam X-Ray Diffraction (PBXRD) data shows peaks at approximately the same locations as the HAXRD scans did, with peaks located close to 36° , 42° , 61° , and 76° . Again,

this hints that the films I produced were what I was intending to produce, but the data is not quite definitive.

In order to define further the exact nature of the PyO films that I produced in my research, the films were analyzed using the D-1 in reflectivity mode, as was done with the Py metal films. Again, once the data was collected, it was input into the REFS Mercury program to attempt to determine the actual details of the films produced.

The screenshot shows the REFS Mercury software interface with the following input parameters:

- Layers: 5
- Points: 501
- Lambda: 1.541
- Incident Intensity: 3E+6
- Range % +/-: 0
- Omega Start: 0
- Omega Finish: 5000
- Background Intensity: 0.1

The main data table is as follows:

Sub	Material		Thickness			Roughness			Density			SI
	X	Y	Start	Low	High	Start	Low	High	Start	Low	High	
	0.0	0.0	Si	NA	NA	NA	2	5	25	1	.95	1
1	0.0	0.0	SiO2	1877	1700	1900	20	1	40	1	.9	1
2	.8	0.0	NiO(x)FeO(1-x)	30	25	50	5	5	10	1	.7	1.2
3	.8	0.0	NiO(x)FeO(1-x)	750	650	900	50	1	200	1	0.5	1.5
4	.8	0.0	NiFe2O3(x)NiFe3O4(1-x)	40	1	80	5	1	10	1	0.5	1.5

At the bottom, the Divergence (sec) is set to 0.

Figure 9-18: Example of REFS Mercury Data Input for PyO Film

It was when these films were analyzed using the computer models that I became convinced that I had indeed produced good, high quality non-magnetic films of Permalloy Oxide containing FeO instead of Fe₂O₃ or Fe₃O₄. When the

initial guess as to what material existed in the sample was input into the program I used a model that had a changeable ratio of NiO to FeO (see Figure 9-18). In both cases, the density and the elemental composition for the materials was based on the monoxide phase of the molecule. The appropriate guess as to the film thickness, interfacial layers, and surface roughness of all layers was also input into the computer modeling software, and the program was allowed to run for just over 40,000 iterations in the example used here.

A close look at Figure 9-19 on the next page shows that the model was fairly accurate at matching up with the experimental data. Notice how each “peak and valley” of the reflectivity model is almost directly on top of the experimental data. As was mentioned in the discussion of the Py metal films, the Best Cost and the Standardized Cost are pieces of information that indicate how closely the model fits to the experimental data. The lower the numbers, the better the fit. For the example used here, the Best Cost was only 1.853 and the Standardized Cost was only 0.065 (see Figure 9-20 on next

page)! All of the XRR scans can be viewed in section 10.7.2 starting on page 301.

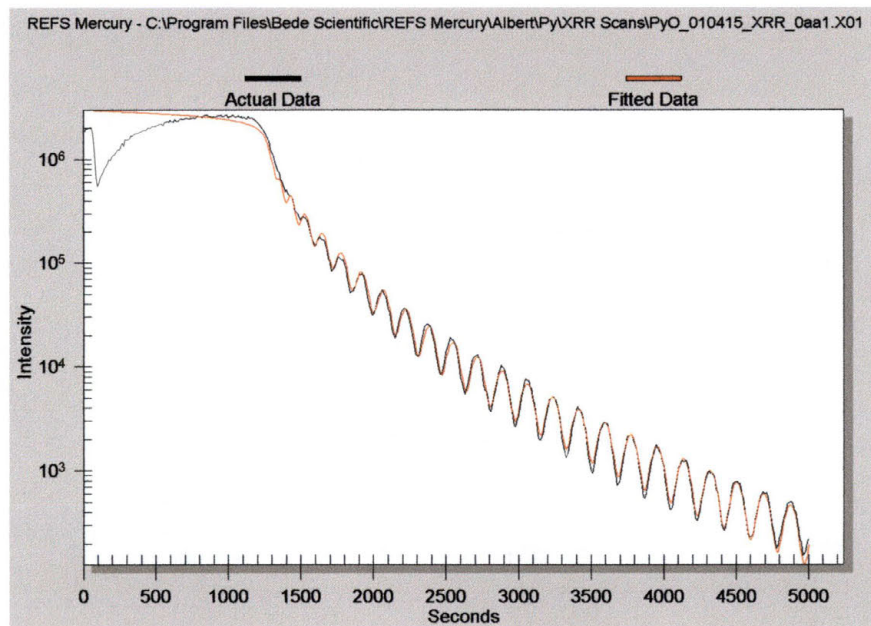


Figure 9-19: REFS Mercury Fit to Experimental Data for a PyO Film

Evaluations: 40120				
Best Cost: 1.853				
Standardized Cost: 0.065				
Incident Intensity: 3000000.000				
TC Mean: TC SD:				
	Thickness	Roughness	Density	SL
Sub		12.68	1.00	
1	1735.85	32.41	0.95	
2	50.00	5.18	0.70	
3	747.25	19.17	1.02	
4	80.00	5.88	1.18	

Figure 9-20: REFS Mercury Calculated Details of PyO Film

When this information is added to the circumstantial information obtained in the HAXRD and PBXRD scans, I feel confident in stating that this goal of the research project that became my thesis was a success! The Permalloy Oxide films that were produced in the Dual Ion-Beam Sputtering system at SWT are indeed what I call Permalloy Monoxide films. These are non-magnetic films containing NiO and FeO with little or no traces of Fe₂O₃ or Fe₃O₄ in their crystal lattice.

10 Raw Data

10.1 Film Production Parameters

10.1.1 Permalloy Metal Films

In the following chart, the following applies:

Ar is Argon Gas

Kr is Krypton Gas

Film	10315	10319	010505A	010505B	010506A	010506B
SiO ₂ Thickness	3000	3000	1877	1877	1877	1877
Target	Py	Py	Py	Py	Py	Py
Thickness (Å)	Metal	Metal	Metal	Metal	Metal	Metal
Beam Volts	800	800	800	800	800	800
Beam Current	20	14.6-14.0	20	20	20	20
Target Gas	Kr 6.0	Kr 6.0	Ar 6.0	Ar 6.0	Kr 6.0	Kr 6.0
Target Gas	N/A	N/A	N/A	N/A	N/A	N/A
Assist Gas	Kr 6.0	Kr 6.0	Ar 6.0	Ar 6.0	Kr 6.0	Kr 6.0
Assist Gas	N/A	N/A	N/A	N/A	N/A	N/A
Film Pre-Sputter	Yes	Yes	Yes	Yes	Yes	Yes
Temp (C)	150	48-47	21-24	24-28	26-28	21-27
Time (S)	1200	600	600	1200	600	1200

10.1.2 Permalloy Oxide Films

In the following chart, the following applies:

Ar is Argon Gas

Kr is Krypton Gas

O (N) is oxygen just bled into the growth chamber

O (R) is oxygen that has been ionized by the Kaufman source.

Film	10305	10312	10314	10323	10415	10501
SiO ₂ Thickness	3000	3000	3000	3000	1877	1877
Target	Py	Py	Py	Py	Py	Py
Thickness (Å)	Lost(?)	1665	893.4	967.2		
Beam Volts	800	800	800	800	800	800
Beam Current	20	20	20	14.9-14.0	20	20
Target Gas	Ar 6.0	Ar 6.0	Ar 6.0	Kr 6.0	Ar 6.0	Ar 6.0
Target Gas	N/A	N/A	N/A	N/A	N/A	N/A
Assist Gas	Ar 6.0	Ar 6.0	Ar 6.0	Kr 6.0	Ar 6.0	Ar 6.0
Assist Gas	N/A	O ₂ 1.0				
Assist Gas	N/A	(N)	(N)	(R)	(N)	(R)
Film Pre-Sputter	Yes	Yes	Yes	Yes	Yes	Yes
Temp (C)	150	150	150	150	27-29	27-29
Time (S)	1200	1200	600	600	600	600

10.1.3 Barium Zirconium Titanate Films

In the following chart, the following applies:

Ar is Argon Gas

Kr is Krypton Gas

O (N) is oxygen just bled into the growth chamber

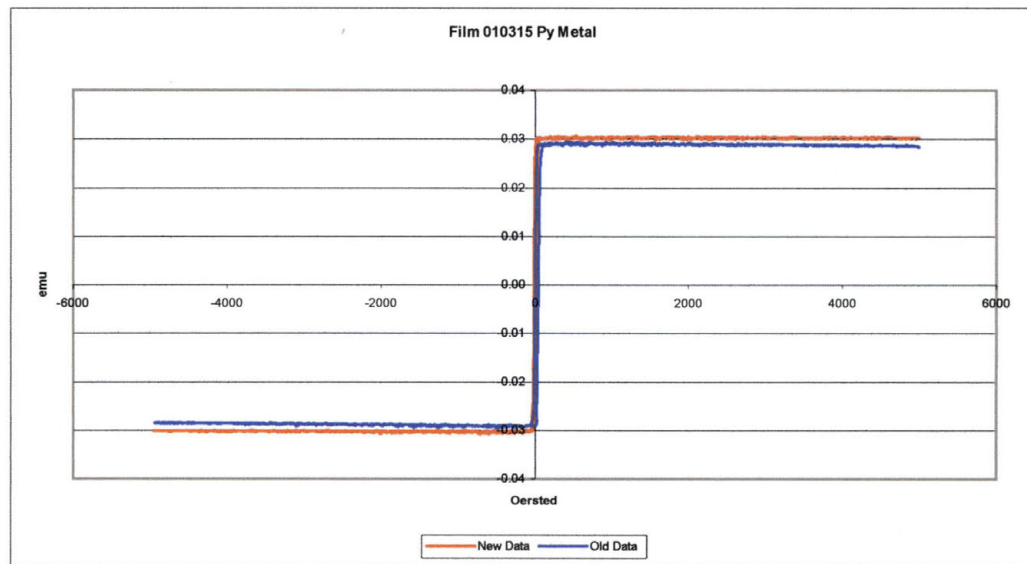
O (R) is oxygen that has been ionized by the Kaufman source.

Film	10206	10208	10209	10326	10410	10413	010415B	010501B	010504AB
SiO ₂ Thickness	3000	3000	3000	3000	1877	1877	1877	1877	1877
Target	BZT	BZT							
Thickness (Å)	910.7	1115	1343	876.6	493.9	2698			
Beam Volts	800	800	800	800	800	800	800	800	800
Beam Current	20.4	30	30	20	20	20	20	20	20
Target Gas	Ar 6.95	Ar 6.95	Ar 6.95	Kr 5.0	Kr 7.5	Kr 7.0	Ar 6.0	Ar 6.0	Ar 6.0
Target Gas	O ₂ 1.0	O ₂ 1.0	O ₂ 1.0	O ₂ 1.0	O ₂ 1.5	O ₂ 1.5	N/A	N/A	N/A
Assist Gas	N/A	Ar 5.0	Ar 6.95	Kr 5.0	Kr 7.5	Kr 7.5	Ar 6.0	Ar 6.0	Ar 6.0
Assist Gas	N/A	O ₂ 1.0	O ₂ 1.0	O ₂ 1.0	O ₂ 1.5	O ₂ 1.5	O ₂ 1.0	O ₂ 1.0	N/A
Assist Gas	N/A	(N)	(N)	(R)	(N)	(R)	(R)	(N)	N/A
Film Pre-Sputter	No	Yes	Yea						
Temp (C)	500	500	68-138 No Htrs	500	600	600	23-28	23-28	24-27
Time (S)	1200	1200	1200	1200	600	3600	600	600	600

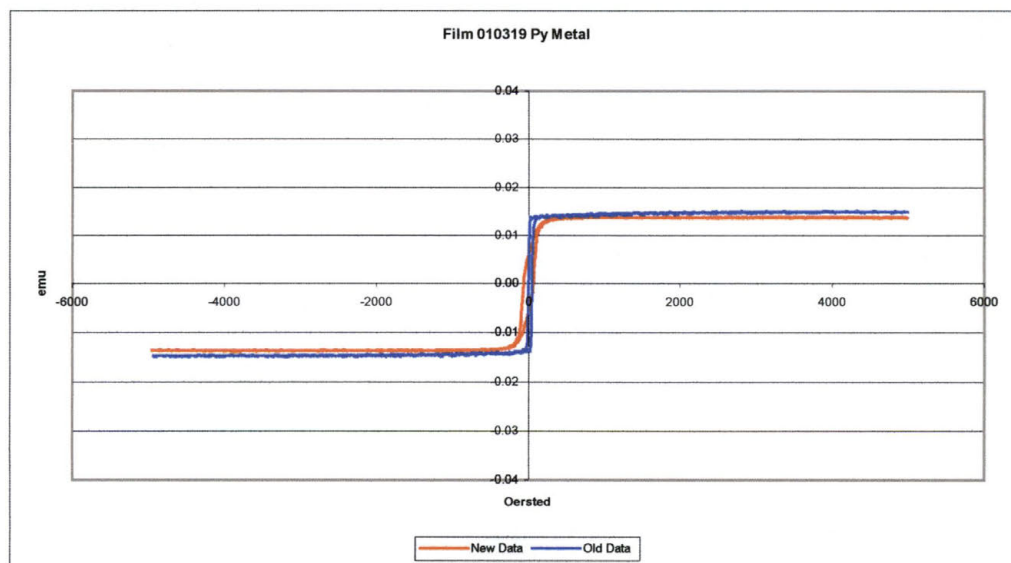
10.2 Vibrating Sample Magnetometry Data

PERMALLOY METAL FILMS

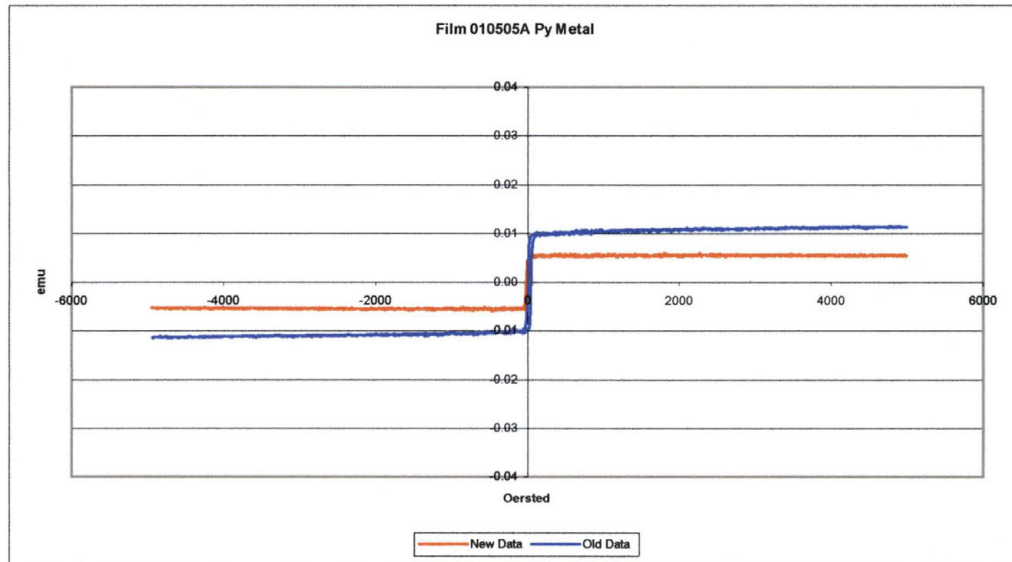
10.2.1 Film 010315



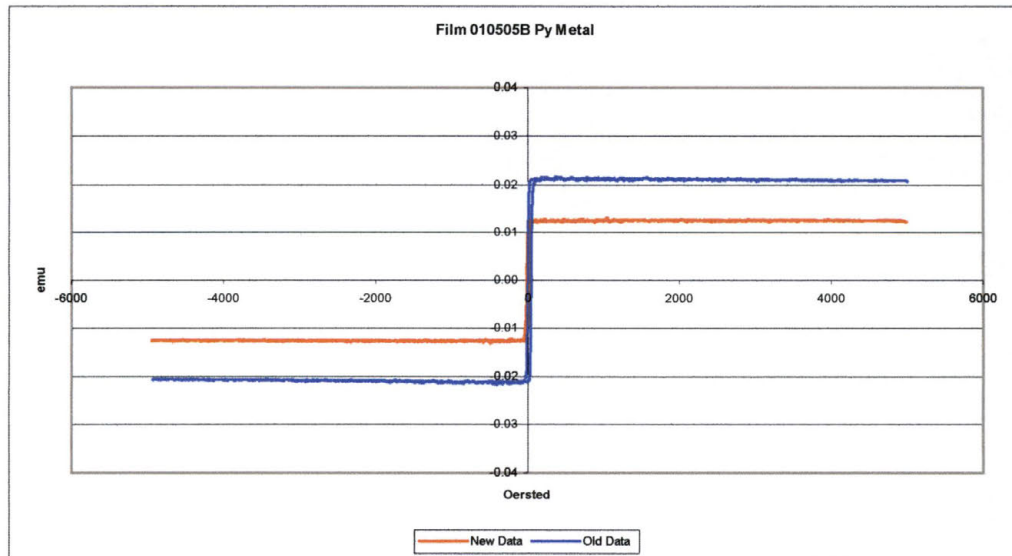
10.2.2 Film 010319

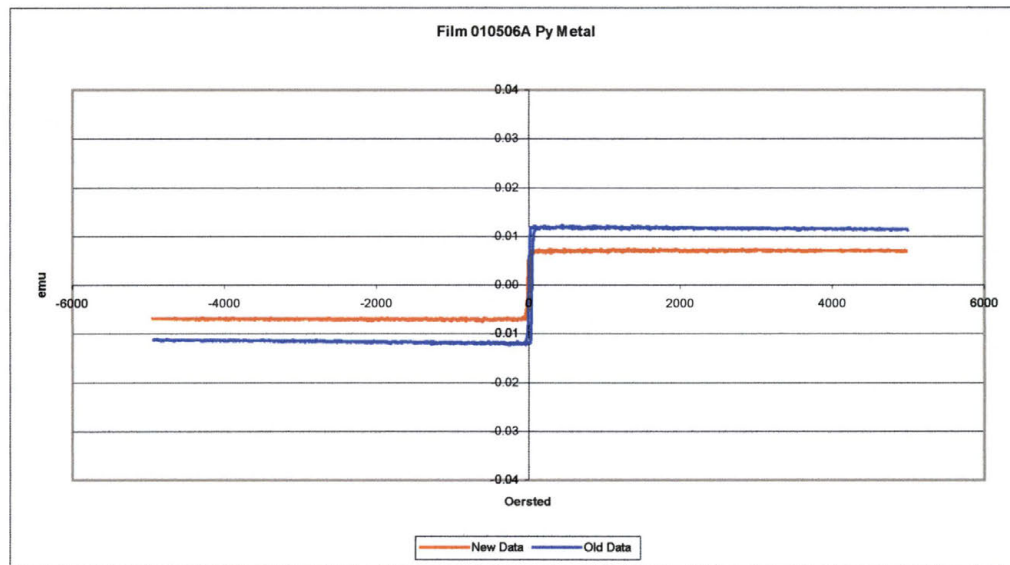
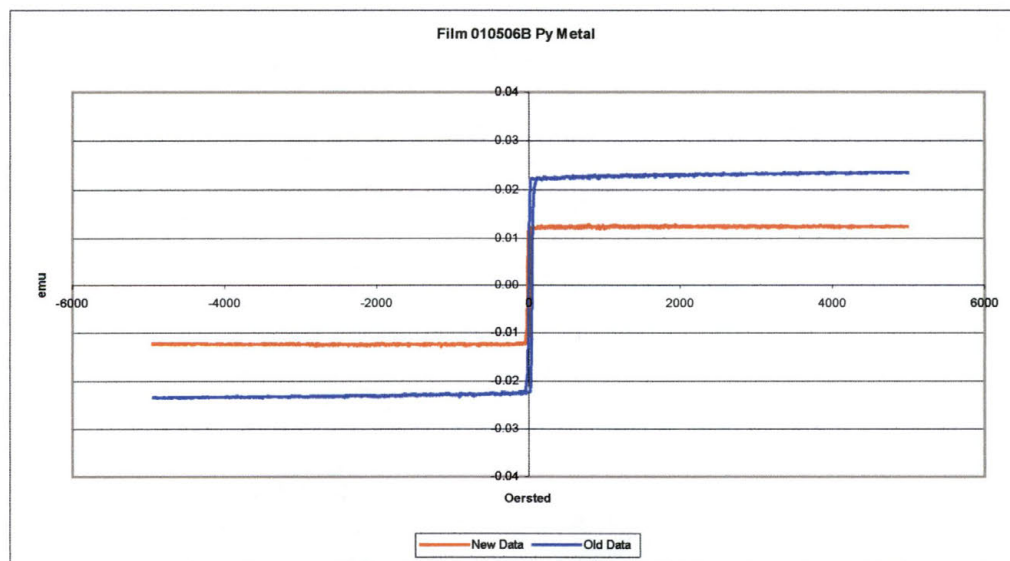


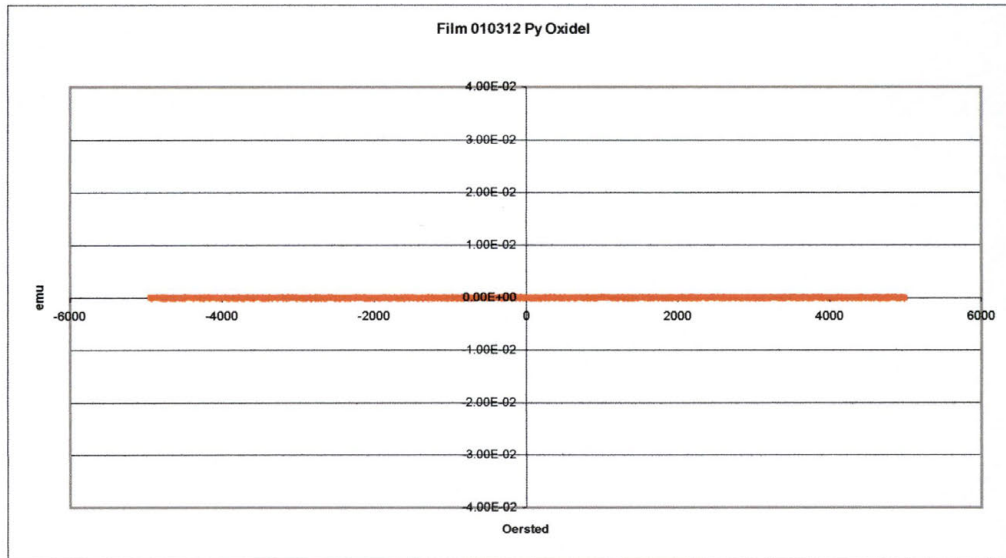
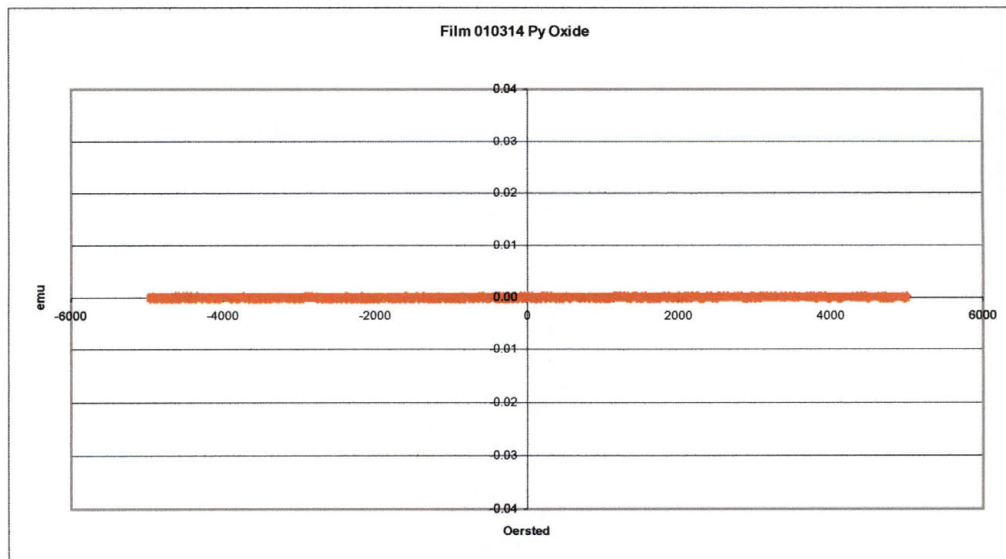
10.2.3 Film 010505A



10.2.4 Film 010505B



10.2.5 Film 010506A**10.2.6 Film 010506B**

PERMALLOY OXIDE FILMS**10.2.7 Film 010312****10.2.8 Film 010314**

10.3 Optical Data

The optical data was taken in a pattern of concentric rings. This was in an attempt to determine the uniformity of the films being produced. The data was collected in locations at 12, 3, 6, and 9 o'clock. The location "a" is at the center of the wafer. The data points on the ring labeled "b" are 0.5 inches from the center of the wafer. The data points on the ring labeled "c" are one inch from the center of the wafer (see Figure 10-1).

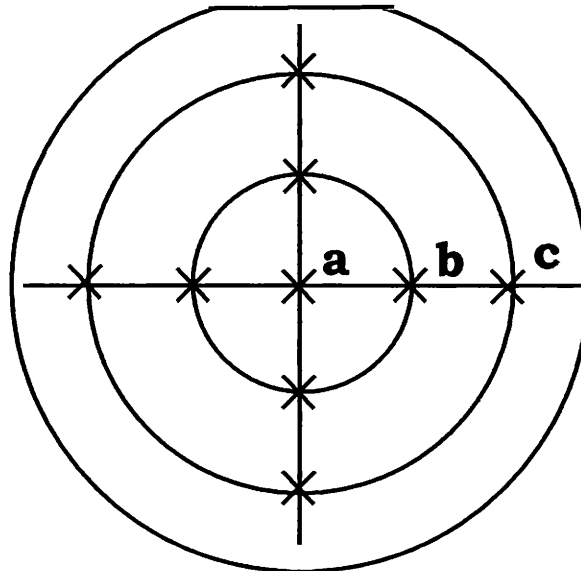


Figure 10-1: F-20 Data Collection Locations

	Scanned by Filmetrics- No error or graphs available
	BZT Films
	PY Oxide Films

	FILM	010206	010208	010209	010326	010410	010413
Avg	Thickness (A)	863.8	1038.2	1310.6	881.3	509.2	2682.2
A	Thickness	910.7	1115	1343	876.6	493.9	2698
A	Error				0.026	0.015	0.038
B-12	Thickness	892.9	1084	1334	900.9	499.1	2677
B-12	Error				0.024	0.013	0.039
B-3	Thickness	885.6	1086	1332	866.3	508.5	2696
B-3	Error				0.030	0.015	0.036
B-6	Thickness	895.6	996.8	1330	865.4	513.5	2695
B-6	Error				0.030	0.016	0.037
B-9	Thickness	901.7	1088	1329	870.3	516.9	2723
B-9	Error				0.021	0.017	0.037
C-12	Thickness	812.7	1001	1281	904.2	512.1	2609
C-12	Error				0.019	0.015	0.027
C-3	Thickness	809.3	996.8	1280	899.8	509.4	2639
C-3	Error				0.036	0.013	0.027
C-6	Thickness	829.8	968.9	1278	898.2	518.9	2708
C-6	Error				0.020	0.018	0.032
C-9	Thickness	835.6	1007	1288	849.9	510.8	2695
C-9	Error				0.021	0.027	0.027

	FILM	010415B	010501B	010504AB
Avg	Thickness (A)	0.0	0.0	0.0
A	Thickness			
A	Error			
B-12	Thickness			
B-12	Error			
B-3	Thickness			
B-3	Error			
B-6	Thickness			
B-6	Error			
B-9	Thickness			
B-9	Error			
C-12	Thickness			
C-12	Error			
C-3	Thickness			
C-3	Error			
C-6	Thickness			
C-6	Error			
C-9	Thickness			
C-9	Error			

Note: No data was taken for these films. I was presented with the opportunity to work as an Intern as International SEMATECH and began my internship before all data was collected. The tool was lent to the technology department while I was away and the opportunity for me to scan these films never presented itself. I decided that the thickness measurements made from the x-ray reflectivity scans would suffice for something as elementary as the thickness of the films produced.

	FILM	010312	010314	010323	010415	010501
Avg	Thickness (A)	1591.0	858.1	935.2	440.6	442.8
A	Thickness	1665	893.4	961.2	447.8	447.2
A	Error	0.022	0.022	0.027	0.031	0.030
B-12	Thickness	1666	887.2	961.9	421.4	435.6
B-12	Error	0.024	0.023	0.026	0.030	0.031
B-3	Thickness	1653	884.8	958.6	443.3	441.4
B-3	Error	0.023	0.020	0.025	0.038	0.021
B-6	Thickness	1605	901.4	948.7	435.1	443.1
B-6	Error	0.026	0.021	0.028	0.041	0.026
B-9	Thickness	1583	878.4	959	442.6	437.3
B-9	Error	0.026	0.021	0.027	0.032	0.025
C-12	Thickness	1574	853.4	925.7	432.1	447.8
C-12	Error	0.021	0.020	0.024	0.030	0.028
C-3	Thickness	1574	869.1	901.4	457.6	443.6
C-3	Error	0.021	0.012	0.020	0.035	0.029
C-6	Thickness	1487	703.9	886	458.8	449.7
C-6	Error	0.024	0.033	0.023	0.031	0.030
C-9	Thickness	1512	851.5	914.6	426.7	439.6
C-9	Error	0.050	0.020	0.022	0.040	0.026

On the charts above, the data is arranged as follows: The location is given for where the data was collected, the resulting film thickness is listed along with the error. The error is an indication of how closely the calculated data matched the experimental data. The calculated data is what was used to determine the thickness of the film, so the smaller the error, the better the fit and the more accurate the fit. The actual scans are shown on the following pages. In all the graphs, the blue line is the experimental data while the pink line is the calculated data. The closer one line is to the other, the better the fit.

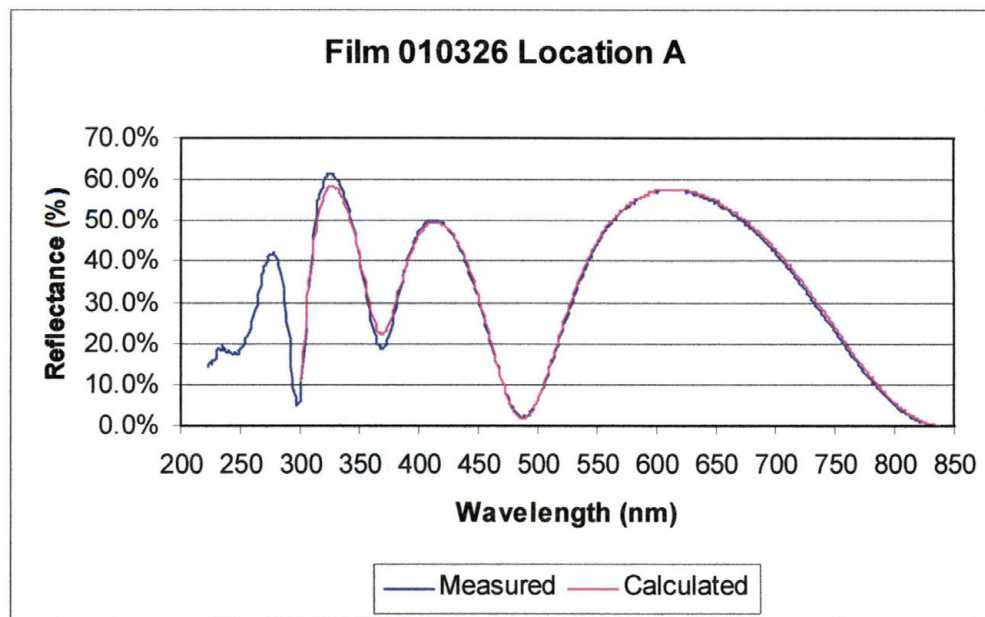
Note: This method only works for films that are at least semi-transparent. It does not work for metal films, only oxides.

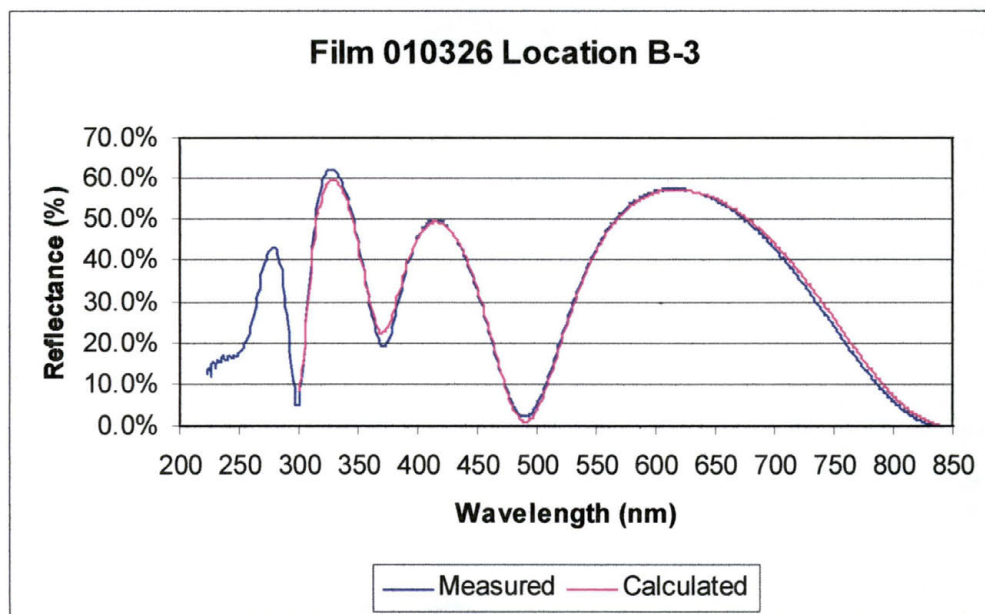
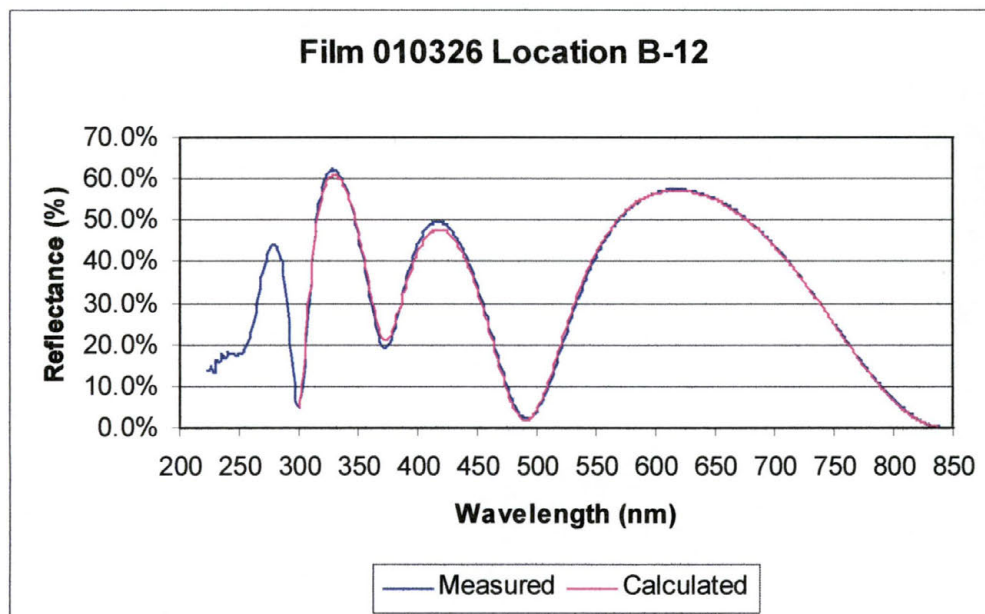
10.3.1 Barium Zirconium Titanate Films

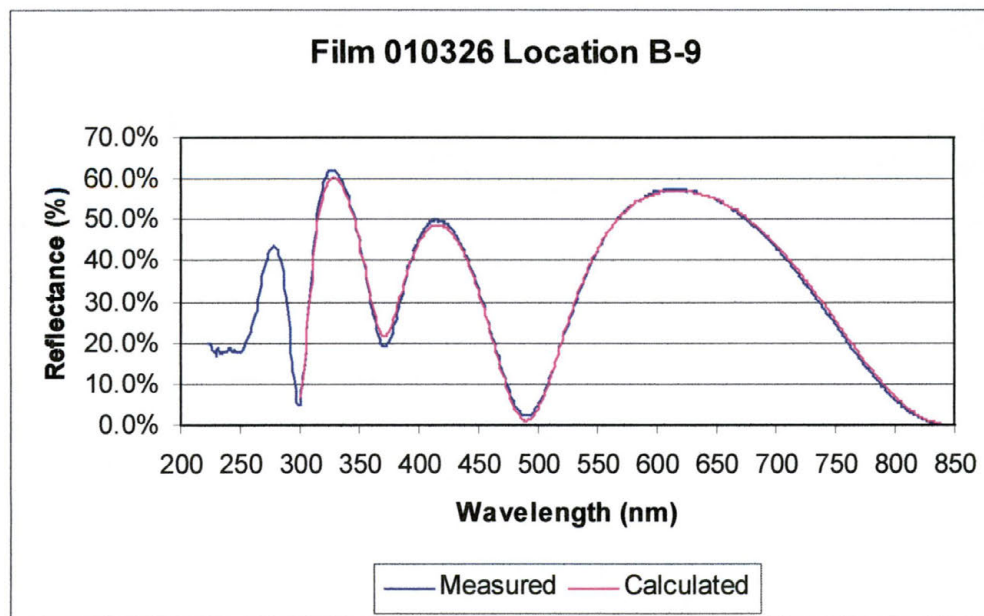
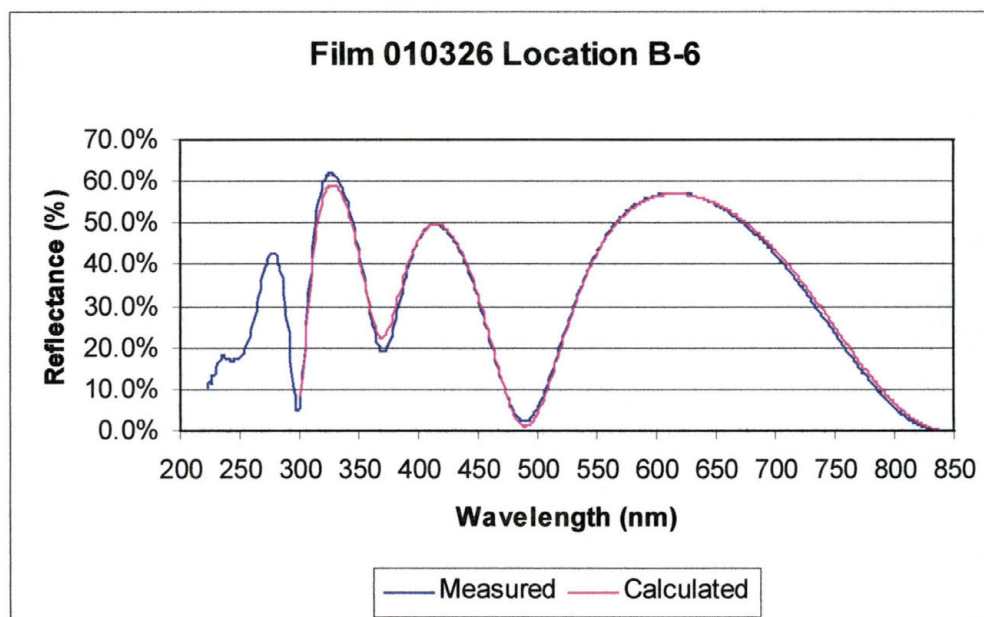
10.3.1.1 Film 010206, 010208, and 010209

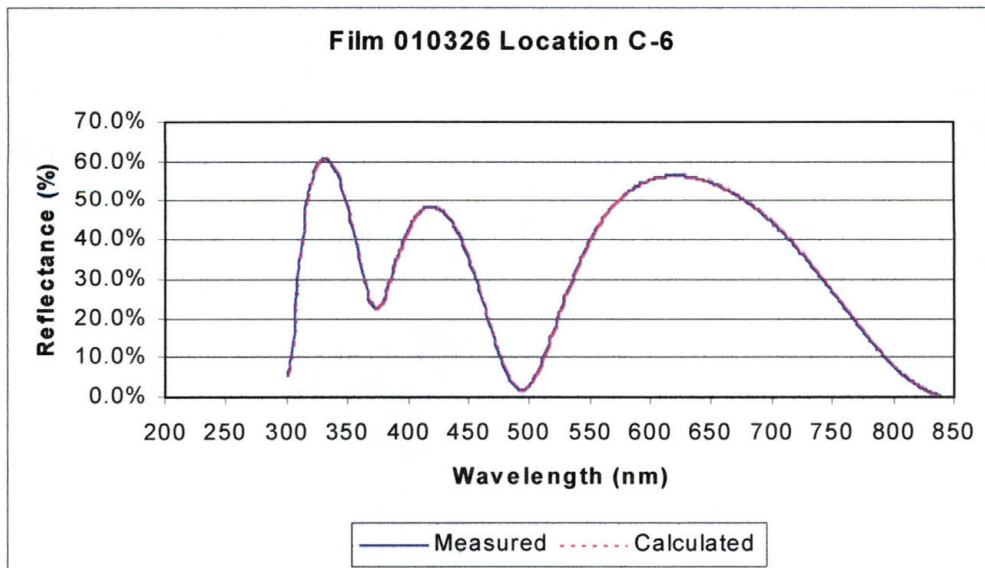
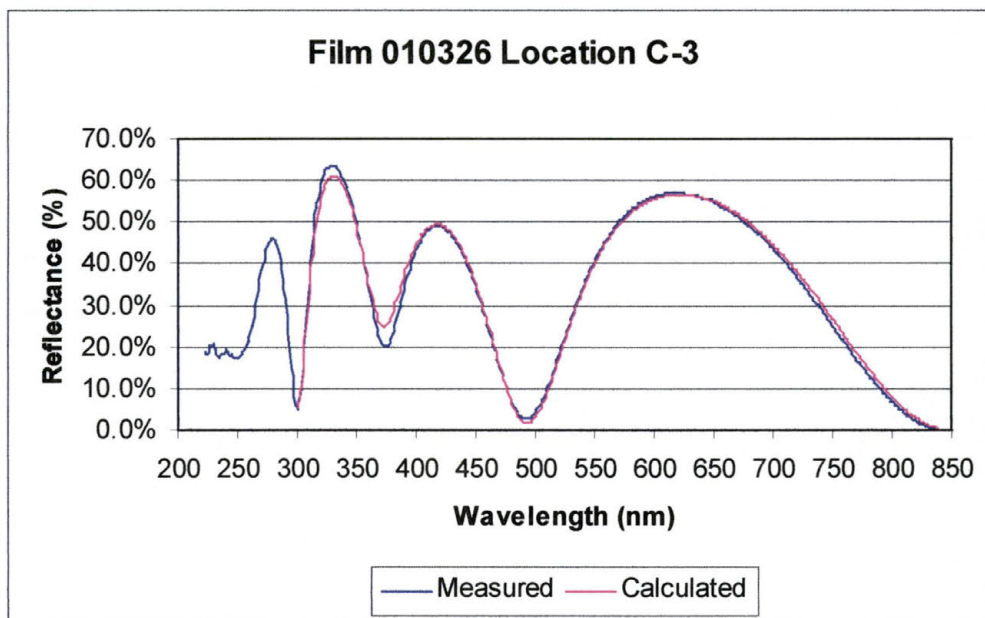
Data was collected by Filmetrics as part of a device demonstration for the tool. The actual scans are not available. The tool has been loaned to the Technology department as is not currently available.

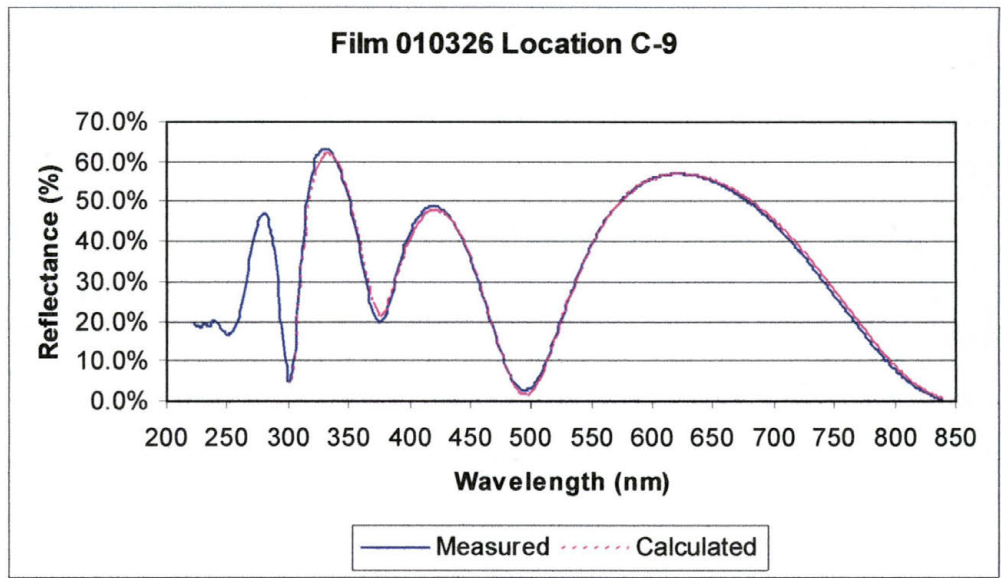
10.3.1.2 Film 010326



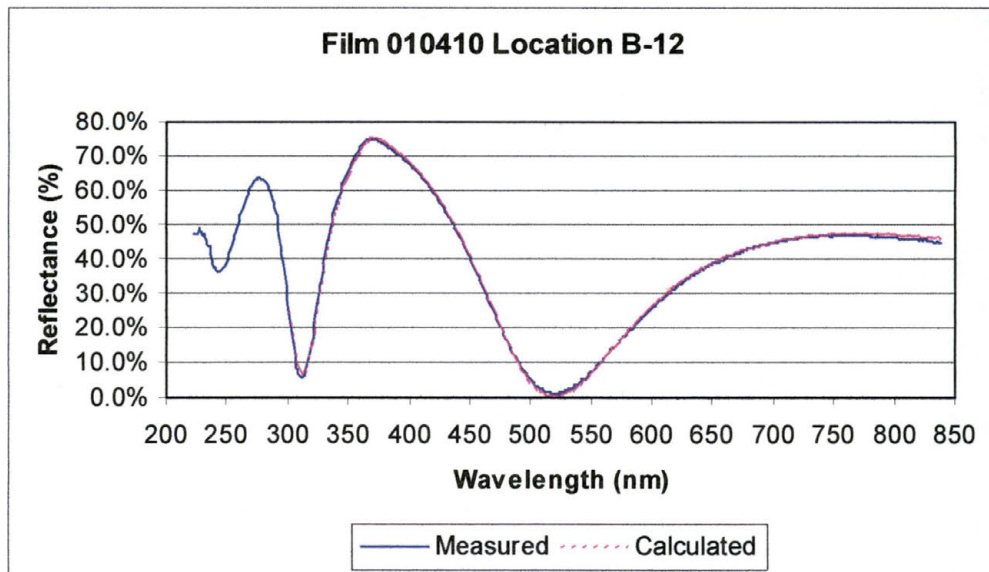
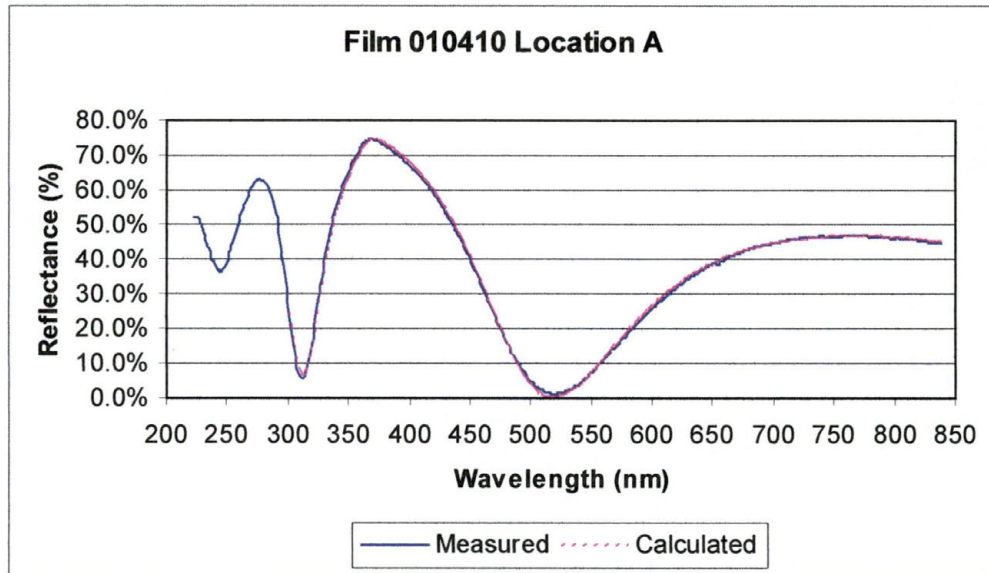


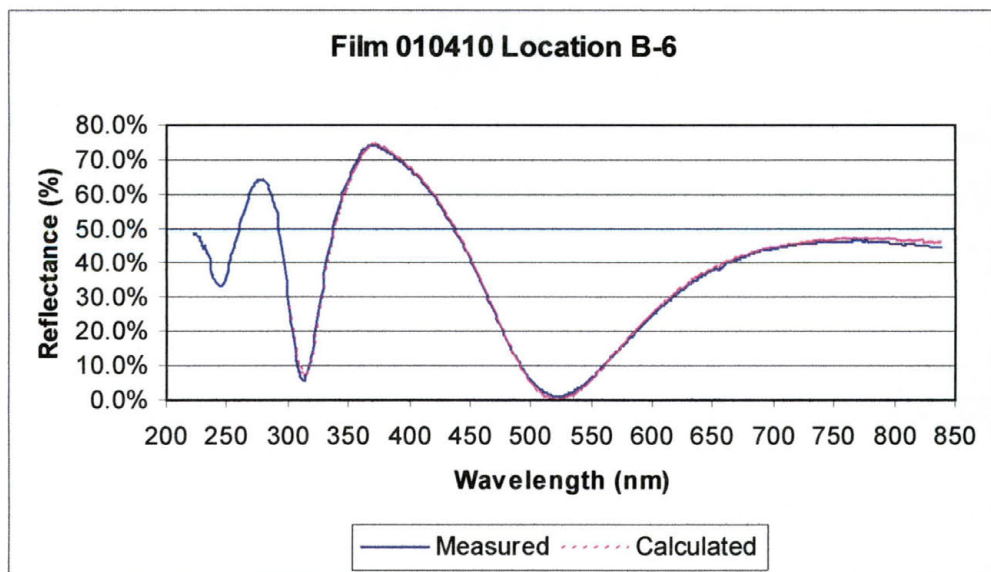
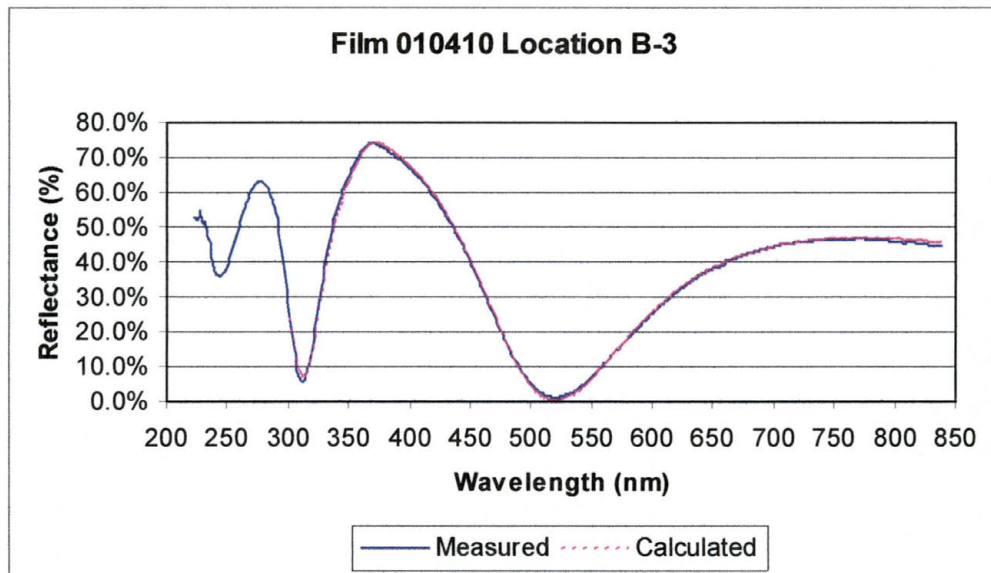


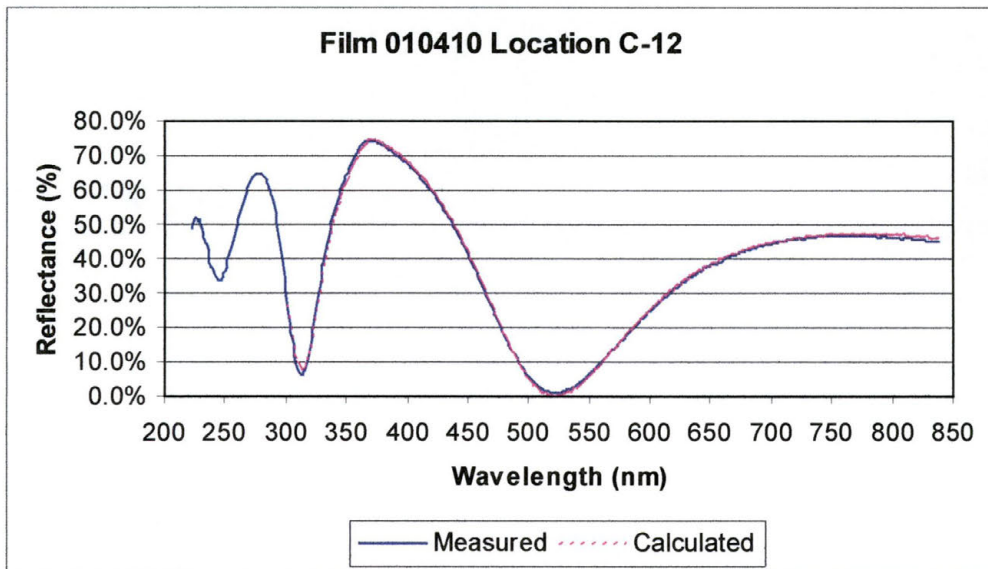
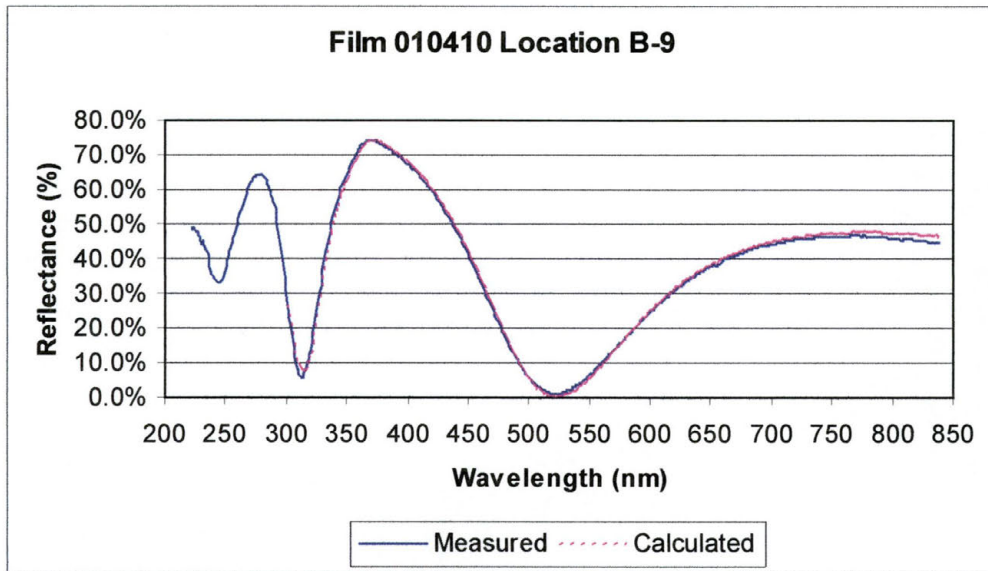


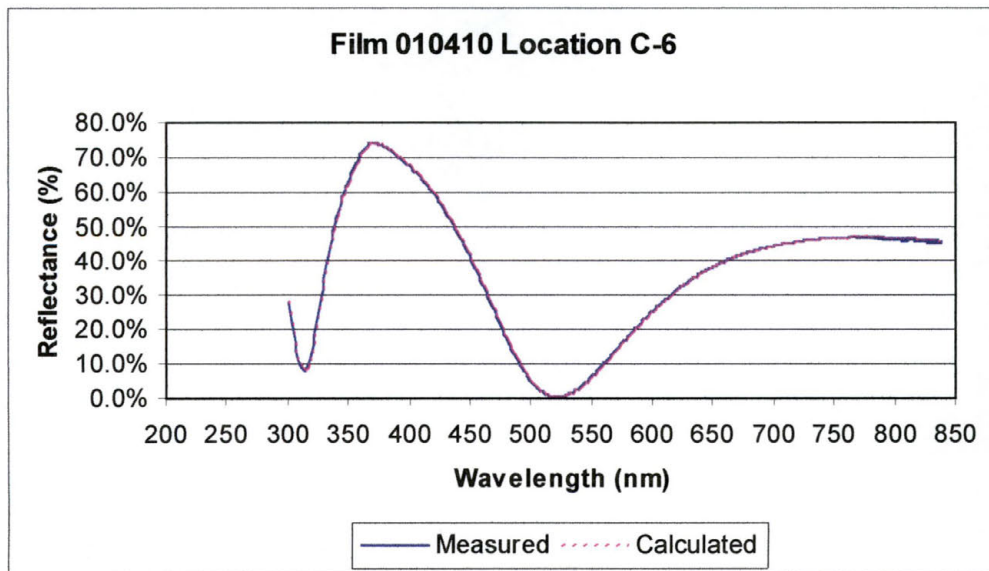
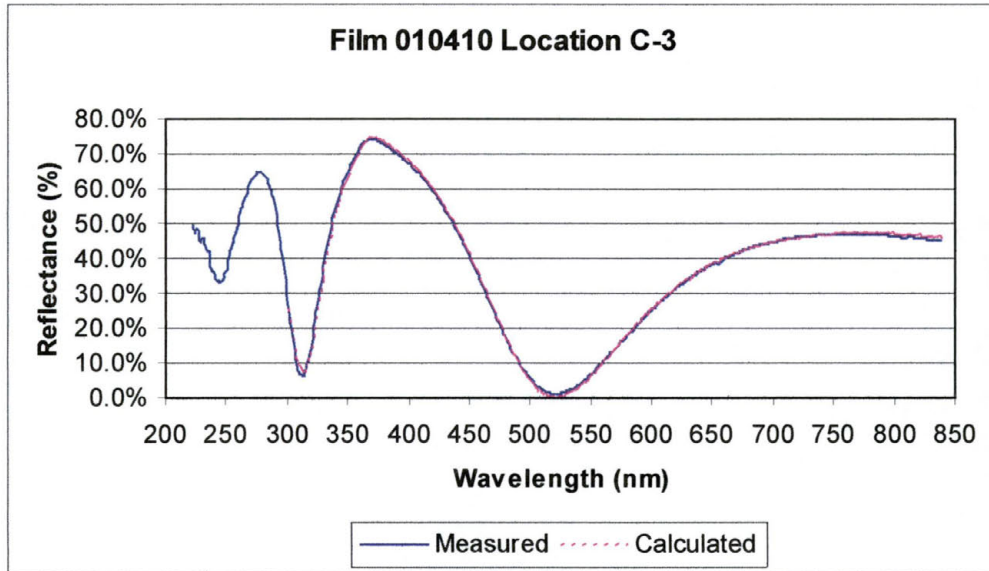


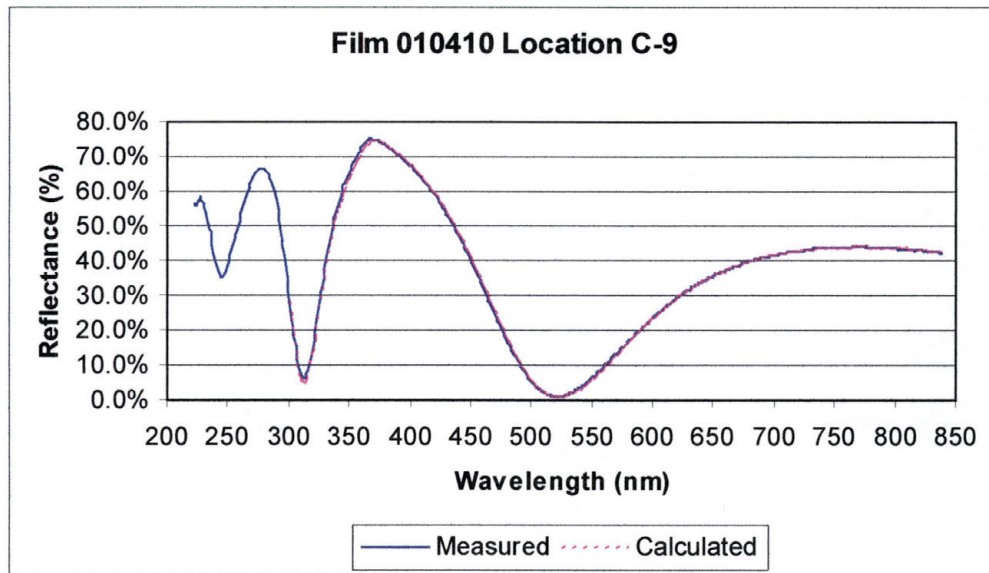
10.3.1.3 Film 010410



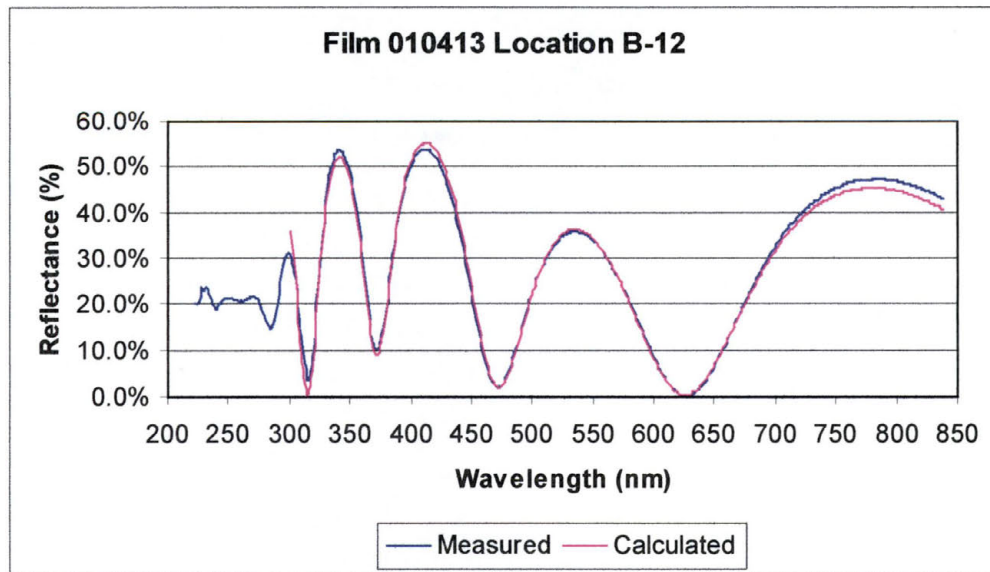
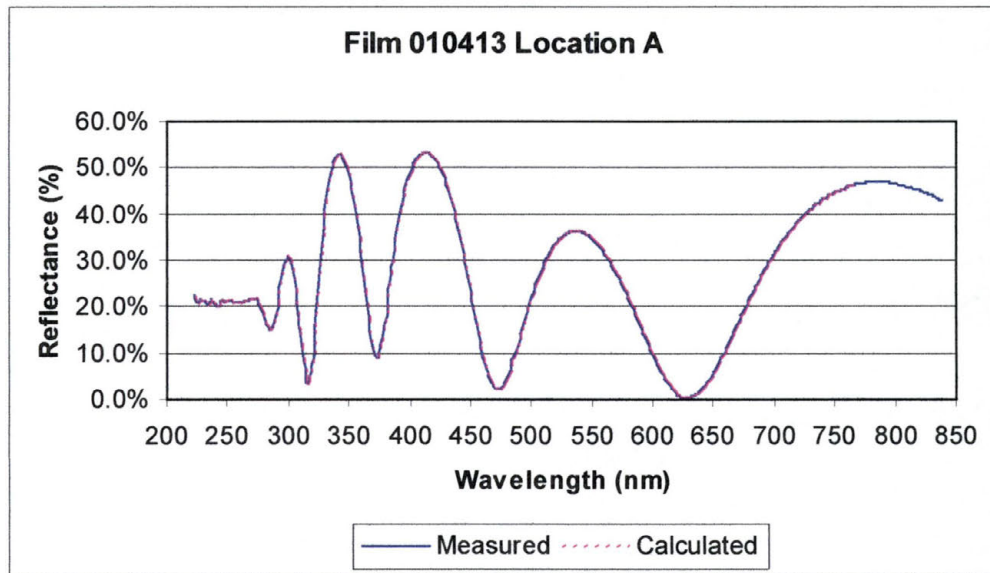


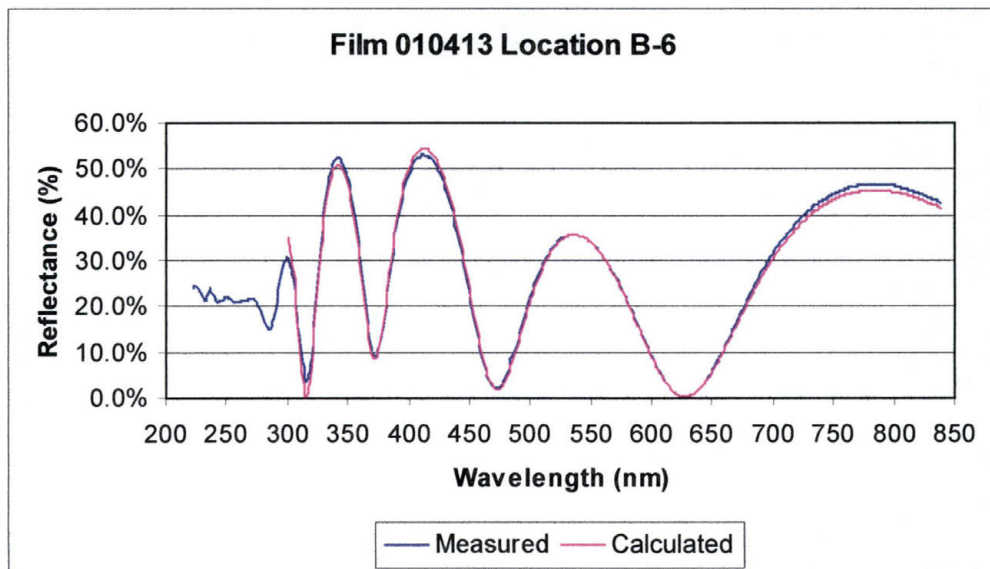
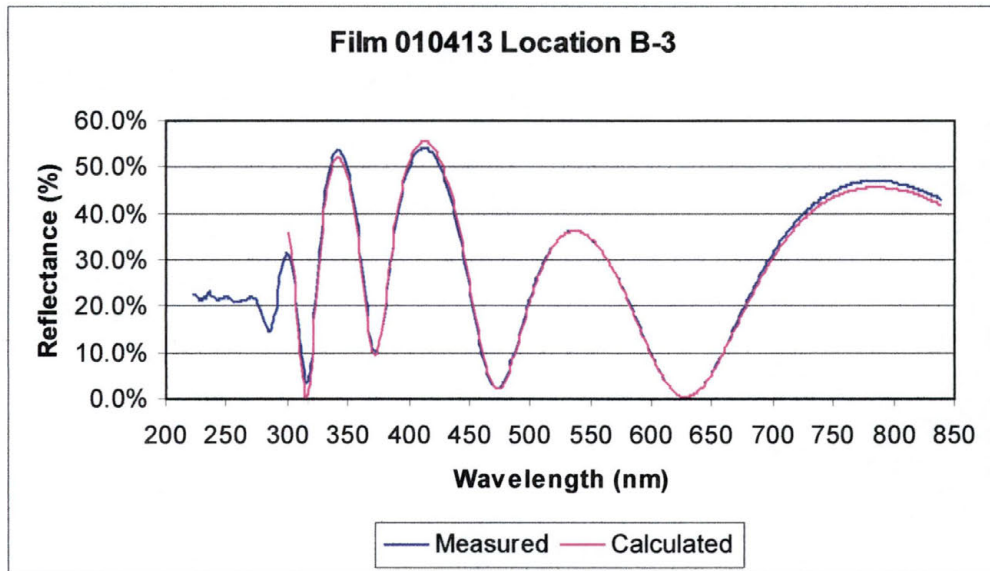


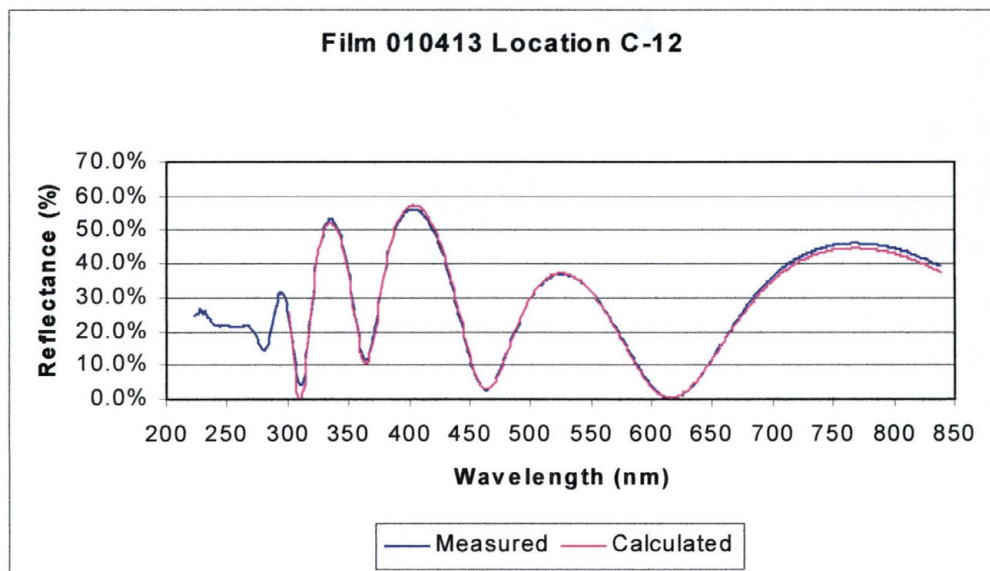
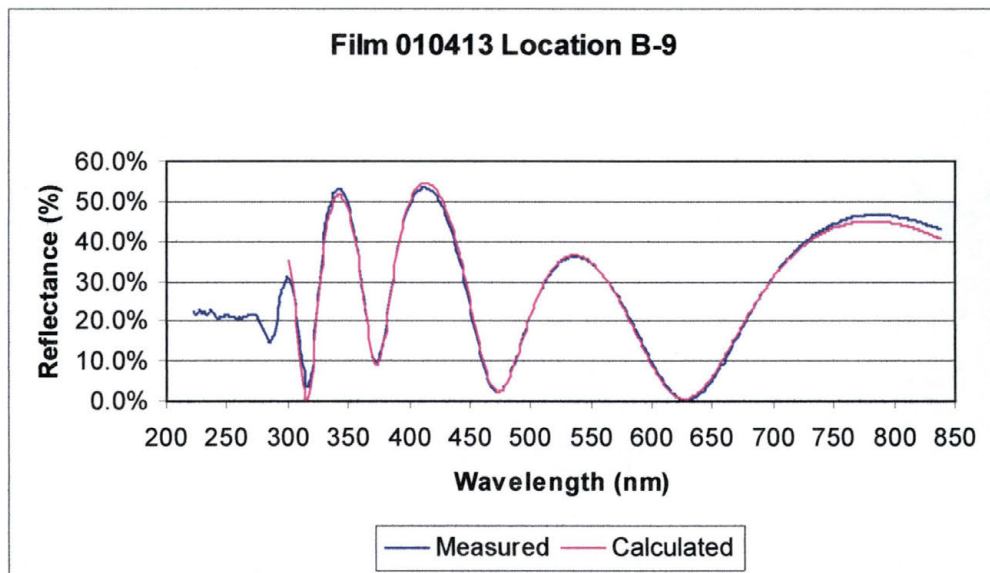


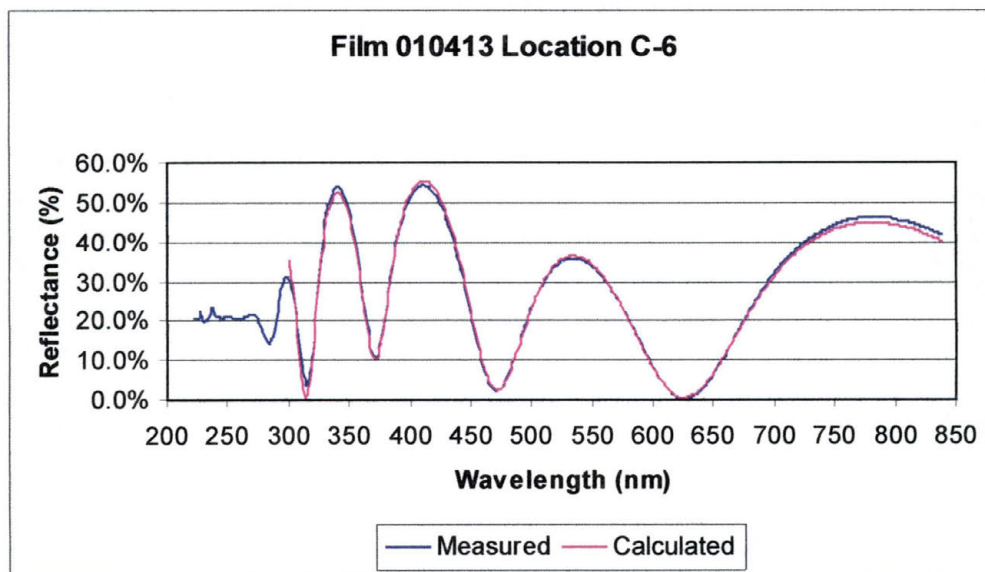
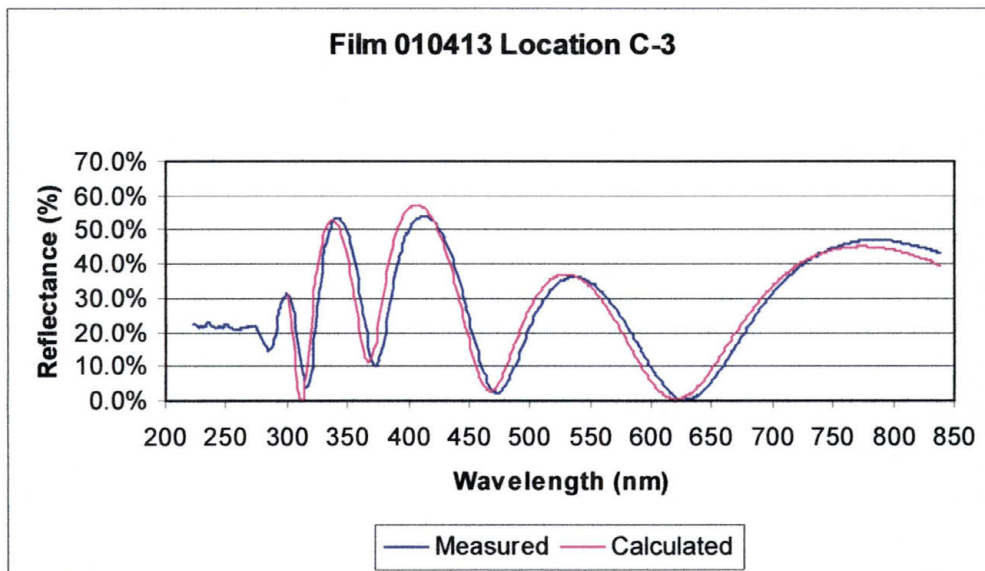


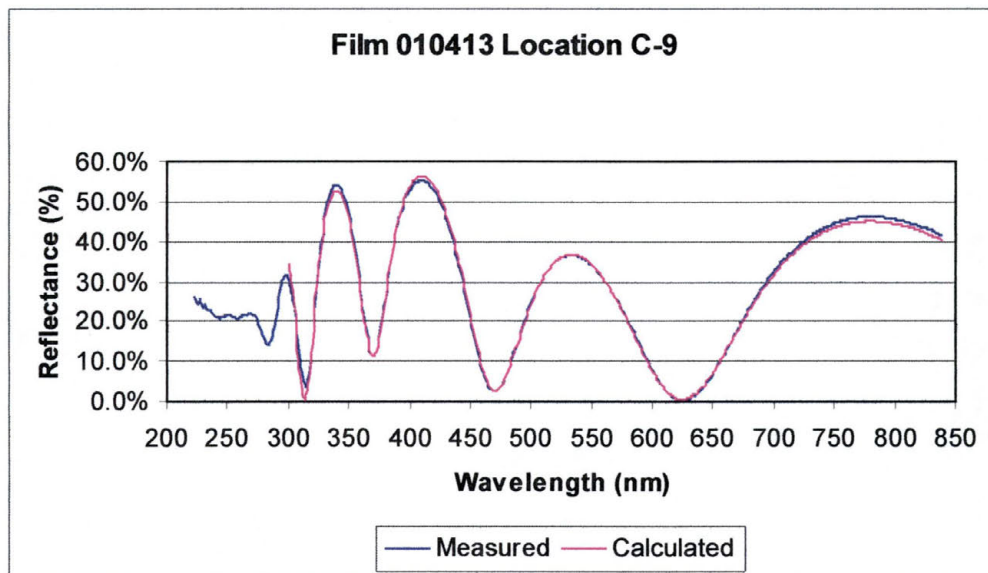
10.3.1.4 Film 010413





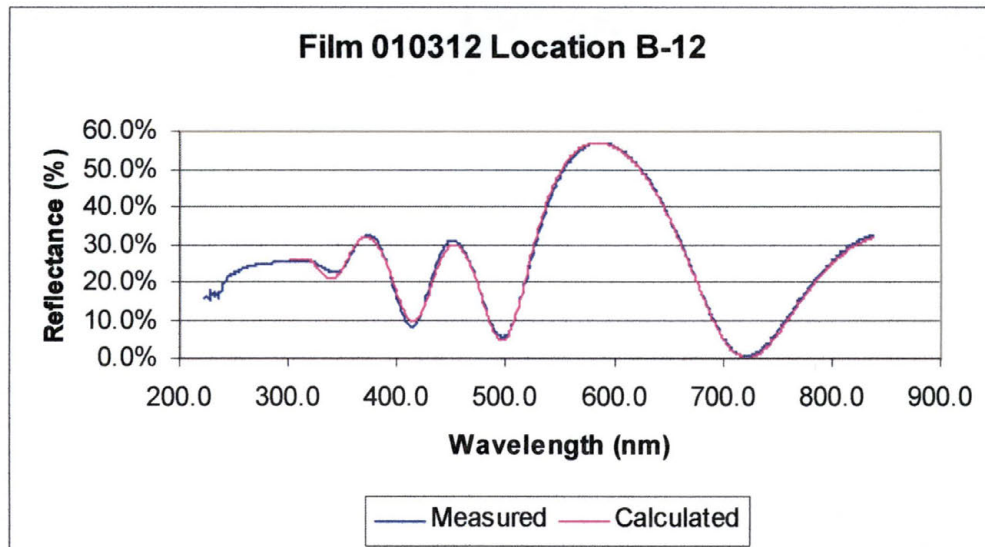
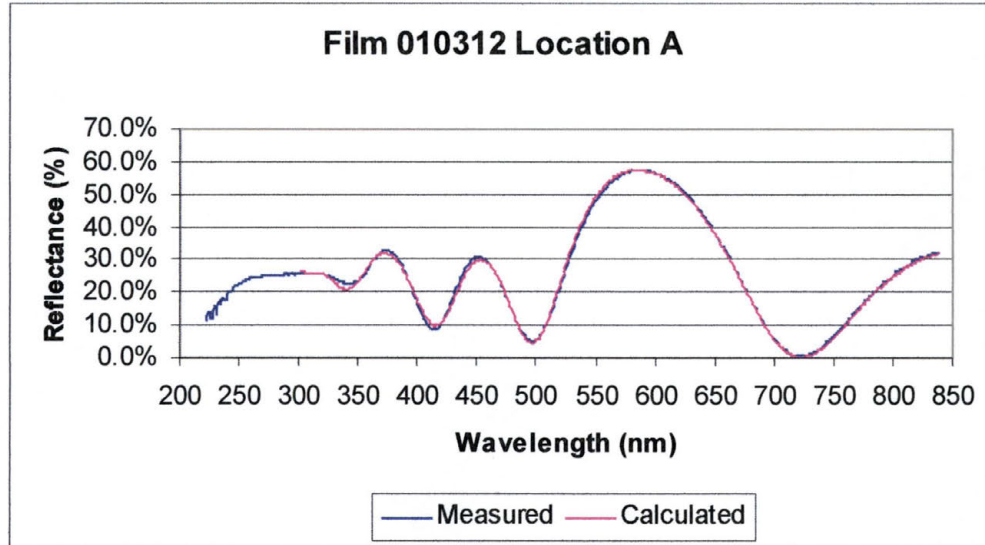


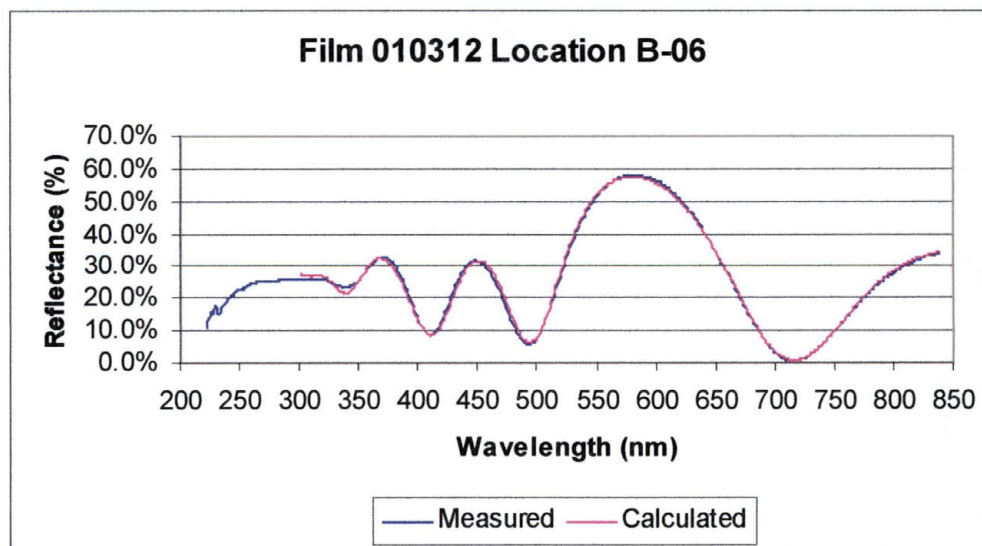
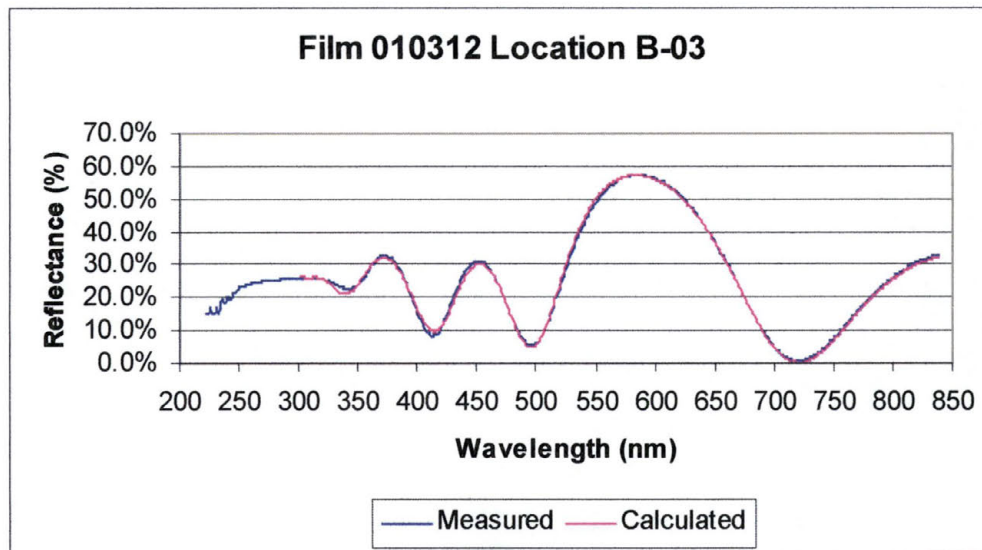


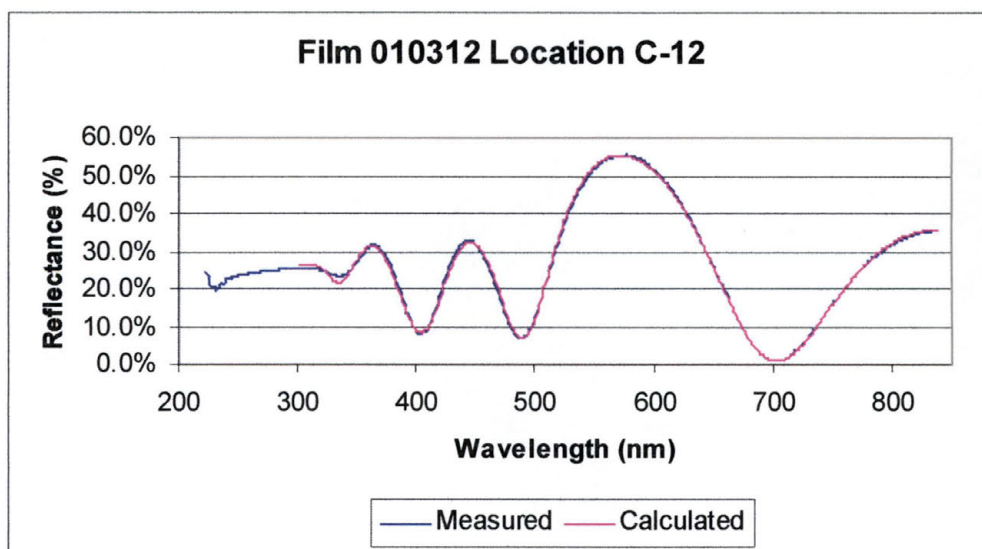
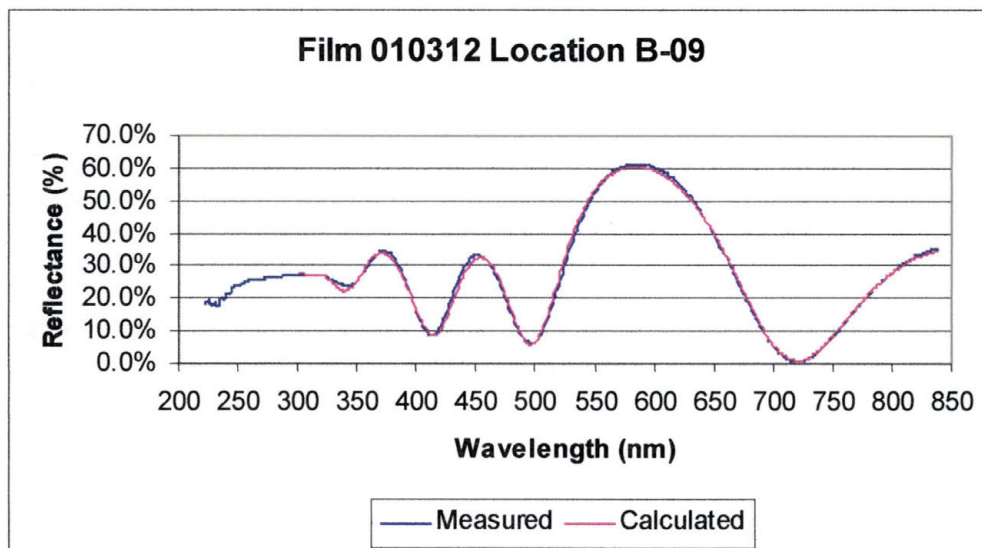


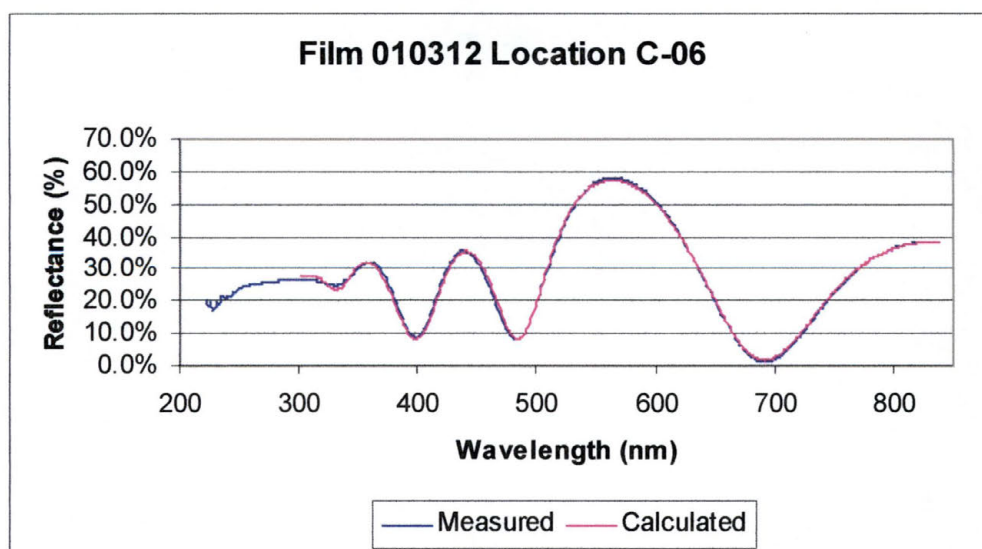
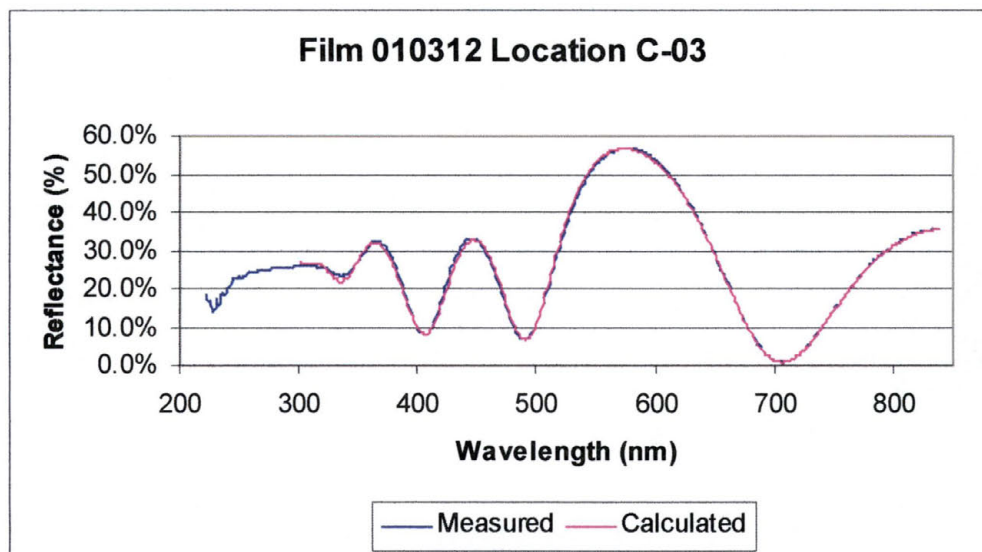
10.3.2 Permalloy Oxide Films

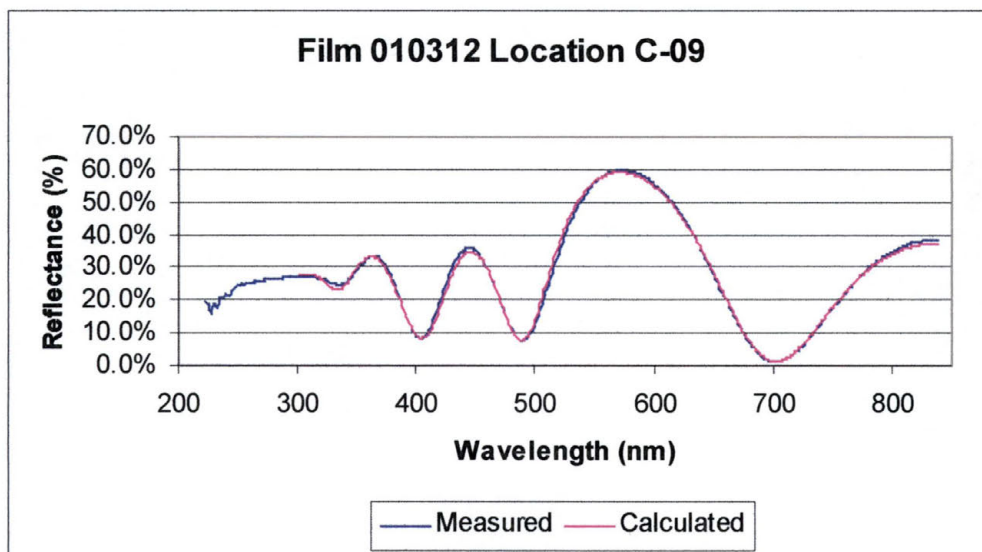
10.3.2.1 Film 010312



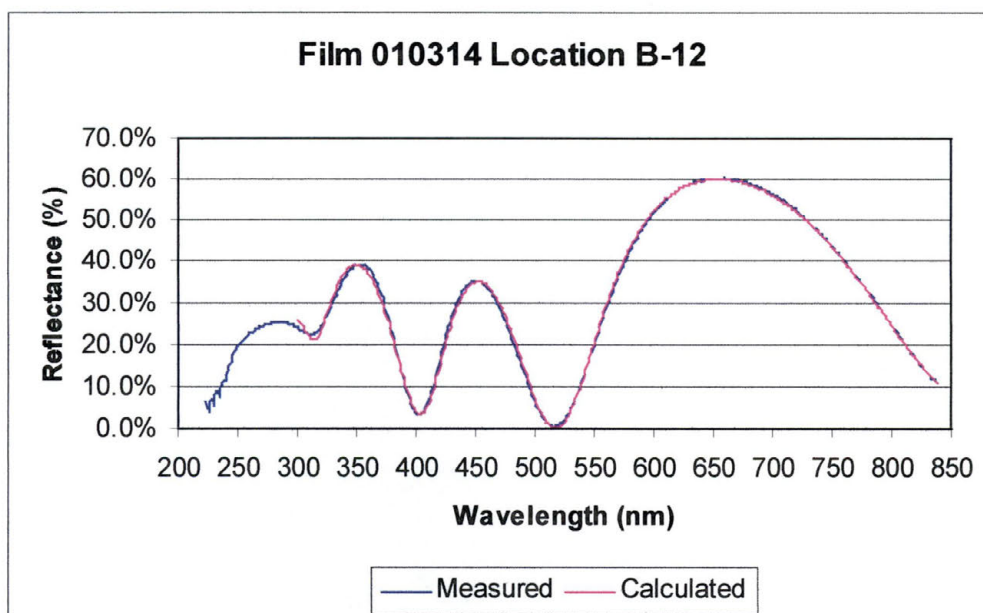
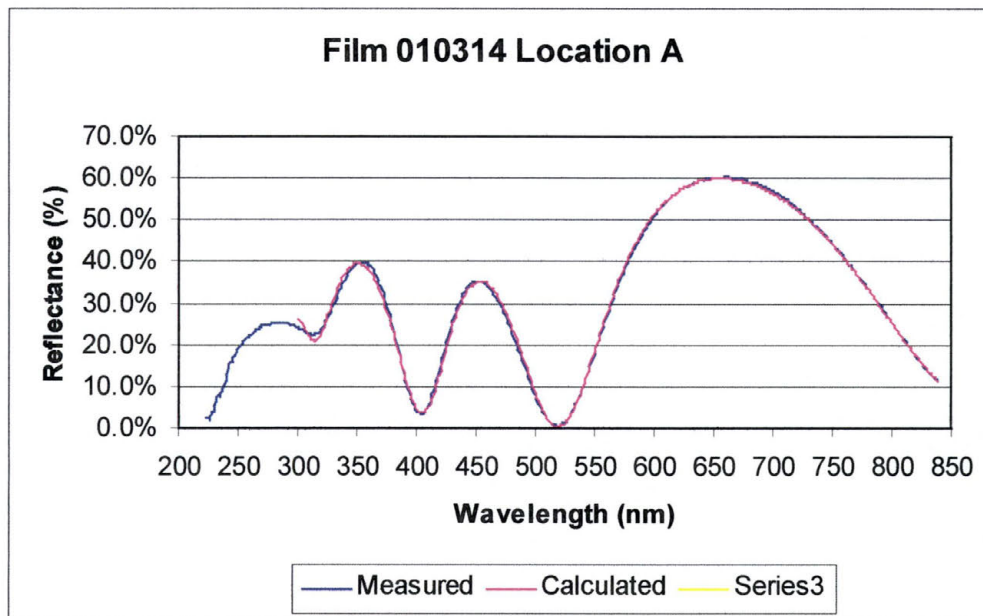


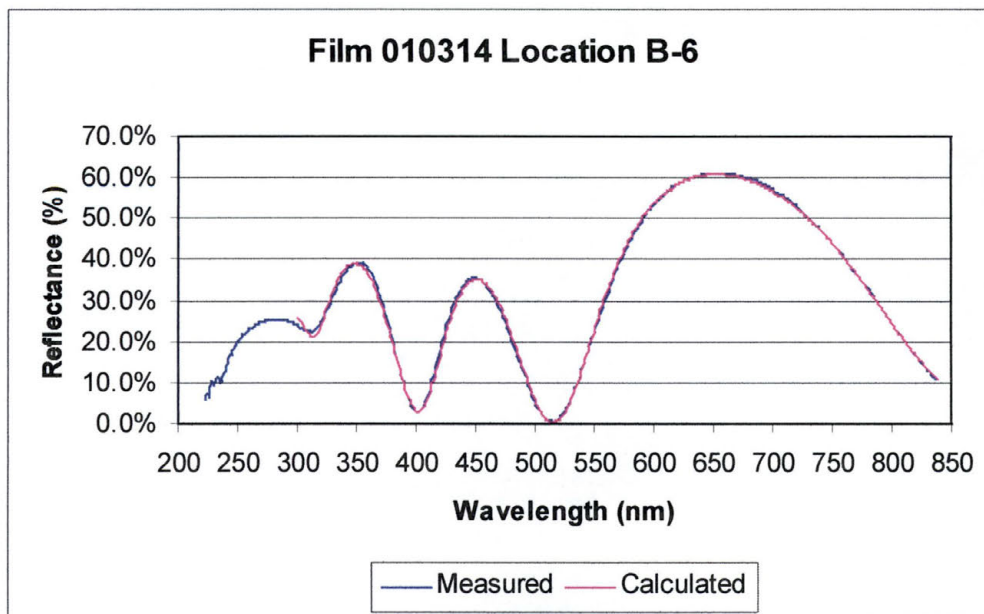
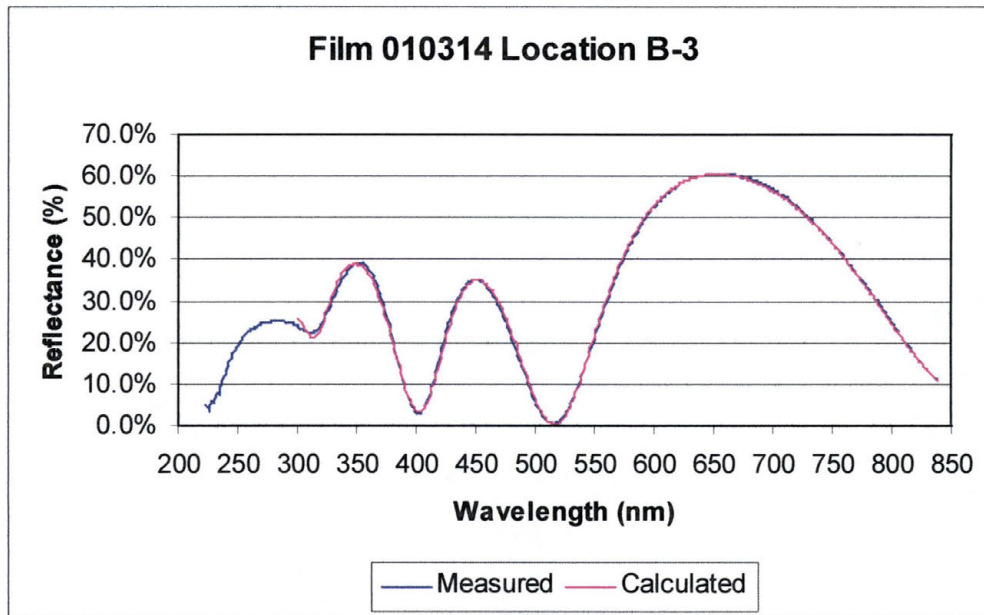


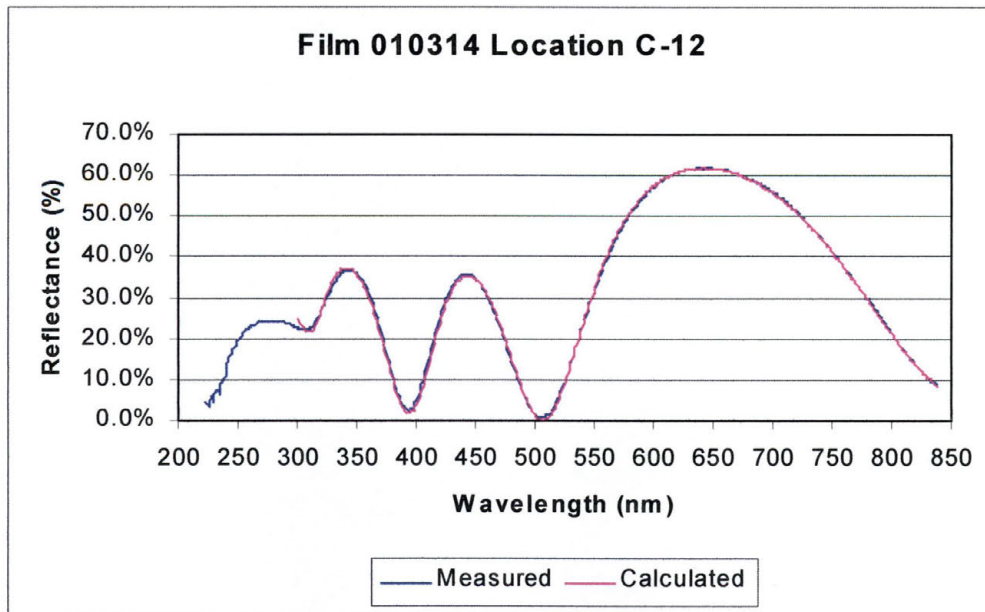
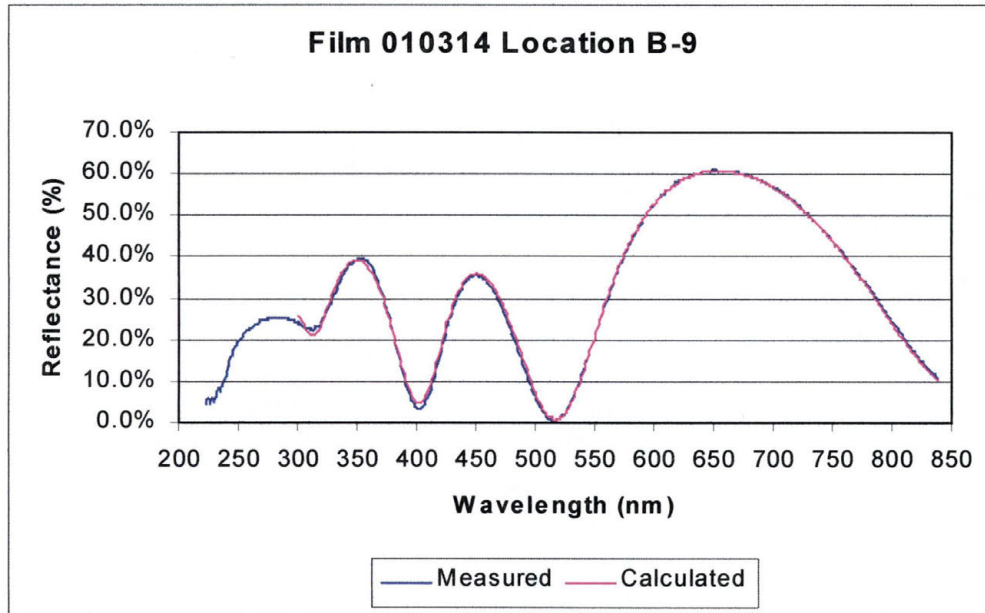


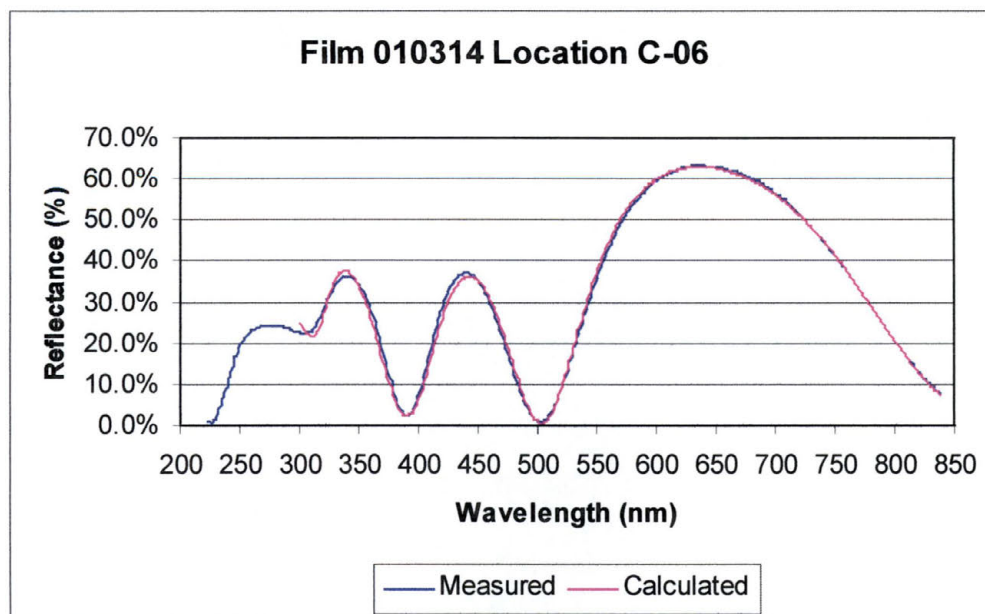
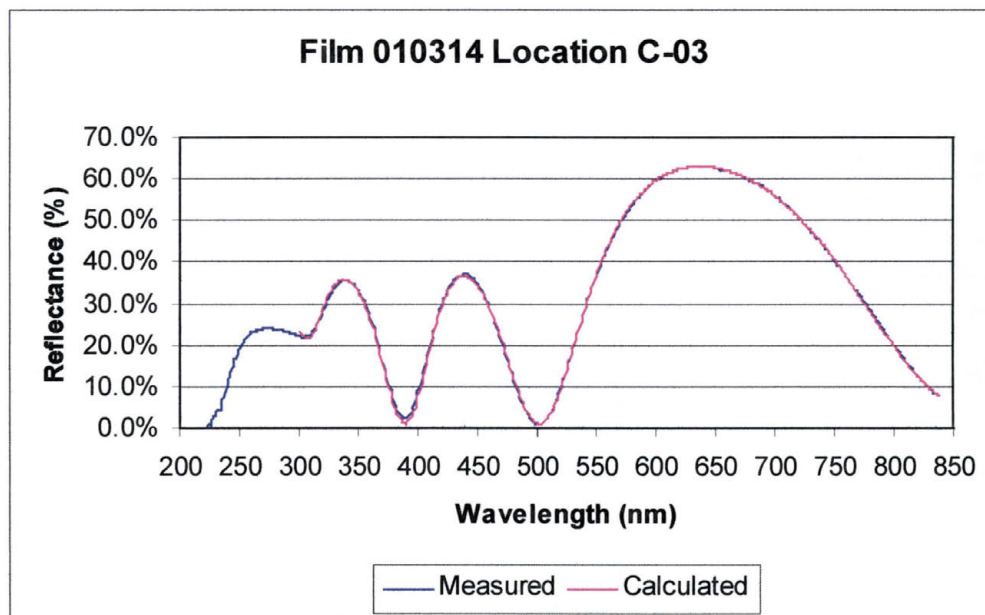


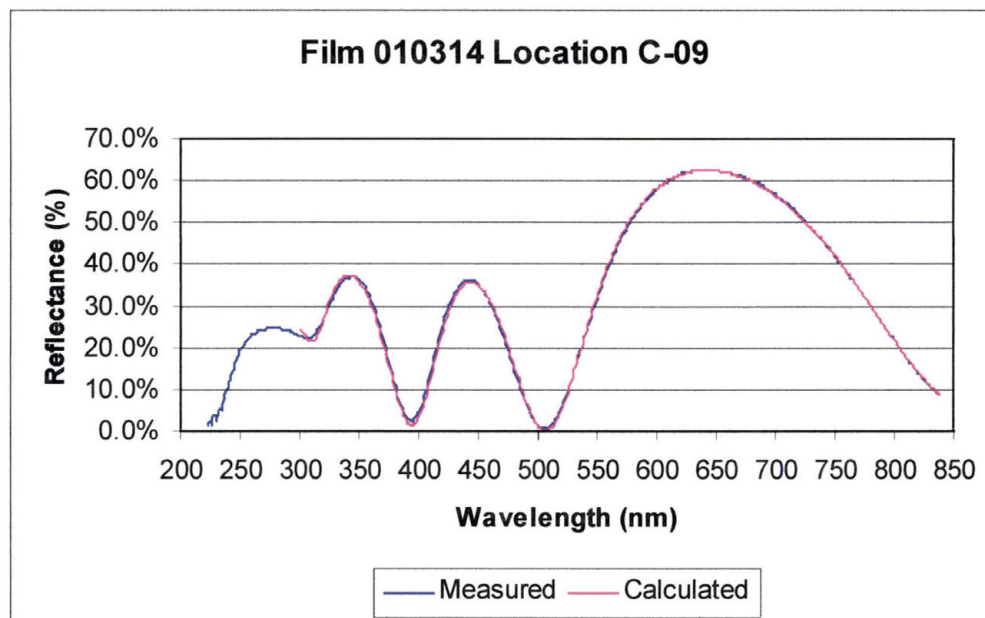
10.3.2.2 Film 010314



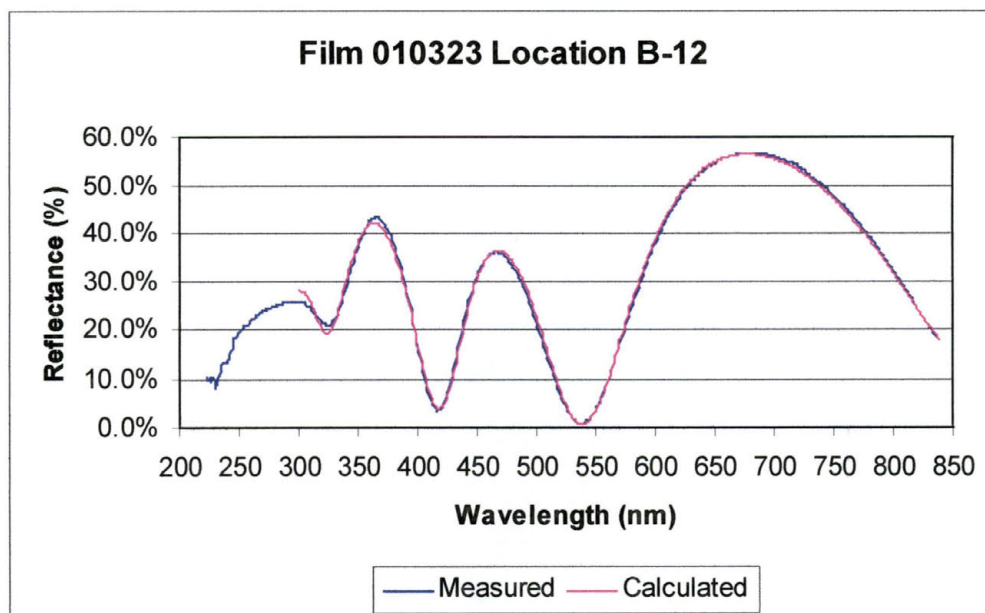
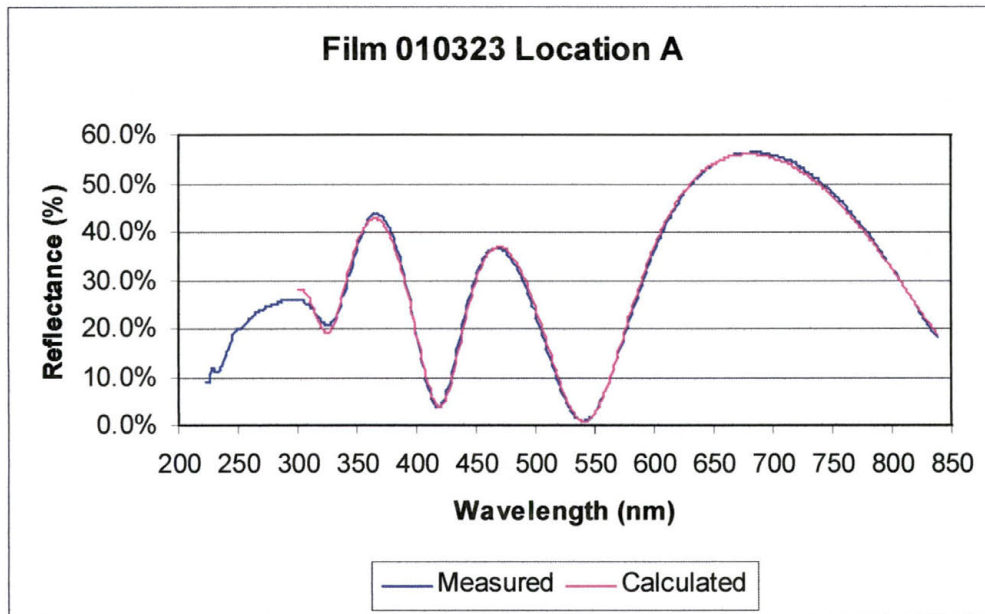


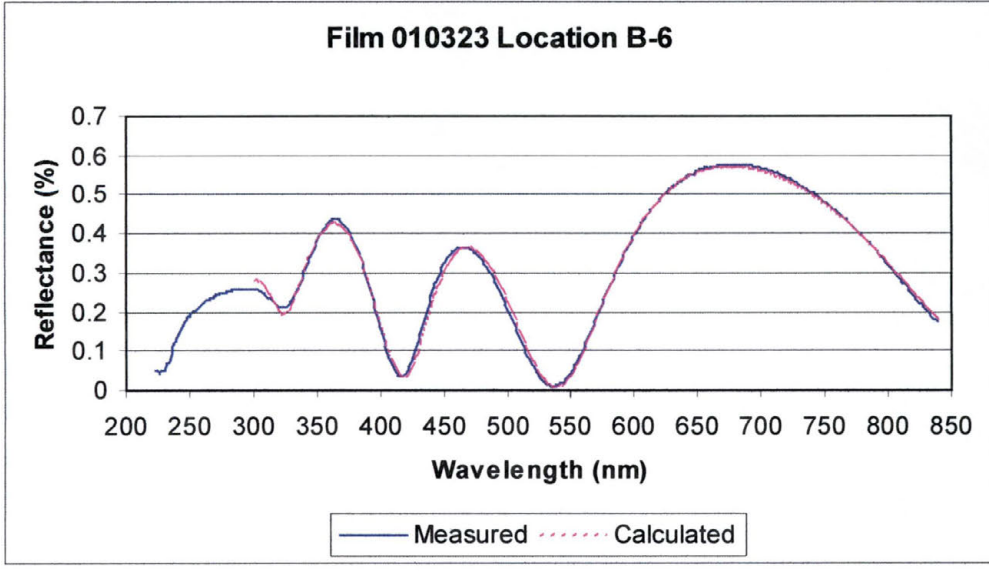
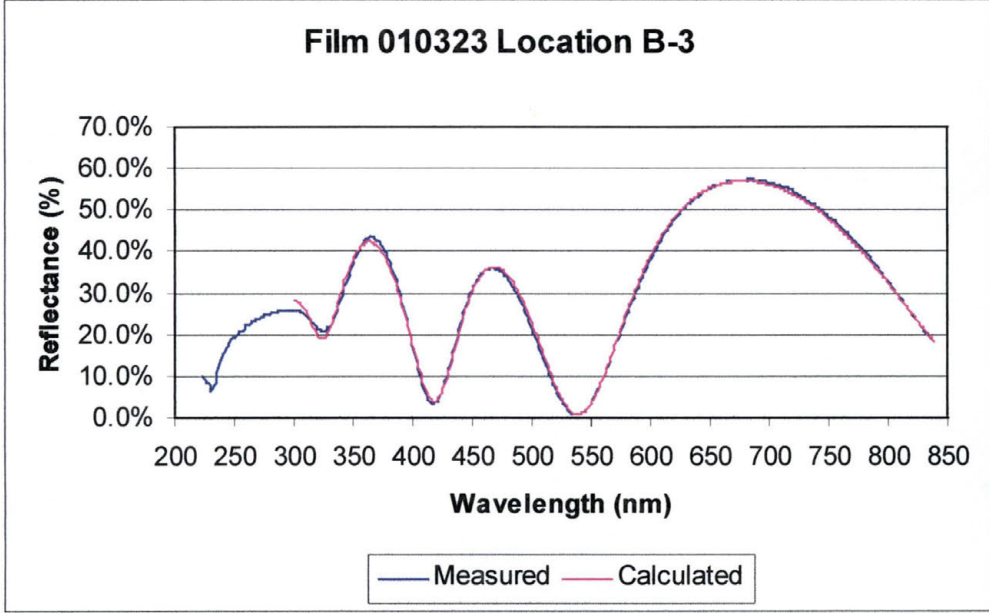


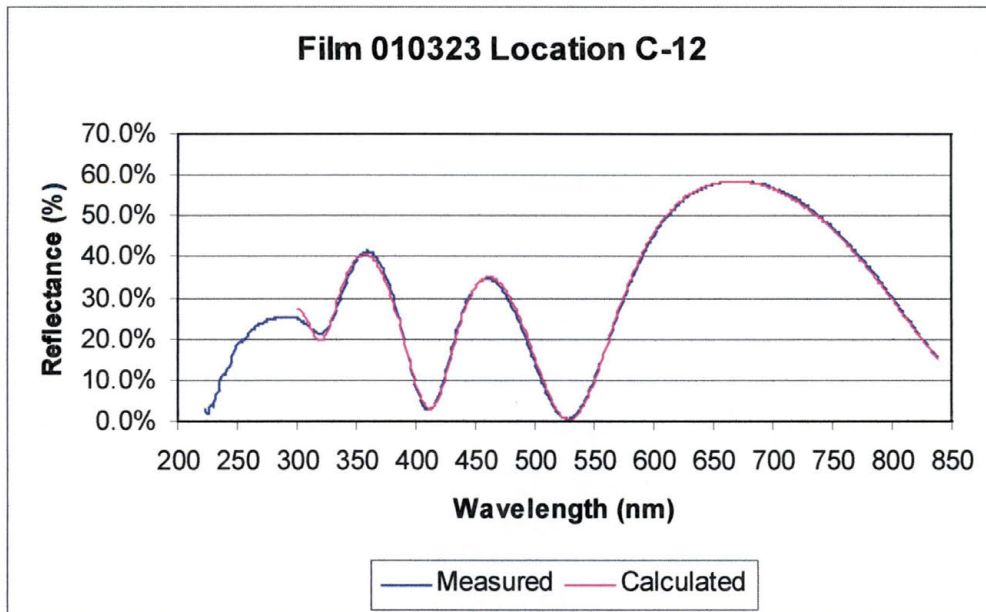
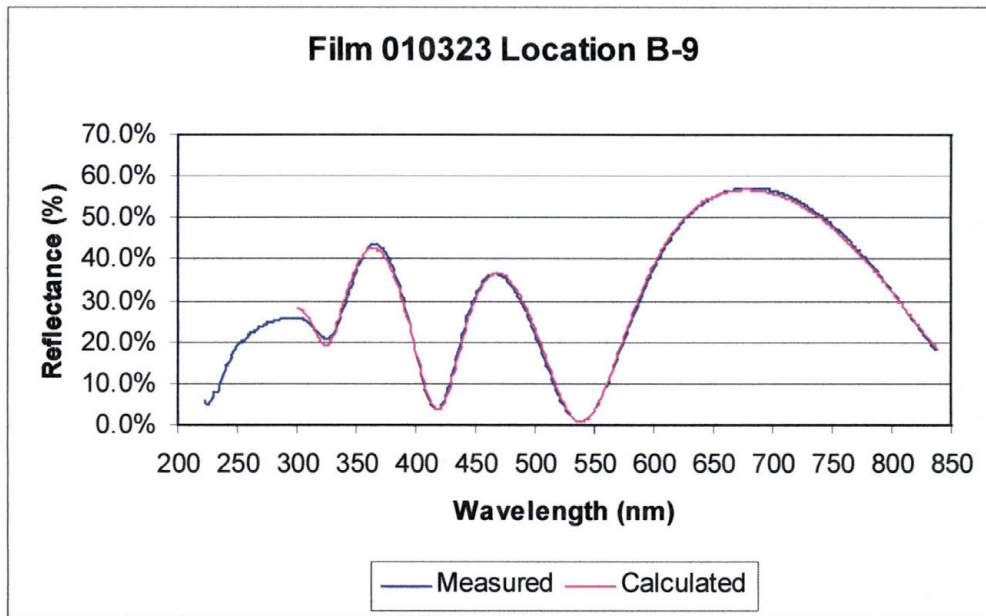


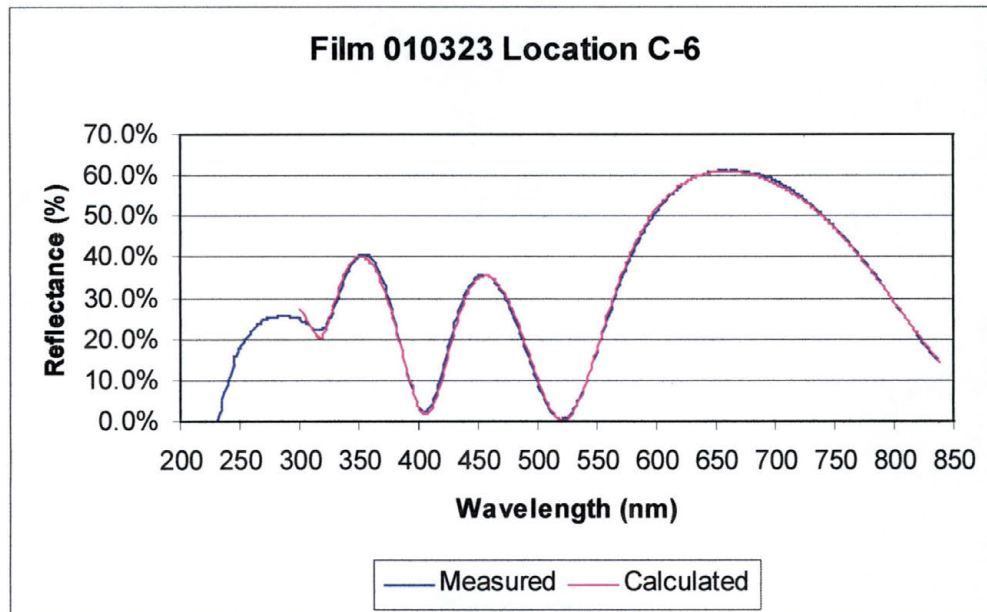
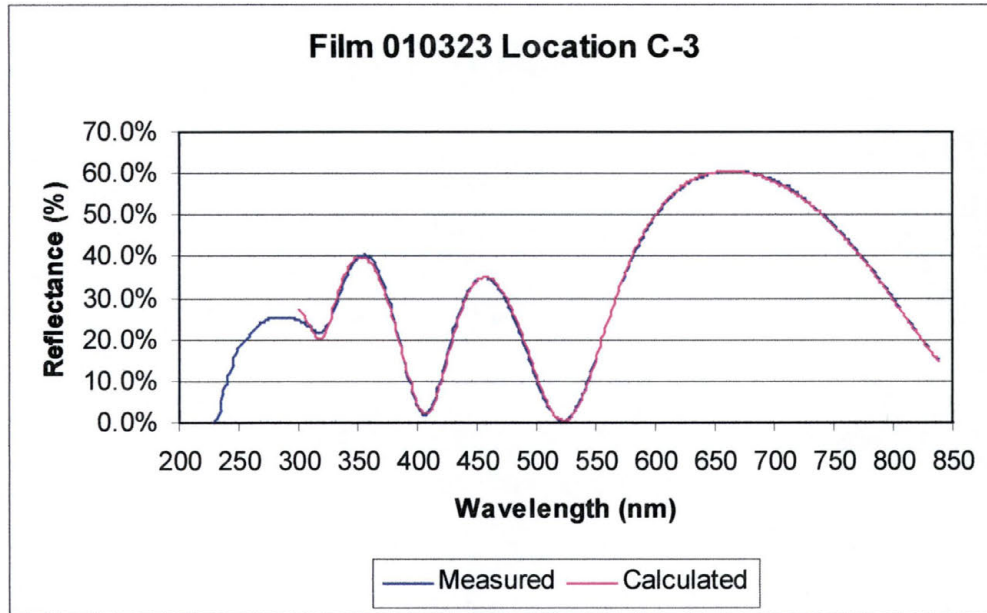


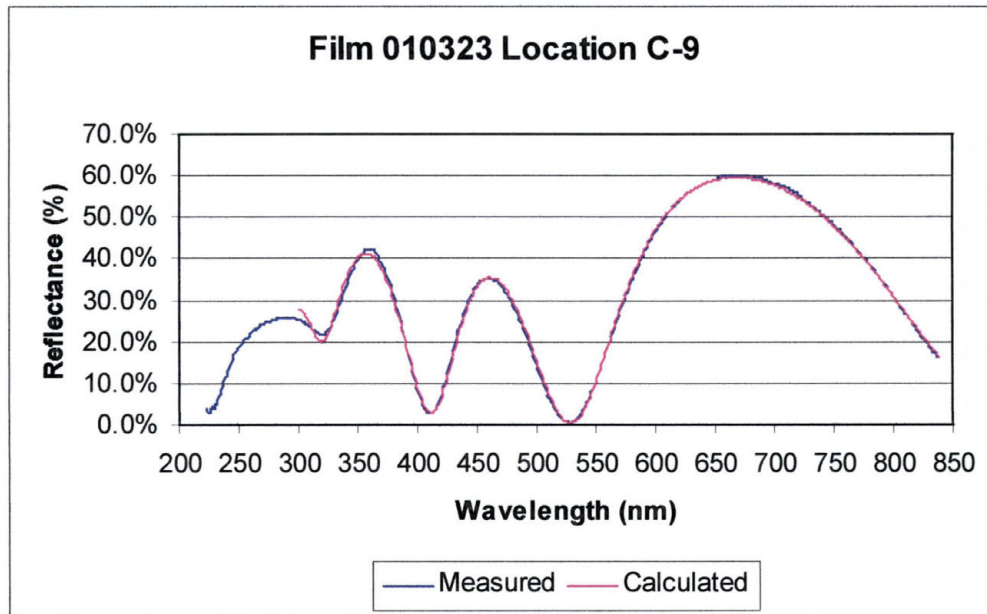
10.3.2.3 Film 010323



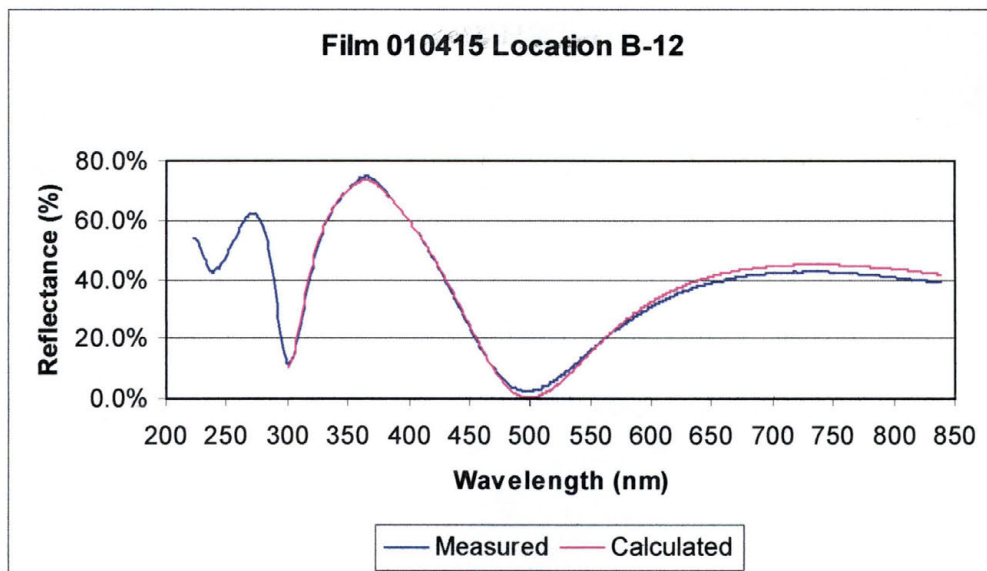
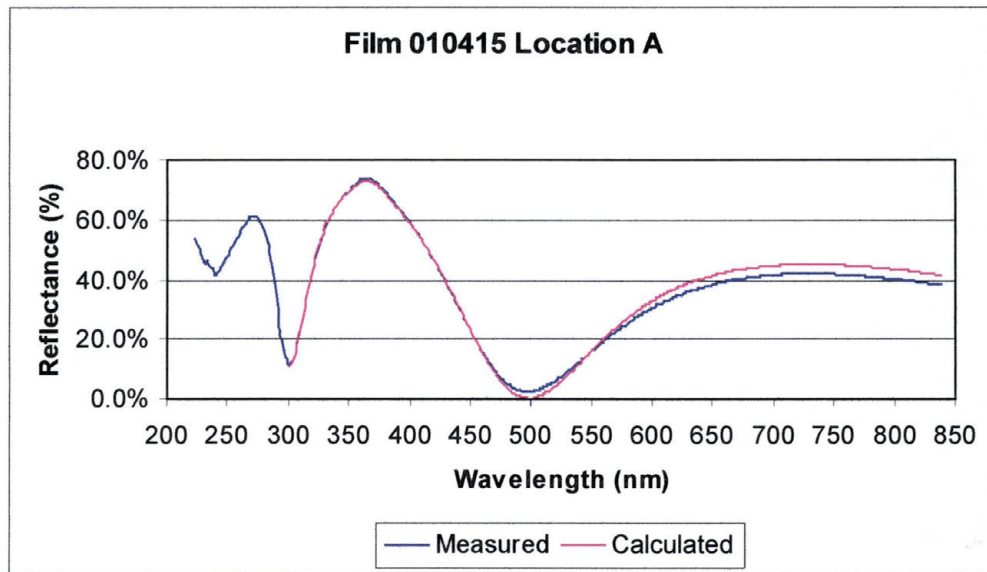


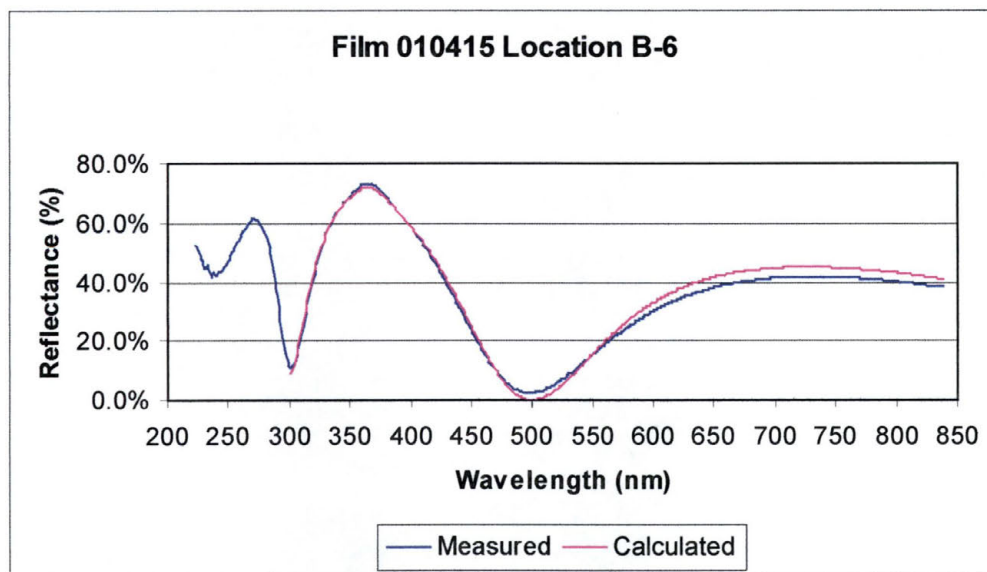
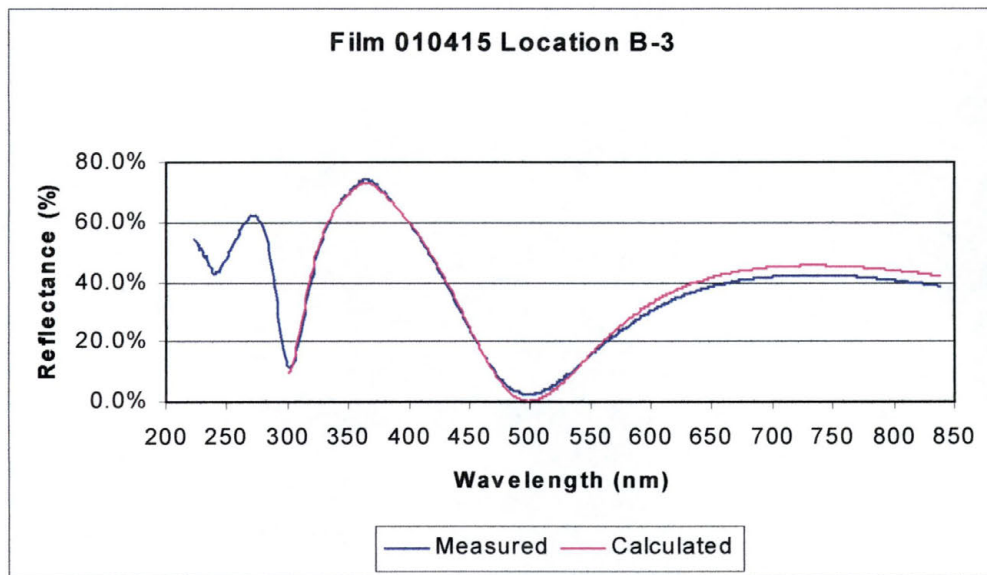


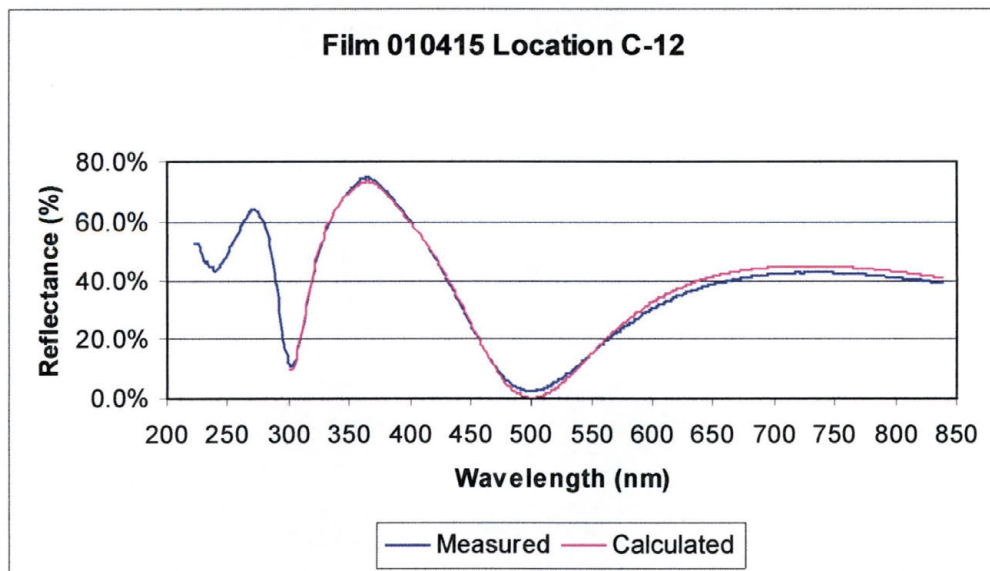
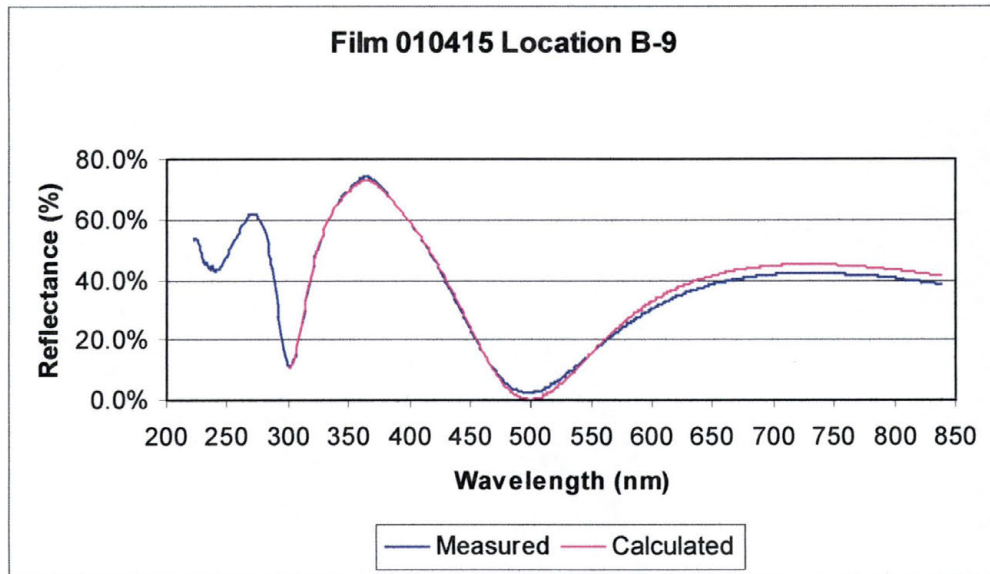


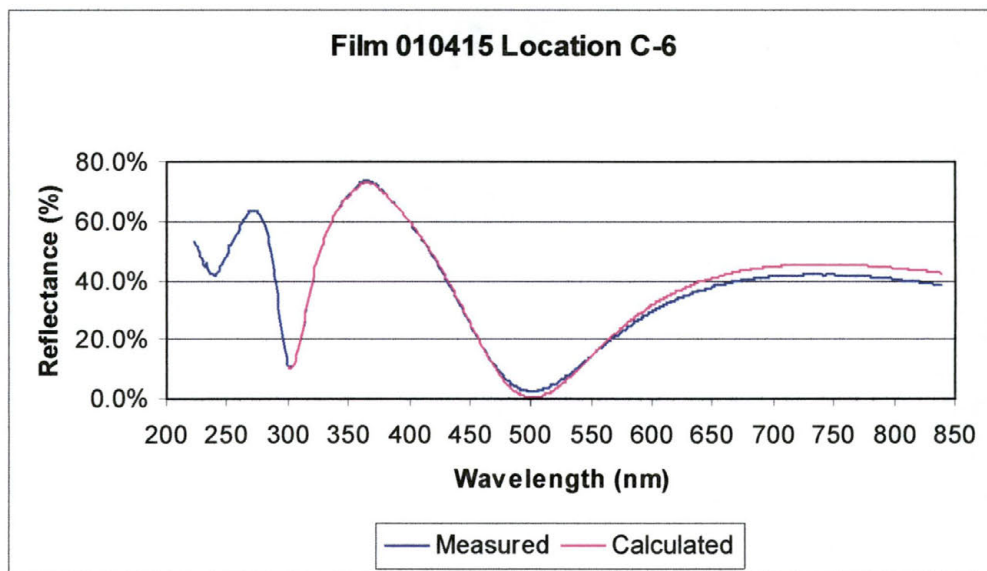
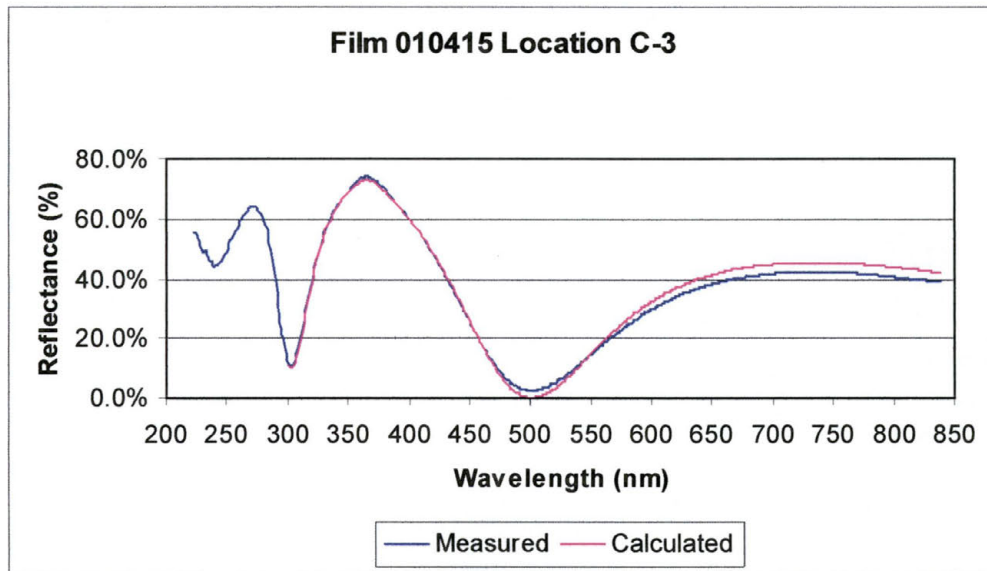


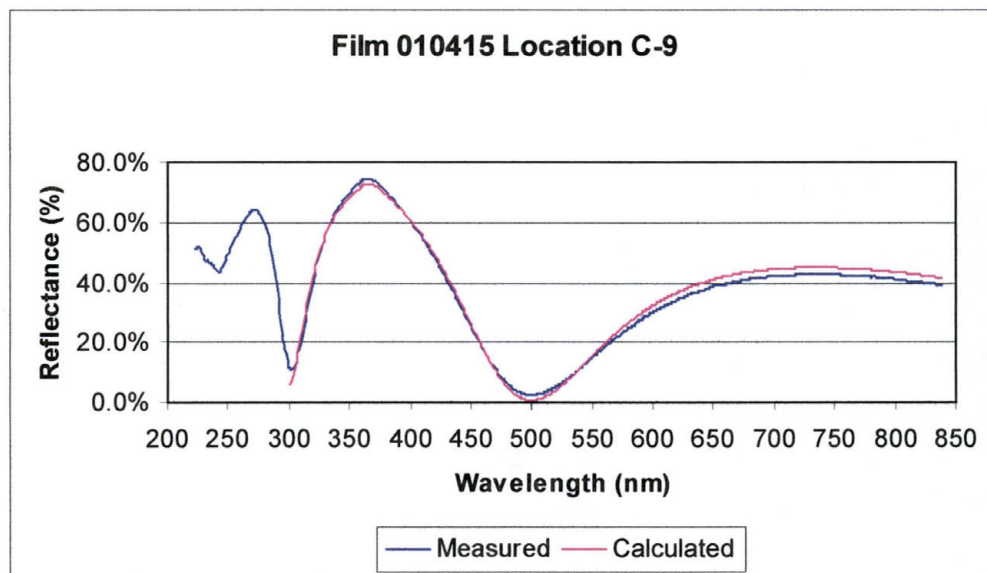
10.3.2.4 Film 010415



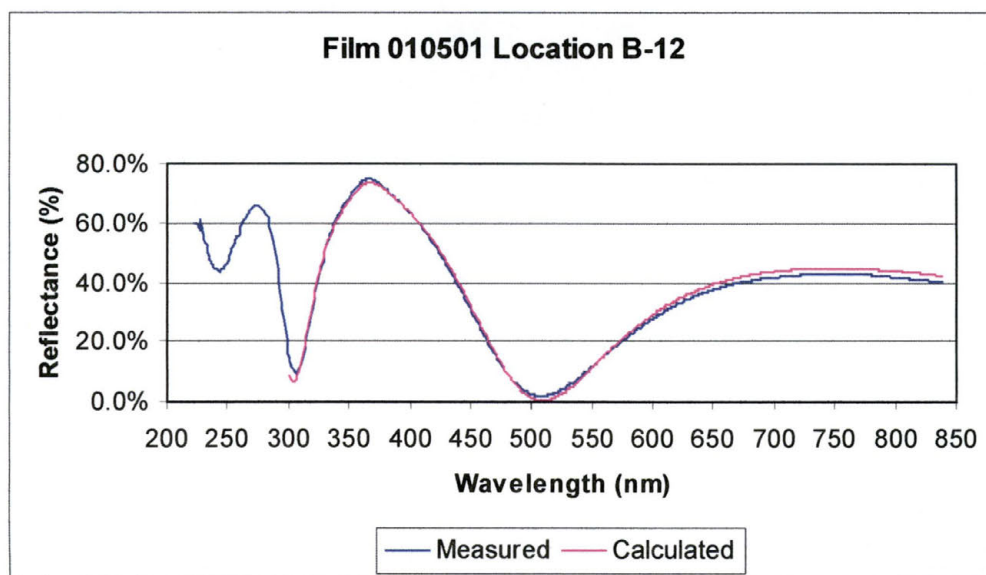
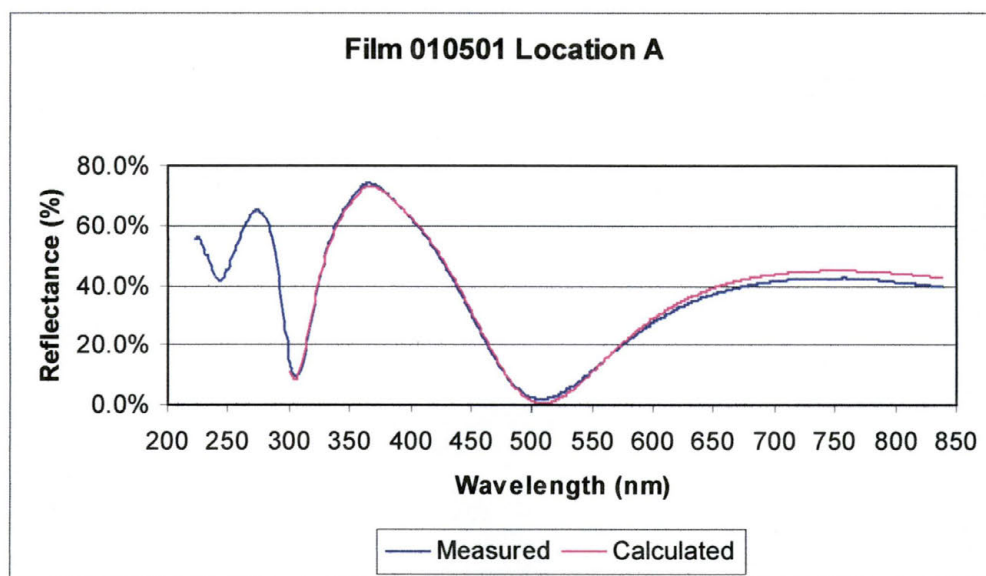


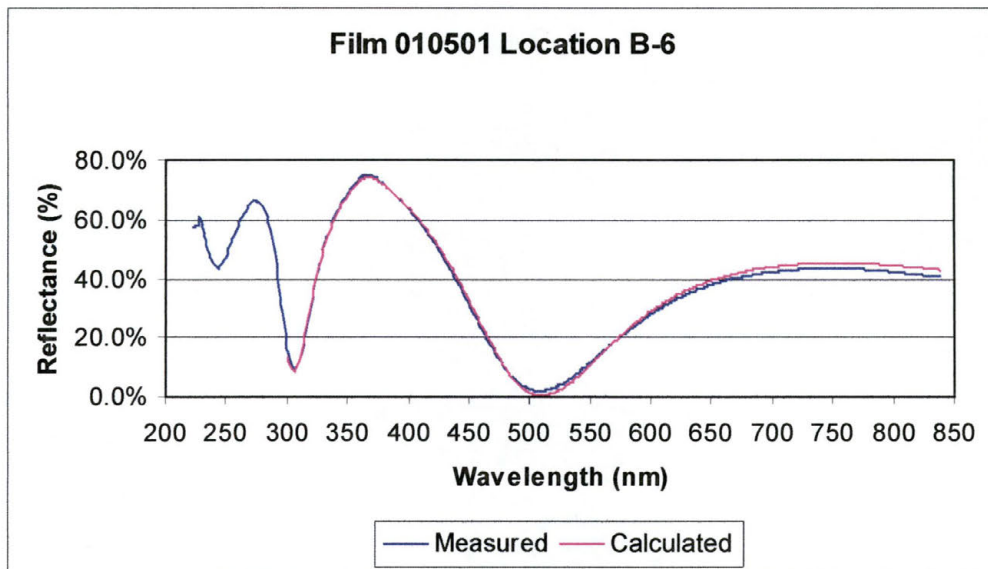
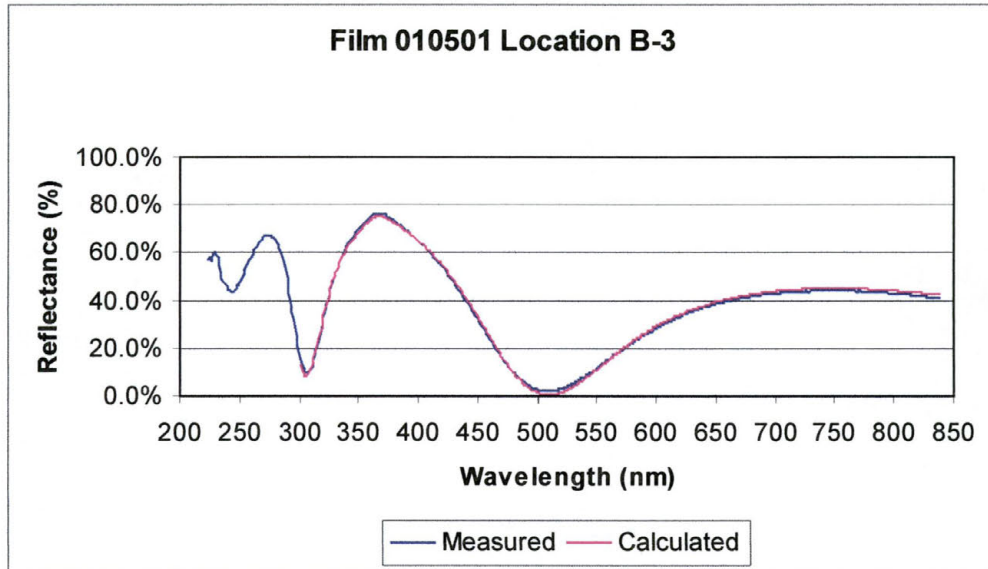


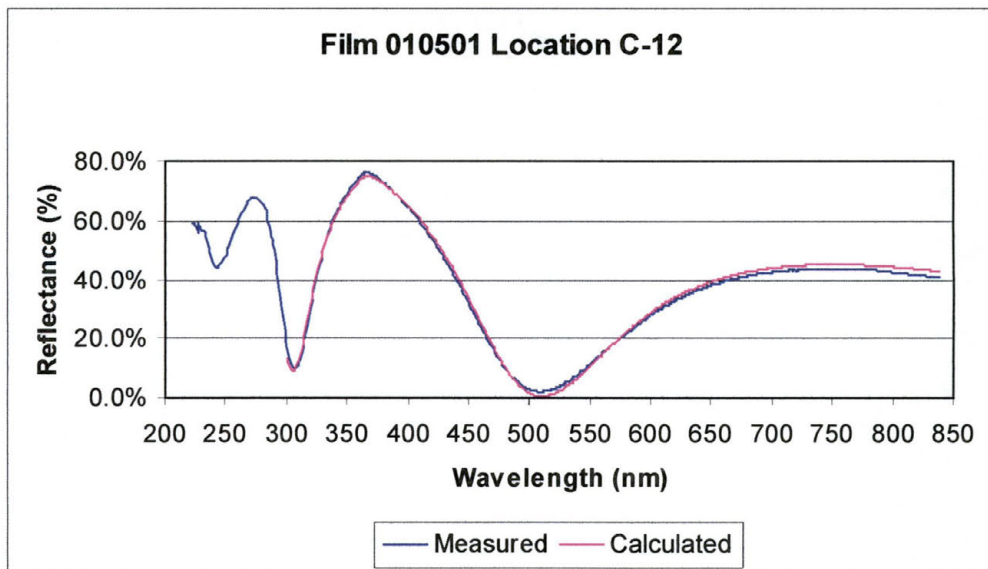
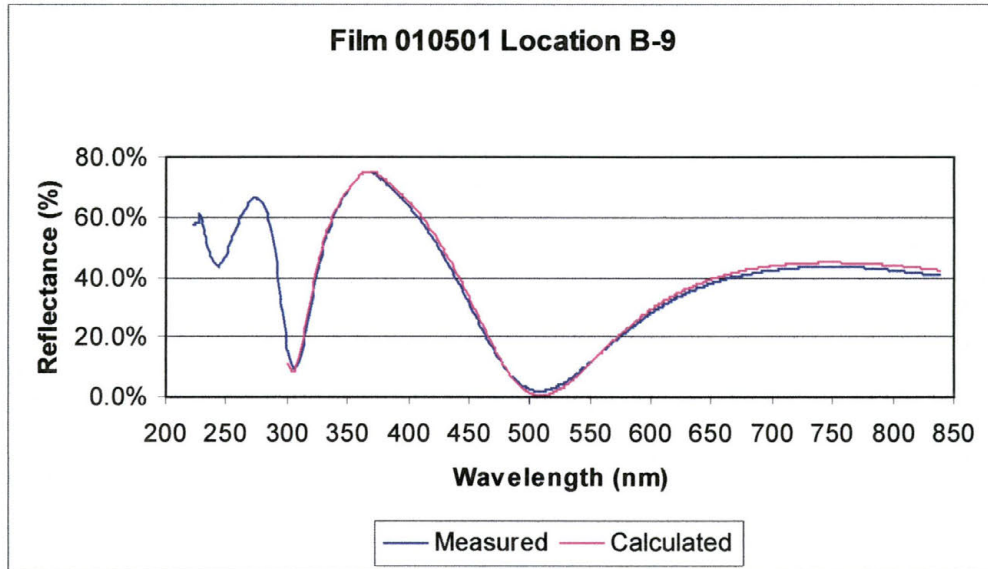


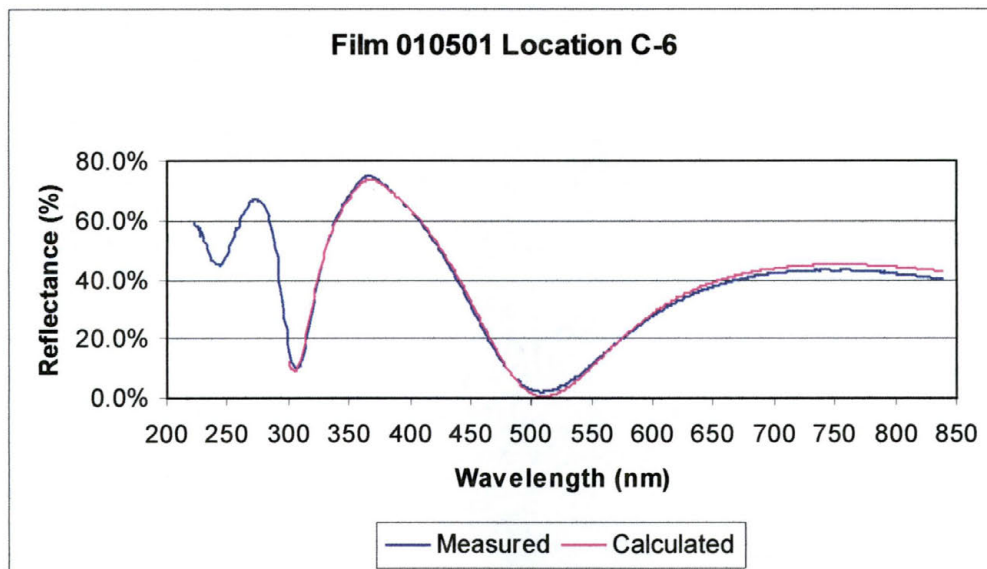
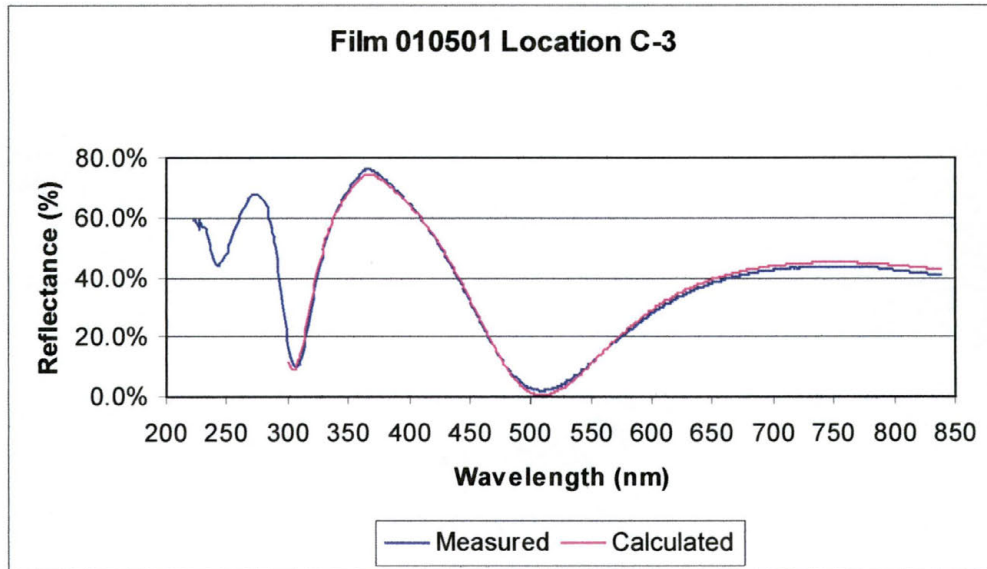


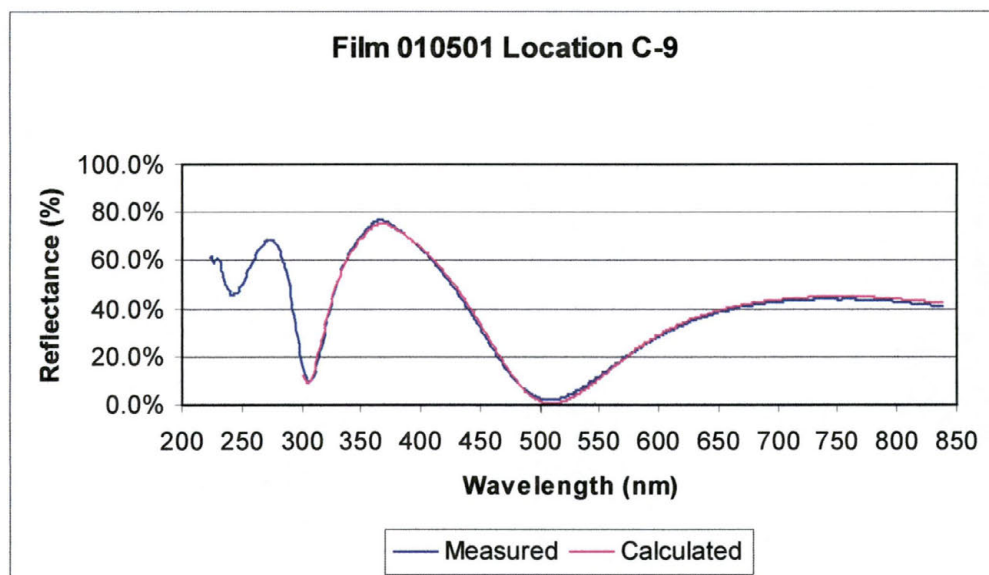
10.3.2.5 010501











10.4 X-Ray Fluorescence Data

I was initially planning on using the Kevex Model 771 X-Ray Fluorescence tool to create a standard from a Py film that could then be used to measure the film thickness of all the rest of the Py films. Figure 10-1 is the data that was collected. Note the large peak at around 7.3 KeV for the Ni $K_{\alpha 1}$ peak and the smaller peak at around 6.3 KeV for the Fe $K_{\alpha 1}$ peak.

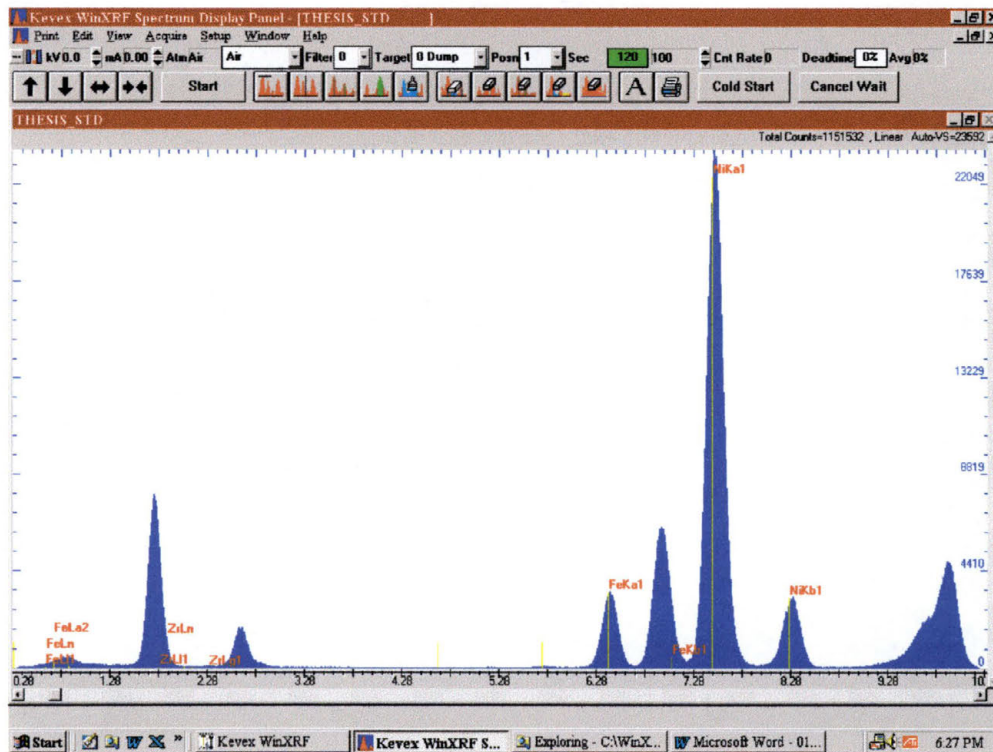


Figure 10-2: XRF Data From Scan Used to Create Py Standard

I also intended to use the Kevex to obtain data about the BZT films that I produced. I scanned the Ion-Beam target that was to be used in the production of my BZT films to get an idea of the elemental composition of the target. There are distinctive peaks for the Ba and the Zr of the target, but the Ti signal is lost in the background radiation and cannot be adequately resolved.

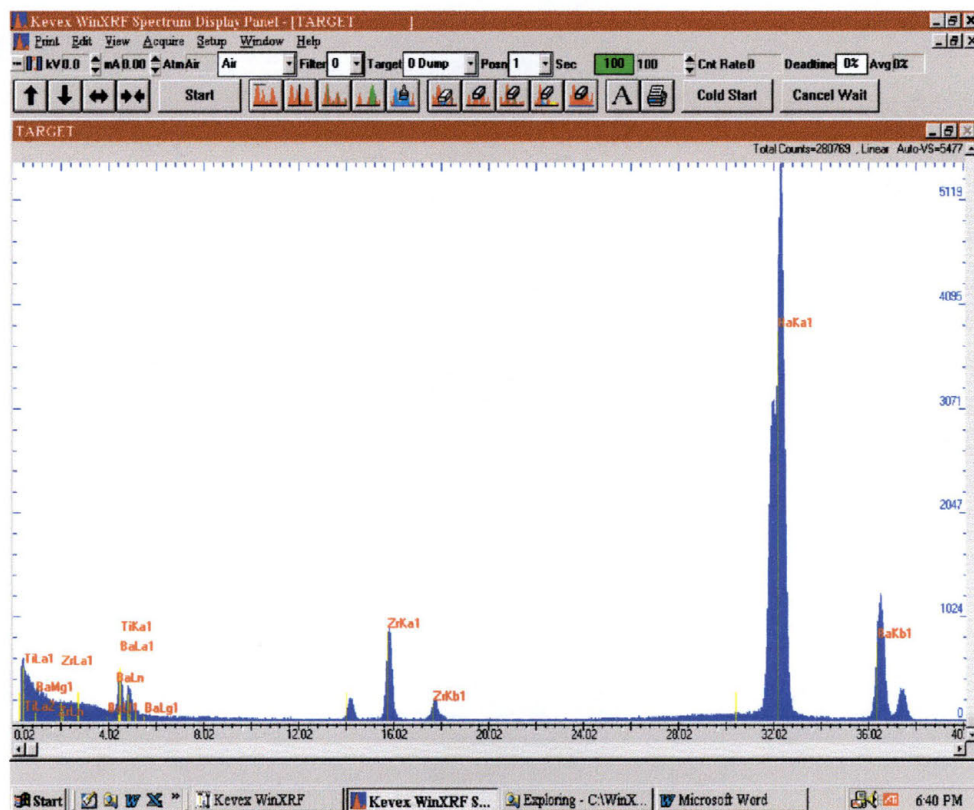


Figure 10-3: XRF Scan Data of BZT Target Used to Produce BZT Films

Film 010413 was then chosen to be the reference standard film for the determination of the BZT films because it was the thickest film as determined by Optical measurement. The film was first scanned using a Gadolinium secondary target in an attempt to get a good signal from the Ba, Zr and Ti on the same scan. This proved unsuccessful, as one look at Figure 10-4 will show.

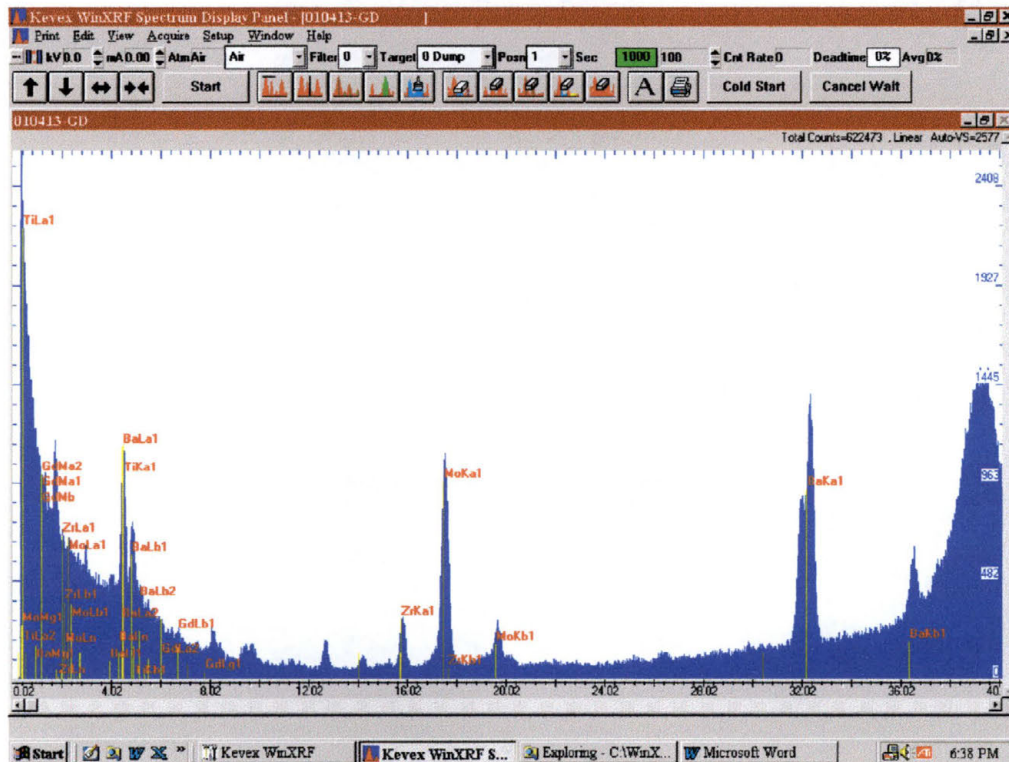


Figure 10-4: XRF Scan of Film 010413 Using Gd Secondary Target

All traces of the Ti signal are completely swamped by the background radiation due to the energy of the secondary target

x-rays. There is also a large peak for Molybdenum present. This is suspected to be trace amounts left from the fact that the substrates that were used in the production of films for my research came from a source that reclaims used Si substrates and resells them. Obviously the cleaning process used, while good enough to allow the use of the reclaimed Si in many applications including my own research, did not completely remove the previous coatings of the Si wafers.

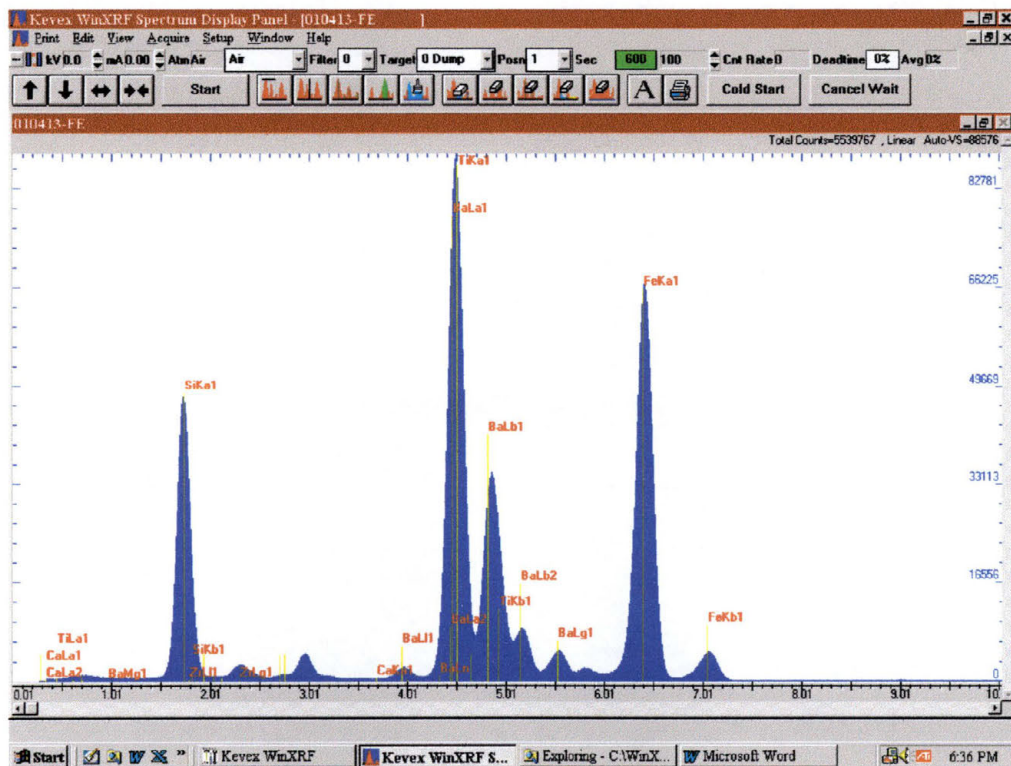


Figure 10-5: XRF Scan Film 010413 Using an Fe Secondary Target

The film was scanned again, this time using an iron secondary target (see Figure 10-5) but the Ba peak disappeared. There is a Ba $L\alpha$ peak present, but this peak is not reliable enough to give accurate data as to the actual number of Ba atoms are present in the material. The Ti peak is also still buried in background noise and is also not a reliable peak for attempting to determine film thickness.

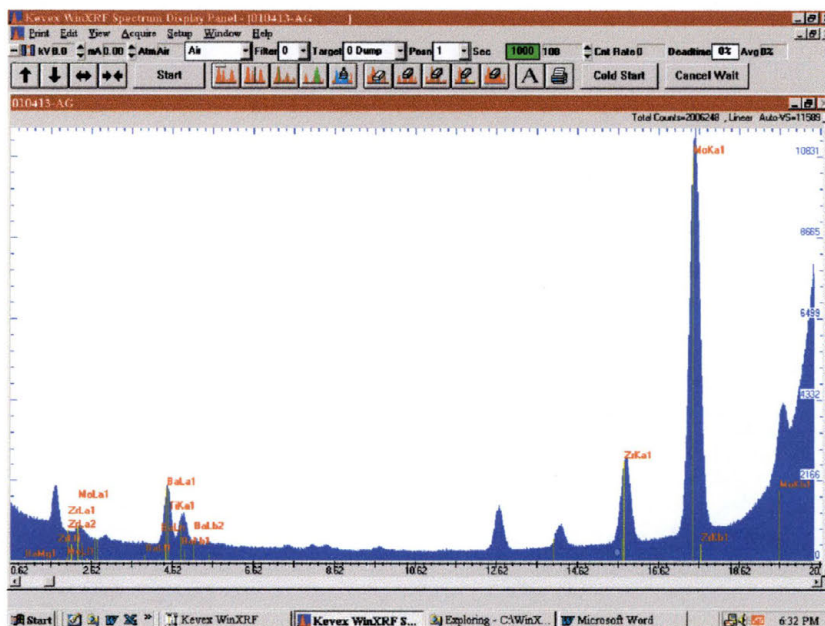


Figure 10-6: XRF Scan of Film 010413 Using a Silver (Ag) Secondary Target

Out of a growing sense of frustration, the same film was scanned using a silver (Ag) secondary target (see Figure 10-6). This proved to be useless also as there was no Ba signal that

could be used for film calibration and the Ti signal was still lost in the background noise.

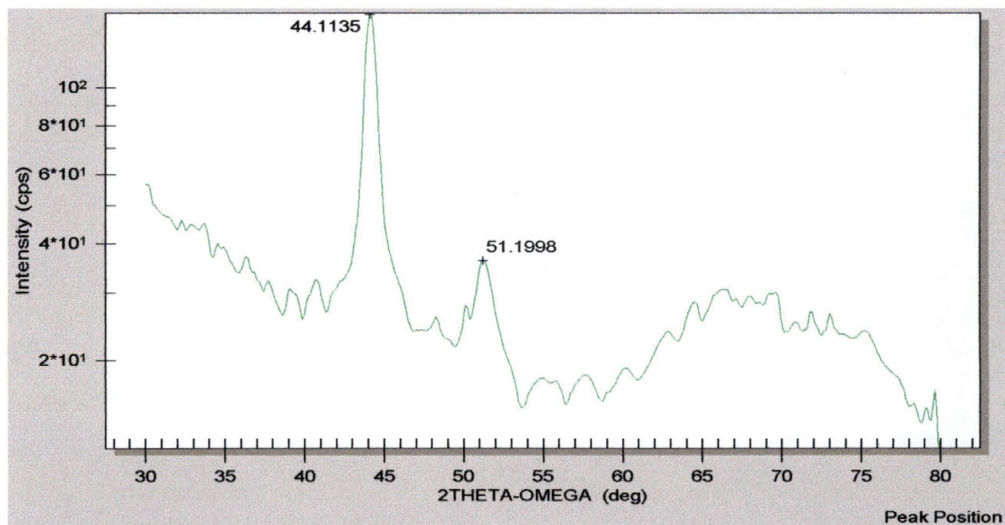
The end result was that, after discussions with my advisor, it was determined that the BZT films were too thin for accurate measurement of them using the XRF tool. Unfortunately, before I could measure all of the Py films, the detector on the Kevex went out and I was unable to collect any further data. I spent the rest of my time collecting data using the other analytical techniques I had available to me.

10.5 High Angle X-Ray Diffraction Data

This data is presented in the following manner: the actual graph of the data as taken from the Bede D-1 system is shown with the major peaks indicated. Immediately below that is the scan data defining the parameters of the scan taken, followed by a listing of the peaks and the relative intensity of each peak shown.

10.5.1 Permalloy Metal Films

10.5.1.1 Film 010315



DCC SCAN DATA:

File: D:\Data\Bede\Albert\High Angle\Py010315_HAXRD_1aa1.X01

User: D1D1

Specimen: Py010315_HA Crystal: Si Reflection: 0 0 4

Wavelength: 1.54056 Å Bragg Angle: 34.5635 kV: 00.00 mA: 00.00

test taken using 1 mm vertical source slit, 1 mm front and 2mm back detector slits (with NO Phi offset)

Time: 12:30 Date: 03/23/2002 Count Time: 3 Datapoints: 540

DCC SCAN DATA:

File: D:\Data\Bede\Albert\High Angle\Py010315_HAXRD_1aa1.X01

User: D1D1

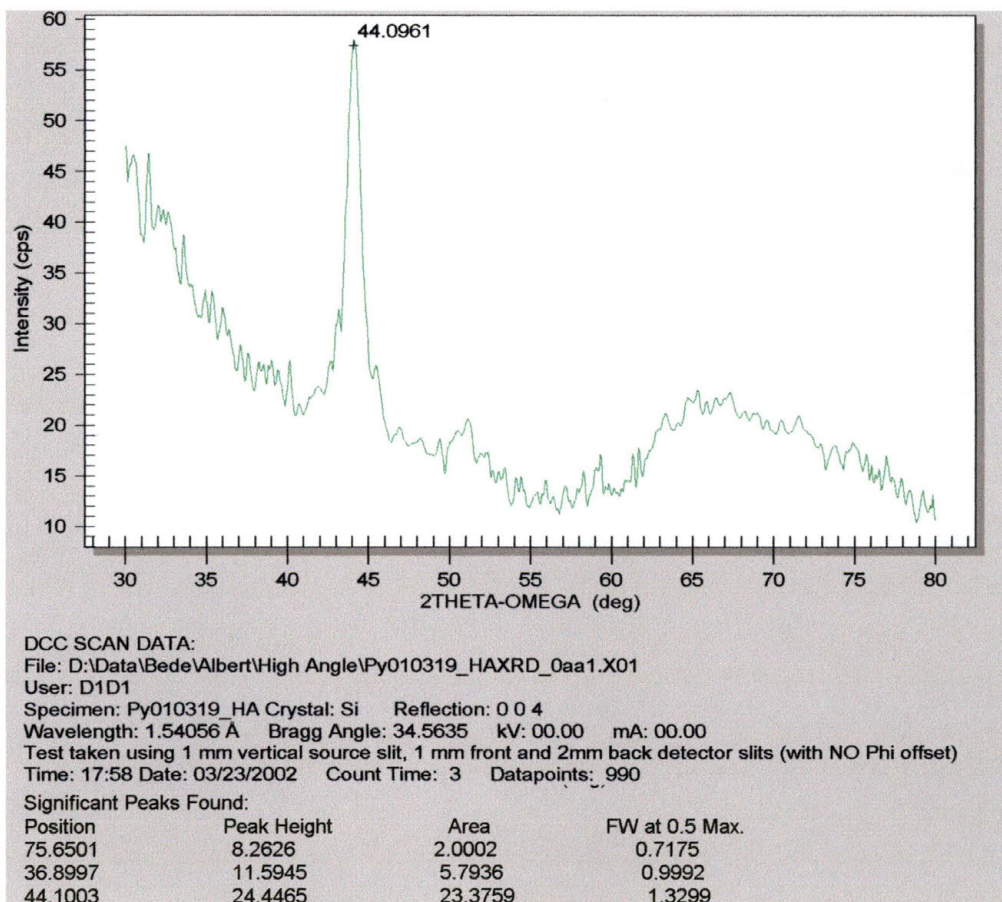
Specimen: Py010315_HA Crystal: Si Reflection: 0 0 4

Wavelength: 1.54056 Å Bragg Angle: 34.5635 kV: 00.00 mA: 00.00

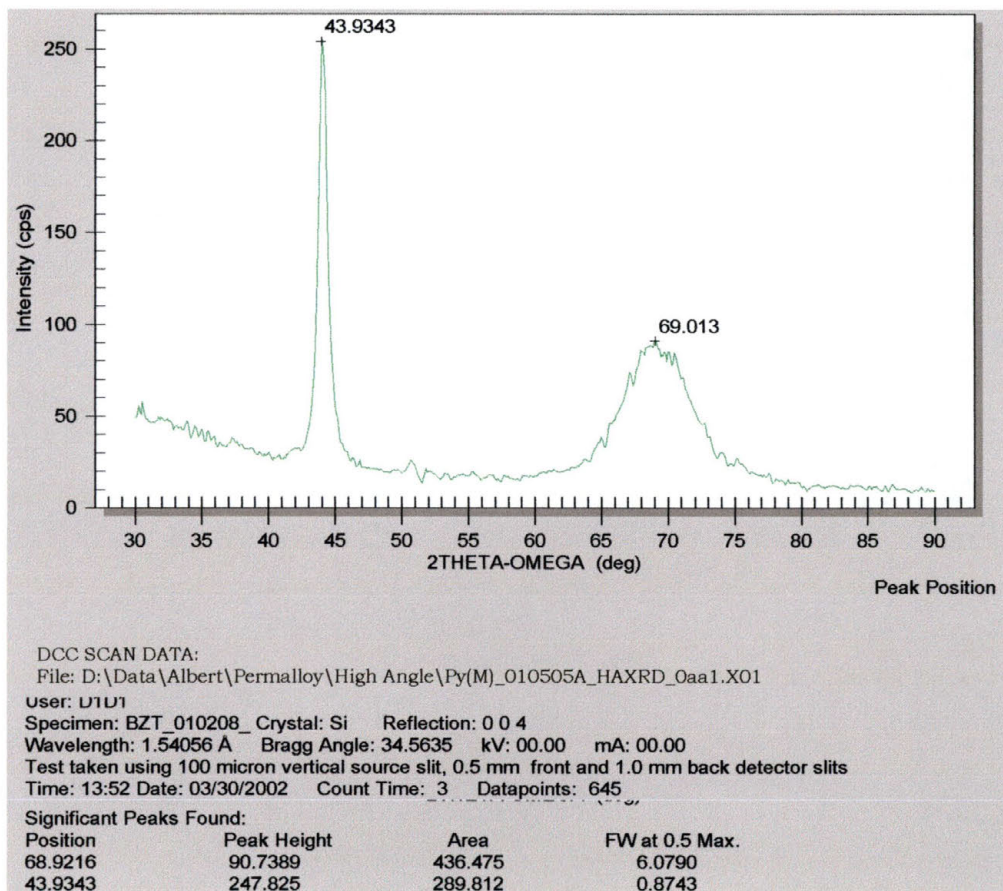
test taken using 1 mm vertical source slit, 1 mm front and 2mm back detector slits (with NO Phi offset)

Time: 12:30 Date: 03/23/2002 Count Time: 3 Datapoints: 540

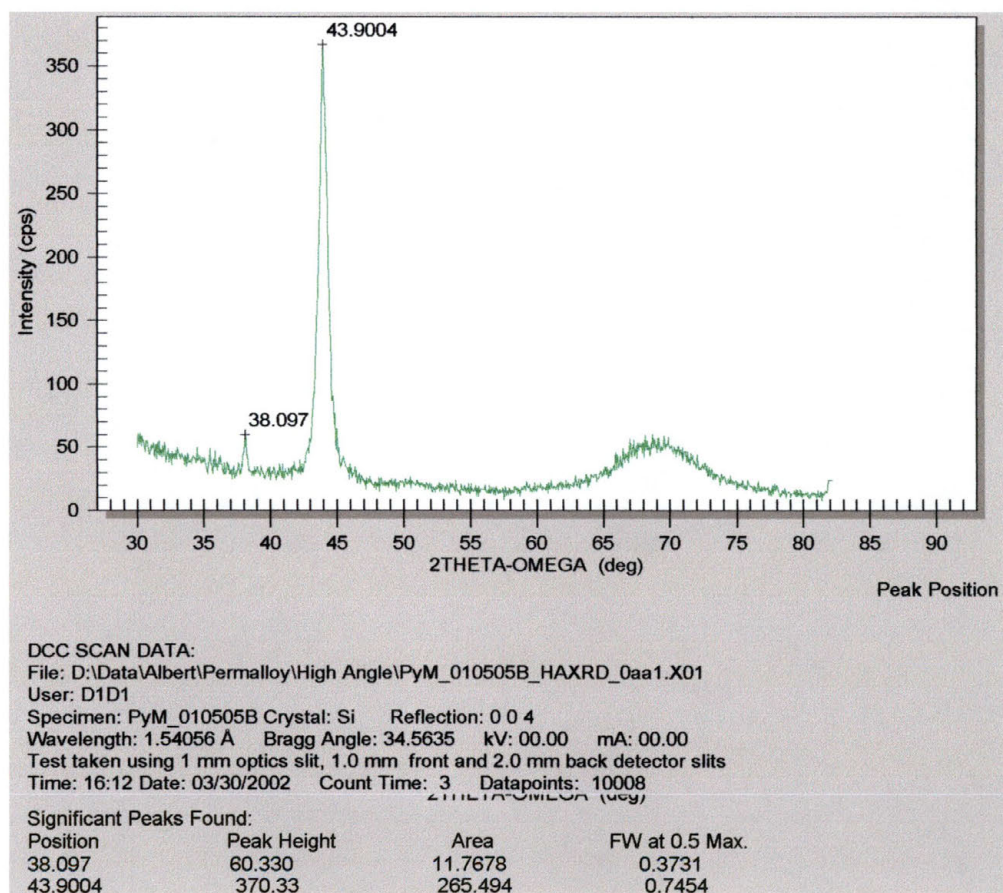
10.5.1.2 Film 010319



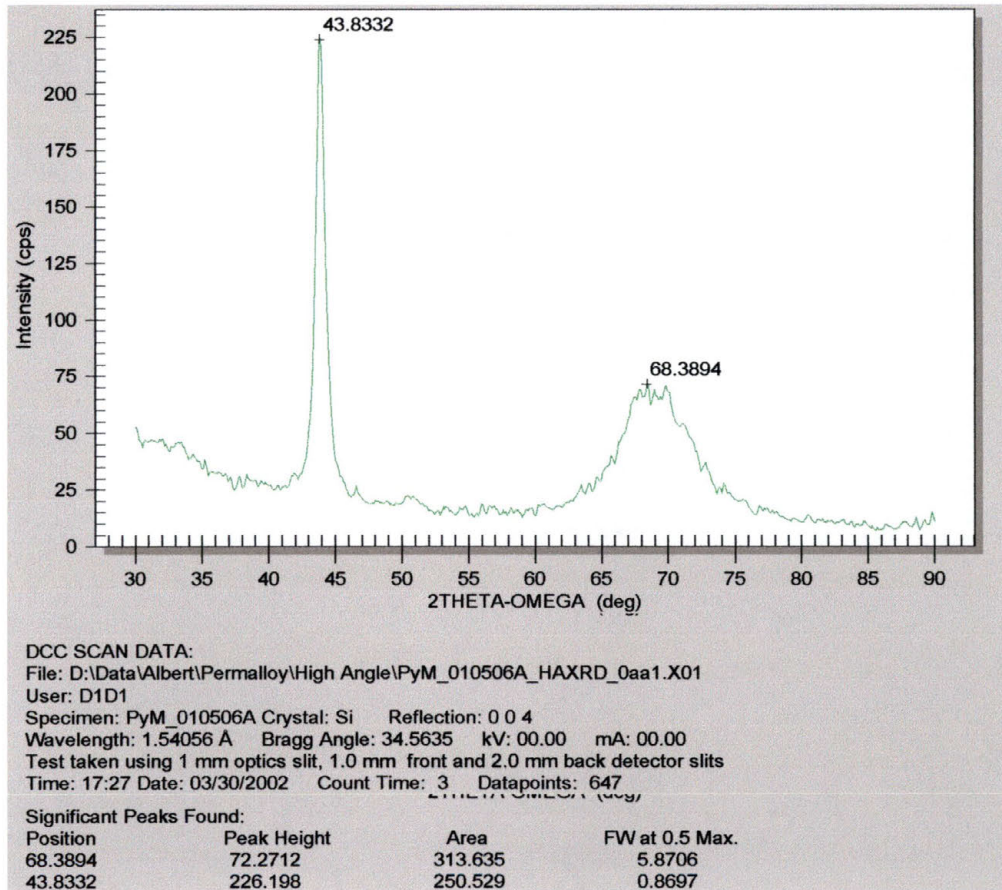
10.5.1.3 Film 010505A



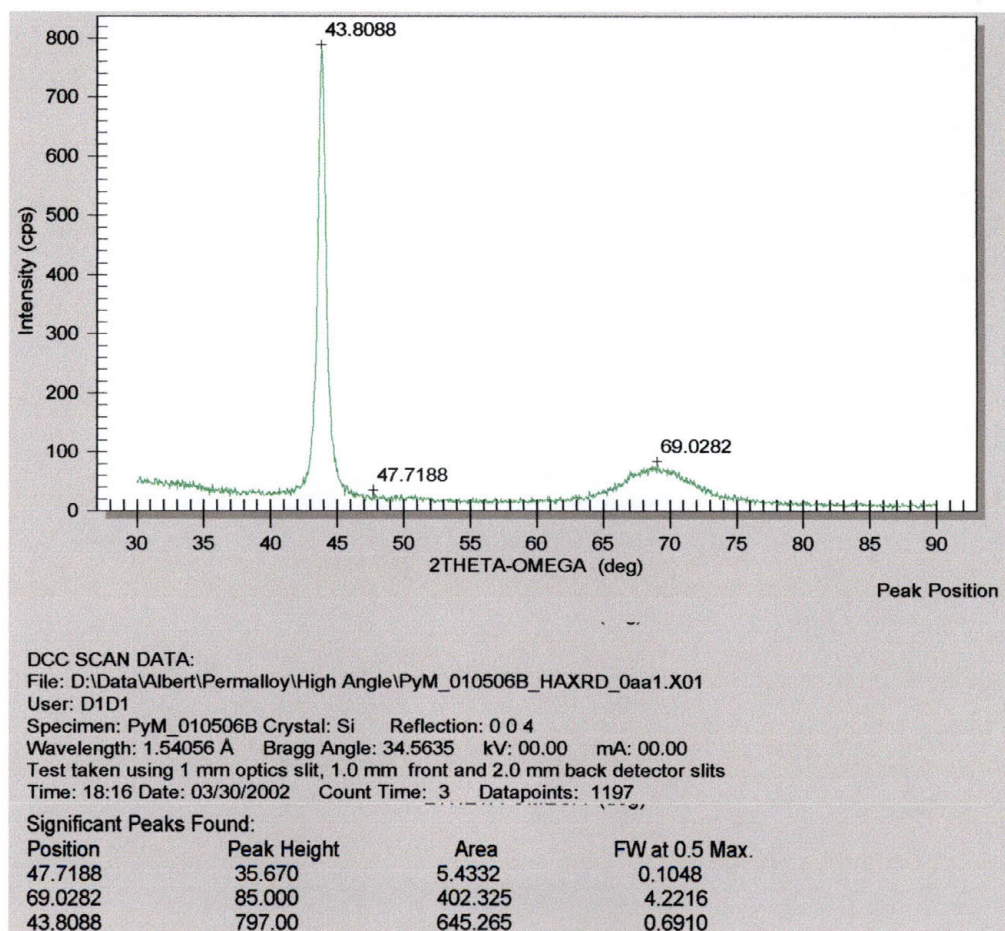
10.5.1.4 Film 010505B



10.5.1.5 Film 010506A

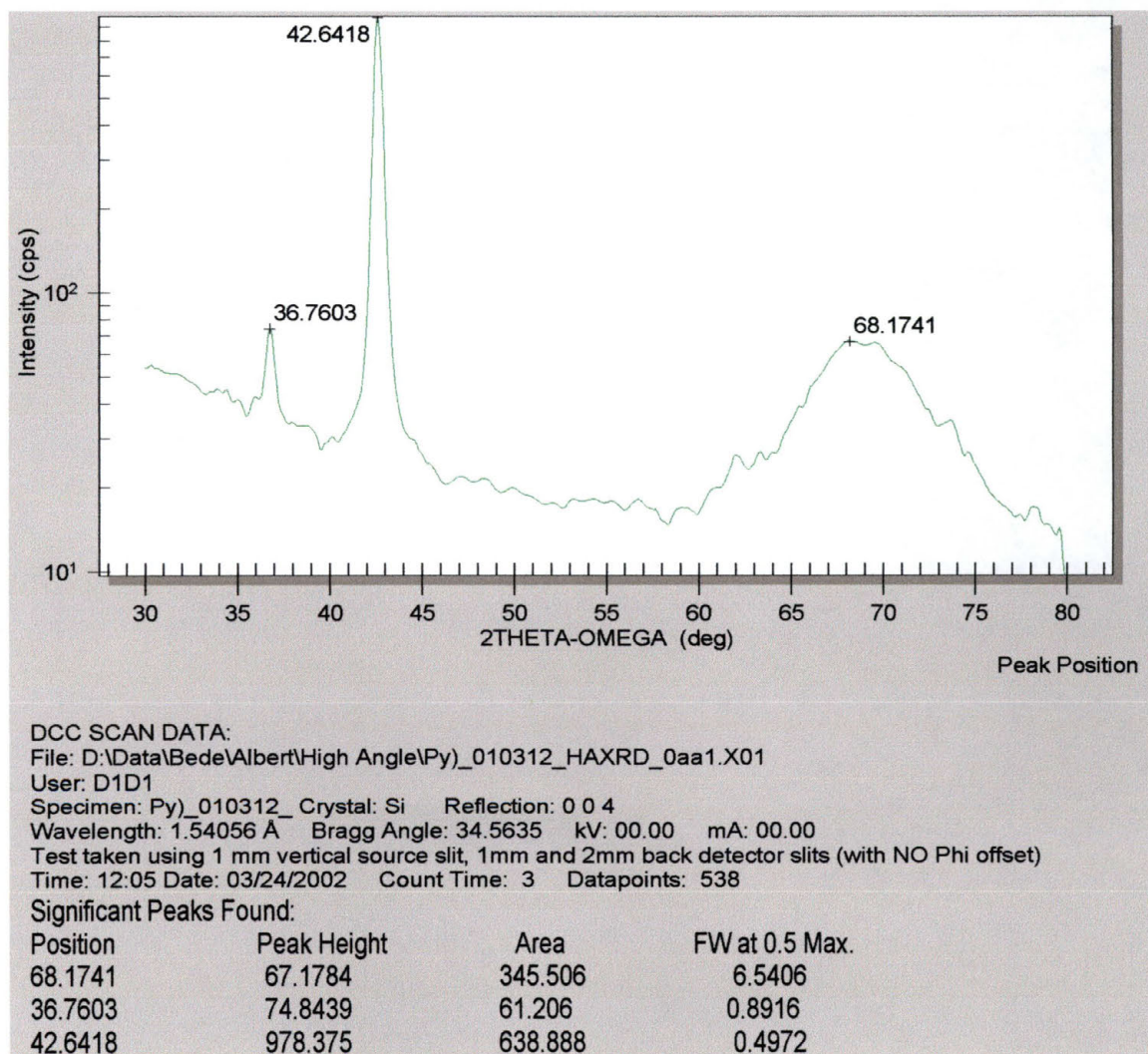


10.5.1.6 Film 010506B

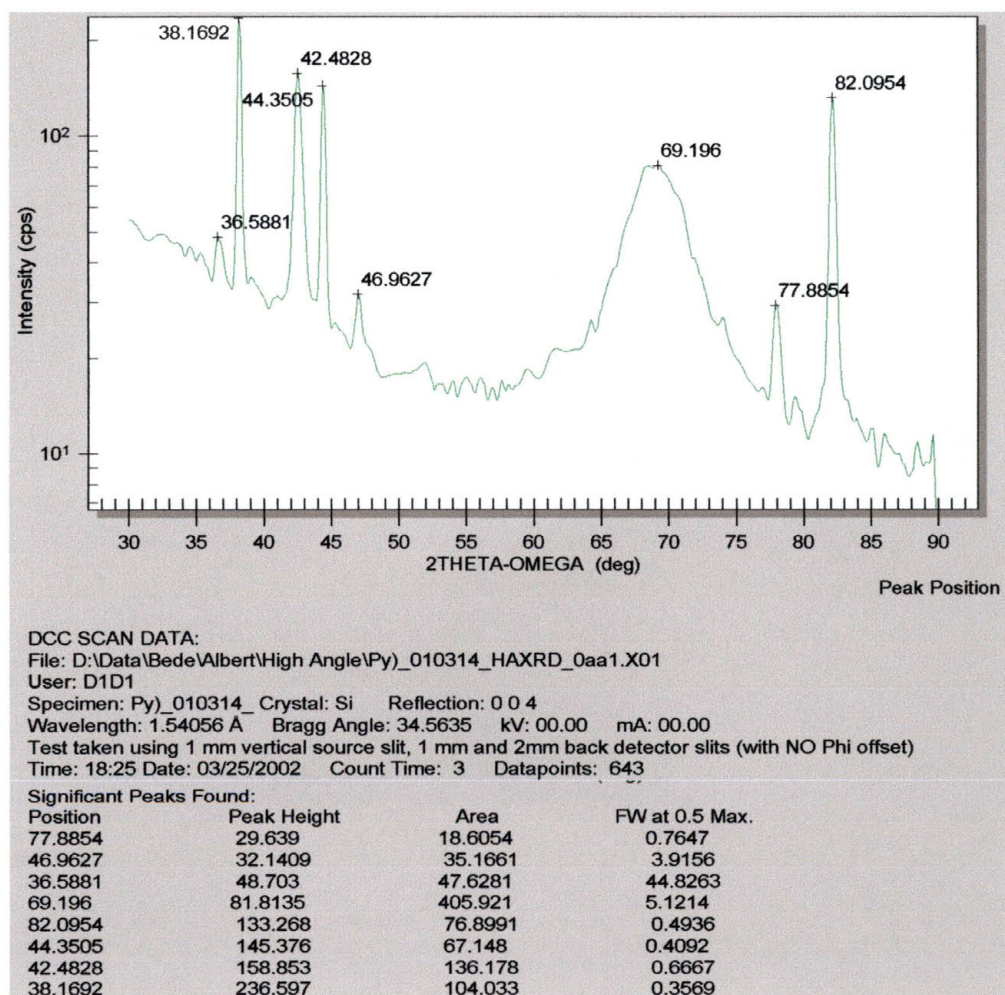


10.5.2 Permalloy Oxide Films

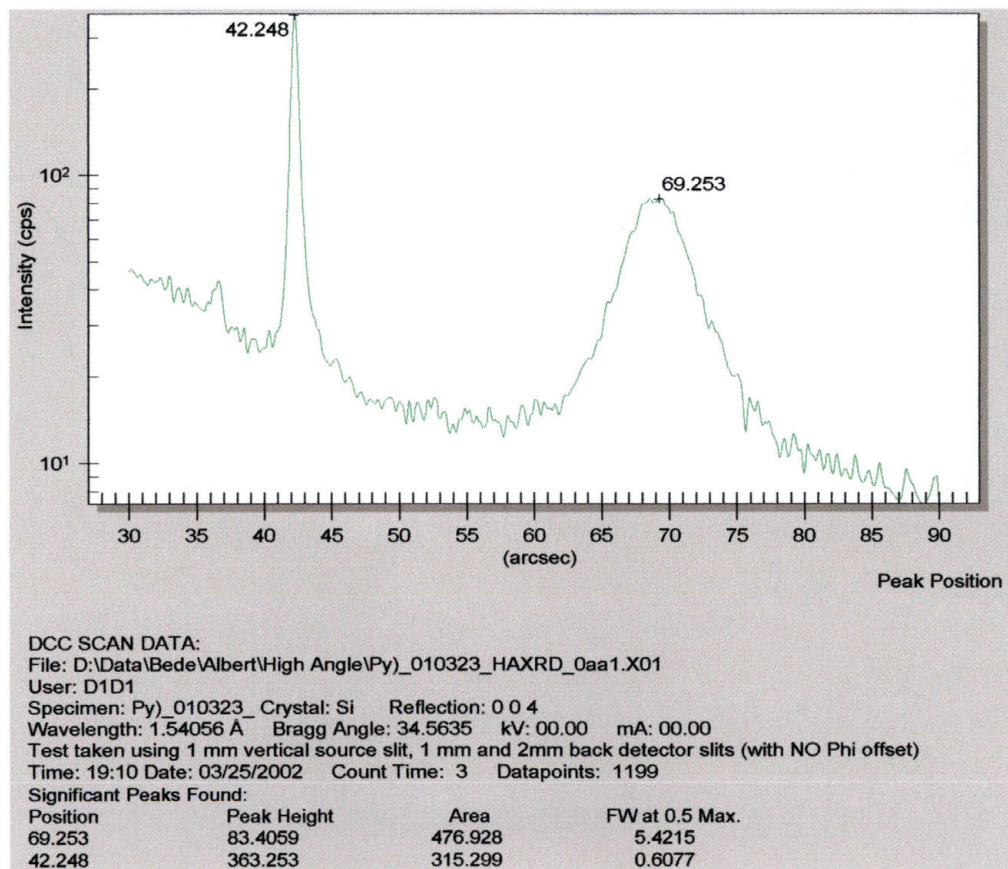
10.5.2.1 Film 010312



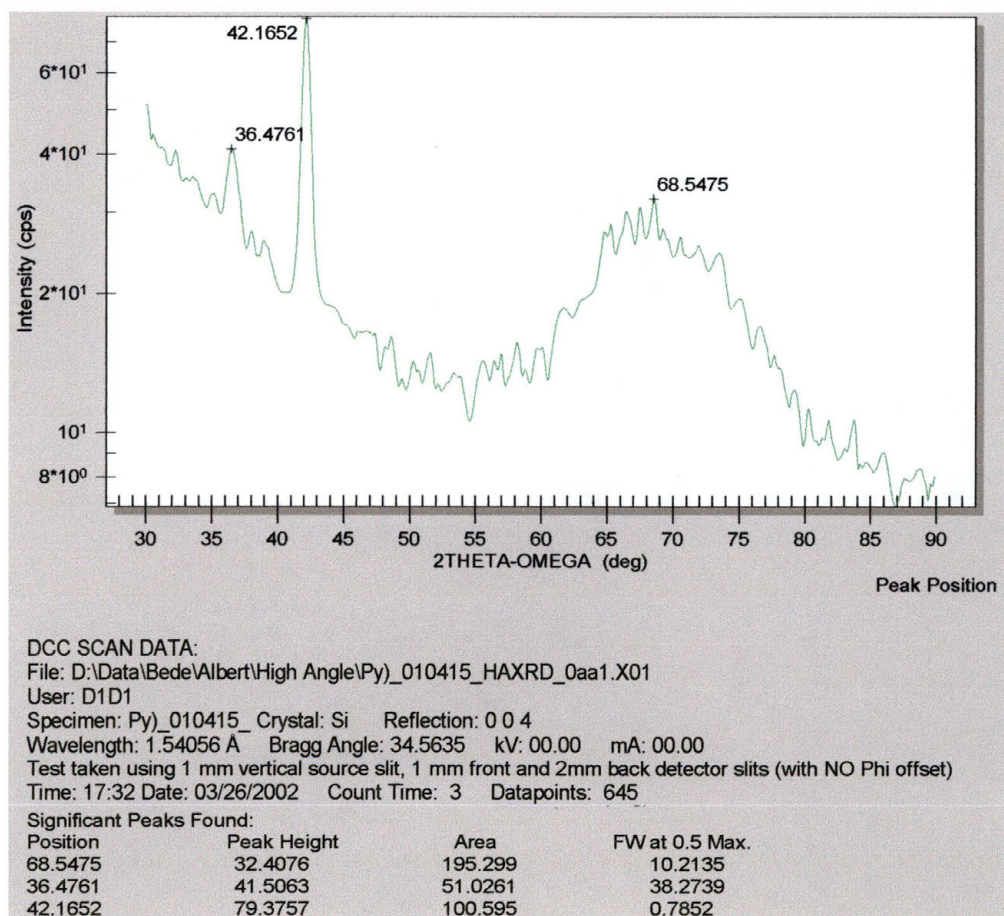
10.5.2.2 Film 010314



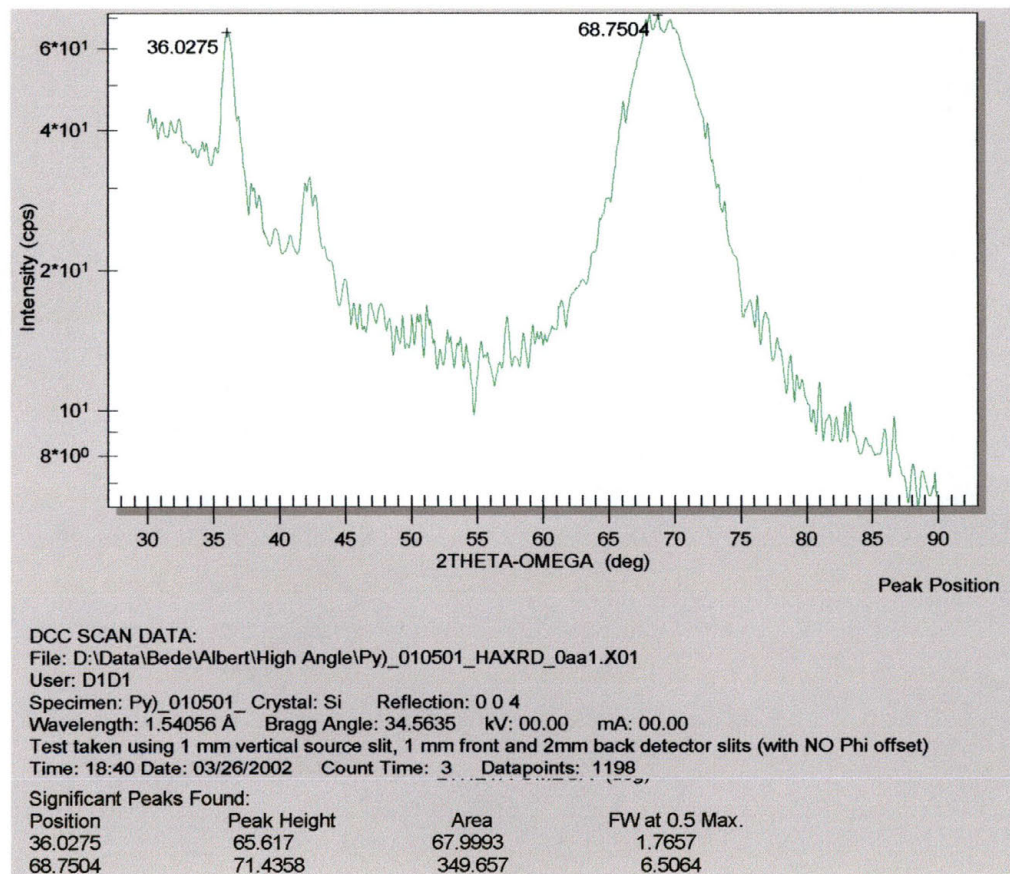
10.5.2.3 Film 010323



10.5.2.4 010415

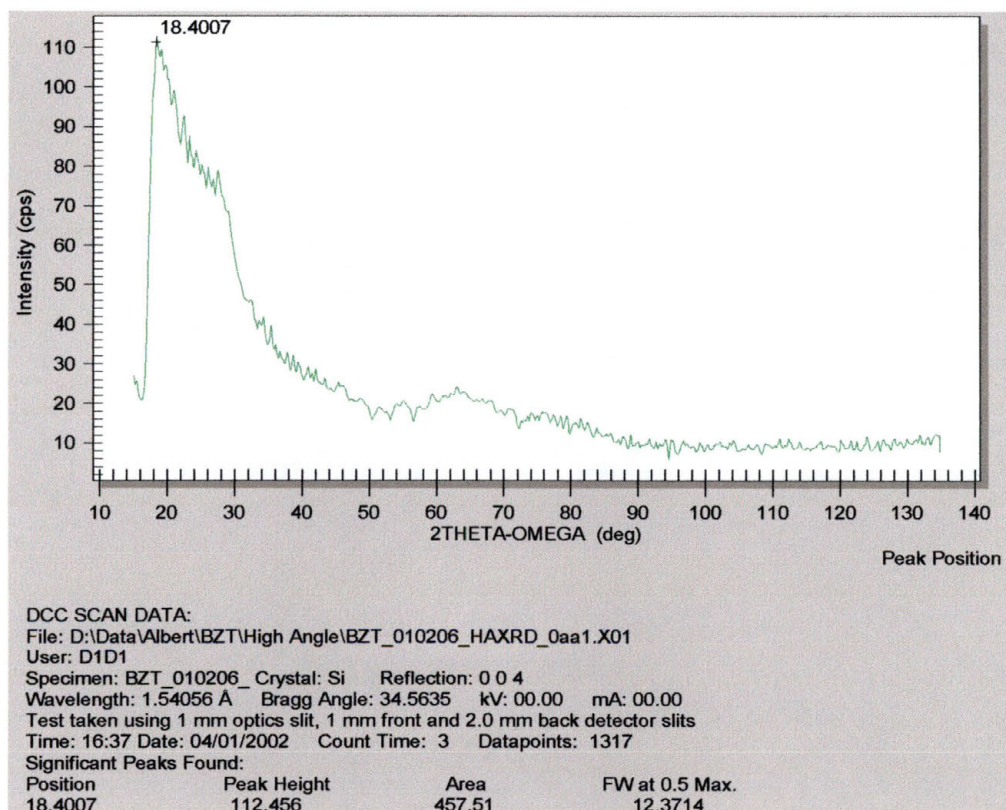


10.5.2.5 Film 010501

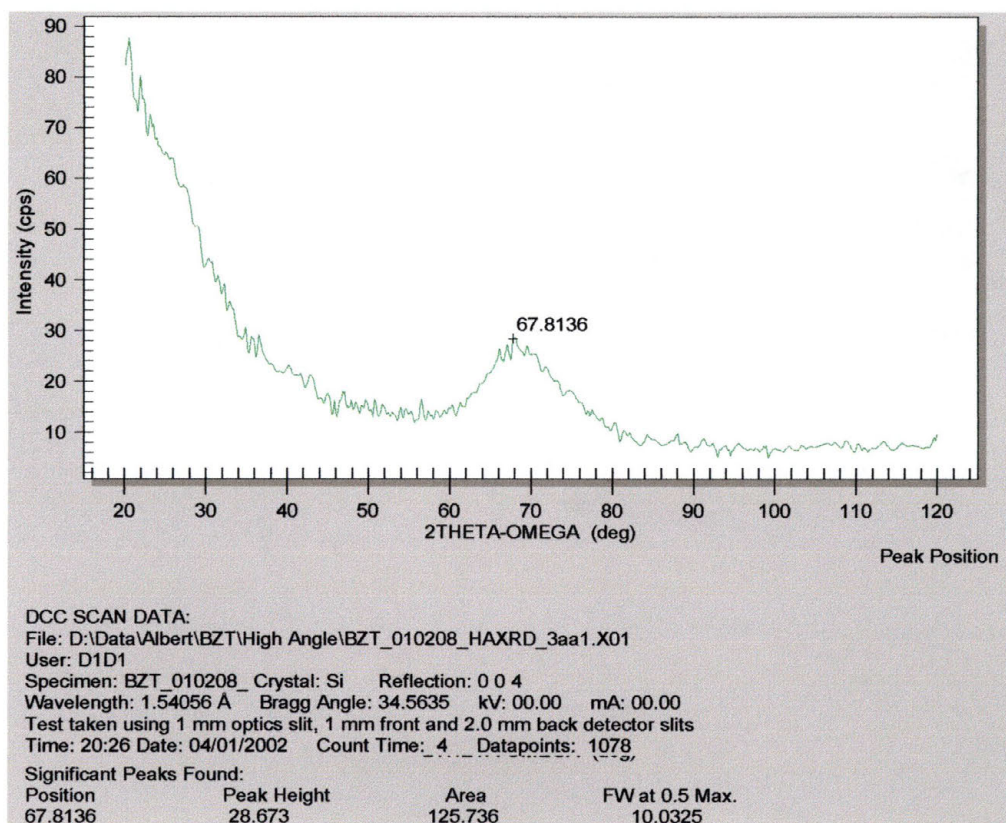


10.5.3 Barium Zirconium Titanate Films

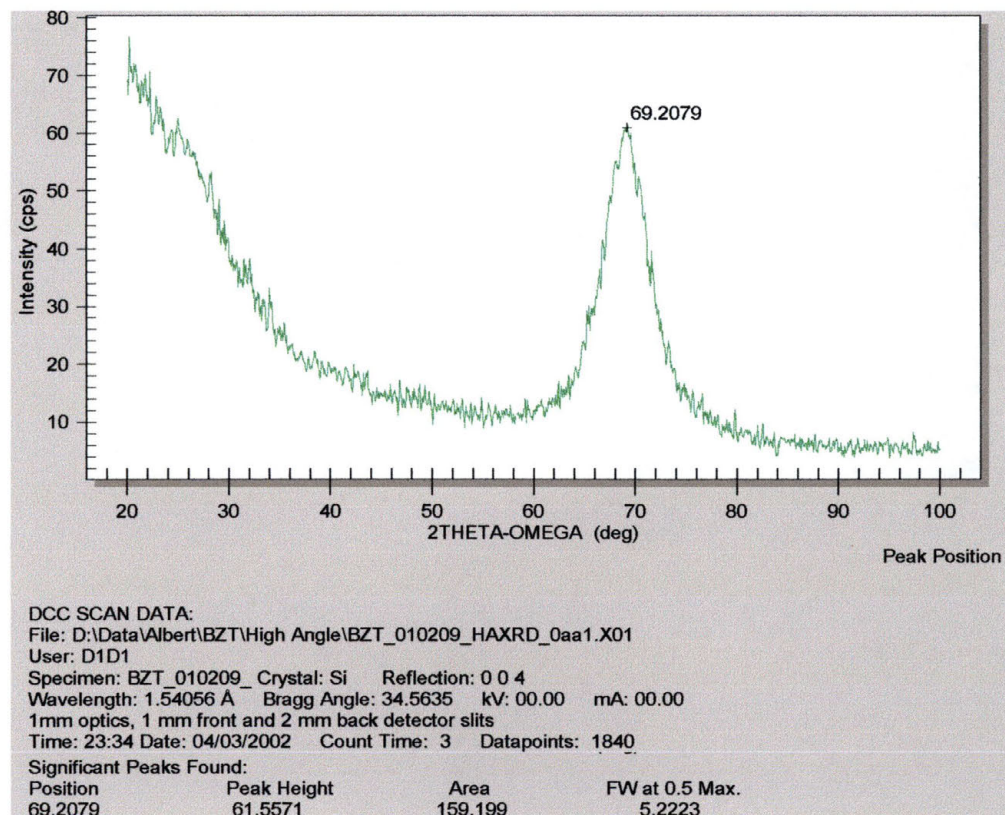
10.5.3.1 Film 010206



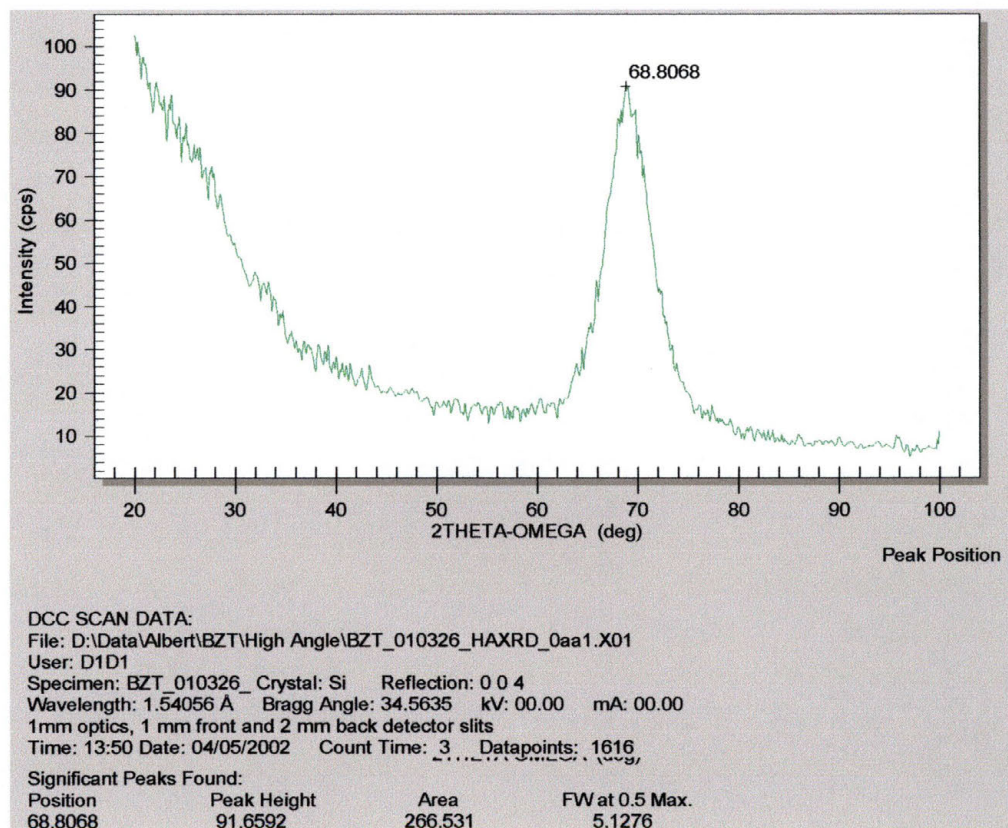
10.5.3.2 Film 010208



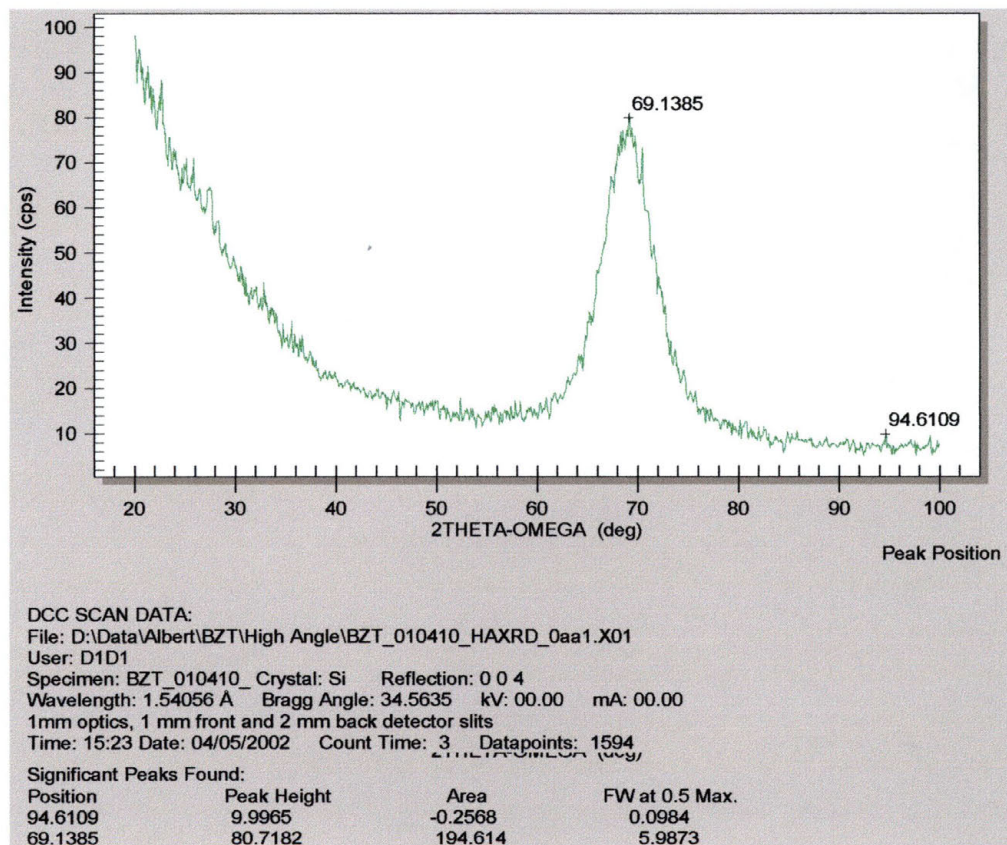
10.5.3.3 Film 010209



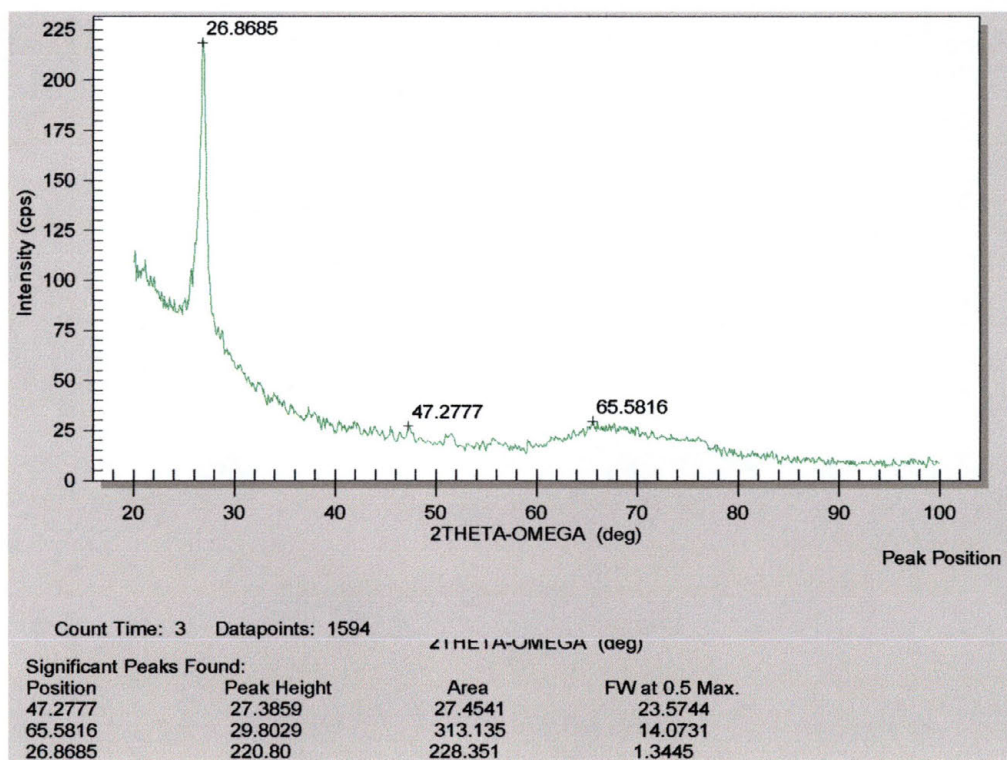
10.5.3.4 Film 010326



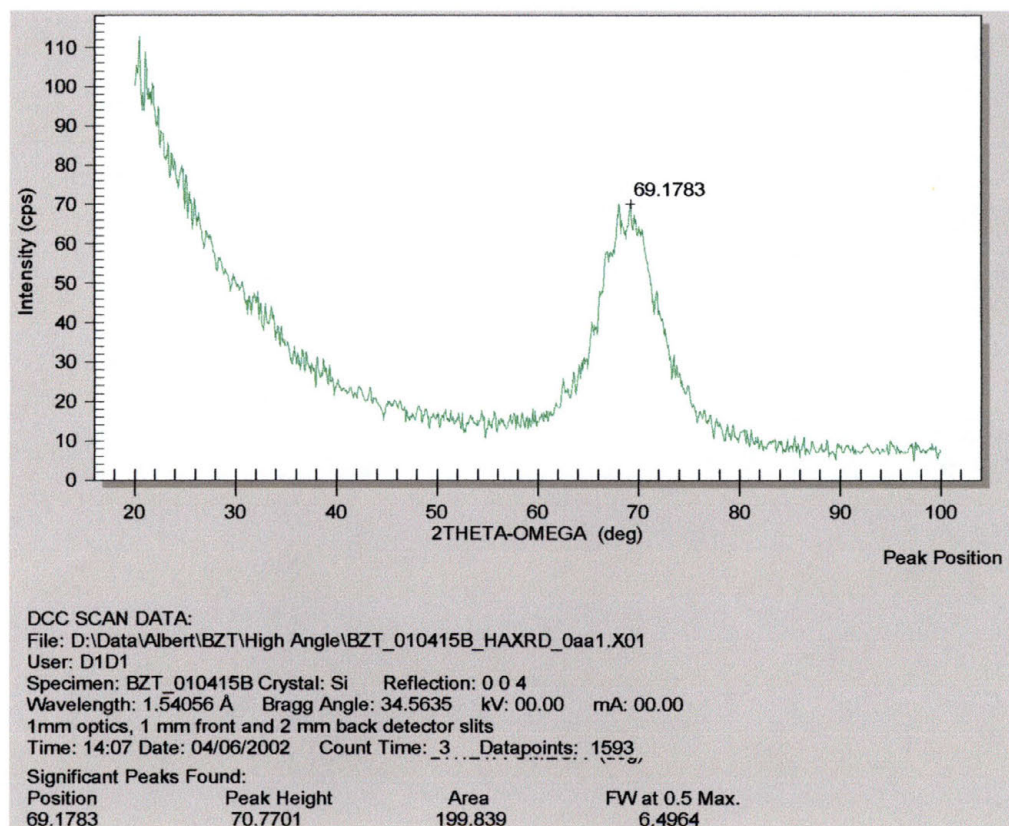
10.5.3.5 Film 010410



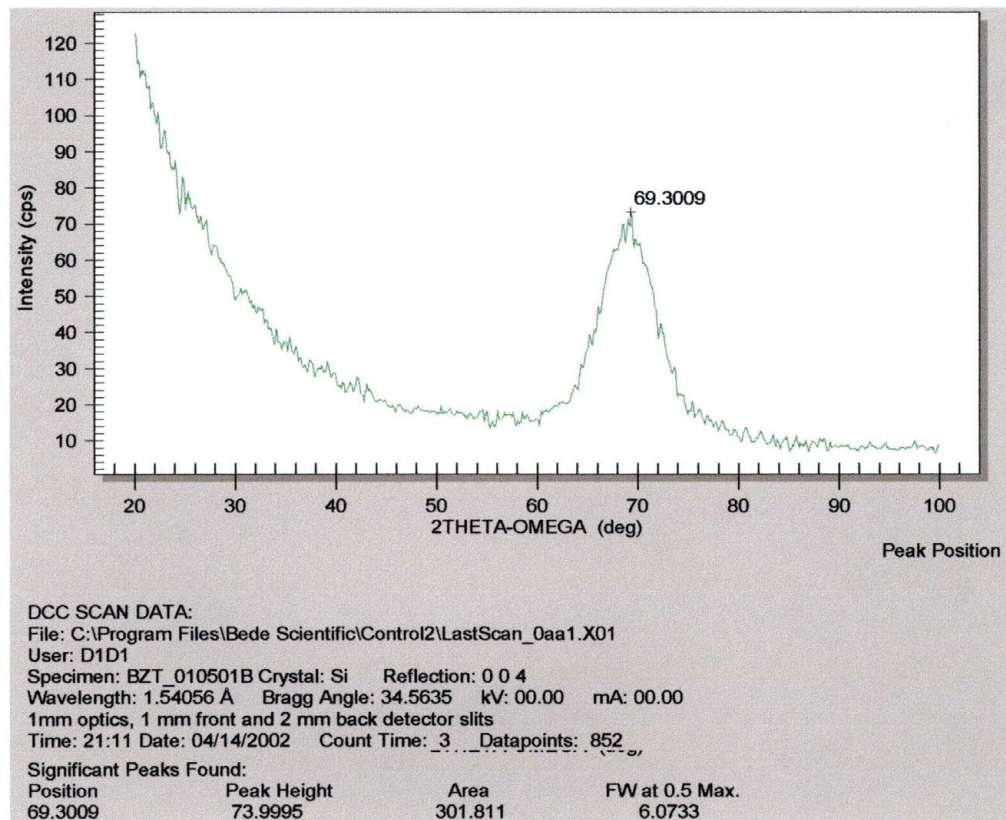
10.5.3.6 Film 010413



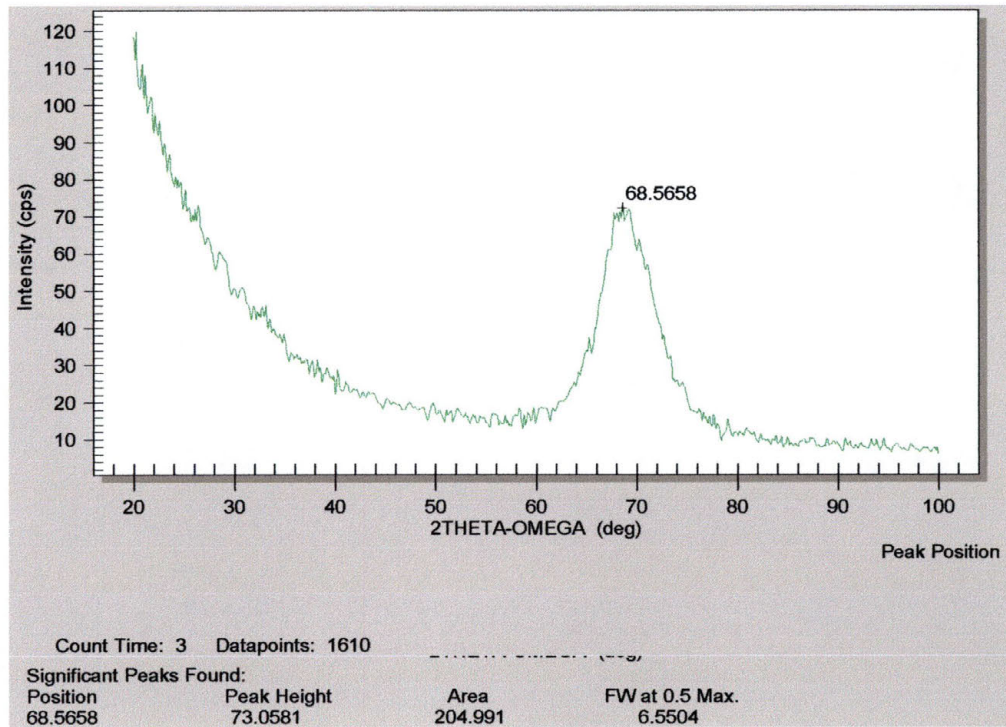
10.5.3.7 Film 010415B



10.5.3.8 Film 010501B



10.5.3.9 Film 010504AB



10.6 Parallel Beam X-Ray Diffraction Data

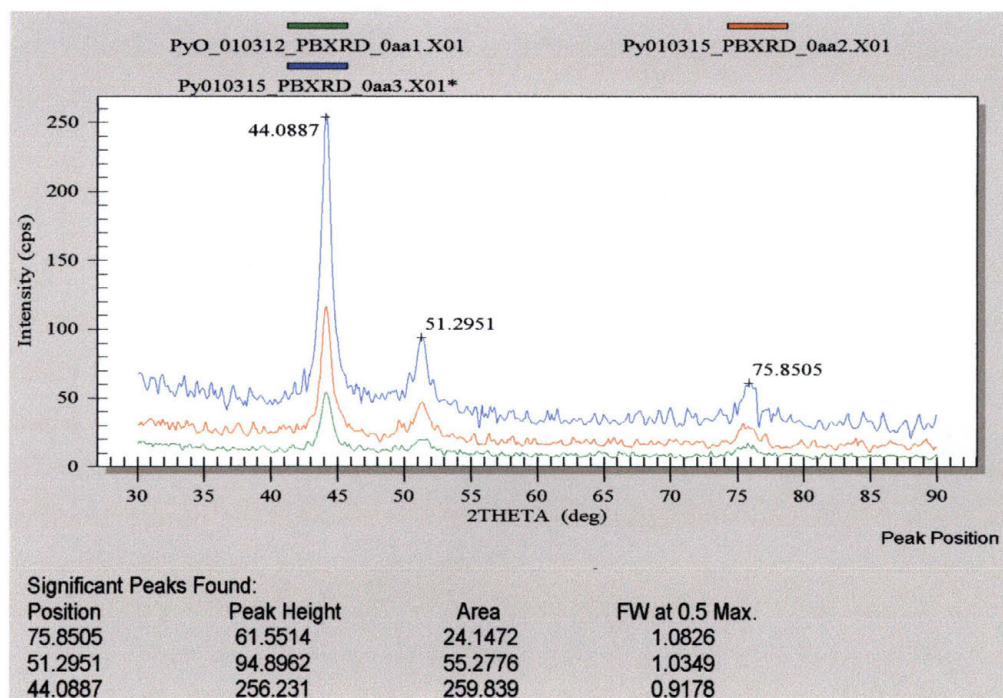
When collecting data for the parallel beam scans, the method used on most films was to adjust the angle of incidence of the x-ray beam from 2.0 to 3.0 degrees. On most of the scans, three sets of data were taken, advancing the angle of incidence by $\frac{1}{2}$ of a degree per scan. On some films, only two sets of data were taken, one set at 2.0 degrees the other at 3.0 degrees. This was done to save time, while still allowing for multiple scans per film. One of the reasons that multiple scans were collected was to show the presence of what is known as a Laue peak. A Laue peak would be visible on one scan, and then be at a slightly different location (shifted by only a few degrees to the right) on the next scan, etc. By finding peaks that are not moving as the angle of incidence is adjusted, it is possible to find the peaks that are truly indicative of the film under investigation.

In addition, all of the scans have been combined to show the relationships between one scan and another more easily. The relative intensity of each peak is actually similar, however, the data has been split by multiplying one set of data by a

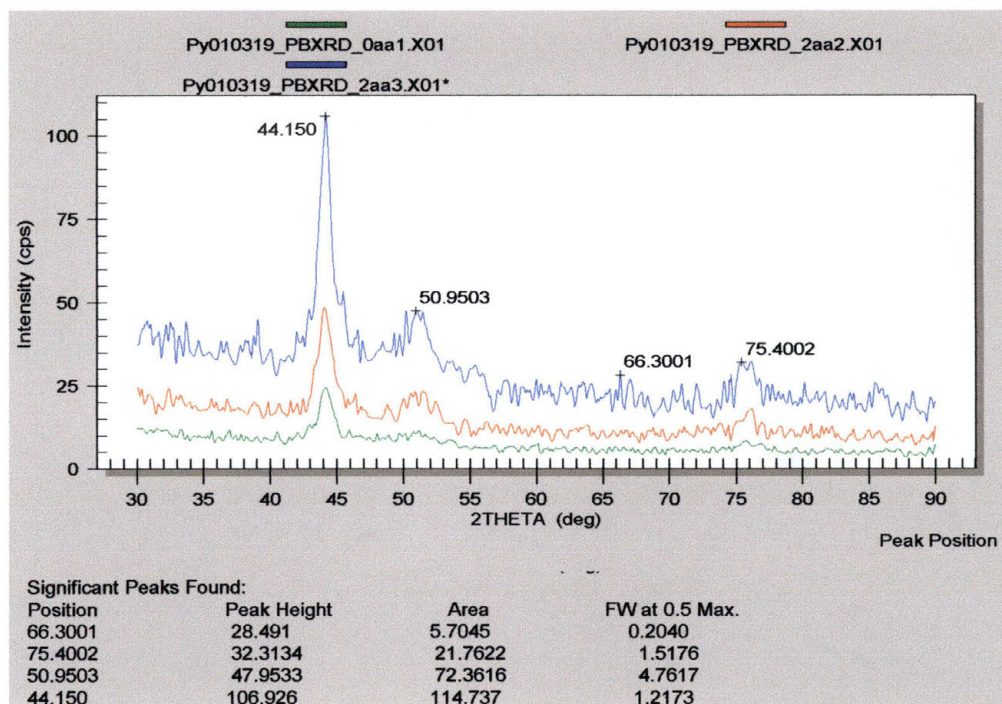
factor of 2 and one set of data by a factor of 3. This was done because resolution of the data would have been lost from one scan to the other as all data sets “sat” on top of each other.

10.6.1 Permalloy Metal Films

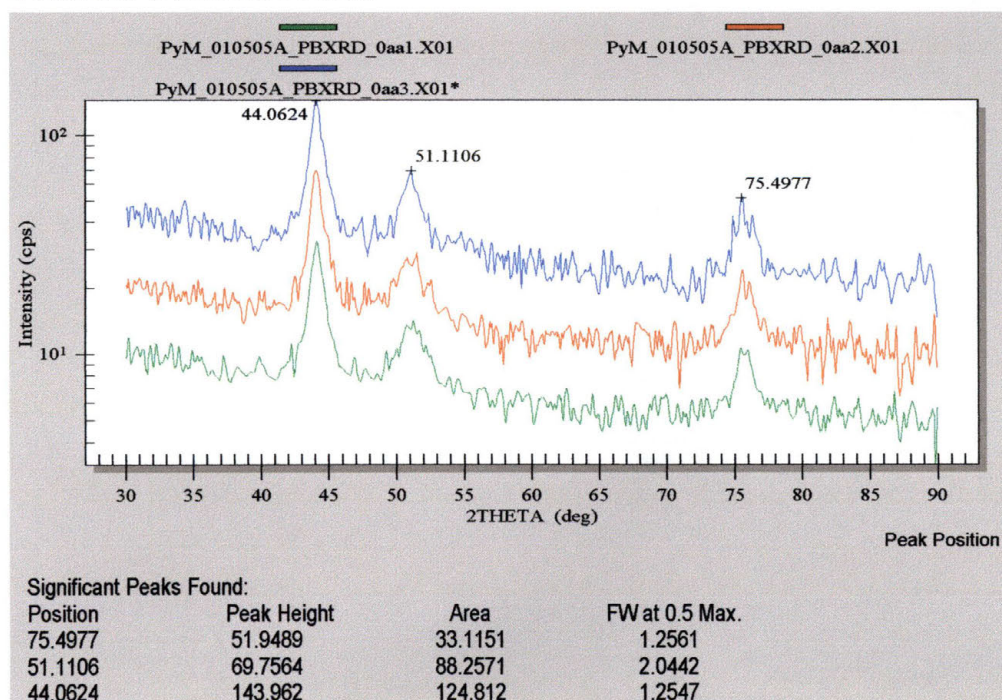
10.6.1.1 Film 010315



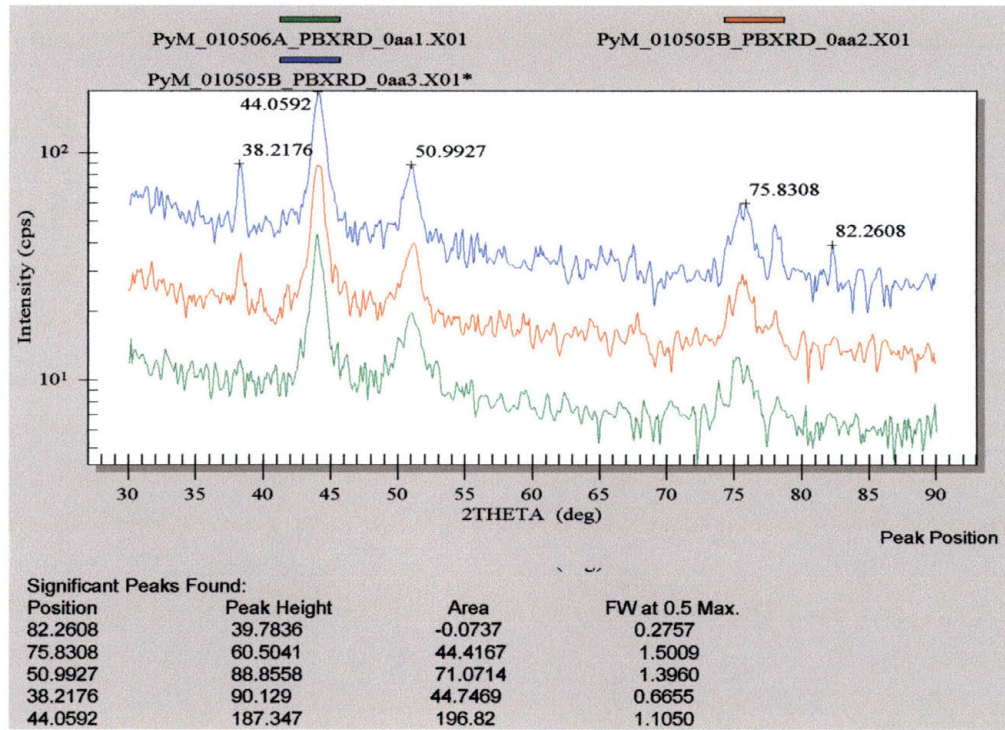
10.6.1.2 Film 010319



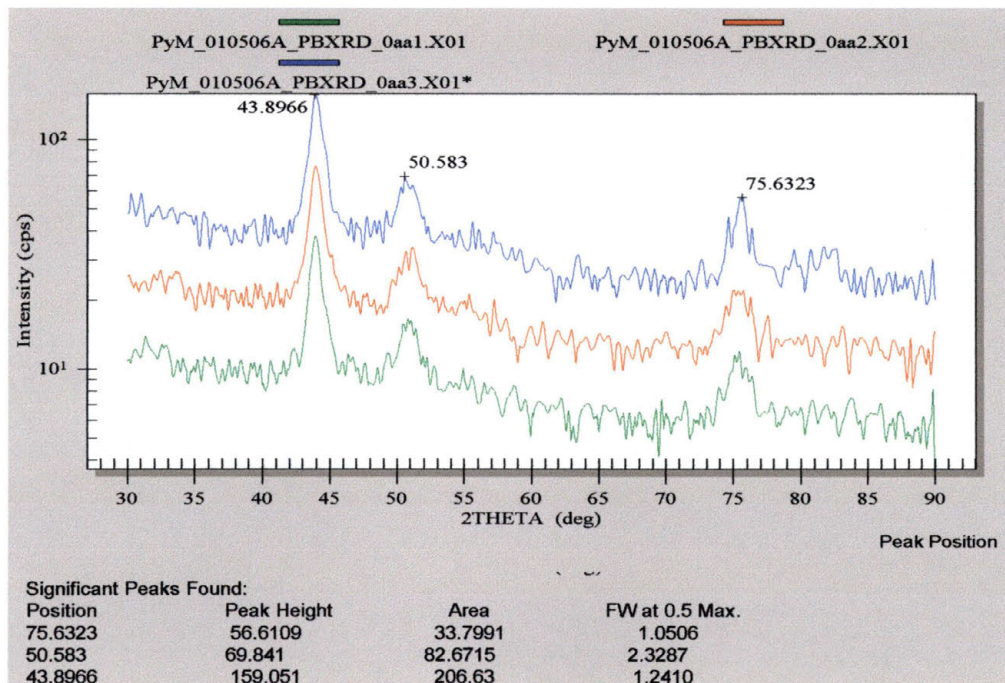
10.6.1.3 Film 010505A



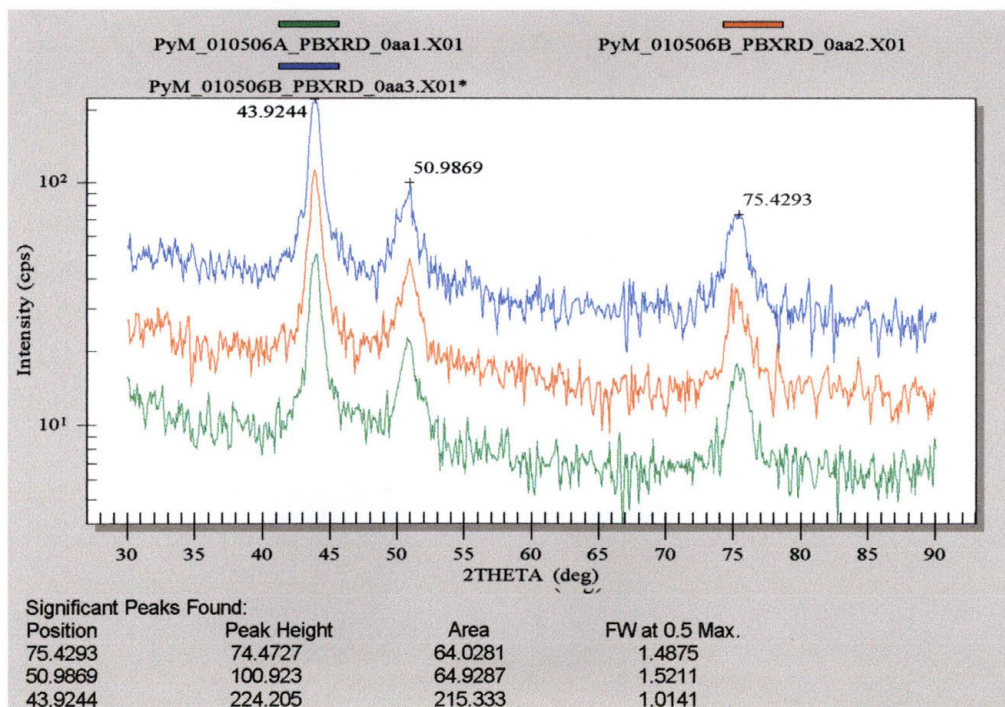
10.6.1.4 Film 010505B



10.6.1.5 Film 010506A

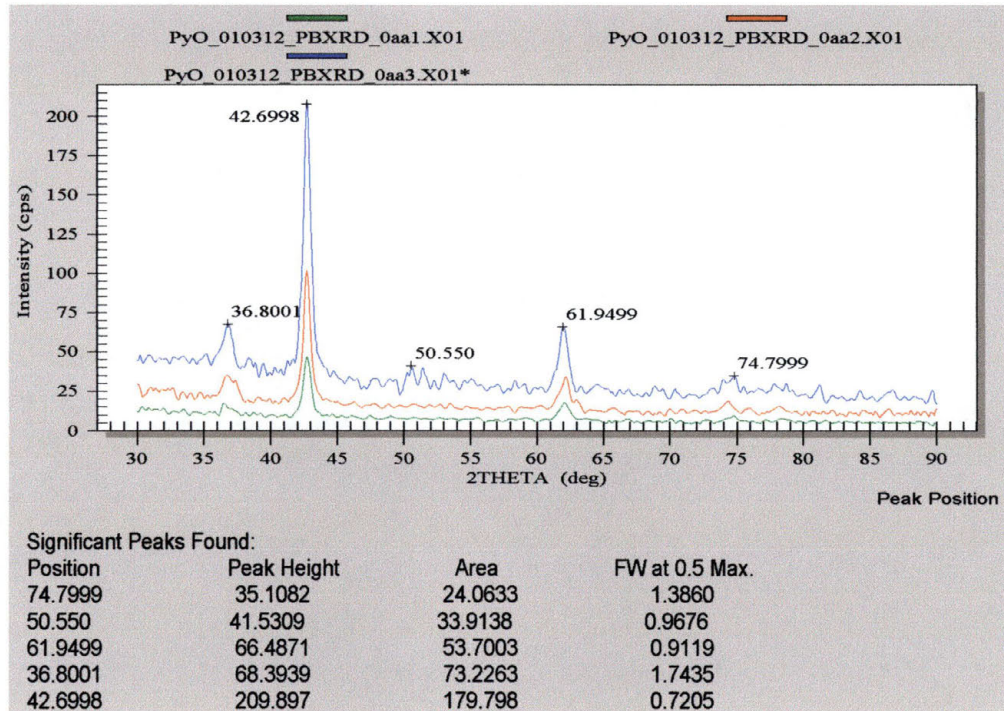


10.6.1.6 Film 010506B

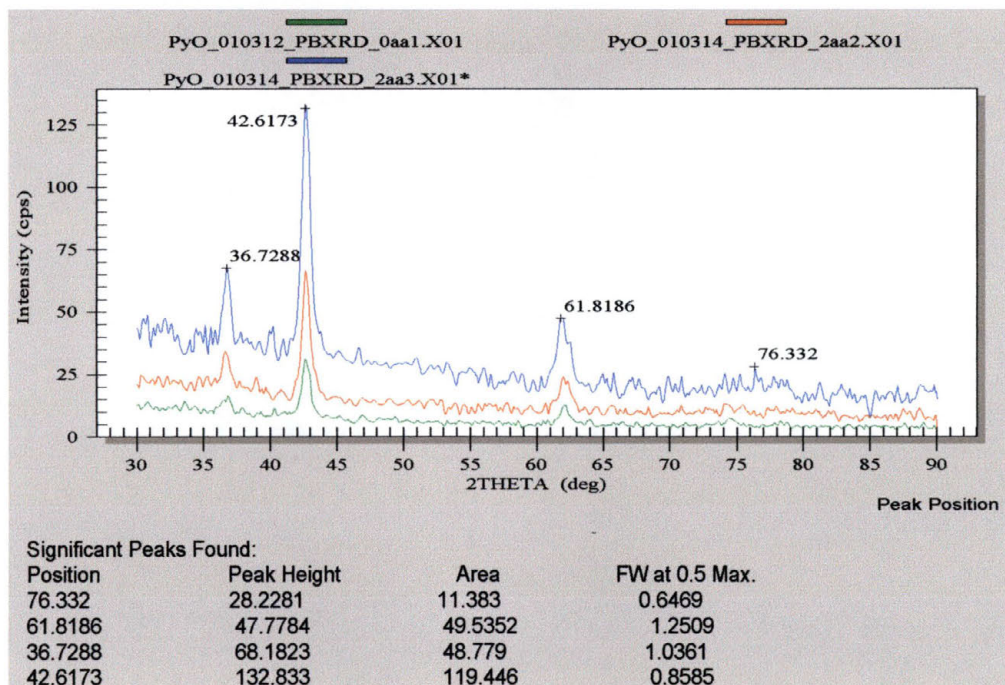


10.6.2 Permalloy Oxide Films

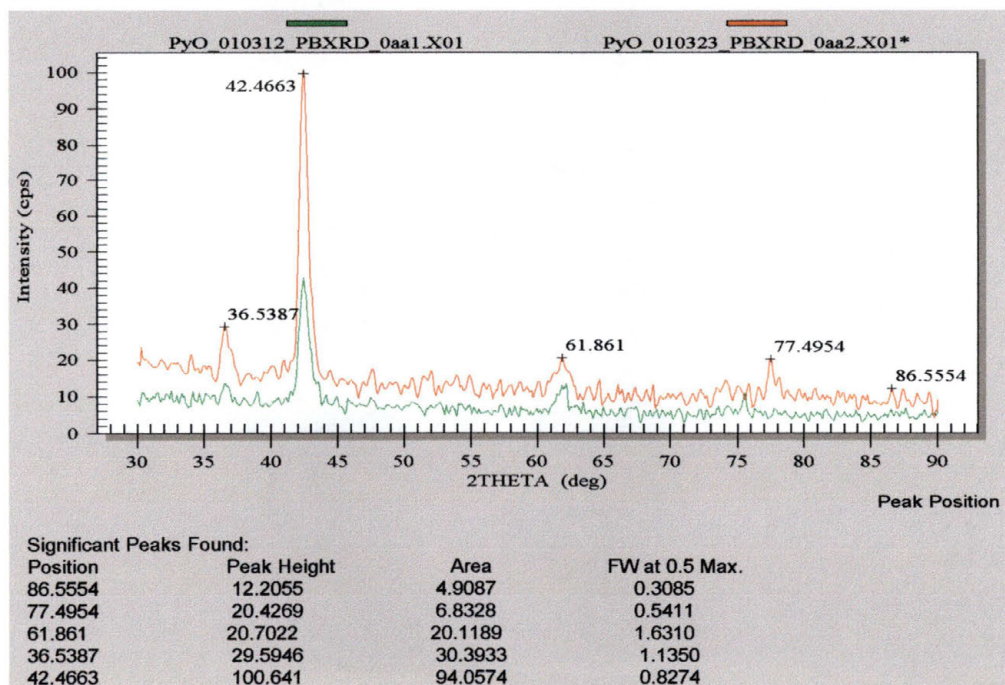
10.6.2.1 Film 010312



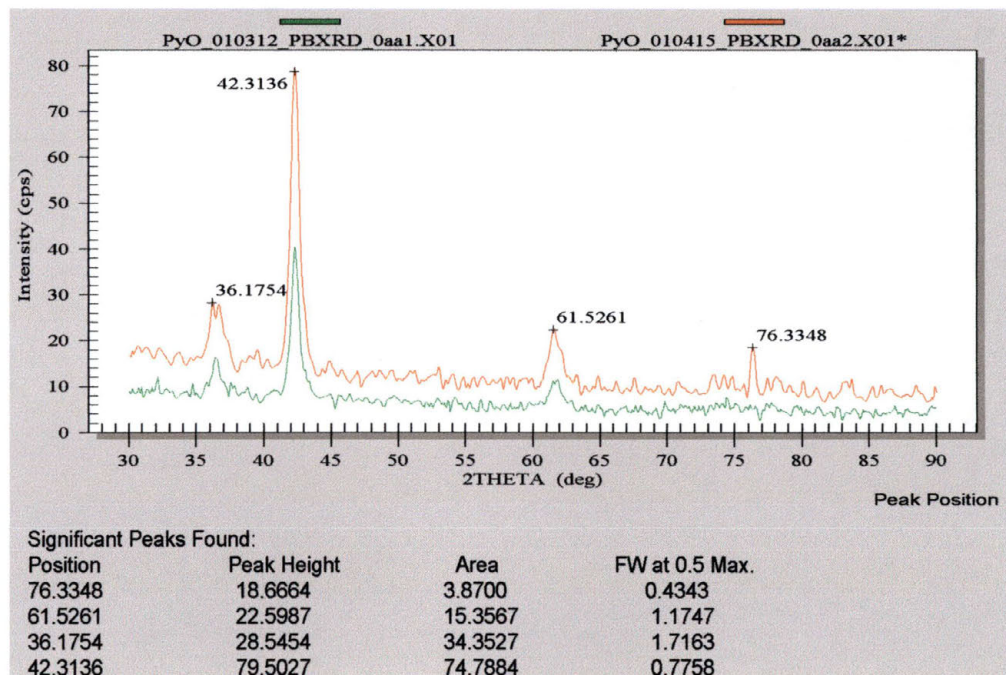
10.6.2.2 Film 010314



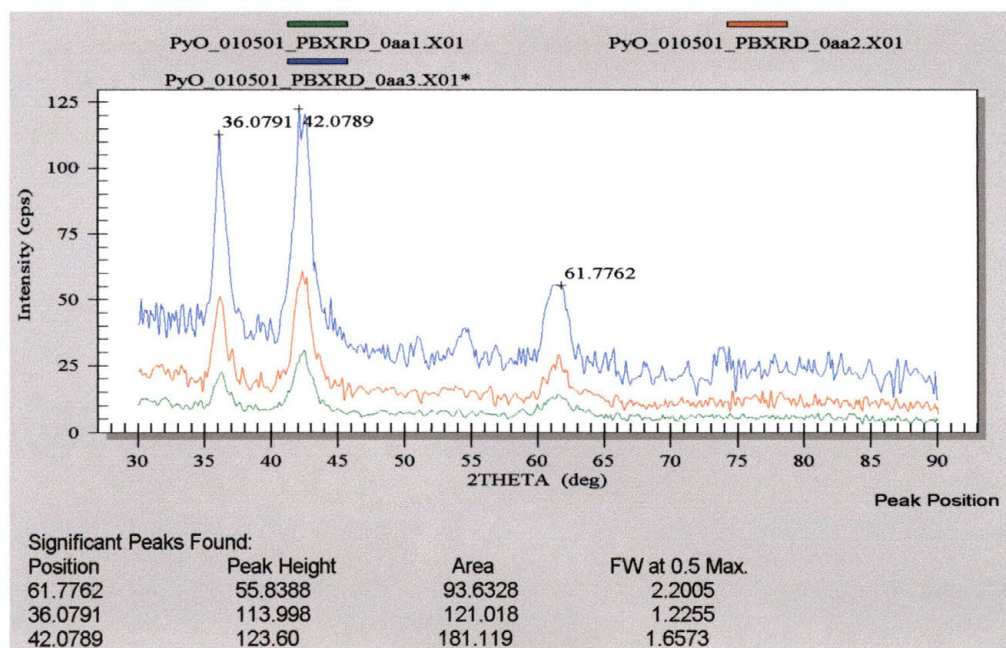
10.6.2.3 Film 010323



10.6.2.4 Film 010415



10.6.2.5 Film 010501



10.7 X-Ray Reflectivity

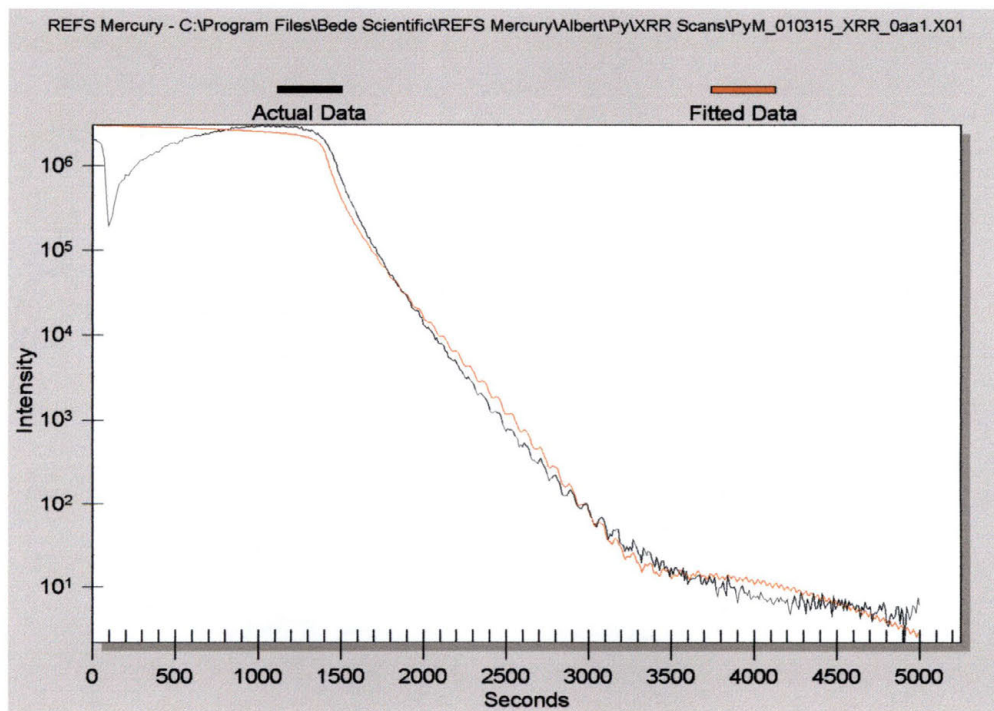
Once a reflectivity scan was performed, the data was transferred to a proprietary computer program written by Bede Scientific called REFS Mercury. The purpose of this program is to calculate the composition and thickness of the layers of a film, based on some pre-determined data. By inputting such information as the number of atoms of a specific element that make up a molecule, and the density in grams per cubic centimeter (which can be found in a variety of chemical resources), the computer program can determine the thickness of a film, how rough the surface or interface of that film is, and the density of the species that are being looked for in the film.

The computer then calculates what the diffraction pattern would be if the “modeled” film was exactly what the experimental data shows. It goes through numerous iterations (sometimes as many as 100,000) in an attempt to make the calculated data match as closely as the experimental data. Information is presented on the thickness of the film, the density of the film, and the roughness of the interface/surface, as well as the relative cost of the calculation (an indication of

how much computing power was needed to match the data) and the standardized cost. As a note, the closer the value of the standardized cost is to zero, the better the fit from the calculated to the experimental data.

10.7.1 Permalloy Metal Films

10.7.1.1 Film 010315



REFS Mercury

File Edit Database Graph Help

Input | Graph | Iterations | Errors | Options

Layers: Points: Lambda: Incident Intensity: Range % +/-:

Omega Start: Omega Finish: Background Intensity:

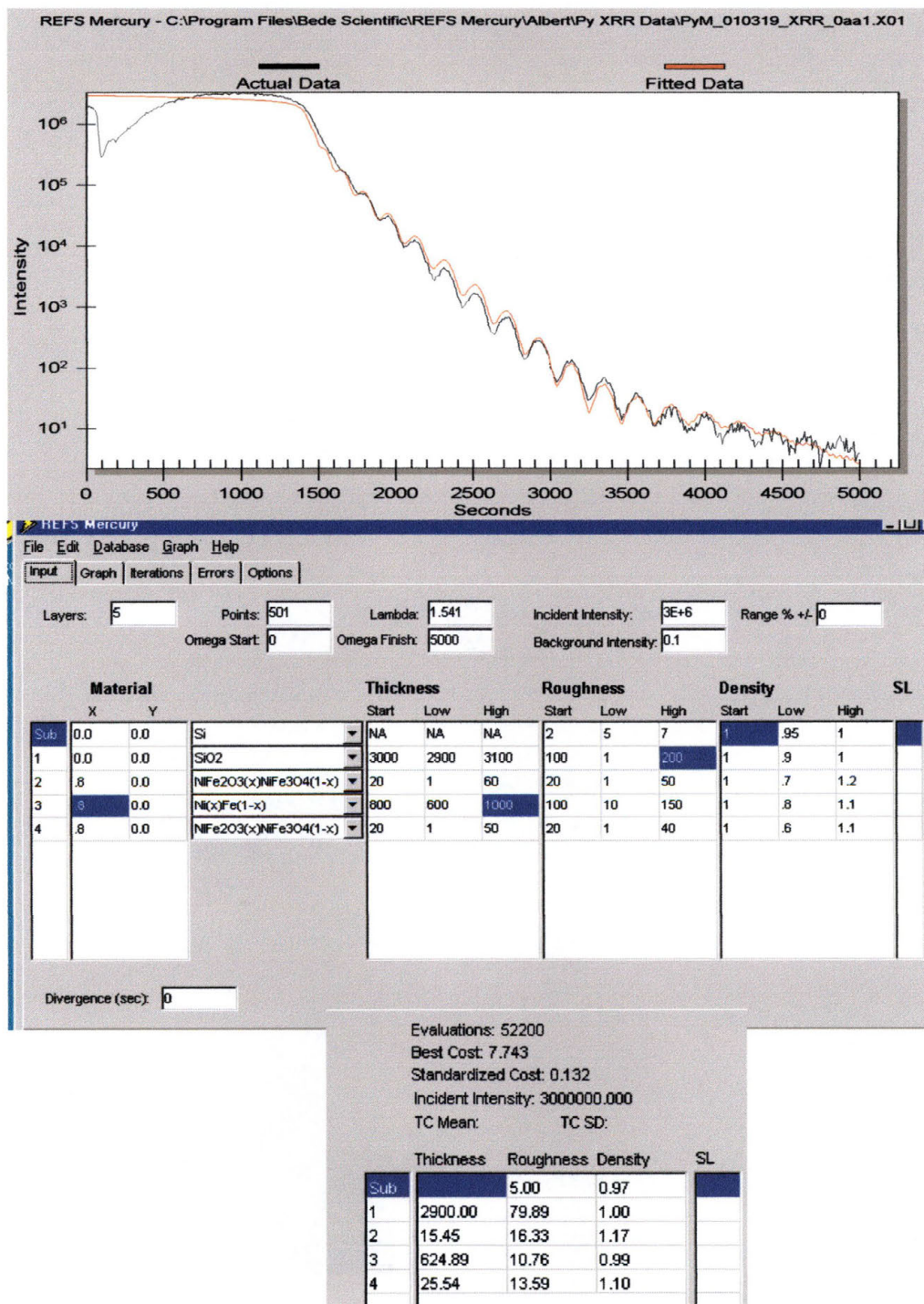
Sub	Material		Thickness			Roughness			Density			SL
	X	Y	Start	Low	High	Start	Low	High	Start	Low	High	
	0.0	0.0	Si	NA	NA	NA	2	5	25	.95	1	
1	0.0	0.0	SiO2	3000	2500	3200	2	1	25	.9	1	
2	.8	0.0	NiFe2O3(x)NiFe3O4(1-x)	100	1	200	100	1	200	.7	1.2	
3	.8	0.0	Ni(x)Fe(1-x)	1570	1000	1700	200	1	400	.8	1.1	
4	.8	0.0	NiFe2O3(x)NiFe3O4(1-x)	100	1	200	100	1	200	.6	1.1	

Divergence (sec):

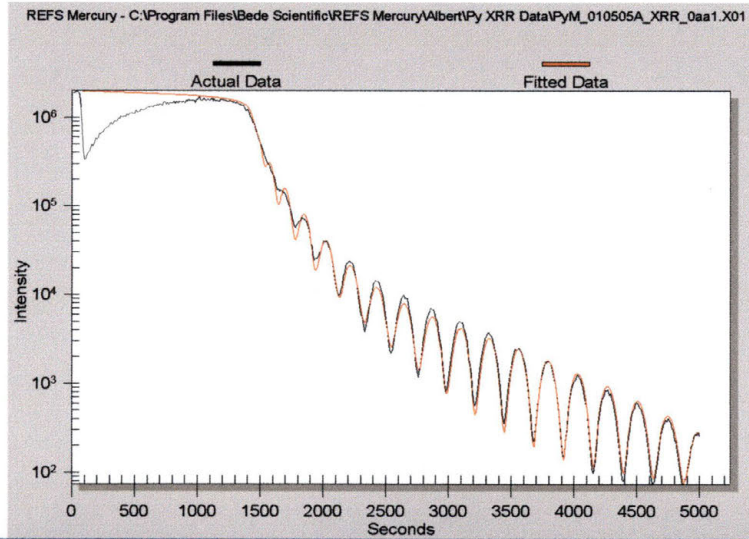
Evaluations: 153360
 Best Cost: 9.917
 Standardized Cost: 0.143
 Incident Intensity: 3000000.000
 TC Mean: TC SD:

Sub	Thickness	Roughness	Density	SL
	5.00	0.98		
1	2735.38	20.71	1.00	
2	1.00	60.02	0.77	
3	1531.23	9.35	0.97	
4	21.52	18.56	1.10	

10.7.1.2 Film 010319



10.7.1.3 Film 010505A



REFS Mercury - C:\Program Files\Bede Scientific\REFS Mercury\Albert\Py XRR Data\PyM_010505A_XRR_0aa1.X01

REFS Mercury

File Edit Database Graph Help

Input Graph Iterations Errors Options

Layers: 5 Points: 501 Lambda: 1.541 Incident Intensity: 2E+6 Range % +/-: 0

Omega Start: 0 Omega Finish: 5000 Background Intensity: 0.1

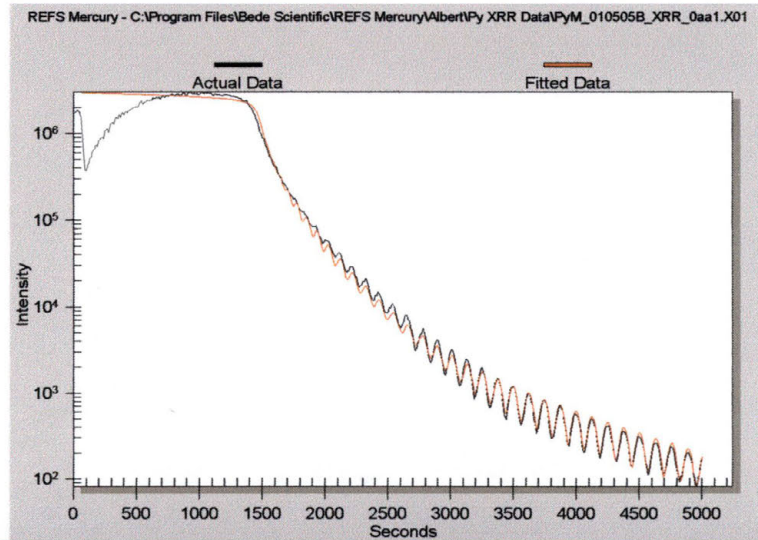
Sub	Material		Thickness			Roughness			Density			SL	
	X	Y	Start	Low	High	Start	Low	High	Start	Low	High		
	0.0	0.0	NA	NA	NA	2	5	7	1	.95	1		
1	0.0	0.0	SiO2	1877	1700	1900	100	1	200	1	.9	1	
2	.8	0.0	NiFe2O3(x)NiFe3O4(1-x)	20	1	60	20	1	50	1	.7	1.2	
3	.8	0.0	Ni(x)Fe(1-x)	800	500	900	100	10	150	1	.8	1.1	
4	.8	0.0	NiFe2O3(x)NiFe3O4(1-x)	20	1	50	20	1	40	1	.6	1.1	

Divergence (sec): 0

Evaluations: 32240
 Best Cost: 3.004
 Standardized Cost: 0.086
 Incident Intensity: 2000000.000
 TC Mean: TC SD:

Sub	Thickness	Roughness	Density	SL
1	1782.52	6.46	1.00	
2	41.23	8.47	0.74	
3	586.81	14.96	1.02	
4	24.59	5.55	1.10	

10.7.1.4 Film 010505B



REFS Mercury

File Edit Database Graph Help

Input Graph Iterations Errors Options

Layers: 5 Points: 501 Lambda: 1.541 Incident Intensity: 3E+6 Range % +/-: 0
 Omega Start: 0 Omega Finish: 5000 Background Intensity: 0.1

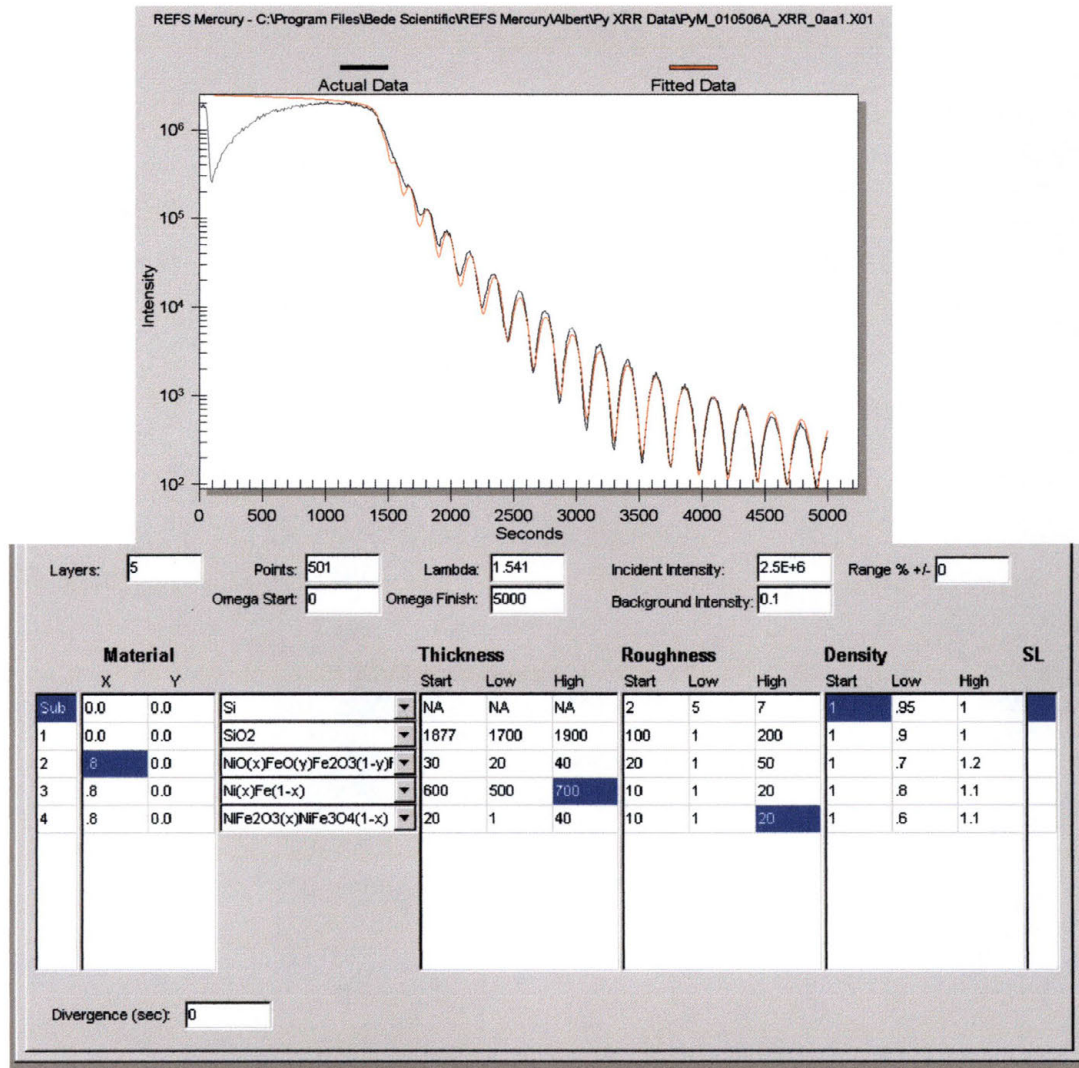
Sub	Material		Thickness			Roughness			Density			SL
	X	Y	Start	Low	High	Start	Low	High	Start	Low	High	
	0.0	0.0	Si	NA	NA	NA	2	5	7	1	95	1
1	0.0	0.0	SiO2	1877	1700	1900	100	1	200	1	9	1
2	.8	0.0	NiFe203(x)NiFe304(1-x)	30	20	40	20	1	50	1	7	1.2
3	.8	0.0	Ni(x)Fe(1-x)	1150	1100	1200	10	1	20	1	8	1.1
4	.8	0.0	NiFe203(x)NiFe304(1-x)	20	1	40	10	1	20	1	6	1.1

Divergence (sec): 0

Evaluations: 61480
 Best Cost: 4.860
 Standardized Cost: 0.079
 Incident Intensity: 3000000.000
 TC Mean: TC SD:

	Thickness	Roughness	Density	SL
Sub		7.00	0.95	
1	1844.97	20.56	0.95	
2	32.24	5.35	1.19	
3	1176.66	3.86	1.07	
4	13.93	15.78	0.96	

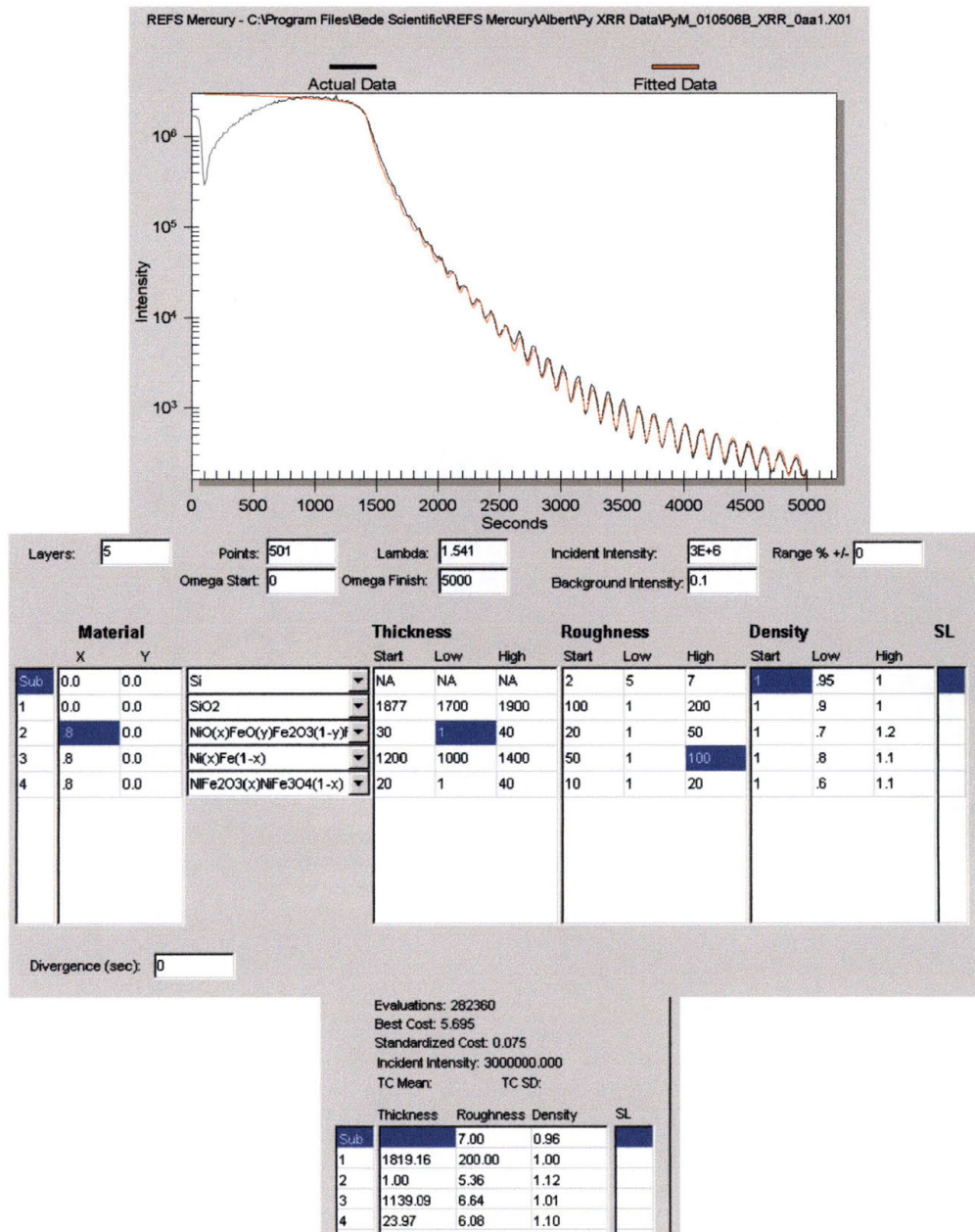
10.7.1.5 Film 010506A



Evaluations: 53440
 Best Cost: 7.090
 Standardized Cost: 0.098
 Incident Intensity: 2500000.000
 TC Mean: TC SD:

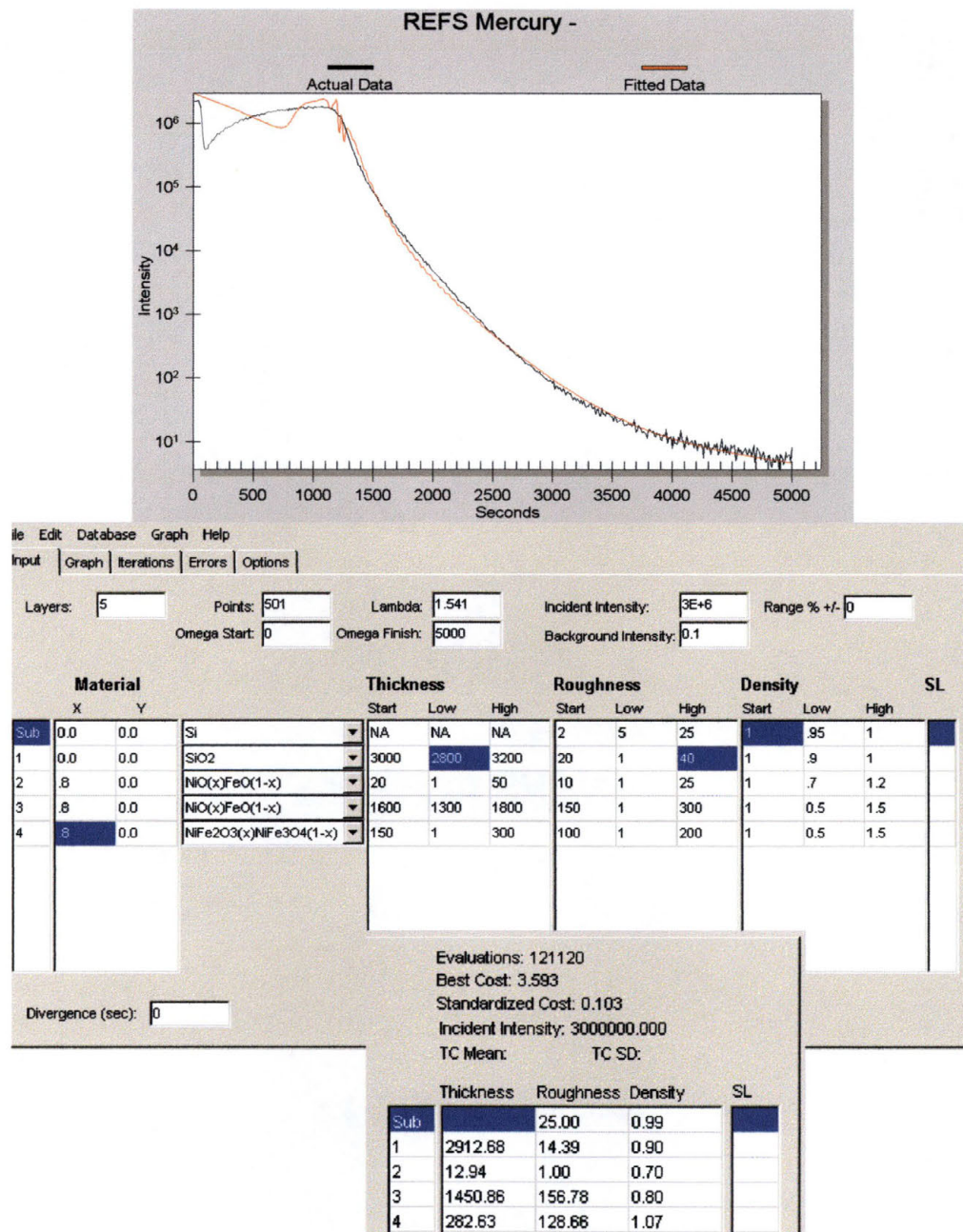
	Thickness	Roughness	Density	SL
Sub		7.00	0.99	
1	1831.41	200.00	1.00	
2	40.00	4.53	0.88	
3	618.34	6.30	1.01	
4	22.51	5.04	1.10	

10.7.1.6 Film 010506B

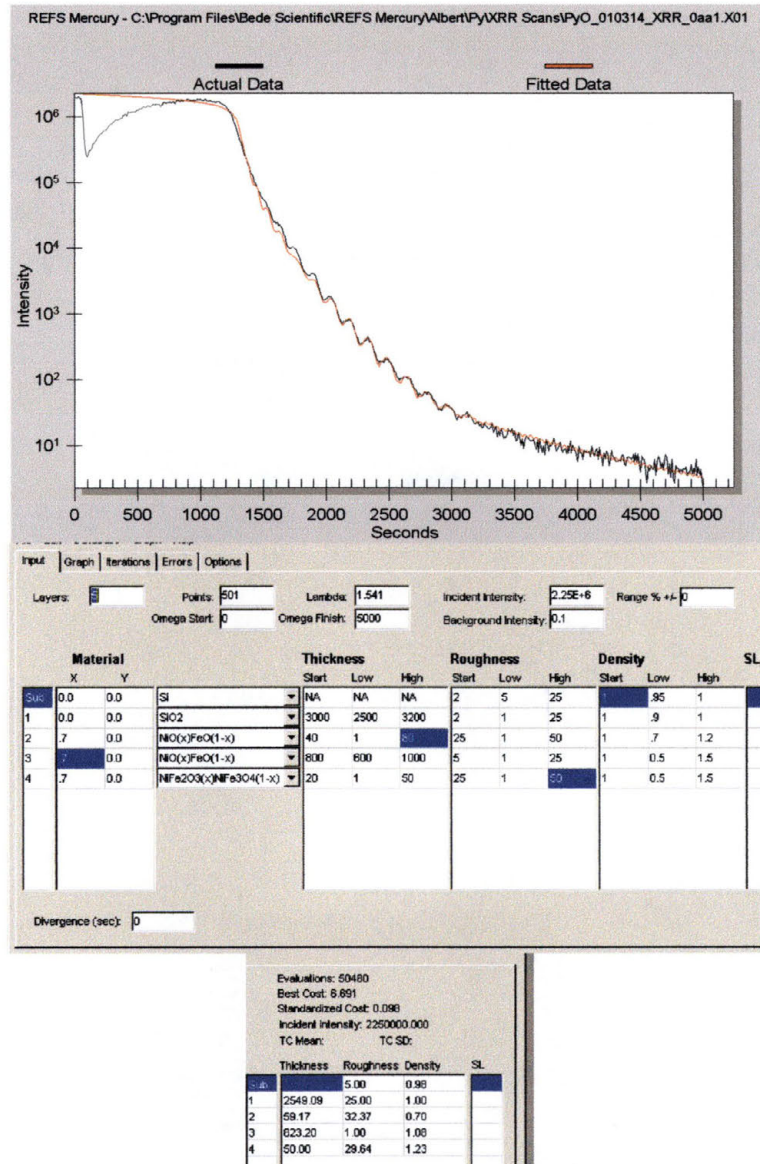


10.7.2 Permalloy Oxide Films

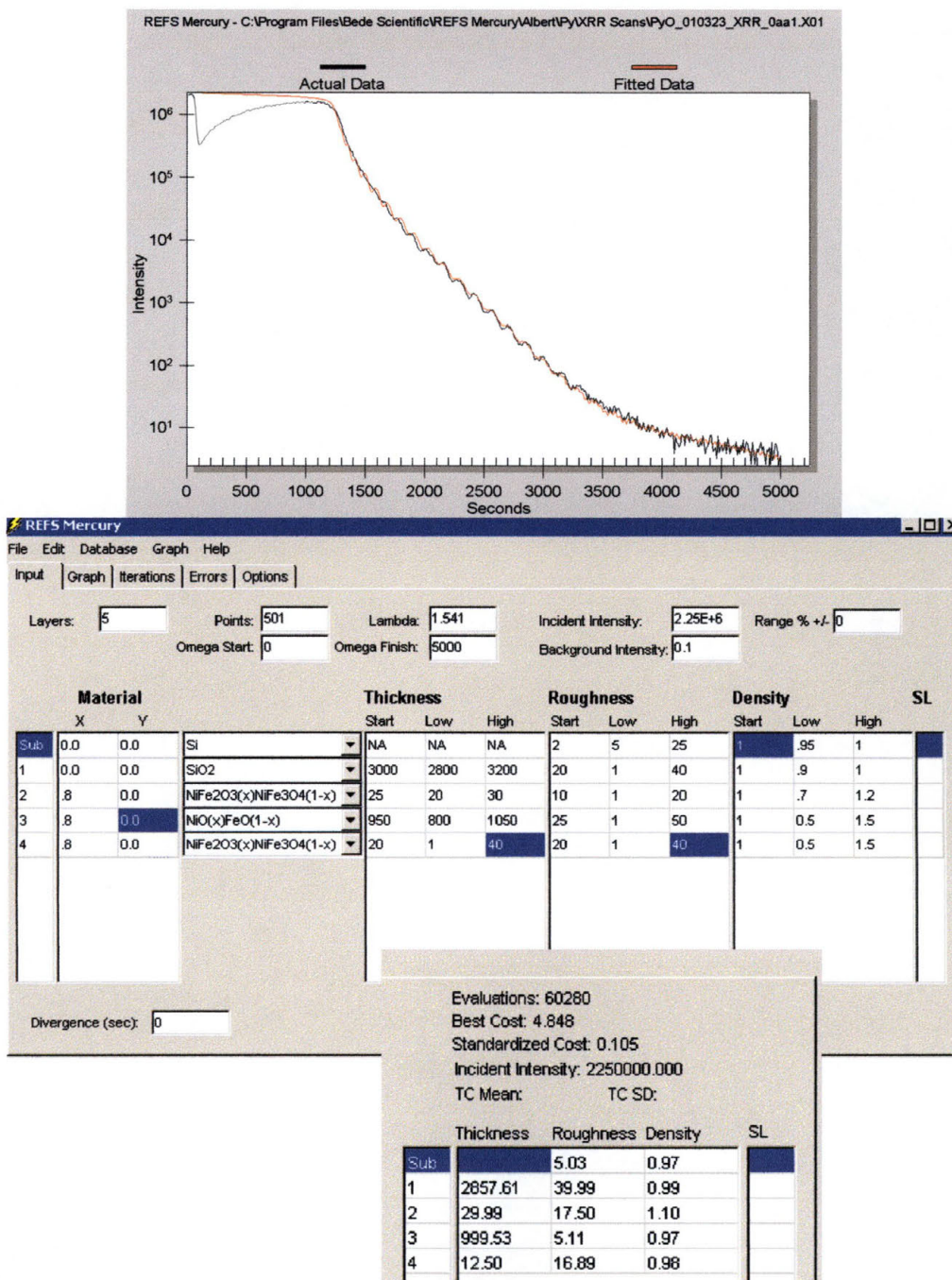
10.7.2.1 Film 010312



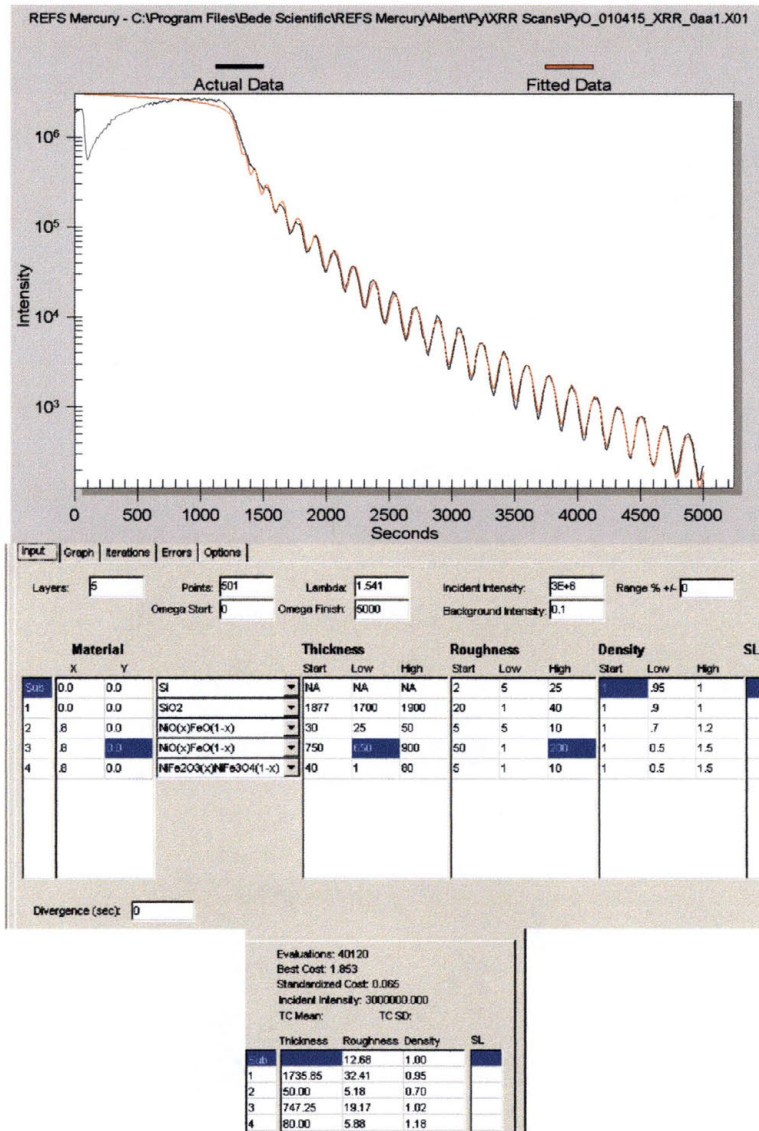
10.7.2.2 Film 010314



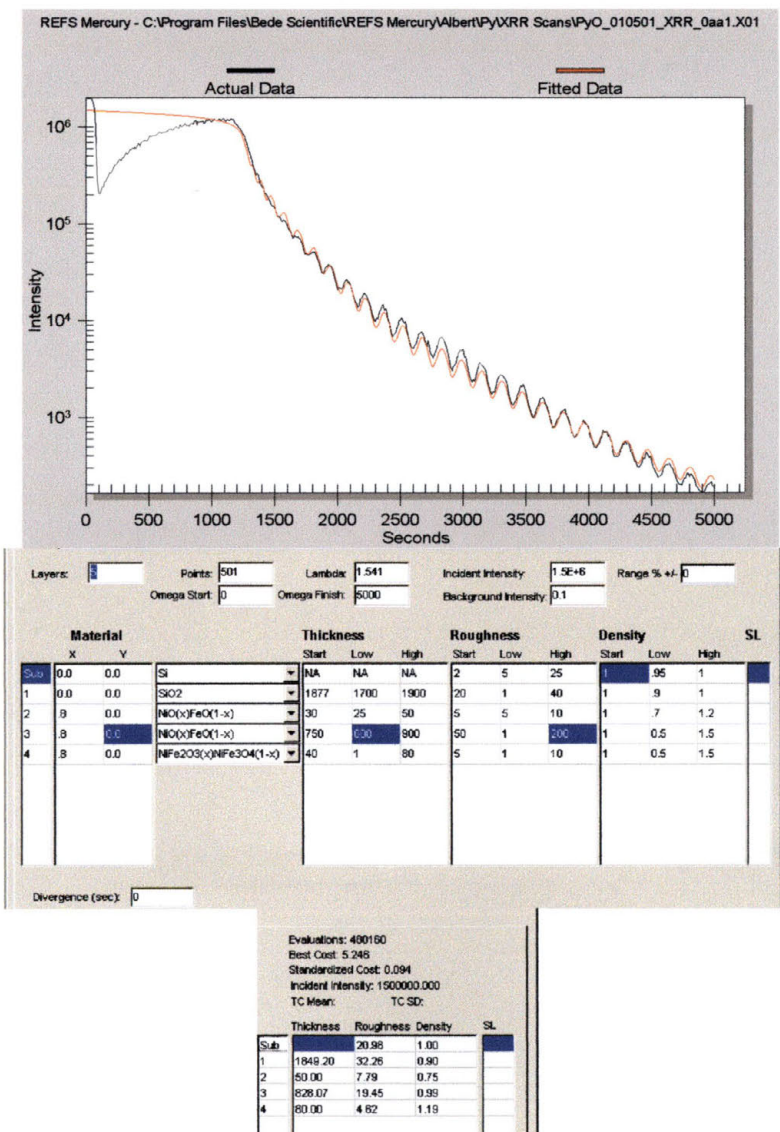
10.7.2.3 Film 010323



10.7.2.4 Film 010415



10.7.2.5 Film 010501



11 Appendices

11.1 How to Operate the VSM

11.1.1 Mounting a Sample

- A. Place a small amount of rubber cement on the back of the sample.
- B. Attach the sample to one of the rods, depending on how the measurement is to be taken.
- C. Stand the rod upright until the cement is dry (around 10 minutes)

11.1.2 Turning on the System Components

Note: It is important that these instructions be followed in the order described to prevent damage to equipment.

- A. Turn on the faucet for the DI water. Ensure that water is running into the sink before proceeding.
- B. Turn on the computer. It should automatically boot to the VSM control software.
- C. Turn on the power supply
- D. Turn on the SS250 Amplifier
- E. Turn on the Control Chassis
- F. Turn on the Lock-In Amplifier
- G. Turn on the Beckman Voltmeter- ensure set to 20 DC Volts range.
- H. Turn on the graph plotter.

11.1.3 Calibration Setup

- A. Carefully attach the Ni calibration sample to the VSM
- B. Under “Setup” on the control software, make the following changes:
 - a. Test Speed = Quick
 - b. Induction Range = 10 emu
 - c. Peak Field = 5,000 Oe
 - d. Field Range = 10,000 Oe
 - e. Time Constant = 0.1 sec.
- C. Under “Set” on the control software, make the following changes:
 - a. Field = 5,000 Oe
 - b. Vibration = On

11.1.4 Optimization

- A. Use the top-most knob on the right side of the VSM to adjust the left-right orientation of the sample with respect to the Hall probe. Find the minimum value attainable by adjusting the position while observing the voltage on the voltmeter.
- B. Use the small knob on the front of the VSM to adjust the front-back orientation of the sample with respect to the Hall probe. Find the maximum value attainable by adjusting the position while observing the voltage on the voltmeter.
- C. Use the large knob on the VSM to adjust the vertical position of the sample with respect to the Hall probe. Find the maximum value attainable by adjusting the position while observing the voltage on the voltmeter.

11.1.5 Calibrating the Lock-In Amplifier

- A. After optimizing the signal, the value of M should be between 3.55 and 3.56 for the Ni calibration sample as read on the Lock-In amplifier. If this is not the case:
 - a. Use the small calibration screwdriver to adjust the calibration potentiometer located next to the voltmeter.
 - b. Verify the calibration by rotating the Quadrant Knob on the Lock-In amplifier to each position with the following results:
 - i. For the first quadrant, M should be 3.55.
 - ii. For the second quadrant, M should be 0.
 - iii. For the third quadrant, M should be -3.55.
 - iv. For the fourth quadrant, M should be 0.
 - c. If any of the values are different than listed above, use the small Phase Knob to set them to the correct values.
- B. Run a quick measurement to verify the calibration.
 - a. Click on "Sample" on the control software.
 - b. Click on "Curve" on the control software.
- C. Once this is accomplished, the VSM should now be calibrated.

Do not move the Hall probe! Moving the probe will require recalibration of the VSM before any data may be collected.

11.1.6 Taking a Measurement

- A. Replace the Ni calibration sample with the rod having the sample to be scanned attached.
- B. Use the large cylinder on top of the VSM to rotate the sample such that the magnetic field of the pole pieces passes through the desired axis of the sample.
 - a. If the sample touches either pole piece, adjust the left-right orientation to provide clearance for the sample as it rotates.
 - b. Center the sample between the pole pieces.
- C. Under "Setup" on the control software, make the following changes:
 - a. Test Speed = Quick
 - b. Induction Range = 0.1 emu
 - c. Peak Field = 5,000 Oe
 - d. Field Range = 10,000 Oe
 - e. Time Constant = 0.1 sec.
- D. Under "Set" on the control software, make the following changes:
 - a. Field = 5,000 Oe
 - b. Vibration = On
- E. Optimize the VSM as in section 11.1.4 with the field at 5,000 Oe.
- F. To begin measurement:
 - a. Click on "Sample"
 - b. Click on "Curve"

11.2 How to Operate the KeveX Model 771 XRF

11.2.1 Starting and preparing the computer and the machine

- A) Ensure that the XRF machine reads “X-RAY ON” and that the Analyzer is on. Then turn on and boot up the computer. For the login name “Default” just hit enter on the keyboard to log on.
- B) When the login is complete, you will see a small box (or “window”) labeled “KeveX WinXRF Monitor” on the screen (See Figure 11-1 below). Click somewhere in the box to activate that window.

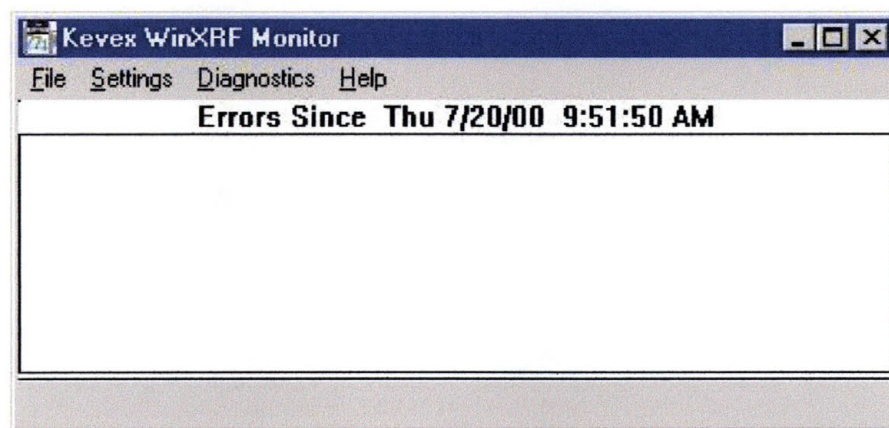


Figure 11-1: KeveX WinXRF Monitor Pop-Up Window

- a) Click on the “File” pull-down menu. Highlight and click on “Download Front-End”. It should be the only choice.
 - b) Click on the “Settings” pull-down menu. Highlight “System”, then highlight and click on “Connect”.
 - c) **DO NOT CLOSE THIS WINDOW!** This is what allows the different parts of the equipment to talk to each other. Minimize the window instead.
- C) Once system is through downloading and you have minimized the “Monitor” window, you need to bring up the actual software programs that do the work.
- a) Open the Win XRF Spectrum Display Panel (SDP) file from the start menu or the icon on the desktop
 - b) Open the WIN XRF file from the start menu or the icon on the desktop.

11.2.2 Setting up a Matrix file.

Now we need to find the excitation values needed for the desired sample and store that information in a new Matrix file. We also need to define a layer structure for the samples to be analyzed. Before this is done, however, you want to create a library to hold all the data.

A) Setting up a library

- a) Find the “blank.kvx” file in the C:\WinXRF folder and highlight it.
- b) Right click on the file and choose “copy”.
- c) Right click on the C:\WinXRF folder again and choose “paste”.
- d) Highlight the “Copy of blank.kvx” file in the WinXRF folder and rename it. Make sure when renaming the file that you include a “.kvx” at the end.
- e) Close Windows Explorer and click on the WinXRF program menu bar (See [Figure 11-2](#) below) to activate it.
- f) Click on the “File” pull-down menu and select “KVX Library”
- g) Click on the file you just created and then select which unit to send it to.
- h) Hit the “OK” button.
- i) You have now created and installed a library for all of your files.

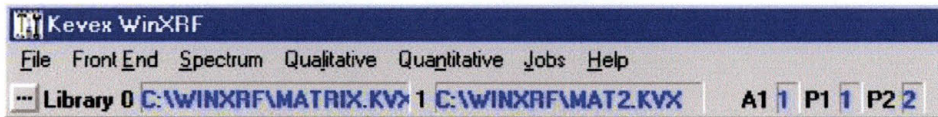


Figure 11-2: Kevex WinXRF Main Program Window Example

B) Setting the excitation conditions

- a) From the WinXRF program, click on the “Front End” pull-down menu, highlight and click on “Condition Code” (See [Figure 11-3](#) on next page).

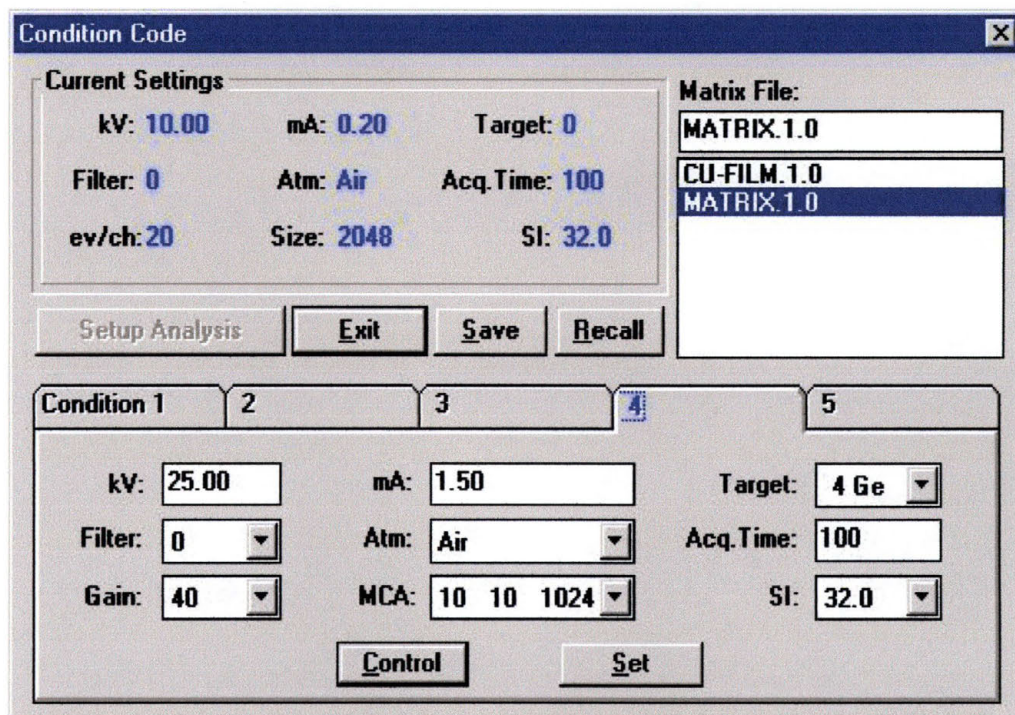


Figure 11-3: Condition Code Pop-up Window

b) Select the Condition Code to be used. This choice must be made keeping in mind that the secondary target x-ray energy must be higher than any element that you plan to identify in the samples to be scanned.

c) Double check to make sure that:

-Gain is at 40

-SI is at 32

-MCA needs to be based on the x-rays generated from the target using the slide cards Kevex provided.

-Acquisition Time should be ~60 sec to start

d) Hit the "Control" button to send the information you just set up to the scanning software program.

e) Keeping the "Condition Code" window open, click on the SDP window (See [Figure 11-4](#) on next page) and click "Start". Once the scan starts, click on the Win XRF window (see [Figure 11-2](#) on previous page) to bring the "Condition Code" window back into the front of the screen.

f) Adjust the voltage and current settings on the "Condition Code" window until you get a "green" dead-time (approx. 40 to 50%)

IMPORTANT NOTE: If the XRF has not been operated at a high voltage for a period longer than two weeks, DO NOT GO TO MAX. POWER without first doing a slow ramp up! See the Kevex manuals for how to do this.

NOTE: When operating at the extremes of the voltage (~64 kV) and current (~3.3 mA) you do not want to adjust until the dead time is green. Instead, increase the data acquisition time until you get enough counts for a useful scan.

f) When the dead time is properly adjusted, you want to save the Condition Codes. Give the file a name and then click “Save”. It is a good idea to name your Matrix with a descriptive name. You then want to click “Recall” and check to make sure you data were properly saved.

g) Excitation conditions are now set so you can click on “Exit”.

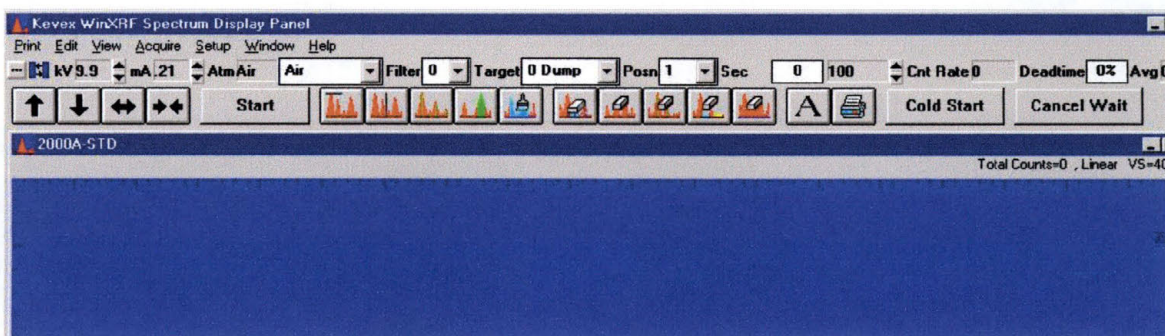


Figure 11-4: KeveX WinXRF Spectrum Display Panel (SDP) Menu Bar

11.2.3 Setting the sample conditions in preparation for making a Standard.

A) Click on the WinXRF program and then click on the “Quantitative” pull-down menu.

B) Highlight “Setup” and then click on “Sample Data”. This will open a new window (See Figure 11-5).

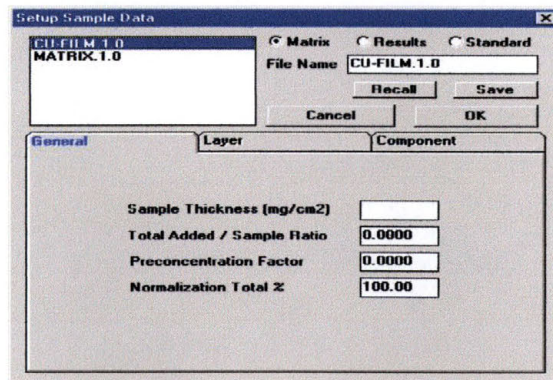


Figure 11-5: Setup Sample Data Pop-up Window

- a) Click on the dot for "Matrix"
- b) Highlight the file that you named earlier (step 2.B.g) and click on the "Recall" button.
- c) Click on the "Layers" tab of the file folders in the window. This will allow you to enter information about the number of layers in your standard, as well as the chemical make-up of those layers.
- d) From this folder (See [Figure 11-6](#)), select that layer you are going to label. List the element(s) in that layer, and give a percent weight for each element. When the data is set, click on "Add/Change" to save it.

NOTE: The Kevex XRF labels layers from the top down (i.e. if you have a Ni layer on top of a Ni/Fe 19% layer on top of a Si substrate, choose layers as follows (See [Figure 6](#) on next page):

Layer 1	Ni
Layer 2	Ni
Layer 2	Fe
Layer 3	Si

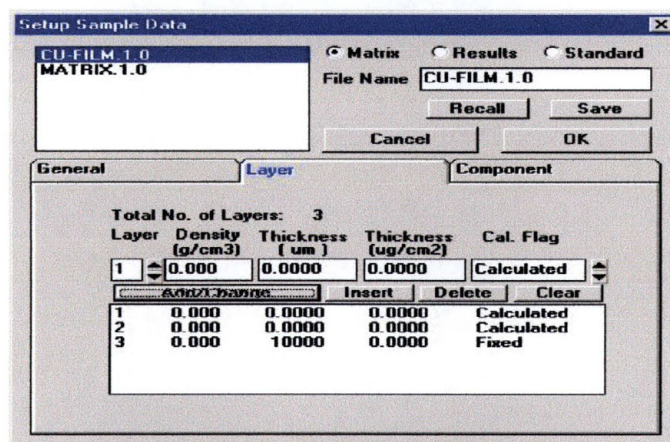


Figure 11-6: "Layers" Example for Sample Data Setup

- e) When you have input the information for the sample to be used as the standard, click on the "Components" tab.
 - i) For each element in a layer, highlight it and give it a weighted percentage. For example (See [Figure 11-7](#) on next page):

Layer 1	Ni	100%
Layer 2	Ni	81%
Layer 2	Fe	19%
Layer 3	Si	100%

f) When all data has been input, click on the “Save” button and then on the “Recall” button to make sure your changes were saved. If all the data was properly saved, click on “OK”.

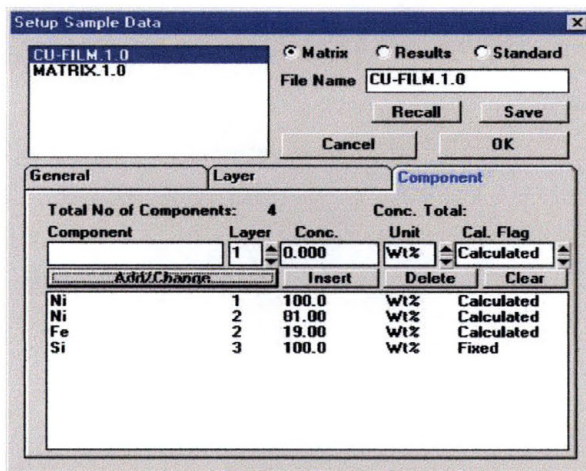


Figure 11-7: "Component" Example for Sample Data Setup

11.2.4 Taking a scan

Note: The method for taking a scan for the standard is identical to the method used for taking any other scan.

A) First, the samples must be labeled. Since the carousel can have up to 16 different samples loaded at one time, it is very important to label each sample location prior to scanning. This not only makes things less confusing, but also simplifies later steps.

a) Click on the SDP program window and then click on the “Setup” pull-down menu.

c) Highlight “Sample Names” and click to open a smaller window that has the sample positions listed (See [Figure 11-8](#)).

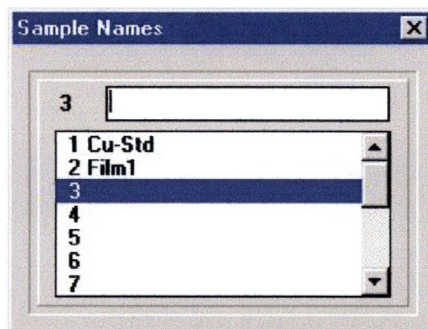


Figure 11-8: Sample Names Pop-up Window

c) Select a sample position and label it. Names must conform to DOS rules (i.e. No more than 8 characters long and no spaces allowed). Make sure to hit "Enter" after you have listed the name of each sample in order to store the information.

d) When you have labeled all of the sample positions for this run, click on the "x" at the top right corner of the window to close it.

e) Click on the "Start" button to begin the scan.

B) When the scan is finished, you want to immediately save the scan.

a) Click on the Win XRF program window.

b) Click on the "Spectrum" pull-down menu.

c) Highlight "Save/Recall" and click on it.

d) When the window opens, the name of the sample should already be listed in the filename position (because of step 4.A). If it is not, then type the name of the sample into the filename position and click on the "Save" button.

C) Scan each of the samples you have loaded, making sure to save each scan before performing the next scan. If you do not save your scans, the data will be lost when the next scan is performed.

Note: There is a way to do all of the scans at one time using the "Job" function that will be discussed later in this report.

11.2.5 Creating a results file

In order to do any analysis on a scan, a results file must first be created. This method is the same for every scan taken. In the case of the scan being used as a standard, the results file will later be edited to include known film thickness levels.

A) Click on the Win XRF program window and then click on the "Spectrum" pull-down menu.

a) Highlight and click on "Save/Recall".

b) When the window opens (See [Figure 11-9](#) on next page), highlight the filename you gave to the scan you want to use as the standard and then click on the "Recall" button. This loads the scan onto the SDP.

c) Click on "Exit" to close the "Save/Recall" window.

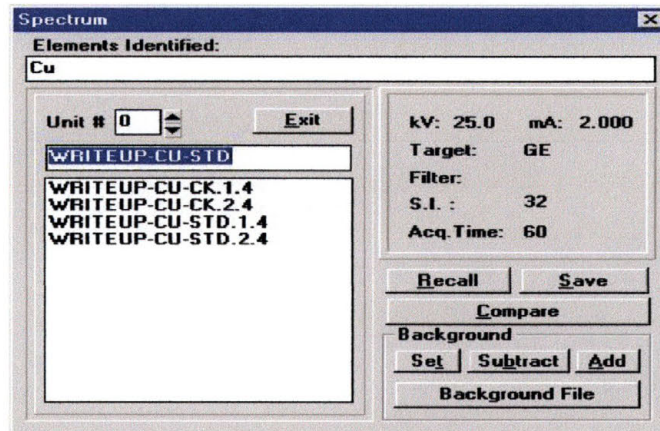


Figure 11-9: Spectrum Save/Recall Pop-up Window

- B) Click on the "Qualitative" pull-down menu.
- a) Highlight and click on "Process". This will open a new window (See Figure 11-10).
 - b) Click on the "Deconvolution" file tab.
 - i) Now you need to tell the results file what elements to look for. Do this by clicking on the "Chart" button.
 - ii) From the window that pops up (See Figure 11-11 on next page), select the elements that you want the software to process the scan for. When you have selected all of the elements that you know are in the sample, click on the "OK" button. This will close the periodic chart.
 - c) Click on the "Process All" button. When this button is pressed, the actual results file will be created. A new window should open up. Just close it.
 - d) Close the "Spectrum Processing" window as well.

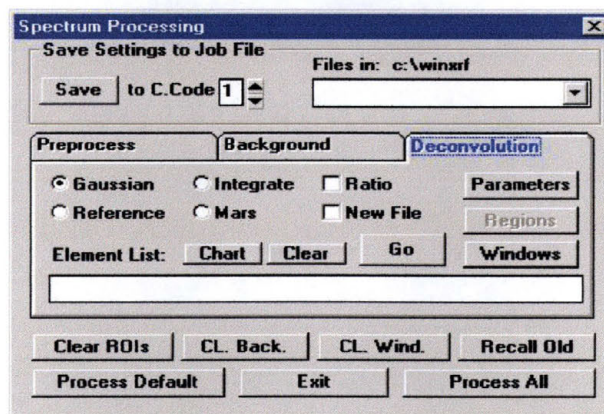


Figure 11-10: "Deconvolution" Example for Spectrum Processing Window

C) It is now important to make sure that the information was processed correctly and the file was properly saved. Click on the Win XRF “File” pull-down menu.

a) Highlight and click on “WinXRF File Manager”. This will open a new window.

b) Click on the “Results” button. When you do this, a list of the current results files will be shown.

c) Double-click on the results file you just saved. This will open a new window that contains the results of the file you just processed.

d) After reviewing the information in the window, close it.

e) Click on the “Exit” button to close the window.

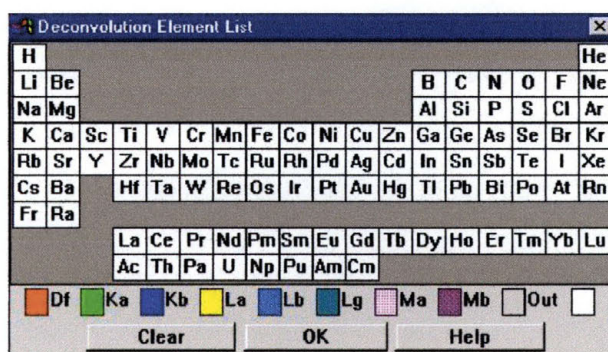


Figure 11-11: Chart to Select Elements from for Deconvolution Processing

11.2.6 Defining the Standard

Now that the file to be used as a standard has been processed and saved as a results file, you need to go back and fill in the information about the thickness of each layer that exists in the sample.

A) From the Win XRF program window, click on the “Quantitative” pull-down menu.

B) Highlight the “Setup” selection, then highlight and click on “Sample Data”. This will open a new window (See [Figure 11-12](#) on next page).

a) Click on the “Results” button. This should present a listing of the results files you have created so far.

b) Highlight the file you intend to use as the standard and click on the “Recall” button.

c) Click on the “Layer” folder tab.

i) Highlight the layer that you want to adjust.

ii) In the boxes above the listed layers, fill in the information about the thickness of the layer you have highlighted. When the

information has been entered, click on the “Add/Change” button to save the new information.

C) When all of the layers have been edited, click on the “Save” button. Then click on the “Recall” button to make sure the new data was saved properly.

D) Once you have verified the new data as being correctly saved, click on “Exit”.

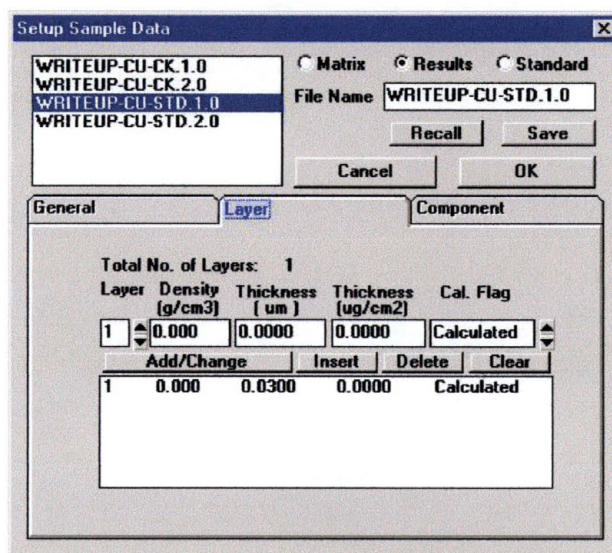


Figure 11-12: Setting the Layer Thickness of the Standard Film

11.2.7 Creating a file that will hold the calibration data.

In order to create a file to calibrate against you now need to create a Least Squares file.

A) From the Win XRF window, click on the “Quantitative” pull-down menu.

a) Highlight the “Setup” selection and then highlight and click on the “Least Squares” selection. This should open up a new window (See Figure 11-13 on next page).

b) Click on the “FP” box first, then click on the “LS” dot. In the blank, supply a filename for the calibration file. It is a good idea to name the LS files the same as the Matrix file that you created earlier.

c) Click on the “Results” dot and then select the file(s) that you want to use for calibrating against.

Note: More than one results file can be used to create the LS file. It is important that film thickness data be accurately edited if doing this in order to get as straight a fit as possible.

d) Click on “OK” and then “OK” again.

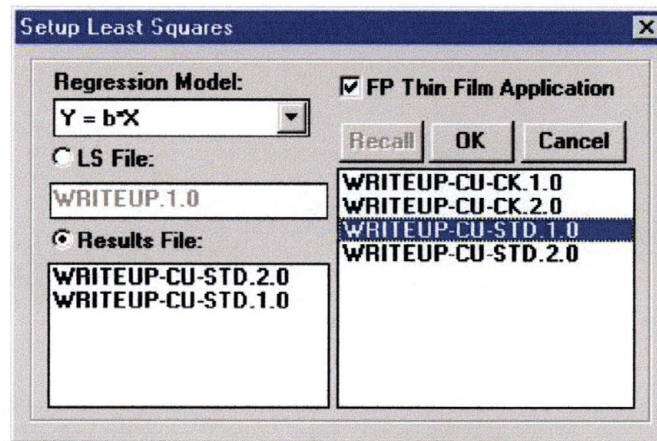


Figure 11-13: Creating a Least Squares File

Now you need to do the actual calibration.

A) From the Win XRF program window, click on the “Quantitative” pull-down menu.

a) Highlight and click on “Calibrate”. This will open a new box (See [Figure 11-14](#) on next page).

b) Click on the “FP” dot, then the “Thin Films” box at the bottom of the window.

c) Click on the “LS” dot and then select the file to be used as the calibration file.

d) Click on the “Go” button. When you do this, a new window will open up (See [Figure 15](#)) which will show the elements you have processed for in the calibration scan and the least squares fit for the data from the scan. If this data looks good to you (i.e. there is a straight line fit for the data) then click on the “OK” button to store the information in the file.

e) Exit this window.

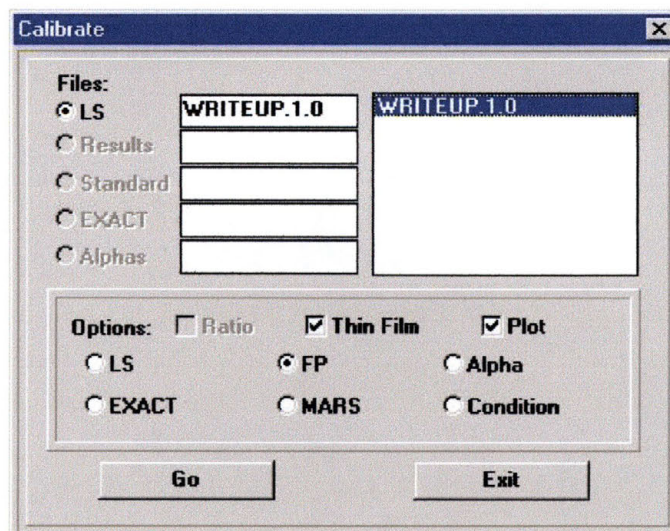


Figure 11-14: Calibration Pop-up Window

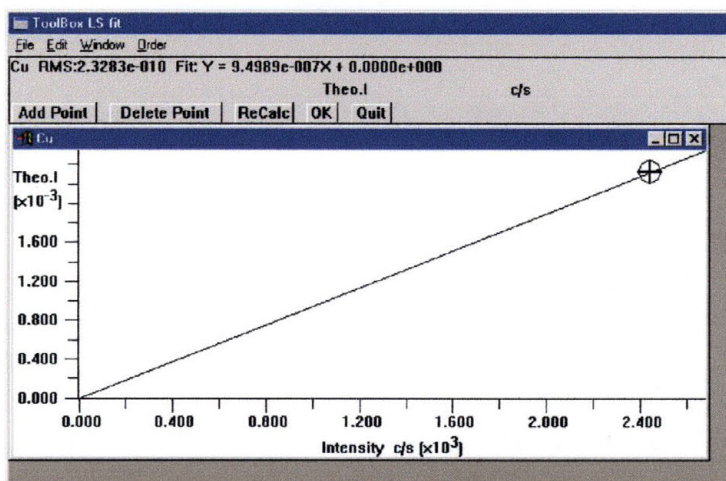


Figure 11-15: Calibrated Data for Use in Future Analysis Window

11.2.8 Comparing an unknown sample to the calibration standard

Now that you have a calibration standard file to compare samples to, you can recall and process data for any samples that you would like to compare with your calibration scan.

- A) From the Win XRF program window, click on the “Spectrum” pull-down menu.
 - a) Highlight and click on “Save/Recall”.

- b) Highlight the file you want to analyze and click on the “Recall” button.
- c) Click on the “Exit” button.
- B) Click on the “Qualitative” pull-down menu.
 - a) Highlight and click on “Process”. This will open a new window (See [Figure 11-16](#))
 - b) Click on the “Deconvolution” file tab.
 - c) Click on the “Chart” button
 - d) Select the elements you want the software to look for.
 - e) Click “OK” to close the “Chart” window.
 - f) Click on “Process All”.
 - g) Close the Notepad pop-up window.
 - h) Click on the “Exit” button.

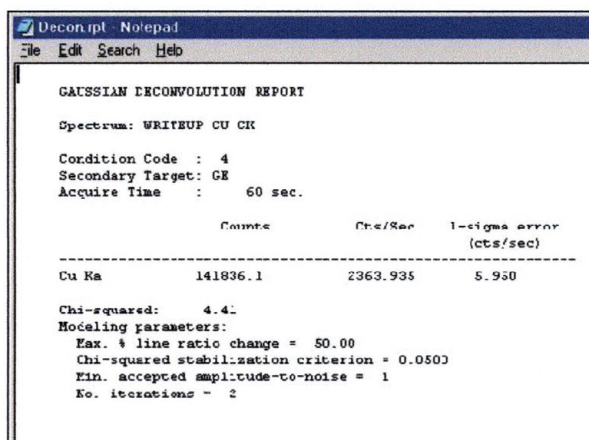


Figure 11-16: Results File for the Unknown Sample

- D) Click on the “Quantitative” pull-down menu.
 - a) Highlight and click on “Quantify”. This will open a new window (See [Figure 11-17](#) on next page).
 - b) Select the “FP” dot and then select the “Thin Films” dot at the bottom of the window.

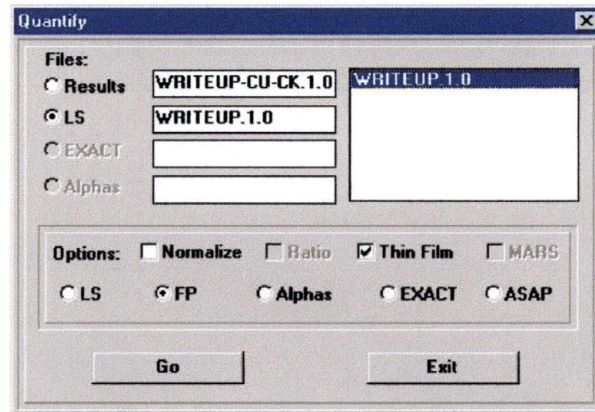


Figure 11-17: Selecting the Least Squares File to Compare to the Unknown Sample

c) Click on the “Results” dot at the top of the window and then select which file you would like to analyze. This should be the file you just created a results file for (Step 8-B).

d) Click on the “LS” dot and select the calibration file you want to compare this file to.

e) Click on the “Go” button. This will open a new window (See [Figure 11-18](#)). The new window will now have the data from the unknown film, such as film thickness of each layer, etc.

f) You have now scanned an unknown sample and determined it’s elemental concentrations and film thickness.

g) Repeat step 8 for any remaining files you wish to analyze.

Quant.rpt - Notepad

File Edit Search Help

```

KEVEX TFFP QUANTITATION REPORT

07/20/00 11:10:57

Results File : WRITEUP-CU-CK.1.0
LS File : WRITEUP.1.0

Element Line Condition Secondary Intensity
          Code Target          (cps)
-----
Cu      Ka      4      CE      2350.72

Component Layer Thickness Conc. Conc.
          No.              (Calc.)100.00 Wt.% (Fixed) 100.00
-----
CU          1  2.8913e-002 um      {Calc.}100.00 Wt.% {Fixed} 100.00

Warning: Default layer density used in calculation.

```

Figure 11-18: Results File for the Unknown Sample Showing Film Thickness

11.2.9 Setting up a Jobs file to automate the process of analyzing materials.

A Jobs file can be created using the steps listed above and a few other steps to automate the taking of a scan as well as the processing and analyzing of the scan data for up to 16 different samples.

A) From the Win XRF program window, click on “Jobs”. This will open the “Jobs” window (See [Figure 11-19](#)).

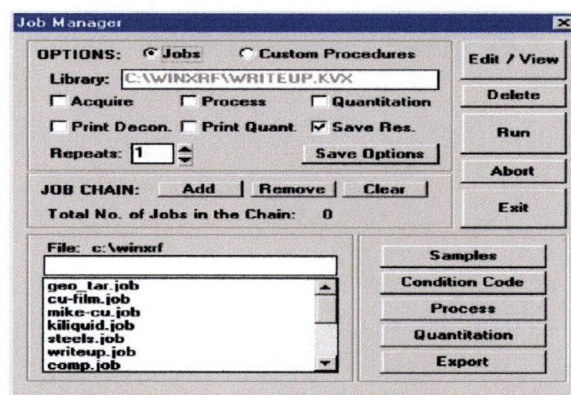


Figure 11-19: Jobs Manager Pop-up Window

- a) In the blank at the bottom right corner, type in the name you wish to give this job. A job file MUST live in the C:\WINXRF folder!
- b) This name is DOS controlled, and must not contain more than eight characters. Spaces are not allowed.

B) Once the name has been selected, click on the “Samples” button. This will open a new window (See [Figure 11-20](#) on the next page).

- a) In the blank provided at the top right corner, provide a name for the “Names File”.
- b) Just below the “Names File”, enter the names of each of the samples located on the carousel. You enter the sample names as you would the film elements and thickness in Step 3.F (i.e. select the sample position, name the sample position, and click on the “Add/Change” button.).
- c) When the sample names have all been entered, click on the “Save Names” button.
- d) On the bottom right corner, select the samples to be scanned from the carousel by clicking on the sample position.

NOTE: The samples will be scanned in the order in which they are selected. This can be seen in the box just below the image of the carousel.

e) Click on “OK”, and then click on “Yes” twice.

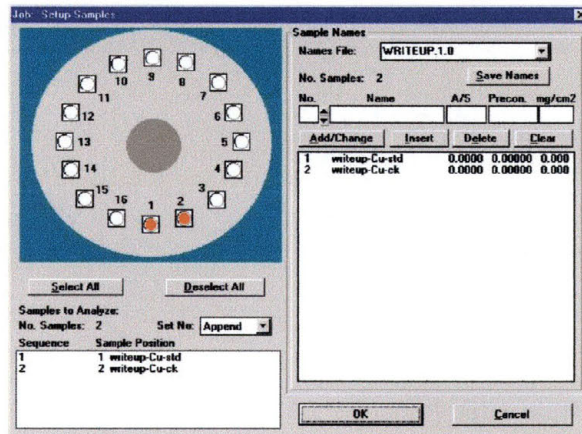


Figure 11-20: Sample Naming Pop-up Window

C) Click on the “Condition Code” button. This will open a new window (See [Figure 11-21](#)).

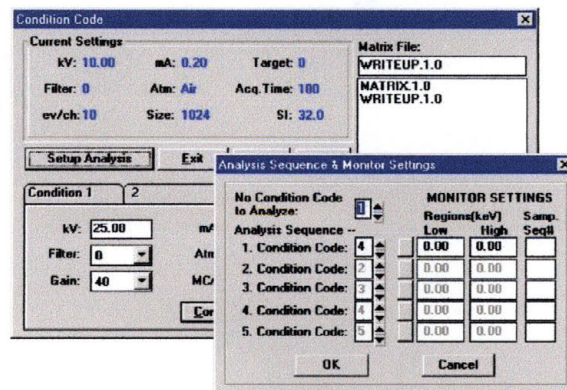


Figure 11-21: Condition Codes for the Jobs Menu

- Select the Matrix file to be used for the sample analysis and click on the “Recall” button.
- Click on the “Setup Analysis” button.
- Select the “Condition Codes” to be used for each “No Condition Code to Analyze”. It is important if only one set of conditions is being

used that in the first Condition Code box in the “Analysis Sequence” listing, the correct Condition Code is selected.

- d) Click on “OK”, then “Yes” and then “Yes” again.
- e) Click on the “Exit” button, then “Yes” and then “Yes” again.

D) Click on the “Process” button. This will open a new window (See [Figure 11-22](#)).

- a) Select the Condition Code to be used. This is done at the top left corner of the pop-up window.
- b) Click on the “Deconvolution” tab.
- c) Click on the “Chart” button and then click on the element(s) to be searched for. Then click on “OK”.
- d) Click on the “Save” button.
- e) Click on the “Exit” button.



Figure 11-22: Spectrum Processing Window for the Jobs Menu

E) Click on the “Quantitative” button. This will open a new window (See [Figure 11-23](#)).

- a) Click on “FP” and then “Thin Film”.
- b) Select the “LS” file to be used for the analysis.
- a) Click on the “OK” button and then “Exit”.

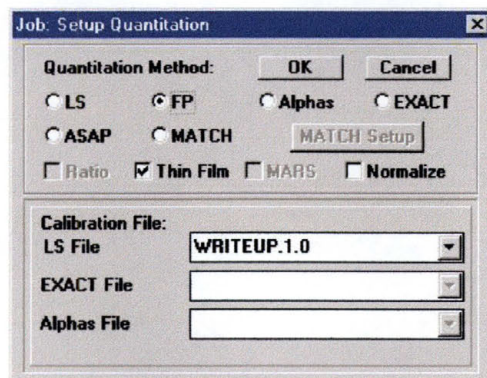


Figure 11-23: Job Setup Quantitation Pop-up Window

F) Click on the “Export” button. This will open a new window (See [Figure 11-24](#)).

a) Select/Provide a name for the exported file. It is important not to use a name with more than eight characters, and spaces are not allowed.

b) Click on the “dots” for what parameters you would like the software to prepare for exportation to another file. If you select “Thickness”, be sure to select what units you would like the data to be provided in.

c) Click on the “Exit” button.

G) From the main “Jobs” window, select the “Acquire”, “Process”, “Quantization”, and “Save Results” buttons.

H) Select the number of times that you would like the software to perform the job.

I) Click on “Save Options”, then “Yes”, and then “Yes” again.

J) Now you are ready to run the Job. All you do is click on the “Run” button and then sit back and let the machine do all the work.

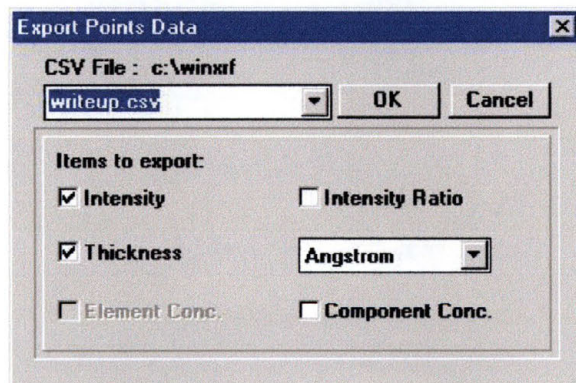


Figure 11-24: Export Pop-up Window

11.3 How to Operate the Dual Ion-Beam System

These instructions are for operating a Standard 3 cm Dual Grid source CSC 1160 System using an Advanced Energy ID-2501 Power Supply

Turning the System "ON"

- A) Make sure the system base pressure is sufficiently low ($\leq 5 \times 10^{-7}$ torr).
- B) Make sure all the system interlocks have been satisfied. This is indicated by the lighted "off" (manual mode) or "on" (automatic mode) indicator light just below the Millatron monitor LED display.
- C) Lower the temperature on the chill water to 10° C to ensure proper cooling of the sample stage and the vacuum chamber.
- D) Establish the desired gas flow using the Mass Flow Controllers (typically use 4-6 standard cubic centimeters per minute to achieve a chamber pressure of approximately 1×10^{-4} torr).
- E) The ID-2501 knobs should all be turned fully CCW, unless they have been purposely preset during a previous run. Fully CCW is the position to set the current and the voltage to zero.
- F) Ensure the ID-2505 is in manual mode & control is in the local position, and that the switches for the source and the beam are in the "off" position. Turn on the ID-2505 power supply, depress the beam "off" switch to make absolutely sure that the source and the beam are "off". The interlock LED should be on continuously.
- G) Turn the source "on". The neutralizer, cathode and source power LED lights on the ID-2505 should continuously light (indicating that the cathode and the neutralizer filaments are not broken), discharge light should blink off and on indicating that the discharge is "off".
- H) Make sure the discharge voltage is set to minimize double-ion production (typically between 35 and 45 volts). Sometimes it may be necessary, however, to increase the voltage to between 70 and 80 Volts to get the discharge started. If this occurs, lower the voltage after the discharge has been turned on.
- I) Establish a cathode current on the source. Typically this will be around 5A to make the filament visibly glow, but at time 6.75A to 7A is needed to get good thermionic emission for the beam current

production. This will establish a discharge causing the discharge light to stop blinking.

- J) Use the adjustments labeled "Filament" to establish a neutralizer current of around 5A. This will be adjusted later when the beam is established (to a value closer to 7A).
- K) Turn the beam "On". The emission, beam, and accelerator LEDs should light continuously. Turn on the beam voltage in stages of approximately 100 Volts, to help minimize the sudden outgassing the will increase pressure as the source is heated.
- L) At the same time that you are increasing the voltage, turn on the accelerator voltage to keep it at a value of approximately 10% to 20% of the beam voltage.
- M) Monitor the beam current to make sure that the accelerator does not have excessive wear due to direct impingement (see Kaufman & Robinson p. 36, Figure IV-3). If beam current (affected by the cathode current) tracks linearly with the accelerator current, the system is working fine. If the accelerator current runs away with an increase in the beam current, there is direct impingement happening. Ensure that the neutralizer current is properly adjusted to neutralize the beam.
- N) Use the cathode to set a useful maximum beam current. Be aware that there are maximum beam currents for the source, depending on the beam energy and grid aperture size, material, and optics.
- O) Use "Auto" mode on the ID-2501 to reduce drift due to filament erosion over time.
- P) Continuously monitor the various currents and voltages to ensure that while you are "growing" your film, the growth parameters are static.

Turing the System "OFF"

- A. If you are going to re-use the settings that you have established for the current film growth, then just turn off the beam and then the source. Leave all control knobs at their current locations.
- B. If you are going to leave the system and not perform another growth using the same parameters, turn all knobs fully counter-

clockwise to ensure that they are at their minimum settings. This prevents large transients on the system when it is cold.

- C. Let gasses flow into the chamber for at least $\frac{1}{2}$ hour to cool the system down.
- D. Raise the temperature of the chill water system to 17°C to prevent frosting on the chamber walls.

11.4 How to Operate the F-20

11.5 How to Operate the D-1

*****NOTE: Whenever you are instructed to manipulate the D-1 physically:**

- 1. Go to the front panel of the D-1.**
- 2. Press the “Shutter Close” button and wait for the light to go out on the “Shutter Open” button.**
- 3. Open the panel and perform whatever operations you need to.**
- 4. Close the D-1 door.**
- 5. Press the “Shutter Open” button until you see it light up.**

Note!!!: Failure to follow the above instructions can lead to physical harm if the safety interlock fails! Do Not Forget!!!

11.5.1 Aligning the Bede D-1 for Parallel Beam and High Angle XRD Scanning

- A) Click on the “Bede Control” icon on the desktop. A Pop-Up-Window (PUW) will open and ask you to login. Type in the password and hit “OK”. The control software will then open up (see Figure 11-25).

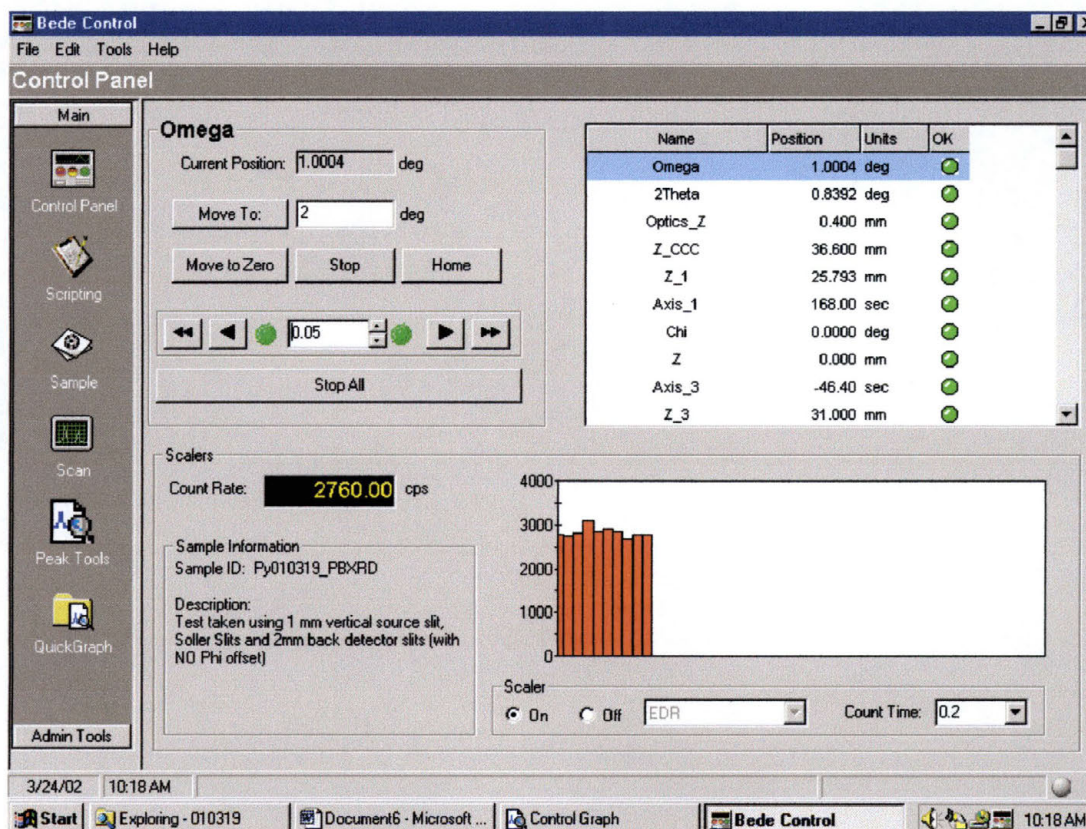


Figure 11-25: Bede Control Opening Window

- B) Click on the “Scripting” button on the left side of the window.
- C) Click on the open folder icon.
- D) Open the file: C:/Program Files/Bede Scientific/Control2/Scripts/Alignment/Align in Powder Mode. The file should say “Aligns the beam in Powder mode for low resolution HAXRD or PBXRD, but does NOT align the sample.” (see Figure 11-26)

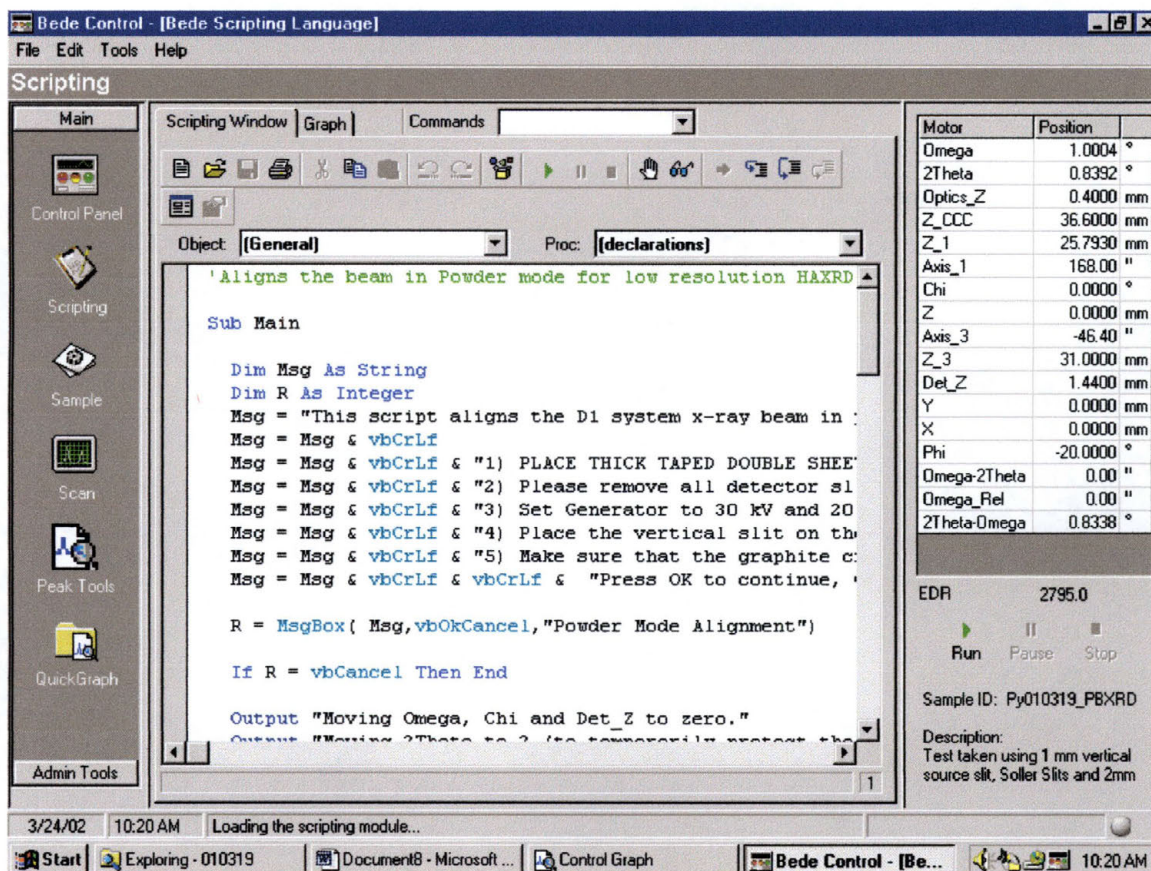


Figure 11-26: Align in Powder Mode Opening Script

E) Click on the “Run” icon on the lower right corner of the window. A new window will open with the title “Powder Mode Alignment”, and will have the following instructions: “This script aligns the D-1 system x-ray beam in powder mode for low resolution (no CCC mode) PBXRD or HAXRD measurements, but does NOT align the sample in the beam.” (see Figure 11-27). It will also list the following instructions that need to be carried out before the alignment procedure can begin:

- 1) PLACE THICK TAPED DOUBLE SHEET ALUMINIM ABSORBER IN PLACE BEHIND THE DETECTOR FRONT SLIT!!!
- 2) Please remove all detector slits.
- 3) Set generator power to 30 kV and 20 mA.
- 4) Place the vertical slit on the horizontal slide at the front of the optics stage, AND the 1 mm vertical slit after the 2nd CCC.
- 5) Make sure that the graphite crystal is removed and that the detector is in the “straight through” position.

“Press OK to continue, Cancel to Abort”.

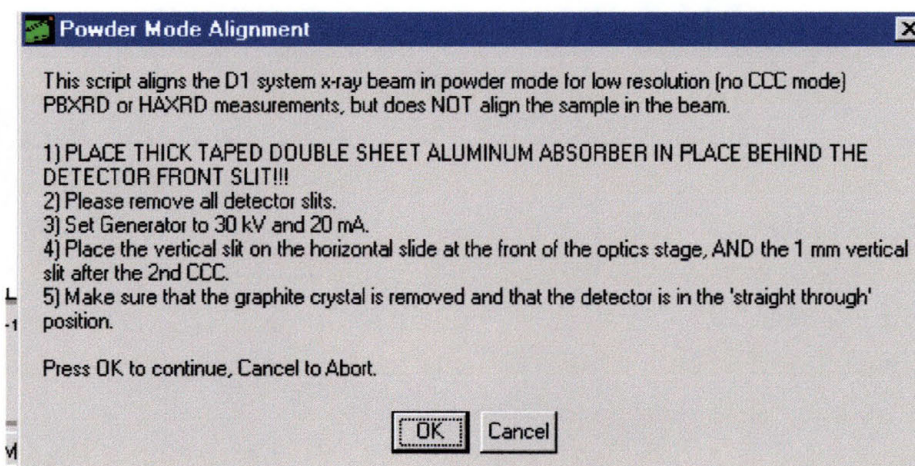


Figure 11-27: Powder Mode Alignment PUW

F) Once you have followed the instructions on the PUW, click the OK button. The script will say:

- Moving Omega, Chi, and Det_Z to zero.
- Moving the sample (Z) out of the way of the beam.
- Moving Z_3, CCC, and Z_1 to positive HW limits.
- Putting movable Al absorber in beam.
- Moving Optics_Z to hardware limit.

G) When this script is finished, a PUW will open that says, “Be sure that you have already placed the 1 mm vertical slit in the front of the optics stage. Be sure that you have already placed the vertical slit on the horizontal slide at the front of the optics stage (unless need a smaller circle to shorten the beam for small samples).” (see Figure 11-28)

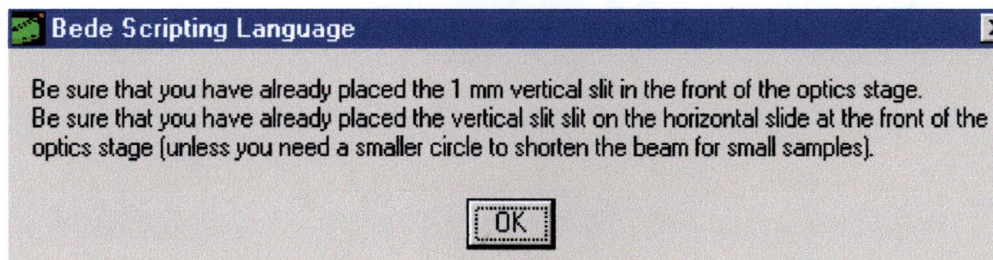


Figure 11-28: Pop-up Window for Step G

- H) The script will then say:
- “Scanning for highest point in Optics_Z” and will perform an alignment scan on the Optics_Z motor.
 - When the scan is complete, the script will then say “Highest scalar value = ### at position ###.”
- I) A new PUW will open (see Figure 11-29) with the instruction “Please insert the 1.0 mm front detector slit.” When you have followed the instruction, click on the OK button.

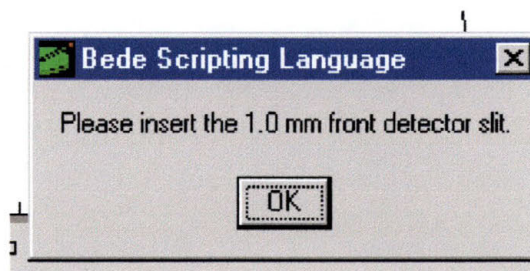


Figure 11-29: PUW for Step I

- J) Script will then say:
- Scanning for highest peak on 2Theta” and will perform a scan on 2Theta.
 - When scan is complete, the script will say, “Highest Scalar Value = ### at position ###.”
- K) A new PUW will open(see) with the following instructions:
- “Please insert the graphite crystal and rotate the detector to its angled graphite position. ALSO, remove the thick double sheet Al absorber and replace it with the thin Al attenuator.”
 - When you have followed the instructions, click on the OK button.

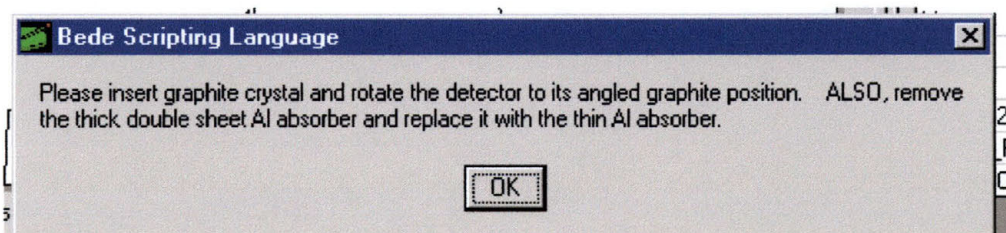


Figure 11-30: PUW for Step K

L) The script will then say,

- Scanning for highest peak on 2Theta” and will perform an alignment scan on the 2Theta motor.
- When the scan is complete, script will say, “Highest Scalar Value = #### at position ###.”

M) A new PUW will appear (see Figure 11-31) with the instruction:

- “Please insert the 2 mm back detector slit (at detector head).”
- When you have followed the instruction click the OK button.



Figure 11-31: PUW for Step M

N) Script will then say:

- “Scanning for peak on Det_Z” and will perform a scan on the Det_Z motor.
- When scan is complete, script will say, “Highest scalar value = ### at position ###.”

O) A new PUW will appear with the question, “Do you want to align the Soller Slit?”

- If you want to perform a PBXRD scan, answer “**yes**” and **go to step 11.5.4** on page .
- If you want to perform a HAXRD scan, answer “**no**” and **go to step 11.5.3** on page .

11.5.2 Aligning the Sample

Note: This is the procedure to align the sample for PBXRD, HAXRD, and Reflectivity scans. For PBXRD and HAXRD, these steps must be performed manually. For Reflectivity, these procedures will be performed automatically by the scripting software immediately after the system is aligned for Reflectivity Mode scanning.

- A) A new PUW will appear with the instruction: “You may want to increase power to 40 kV and ~35 mA to get ~400k cps with the thin Al attenuator sheet for sample placement in the beam.” Click the OK button.

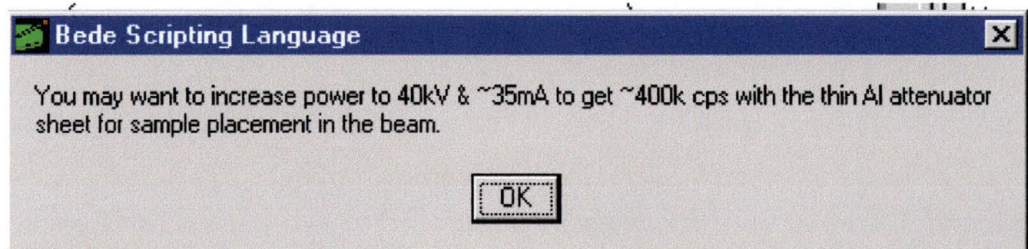


Figure 11-32: PUW for Step A

- B) Script will then open a new PUW that says: “You are now ready to position the sample in the x-ray beam.” Don’t forget that you have the Al attenuator in place!” Click the “OK” button.
- C) Click on the “Control Panel” button on the left side of the screen. The control panel main screen will appear as in Figure 11-33.

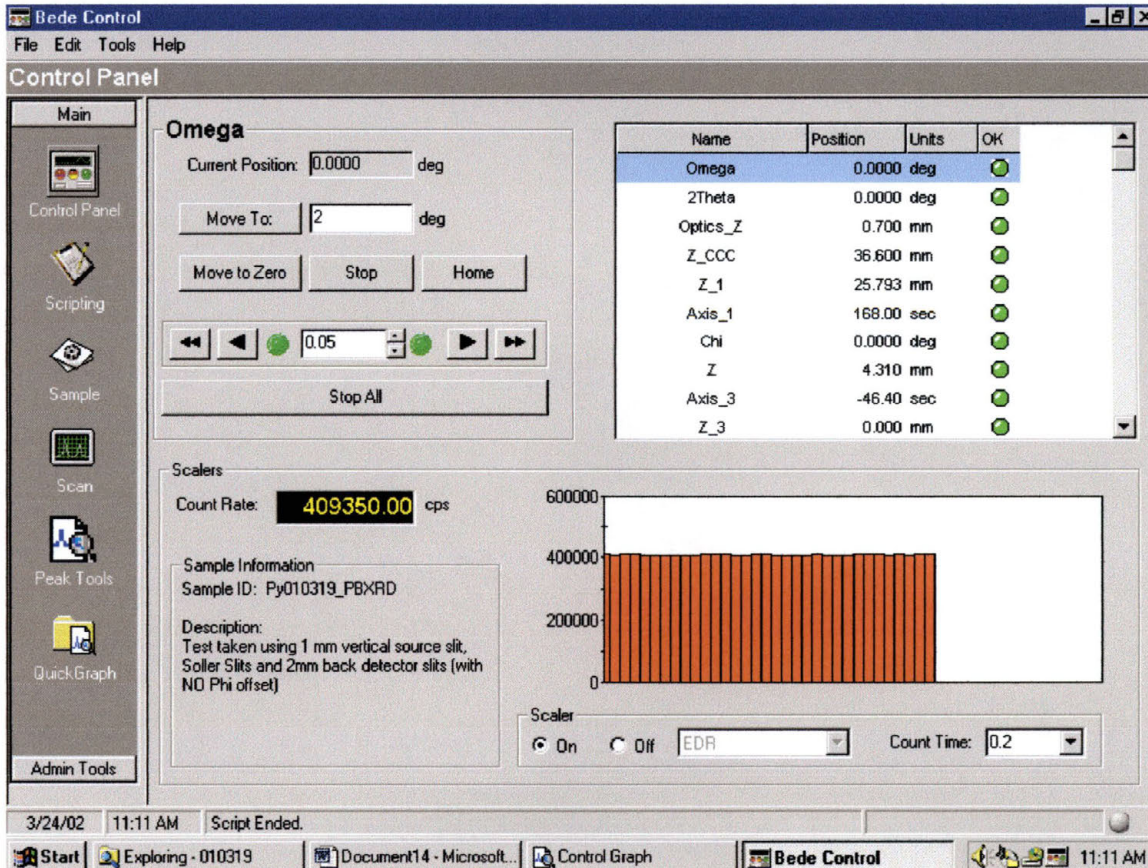


Figure 11-33: Control Pane Main Window for Sample Alignment

- D) Now it is time to align the sample in the beam.
- E) If you have not done so yet, rotate “Phi” to -20.0 degrees. This is to cut down on scattering of the lattice planes.
 - 1) You do this by highlighting Phi (just like Omega is highlighted in Figure 11-33).
 - 2) Type in “-20.0” in the window just next to the “Move To” button.
 - 3) Hit the “Move To” button.
 - 4) Watch the motor position to ensure that it is moving as directed.
 - 5) Open the D-1 panel and observe the location of the screws on the D-1 sample holder plate. Ensure that they are not blocking the x-ray beam. If they are, you will need to adjust the position of the Phi motor until the beam is clear.
- F) Adjust the power until you get $\sim 400,000$ counts-per-second on the EDR detector.
- G) Move the “Z” motor (the sample stage) until you lose half of your counts ($\sim 200\text{k}$ cps).
- H) Click on the “Scan” button on the left side of the screen to set up for a scan on Omega. This will open the scan main window (see Figure 11-34).

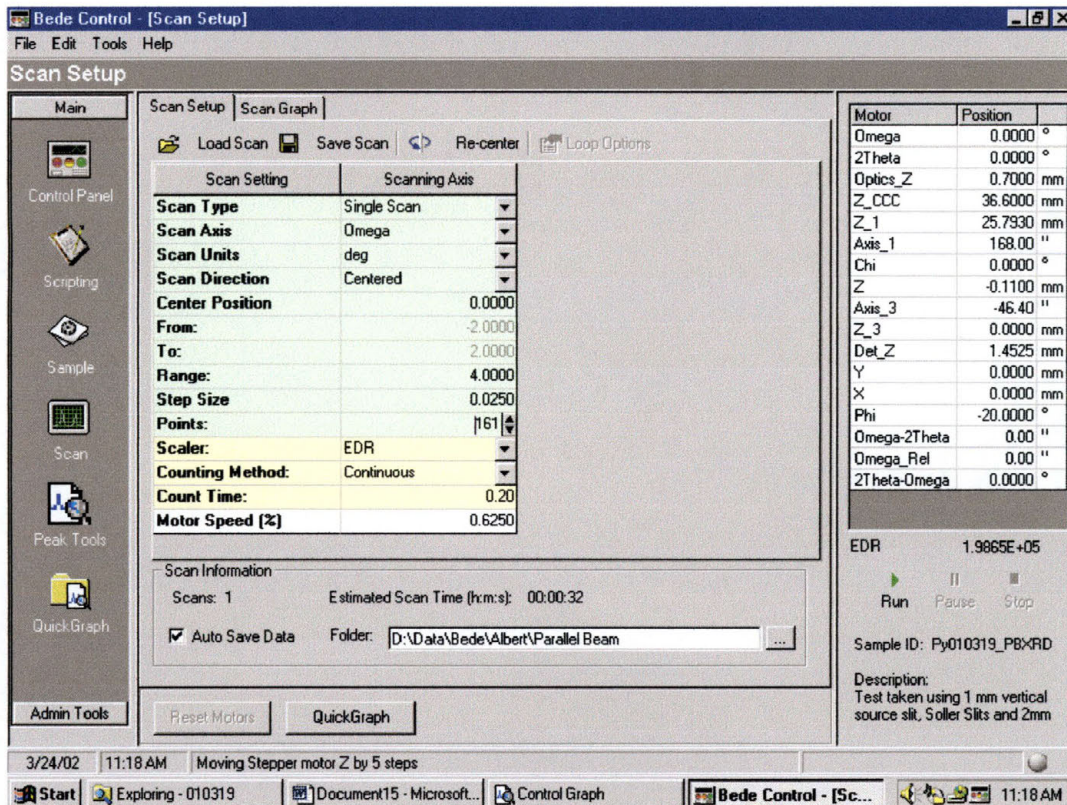


Figure 11-34: Main Window for Scan Setup

1) Select the following settings for a scan on Omega:

Scan Type	: Single Scan
Scan Axis	: Omega
Scan Units	: degrees
Scan Direction	: Centered
Center Position	: 0
From	: N/A
To	: N/A
Range	: 4.0
Step Size	: 0.0250
Points	: 161
Scaler	: EDR
Counting Method	: Continuous
Count Time (sec)	: 0.20

Note: When simply aligning the sample, remove the check on the box for "Auto Save Data". This will prevent your data folder from becoming cluttered with alignment scans.

- I) Click on the “Run” button on the lower right corner of the screen.
- 1) The D-1 will now perform a scan for the parameters you selected.
 - 2) When the scan is complete, click on the peak finder at the top of the graph. This will put a point and a value at the highest peak on the scan.
 - 3) Right click on this point and highlight “Motor Commands”, and then highlight “Move Omega to ### deg.”. Click on it (see Figure 11-35 on the next page).
- J) Click on the “Control Panel” icon, highlight “Omega” and press the letter “c” on the keyboard.
- 1) This will open a new PUW titled “Recalibrate Motor Position”.
 - 2) Type in 0 and hit enter.

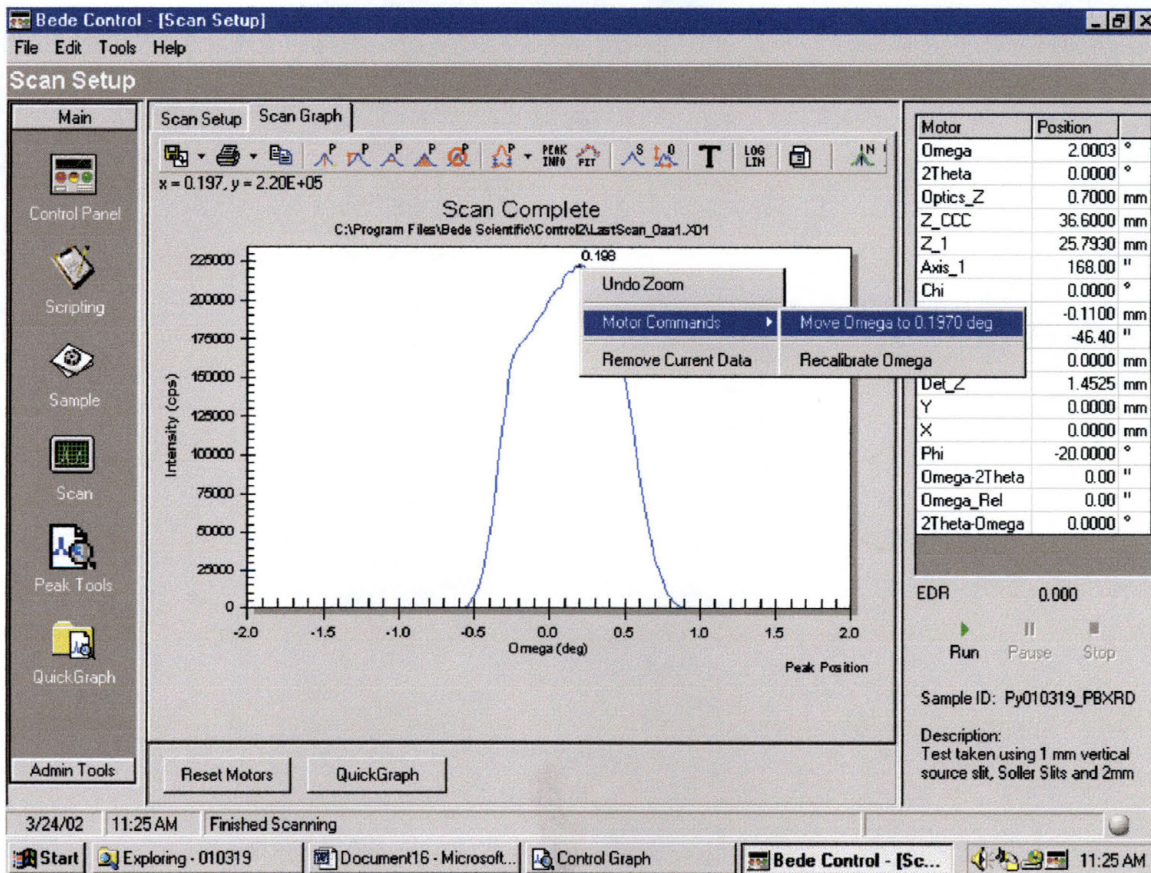


Figure 11-35: Scan Peak Selection for Scan on Omega

- K) If the count rate is higher than ~200,000 cps, repeat steps G thru J until the peak value on the Omega scan is ~200,000 cps.

- L) Move “Z” from ~200,000 cps to ~40,000 cps.
- M) Click on the “Scan” icon on the left side of the screen to set up for a scan on Chi.

- 1) Select the following parameters for a scan on Chi:

Scan Type	: Single Scan
Scan Axis	: Chi
Scan Units	: degrees
Scan Direction	: Centered
Center Position	: 0
From	: N/A
To	: N/A
Range	: 10.0
Step Size	: 0.1
Points	: 101
Scalar	: EDR
Counting Method	: Continuous
Count Time (sec)	: 0.50

- N) Click on the run button on the lower right corner of the screen (see Figure 11-35 on previous page).
- 1) The D-1 will now perform a scan on the parameters selected.
 - 2) When the scan is complete, find the lowest point on the graph and record it.
 - 3) Click on the Control Panel icon on the left side of the screen.
 - 4) Move the Chi motor to the value you recorded and zero the motor calibration.
 - 5) Repeat steps G thru K.
- O) You have now aligned the sample for scanning. For HAXRD, go to Step C on page 185. For PBXRD, go to Step F on page 186.

11.5.3 Performing a High Angle X-Ray Diffraction Scan

- A) If you have not done so yet, click on the “Sample” button. This will open the “Sample Information” window (see Figure 11-36).

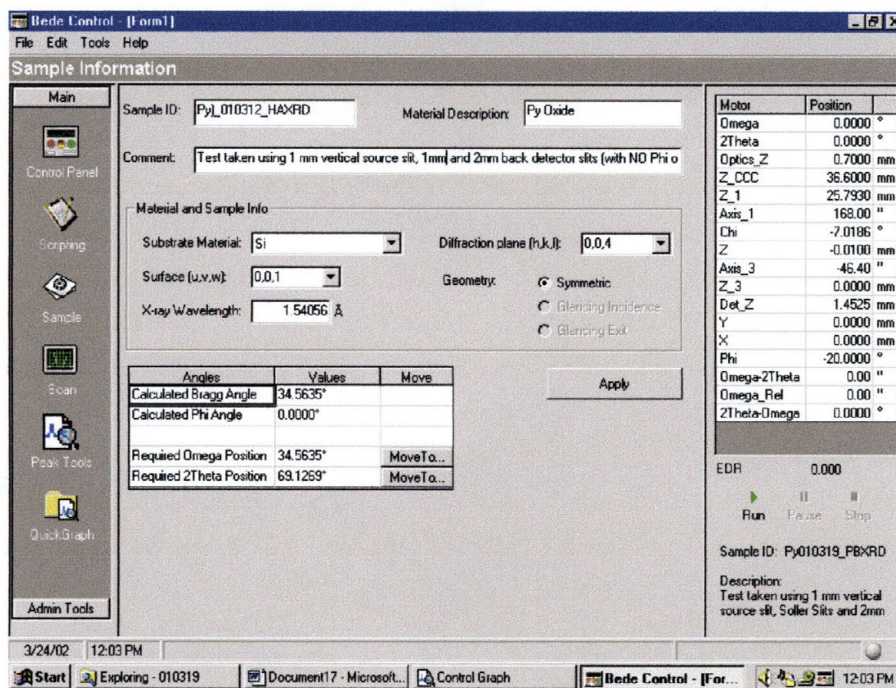


Figure 11-36: Sample Information Window

- 1) Adjust information as necessary and click on “Apply”.
- B) Follow the steps of Section 11.5.2 on page
- C) Move Omega to -2.0 degrees and recalibrate it to 0. This is to remove the Si Laue peaks from your scan.
- D) Remove the thin Al attenuator from in front of the detector.
- E) Raise the power on the power supply to 45 kV and 40 mA.
- F) Click on the “Scan” button on the left side of the screen to set the parameters for your scan.
- 1) Select the following parameters for your scan:

Scan Type : Single Scan
 Scan Axis : 2Theta-Omega
 Scan Units : degrees

Scan Direction	: Positive
Center Position	: N/A
From	These parameters will depend on where you expect to find peaks in your scan.
To	
Range	
Step Size	: 0.05
Points	: Depends on size of your scan
Scalar	: EDR
Counting Method	: Continuous
Count Time (sec)	: ~ 3.0

- G) Check the box for “Auto Save Data”
- H) Select which folder you want to save your scan in.
- I) When you have verified all the scan parameters, click on “Run”. Now you will get to wait a while as the scan takes place.

11.5.4 Performing a Parallel Beam X-Ray Diffraction Scan

- A) The scripting will say:
- 1) You may want to increase power to 40 kV and ~30 mA to get ~400k cps with the thin Al attenuator sheet placement in the beam. Also remove the front detector slit.”
 - 2) When you have followed the instructions, click on “OK”
- B) The script will say, “Scanning for highest point on Axis_3” and will perform a scan on the Axis_3 motor.
- C) When the scan is complete, the scripting will say, “Highest Scalar Value = ### at position ###” and will move the Axis_3 motor to that point.
- D) The script will open a new PUW with the following instructions”
- “You are now ready to position the sample in the x-ray beam. Don’t forget that you have the thin sheet Al attenuator in place!”
 - Click on “OK”
- E) Follow the steps from section 11.5.2 on page 184.
- J) If you have not done so yet, click on the “Sample” button. This will open the “Sample Information” window (see Figure 11-36).

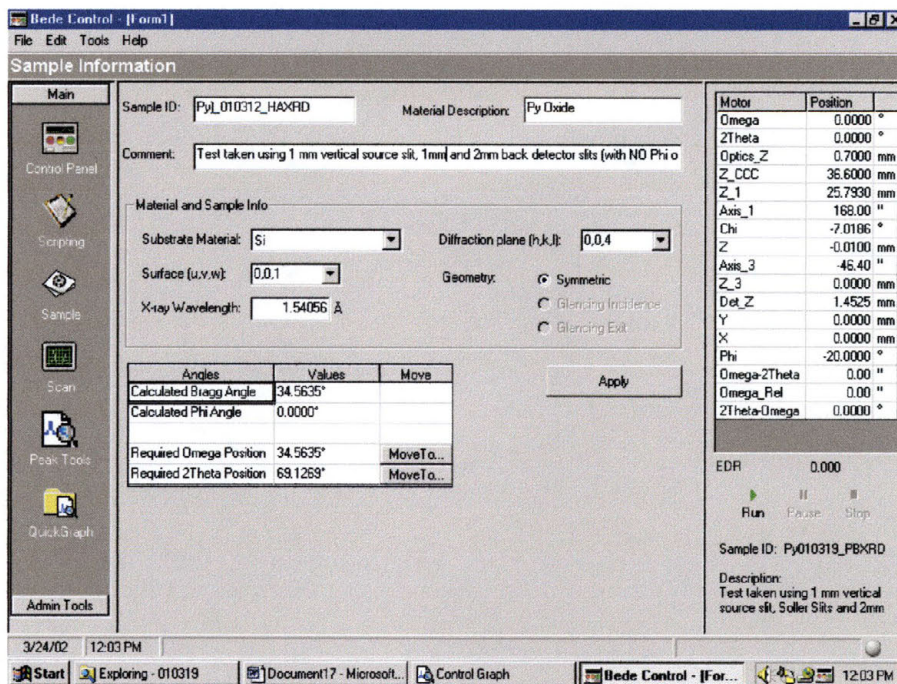


Figure 11-37: Sample Information Window

- F) Adjust information as necessary and click on “Apply”.
- G) Click on the “Scan” icon on the left side of the screen to set the parameters for your scan.
- 1) Select the following parameters:

	Scanning Axis	Loop Axis 1
Scan Type	: Single Scan	: On
Scan Axis	: 2Theta	: Omega
Scan Units	: degrees	: Degrees
Scan Direction	: Positive	: Positive
Center Position	: N/A	: N/A
From	These parameters will depend	: 2.0
To	on where you expect to find	: 3.0
Range	peaks in your scan.	: 1.0
Step Size	: 0.05	: 0.50
Points	: Depends on size of your scan	: 3
Scalar	: EDR	: N/A
Counting Method	: Continuous	: N/A
Count Time (sec)	: ~ 3.0	: N/A

- H) Remove the thin sheet Al attenuator from in front of the detector.

- I) Check the box for “Auto Save Data”.
- J) Select the folder that you want to save your data in.
- K) When you have verified all scan parameters, click on “Run”.

11.5.5 Aligning the D-1 for and Performing a Reflectivity Mode X-Ray Scan

- A) Click on the “Bede Control” icon on the desktop. A Pop-Up-Window (PUW) will open and ask you to login. Type in the password and hit “OK”. The control software will then open up (see Figure 11-25).

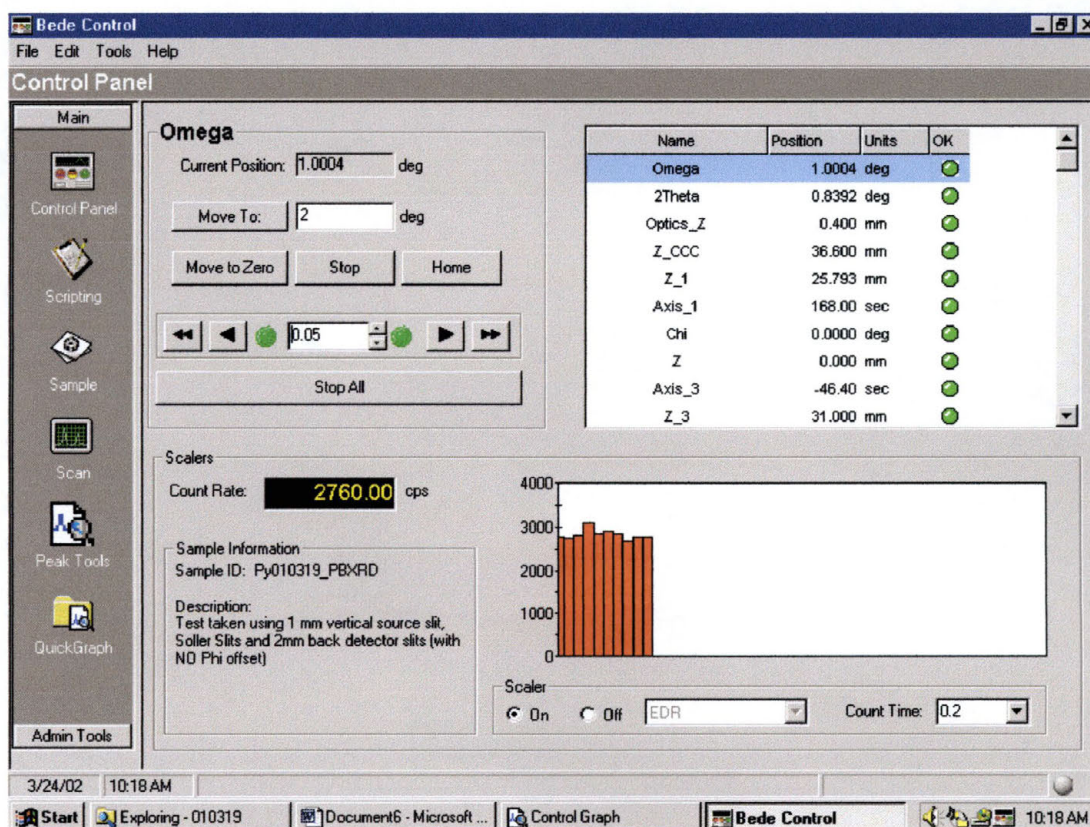


Figure 11-38: Bede Control Opening Window

- B) Click on the “Scripting” button on the left side of the window.
- C) Click on the open folder icon.

D) Open the file: C:/Program Files/Bede Scientific/Control2/Scripts/Alignment/Align in 2 Bounce Mode. The file should say “This script aligns the D1 system in 2-Bounce mode using the 2nd CCC for XRR and high resolution XRD measurements, but does NOT position the sample for measurement.”

E) A new PUW will open which says Figure 11-39:

“This script aligns the D-1 system in 2-Bounce mode using the 2nd CCC for XRR and high resolution XRD measurements, but does NOT position the sample for measurement.”

The script will also have the following instructions:

- 1) Please remove all detector slits (except tube shield).
- 2) Remove graphite monochromator (if present).
- 3) Move detector head to straight indentation.
- 4) Set generator to 20 kV and 10 mA.
- 5) Ensure the 2nd CCC (Axis_1) is mounted in place.
- 6) Place the vertical slit on the horizontal slide at the front of the optics stage, remove any other vertical slit on the vertical 2nd CCC mount.

“Press OK to continue, Cancel to abort.”

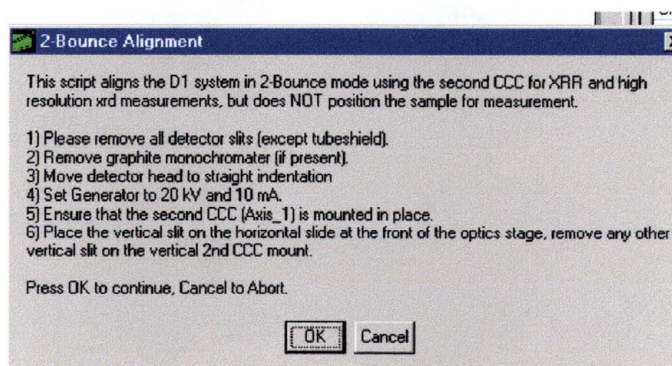


Figure 11-39: Opening PUW of D-1 XRR Alignment

F) The script will then say:

- Moving sample (Z) out of the way
- Moving Omega, Chi, and 2Theta to zero
- Moving soller slits and triple axis crystal out of the way (wide open, NO Al beam attenuator in place).
- Moving Z_CCC (1st CCC) to positive hardware limit.

- Moving Z_1 (2nd CCC) to positive hardware limit, then returning to its approximate proper position for 2 Bounce beam conditioning.
- Moving Optics_Z to its positive hardware limit, then returning to its ~ 3mm offset translated position for single CCC operation.
- Optimizing 2nd CCC Axis_1 rotation for max counts
- Scanning for highest point on Axis_1
- Highest Scalar Value = ### at position ###

G) When the script is finished, a new PUW will open with the following instructions:

“Place the 100 micron (precision) vertical slit in the front of the optics stage”

“Place the largest circular aperture slit on the horizontal slide at the front of the optics stage, unless you need to choose a smaller circular aperture to restrict the beam height for smaller samples.”

When you have followed the instructions, press the OK button.

H) The script will then say the following”

- Scanning for peak on Optics_Z
- Scanning for highest point on Optics_Z
- Highest Scalar Value = ### at position ###
- Optimizing 2nd CCC Axis 1 rotation again at higher resolution for max counts
- Scanning for highest point on Axis_1
- Highest Scalar Value = ### at position ###

I) When the script is finished, a new PUW will open with the following instructions:

“Please insert the 0.5 mm front detector slit”

J) The script will then say:

- Scanning for peak on 2Theta, then calibrating to zero at its peak
- Scanning for highest point on 2Theta
- Highest Scalar Value = ### at position ###

K) When the script is finished, a new PUW will open with the following instructions:

“Please insert the 1.0 mm back detector slit (at detector head)”

L) The script will then say:

- Scanning for peak on Det_Z
- Scanning for highest point on Det_Z
- Highest Scalar Value = ### at position ###
- Alignment Complete

11.5.6 Alignment and Scanning of Sample for Reflectivity Mode

A) Click on the “Scripting” button on the left side of the window.

B) Click on the open folder icon.

C) Open the file: C:/Program Files/Bede Scientific/Control2/Scripts/Alignment/D1_Reflectivity

D) A new PUW will open (see Figure 11-40). Select the parameters you want to use for your scan. When you have completed selecting your parameters, click on the OK button.

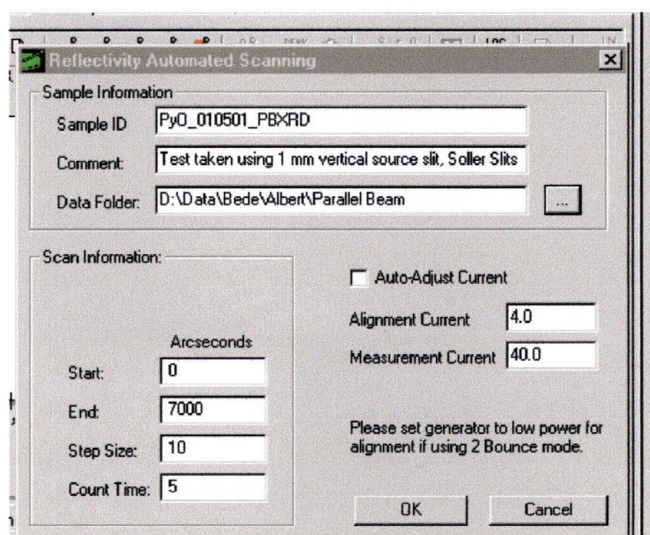


Figure 11-40: Opening Pop Up-Window for XRR Sample Alignment and Scanning

E) The script will open a new PUW with the following instruction:

“Please set XRG to 40 kV and 4.0 mA”

Click on the OK button when you have finished following the instructions.

F) The script will then say:

- Aligning 2Theta
- Scanning for highest point on 2Theta
- Highest Scalar Value = ### at position ###
- Aligning the Z Axis (placing sample in the beam)
- Z is set, Accuracy = ### %
- Scanning for highest point on Omega
- Aligning the Z Axis (placing sample in the beam)
- Scanning for highest point on Omega
- Scan Started: MM/DD/YY HH:MM:SS am/pm

G) The D-1 has now started the scan.

H) When the D-1 recognizes that it is at the appropriate location in the scan, it will open a new PUW that says:

Reset the beam current to a value of 40 mA.

When you have followed the instructions, click on the OK button. Scan will resume until it is finished and it presents you with data.

12 Bibliography

- ¹ Kim K., Perspectives on Giga-Bit Scaled DRAM Technology Generation, *Microelectronics Reliability*, Vol. 40, 2000, p 191
- ² Liang H., Spin Valve Transistor and Magnetic RAM, University of Maryland, <http://www.ece.umd.edu/class/enee697.S99/projects/lianghy/Paper.htm>
- ³ <http://cst-www.nrl.navy.mil/lattice/mainpage.html>
- ⁴ Ghibaudo G., Clerc R., Vincent E., Bruyere S., Autran J.L., Gate dielectrics for ultimate CMOS technologies- Limitations and alternative solutions, in: *Challenges in Microelectronics*, The Academy of Science of the Institute of France, Paris, t. 1, Series IV, p 919
- ⁵ Degraeve R., Groeseneken G., Bellens R., Depas M., Maes H.E., A consistent model for the thickness dependence of intrinsic breakdown in ultra-thin oxides, in: *Institute for Electrical and Electronics Engineers Int. Electron Devices Meeting Tech. Digest*, 1995, p 863
- ⁶ McPherson J., Reddy V.K., Mogul H.C., Field enhanced Si-Si bond breakage mechanism for time dependent dielectric breakdown in thin-film SiO₂ dielectrics, in: *Journal of Applied Physics*, Vol. 84, 1998, p 1513
- ⁷ Vincent E., Bruyere S., Papadas C., Morinin P., Dielectric reliability in deep submicron technologies: from thin to ultra-thin oxides, *Microelectron Reliability*, Vol. 37, 1997, p 761
- ⁸ Maserjian J., Zamani N., Behavior of the Si/SiO₂ interface observed by Fowler-Nordheim Tunneling, *Journal of Applied Physics*, Vol. 53, 1982, p 559
- ⁹ Depas M., Nigam T., Heyns M.M., Soft breakdown of ultra-thin oxide layers, *Institute for Electrical and Electronics Engineers Transactions on Electron Devices*
- ¹⁰ Yang N., Wortman J., A Study of the Effects of Tunneling Currents and Reliability of sub-2 nm Gate Oxides on Scaled n-MOSFETs, *Microelectronics Reliability*, Vol. 41, 2001, p 37
- ¹¹ Chang C.-Y., Chen C.-C., Lin H.-C., Liang M.-S., Chien C.-H., Huang T.-Y., Reliability of Ultrathin Gate Oxides for ULSI Devices, *Microelectronics Reliability*, Vol. 39, 1999, p 558
- ¹² Tarui Y., Hirai T., Teramoto K., Koike H., Nagashima K., Application of the Ferroelectric Materials to ULSI Memories, *Applied Surface Science*, Vol. 113, 1997, p 656
- ¹³ Moll J.L., Tarui Y., *Electronic Devices, (Solid-State Res. Conference Abs.)*, ED-10, 1963, p 338
- ¹⁴ Ezhilvalavan S., Tseng T.Y., Progress in the Development of (Ba,Sr)TiO₃ (BST) Thin Films for Gigabit era DRAMs, *Materials Chemistry and Physics*, Vol. 65, 2000, p 228
- ¹⁵ Kuroiwa T., Tsunemine Y., Horikawa T., Makita T., Tanimura J., Mikami N., Sato K., Dielectric Properties of (Ba xSr1- x)TiO₃ Thin Films Prepared by RF Sputtering for Dynamic Random Access Memory Application, *Japanese Journal of Applied Physics*, Vol. 33, 1994, p 5187
- ¹⁶ Wang Y.P., Tseng T.Y., *Journal of Applied Physics*, Vol. 81, 1997, p 6765
- ¹⁷ Wu T.B., Wu C.M., Chen M.L., Highly Insulative Barium Zirconate-Titanate Thin Films Prepared by RF Magnetron Sputtering for Dynamic Random Access Memory Applications, *Applied Physics Letters*, Vol. 60, 1996, p 2659
- ¹⁸ Jaffe B., Cook R. Jr., "Piezoelectric Ceramics", Academic Press, London and New York, 1971, p 91
- ¹⁹ Lin J.N., Wu T.B., *Journal of Applied Physics*, Vol. 68, 1990, p 985

-
- ²⁰ Weber U., Dielectric Properties of Ba(Zr,Ti)O₃-Based Ferroelectrics for Capacitor Applications, *Journal of the American Ceramic Society*, Vol. 84, 2001, p 759
- ²¹ Armstrong T.R., Buchanan R.C., Influence of Core-Shell Grains on the Internal Stress State and Permittivity Response of Zirconia-Modified Barium Titanate, *Journal of the American Ceramic Society*, Vol. 71, 1990, p 1270
- ²² Yamamichi S., Sakuma T., Hase T., Miyasaka Y., SrTiO₃ and (Ba,Sr)TiO₃ Thin Films Preparation by Ion Beam Sputtering and their Dielectric Properties, *Material Research Symposium Procedures*, Vol. 243, 1992, p 297
- ²³ Peng C.-J., Hu H., Krupanidhi S.B., Low-energy Oxygen Ion Bombardment Effect on BaTiO₃ Thin Films Grown by Multi-Ion-Beam Reactive Sputtering Technique, *Applied Physics Letters*, Vol. 63, 1993, p 734
- ²⁴ GMR: A Giant Leap for IBM Research, <http://www.research.ibm.com/research/gmr>, p 1
- ²⁵ Mallinson J., *Magneto-Resistive Heads: Fundamentals and Applications*, Academic Press, San Diego, 1996
- ²⁶ J.M. Daughton, GMR Applications, *Journal of Magnetism and Magnetic Materials*, Vol. 192, 1999, pp. 334-342.
- ²⁷ B. Dieny, Giant magnetoresistance in spin-valve multilayers, *Journal of Magnetism and Magnetic Materials*, Vol. 136, 1994, pp. 335-359
- ²⁸ J.C.S. Kools, Exchange-Biased Spin-Valves for Magnetic Storage, *Institute for Electrical and Electronics Engineers Transactions on Magnetics*, Vol. 32, No. 4, July 1996, pp 3165-3184.
- ²⁹ P. Perera, A.G. Ayala, C. Gutierrez, Metastable Permalloy Monoxide Based Spin Valves and Pseudo Spin Valves, *Journal of Applied Physics*, Vol. 85, p 6121, 1999
- ³⁰ H.Y. Liang, Spin Valve Transistor and Magnetic RAM, <http://www.ece.umd.edu/class/enee697.S99/projects/lianghy/Paper.htm>
- ³¹ W/ Brückner, S. Baunack, M. Hekcer, J. Thomas, S. Groudeva-Zotova, C.M. Schneider, Oxidation of NiFe(20 wt. %) Thin Films, *Materials Science and Engineering*, B86, 2001, pp272-275.
- ³² R. Bozorth, *Ferromagnetism*, fourth Printing, D. Van Nostrand company, Inc. ,1978
- ³³ M. Kitada, *Journal of Material Science* 26, 1991, p4150
- ³⁴ R.M. Valetta, C. Hwang, H. Lefakis, *Journal of Material Science*, Vol A9, 1991, p. 2107.
- ³⁵ VSM, <http://www.physics.hull.ac.uk/magnetics/Research/Facilities/VSM/vsm.html>
- ³⁶ Jauncey, G.E.M., *Physical Review* Volume 19, 1922, pp 64-67
- ³⁷ Weisskopf, V., Wigner, E., *Z. Phys.* Vol. 63, 1930, pp 54-65.
- ³⁸ Cullity, B.D., *Elements of X-Ray Diffraction*, Addison-Wesley Pub. Co., 1956, p. 7
- ³⁹ http://www.apace-science.com/radsens/images/thin_int.gif
- ⁴⁰ <http://www.bede.co.uk/homeindex.htm>
- ⁴¹ Hammond, C. *The Basics of Crystallography and Diffraction*, Second Edition, Oxford University Press, 2001
- ⁴² Cullity, B.D., *Elements of X-Ray Diffraction*, Addison-Wesley Publishing Co, Inc., Reading, MA, 1959
- ⁴³ Toney, M., *X-Ray Diffraction*, *Encyclopedia of Materials Characterization: Surfaces, Interfaces, Thin Films*, C. Brundle, C. Evans, S. Wilson, editors, Butterworth-Heinemann, London, England.
- ⁴⁴ Introduction to Thin Films, http://www.filmetrics.com/bt_intro.html, p. 3

Vita

Albert Anthony Tijerina was born on November 2, 1966 at Webb Air Force Base in Big Springs Texas to Albert Tijerina and Amanda Ann (Duke) Tijerina. A 1985 graduate of San Angelo Central High School, he joined the United States Navy in 1989 and proudly served aboard the U.S.S. Long Beach (CGN-9) as a nuclear trained Electrician's Mate. It was there (much to his surprise) that he discovered not only a passion, but also an aptitude for physics. He attended Angelo State University (ASU) in San Angelo, TX where he became the first person to ever win the Jody C. Minnick award for the outstanding physics major twice (1998 & 1999). In addition, he was selected for Who's Who in American Colleges and Universities (1998), he was a Robert and Nona Carr Research Fellow for research he did on Integral Wavelet Analysis (1998-1999), and he was elected President of the Society of Physics Students for the 1998-1999 academic year. Between his junior and senior years, he also participated in the Research Experience for Undergraduates at the University of Arkansas where he worked with Dr. Paul Thibadeau in the Molecular Beam Epitaxy lab. In 1999, he was inducted into Sigma Pi Sigma, the National Physics Honor Society sponsored by the American Institute of Physics. It was while he was teaching in the computer lab at ASU that he made the most important discovery of his life... he met Amy Michelle Brooks.

In 1999 Albert graduated from ASU with a B.S. in Applied Physics, after which was he accepted into the graduate program at Southwest Texas State University (SWT) in the Department of Physics. AT SWT he was fortunate enough to have Dr. Carlos J. Gutierrez as his advisor and his friend. On June 3, 2000 Albert and Amy were married and consider themselves lucky enough to still be on their honeymoon. In the spring semester of 2001, Albert was given the privilege of teaching at the college level when he was asked to teach the second half of Introductory Physics at SWT. Also, in 2001, he was presented with an award for Academic Excellence by the Department of Physics. In May of 2001 he began work as an Intern at International SEMATCH in the Front End Process Division where, under the tutelage of Dr. Larry Larson, he contributed to the Advanced Annealing, Doping Development, Gate Stack, and High K projects. In 2002, Albert was also presented with an award for Excellence in Graduate Research by the Department of Physics at SWT.

Permanent Address: 2463 Oxford Avenue
San Angelo, TX 79604

This thesis was typed by Albert A. Tijerina